



HAL
open science

Mixotrophy of photosymbiotic Radiolaria

Joost Mansour

► **To cite this version:**

Joost Mansour. Mixotrophy of photosymbiotic Radiolaria. Oceanography. Sorbonne Université, 2021. English. NNT: 2021SORUS425 . tel-03696691

HAL Id: tel-03696691

<https://theses.hal.science/tel-03696691>

Submitted on 16 Jun 2022

HAL is a multi-disciplinary open access archive for the deposit and dissemination of scientific research documents, whether they are published or not. The documents may come from teaching and research institutions in France or abroad, or from public or private research centers.

L'archive ouverte pluridisciplinaire **HAL**, est destinée au dépôt et à la diffusion de documents scientifiques de niveau recherche, publiés ou non, émanant des établissements d'enseignement et de recherche français ou étrangers, des laboratoires publics ou privés.

Sorbonne Université

Sciences de la nature et de l'Homme : écologie et évolution – ED227

Station Biologique de Roscoff / Adaptation et diversité en milieu marin, UMR 7144

Mixotrophy of photosymbiotic Radiolaria

Par Joost Samir Mansour

Thèse de doctorat de ‘marine microbial physiology’

Dirigée par Fabrice Not

Présentée et soutenue publiquement le 17 Novembre de 2021

Devant un jury composé de :

Paola Furla— Professeure, University Cote d'Azur	Rapportrice
John Burns— Senior Research Scientist, Bigelow Laboratory for Ocean Sciences	Rapporteur
Susanne Wilken— Assistant Professor, University of Amsterdam	Examinatrice
Johan Decelle—Chargé de recherche, Université Grenoble Alpes, CNRS, CEA, INRAe	Examinateur
Laure Guillou— Directrice de recherche, Station Biologique de Roscoff, Sorbonne Université, CNRS	Examinatrice
Fabrice Not—Directeur de recherche, Station Biologique de Roscoff, Sorbonne Université, CNRS	Directeur de Thèse



Summary

Mixoplanktic photosymbioses are ubiquitous trophic relationships among marine plankton in the global ocean and can be important to ecosystems functioning, in particular in low nutrient settings. Radiolaria (Rhizaria) are abundant and ubiquitous single-celled eukaryotes (*i.e.* protists), many of which harbour photosynthetic endosymbionts. The abundance and mixotrophic physiology of photosymbiotic Radiolaria makes them both significant primary producers and consumers in oceanic food webs, as well as great contributors to biogeochemical cycles, including silicon, strontium, and the vertical export of organic matter. Because photosymbiotic Radiolaria cannot currently be cultured, physiological information for these organisms is limited and depends on cultivation-independent approaches. Research on Radiolaria will be important to understand photosymbiotic processes in planktic protists. Additionally, understanding their nutrient uptake capabilities will help to predict plankton dynamics by providing data for (e.g. system dynamics or global ocean) model input. In this thesis, my primary objective aimed at elucidating the mixotrophic physiology of photosymbiotic Radiolaria.

Analyses of carbon and nitrogen content of specific planktic organisms are pivotal information for studies of ocean ecology and in particular for carbon or nitrogen-based models. In Chapter 2, we established biovolume to carbon (and nitrogen) content equations for several Rhizaria taxa, giving more accurate predictions than mean or central capsule normalised C and N density values previously available. Overall, we show that generalised estimations for protists would underestimate the carbon content of Rhizaria by a factor of up to 35. The Radiolaria-specific carbon content to volume estimations provides a first step to better incorporate these mixotrophic organisms into predictive models.

Subsequent chapters focus on the photosymbiotic association between Acantharia (Radiolaria) and *Phaeocystis* (haptophyte algae). In particular, we aimed to establish phototrophic and phagotrophic rates for Acantharia using bulk stable isotope analyses. As well as elucidate the metabolic connectivity between host and symbiont using single-cell NanoSIMS and transcriptomic methods. We established the estimate for total inorganic carbon uptake rate of Acantharia as $1112.7 \pm 82.1 \text{ pg C h}^{-1} \text{ Acantharia}^{-1}$. Despite that the grazing rates of Acantharia remained unclear, based on our experiments and considering that the observed photosynthetic carbon uptake rates would only account for 14.5% of the acantharian carbon content, we suggest photosynthetic carbon uptake might thus mainly be used for energy. Therefore, photosynthates could be preferentially used for respiration. Transcriptomic analyses show an overall rapid gene expressional response to nutrient changes within the first few hours for genes from the photosymbionts. Concurrently, localisation of assimilated inorganic nutrients showed that both carbon and nitrogen are predominantly assimilated at the symbiont's plastids, and nitrogen assimilation is most prominent in the symbiont's nucleolus. Carbon translocation from symbionts to host could not be seen in our experiments and further suggest that photosynthates are used mainly for respiration or, transferred in low molecular weight compounds. Nitrogen assimilation in the symbiont's plastids and nucleolus suggests allocation of nutrients to photosynthesis machinery maintenance. Gene expression data further shows pathways present in nitrate metabolism in both host and symbiont, further indicating the intertwined nature of the Acantharia and symbiont.

Taken together, we propose Acantharia can use both nitrate and ammonium as inorganic nitrogen sources and use photosynthesis mainly as an energy source, and we suggest that carbon acquired by predation would be preferentially allocated (and is needed for) to growth.

Résumé

Associant photosynthèse et prédation chez un même individu, la photosymbiose est un type de relation mixo-trophique très répandue dans le plancton marin. Elle joue un rôle important dans le fonctionnement des écosystèmes, en particulier dans les milieux pauvres en nutriments. Les radiolaires (Rhizaria) sont des organismes eucaryotes unicellulaires (i.e. protistes) abondants dans tous les océans. De nombreuses espèces de radiolaires abritent des endosymbiontes photosynthétiques ce qui en fait à la fois d'importants producteurs primaires et mais aussi consommateurs dans les réseaux trophiques océaniques. Ils contribuent également de façon significative aux grands cycles biogéochimiques comme ceux du silicium, du strontium, ou du carbone via l'exportation verticale de matière organique. Les radiolaires photosymbiotiques ne peuvent être cultivés en laboratoire, limitant fortement les connaissances sur leur physiologie qui requièrent nécessairement des approches indépendantes de la mise en culture. La compréhension fine, aussi bien qualitative que quantitative, de leurs capacités à acquérir des nutriments est précieuse pour comprendre les processus fondamentaux régulant les relations photosymbiotiques ainsi que pour fournir des paramètres essentiels afin de modéliser les écosystèmes océaniques. Dans cette thèse, mon objectif principal a été de caractériser la physiologie des radiolaires photosymbiotiques.

Nous avons dans un premier temps établi des équations décrivant le biovolume en fonction de la masse de carbone et d'azote pour plusieurs taxa de Rhizaria. Cela a permis d'obtenir des valeurs de masses de carbone et d'azote plus précises que celles disponibles jusqu'ici. Ces nouvelles données, spécifiques aux différents taxa de radiolaires, ont pu montrer que les estimations généralisées pour les protistes conduisent à une sous-estimation jusqu'à un facteur 35 du contenu en carbone des radiolaires.

Les chapitres suivants se concentrent sur l'association photosymbiotique entre les Acantharia (Radiolaria) et Phaeocystis (algues haptophytes). Plus spécifiquement, nous avons cherché à établir les taux de photosynthèse et phagotrophie chez les Acantharia en utilisant des approches mettant en œuvre des isotopes stables sur des ensembles de cellules collectés dans l'environnement. Nous avons également étudié la connectivité métabolique entre l'hôte et le symbiote à l'aide de méthodes sur cellule unique comme le NanoSIMS et la transcriptomique. Nous avons pu estimer le taux d'absorption du carbone inorganique total des Acantharia à $1112,7 \pm 82,1 \text{ pg C h}^{-1} \text{ Acantharia}^{-1}$. Sur la base de nos expériences, les taux de prédation par les Acantharia restent incertains et les taux d'absorption de carbone photosynthétique ne représentent pas plus de 14,5% du contenu en carbone des Acantharia. Les analyses transcriptomiques montrent une réponse rapide de l'expression des gènes des photosymbiontes aux changements de nutriments dans les premières heures. Parallèlement, la localisation des nutriments inorganiques assimilés a montré que le carbone et l'azote sont principalement assimilés au niveau des plastes du symbiote, et que l'assimilation de l'azote est plus importante dans le nucléole du symbiote. La translocation du carbone des symbiotes vers l'hôte n'a pas pu être observée dans nos expériences, ce qui suggère que les produits de la photosynthèse sont principalement utilisés pour la respiration ou transférés dans des composés de faible poids moléculaire. L'assimilation de l'azote dans les plastes et le nucléole du symbiote suggère l'allocation des nutriments à la maintenance de la machinerie de la photosynthèse. Les données d'expression des gènes montrent en outre que certaines voies de transcription liées au métabolisme du nitrate sont présentes aussi bien dans l'hôte que le symbiote.

La synthèse de l'ensemble de nos résultats tend à montrer que les Acantharia pourraient utiliser à la fois le nitrate et l'ammonium comme sources d'azote inorganique. La photosynthèse semble être la principale source d'énergie pour le fonctionnement énergétique de la cellule, et le carbone acquis par prédation serait alloué préférentiellement à la croissance.

Table of Contents

GLOSSARY	8
CHAPTER I INTRODUCTION.....	11
1. PLANKTIC PROTISTS	13
1.1. Trophic modes in microorganisms.....	13
2. PHOTOSYMBIOSIS - ENDOSYMBIOTIC MIXOTROPHS	15
2.1. Symbiosis	15
2.2. Photosymbiosis and the relation between the host and algal partners	17
3. RADIOLARIA	18
3.1. Occurrence/importance	19
3.2. Radiolarian physiology.....	20
OBJECTIVES	26
CHAPTER II CARBON AND NITROGEN CONTENT TO BIOVOLUME RELATIONSHIPS FOR MARINE PROTIST OF THE RHIZARIA LINEAGE (RADIOLARIA AND PHAEODARIA).....	29
BRIEF CONTEXT	31
1. ABSTRACT	32
2. INTRODUCTION.....	33
3. METHODOLOGY.....	34
3.1. Study sites and Sampling	34
3.2. Elemental analysis	35
3.3. Image analyses.....	37
3.4. Molecular identification	37
3.5. Data analysis	37
3.6. Validation of prediction equations	38
4. RESULTS	38
4.1. Colonial Radiolaria	38
4.2. Nassellaria and Spumellaria.....	42
4.3. Acantharia.....	42
4.4. Phaeodaria.....	43
5. DISCUSSION	44
5.1. Mean Rhizaria carbon and nitrogen densities and mass estimations	44
5.2. C:vol relationship of Collodaria - comparison of prediction methods	45
6. CONCLUSION	47
7. ACKNOWLEDGEMENTS	48
SUPPLEMENTARY MATERIAL TO CHAPTER II	49
Supplementary Methodology 1	49
Supplementary Methodology 2	51
Supplementary Figures and Tables.....	52

CHAPTER III CARBON AND NITROGEN UPTAKE THROUGH PHOTOSYNTHESIS AND FEEDING BY PHOTOSYMBIOTIC ACANTHARIA	61
BRIEF CONTEXT	63
1. INTRODUCTION.....	65
2. METHODOLOGY.....	67
2.1. Experimental designs for photosynthesis and grazing	67
2.2. Isotopic analysis.....	70
2.3. Microscopy chlorophyll fluorescence measurements.....	72
2.4. Growth and ingestion rate calculations.....	72
2.5. Fluorescence Microscopy	73
2.6. Algal cell enumeration.....	73
2.7. Chlorophyll content	73
2.8. Algal photosynthetic rates measurements.....	73
2.9. Statistical analyses.....	74
3. RESULTS	74
3.1. Inorganic nutrient uptake rates—photosynthesis.....	75
3.2. Organic nutrient uptake—predation	76
4. DISCUSSION.....	79
4.1. Photosynthetic carbon uptake by Acantharia	79
4.2. Nitrogen uptake by Acantharia.....	80
4.3. Grazing by Acantharia.....	81
4.4. Natural isotopic ratios to investigate trophic of Radiolaria	81
4.5. Inorganic and organic nutrient uptake balance of Acantharia	83
5. ACKNOWLEDGEMENTS	84
SUPPLEMENTARY MATERIAL TO CHAPTER III	85
Supplementary Tables and Figures.....	85
Supplementary Methodology and Results	88
CHAPTER IV THE ACANTHARIAN HOLOBIONT—NUTRIENT UPTAKE CAPABILITIES INVESTIGATED BY CHEMICAL IMAGING AND TRANSCRIPTOMICS	91
CHAPTER OVERVIEW.....	93
CHAPTER IV.1 THE ACANTHARIAN HOLOBIONT—NUTRIENT UPTAKE CAPABILITIES INVESTIGATED BY CHEMICAL IMAGING AND TRANSCRIPTOMICS	94
1. INTRODUCTION.....	94
2. EXPERIMENTAL SETUP	96
2.1. Sampling	96
2.2. Isotopic Pulse-Chase Experiment	96
CHAPTER IV.2 NOVEL TRANSCRIPTOME OF PHOTOSYMBIOTIC ACANTHARIA AND AN INVESTIGATION OF NUTRIENT UPTAKE CAPABILITIES OF BOTH SYMBIONT AND HOST	99
1. METHODOLOGY.....	99
1.1. RNA extraction, cDNA library preparation and sequencing	99
1.2. Acantharia transcriptome assembly and binning.....	100
1.3. Differential gene expression analysis	101

2. RESULTS	101
2.1. Transcriptome assembly, assessment, and binning	101
2.2. Transcript annotations.....	102
2.3. Differential expression exploration	103
3. DISCUSSION	104
3.1. Dataset features	104
3.2. Identifying holobiont taxonomy and possible prey items	104
3.3. Symbiont and host pathways	105
SUPPLEMENTARY MATERIAL TO CHAPTER IV.2	106
Supplementary Material 1: Methods and analyses on Acantharia holobiont transcriptome assembly and annotation	106
Supplementary Material 2: Methods and analyses for differential expression	129
CHAPTER IV.3 SINGLE-CELL VISUALISATION OF CARBON AND NITROGEN ASSIMILATION AND TRANSLOCATION WITHIN ENDOSYMBIOTIC ACANTHARIA	137
1. METHODOLOGY	137
1.1. Sample preparation for electron microscopy and chemical imaging.....	137
1.2. Electron Microscopy	138
1.3. NanoSIMS analyses.....	138
2. RESULTS	139
2.1. Electron microscopy observations.....	139
2.2. Chemical imaging.....	140
3. DISCUSSION	143
3.1. Methodological considerations	143
3.2. Carbon assimilation and transfer in the Acantharia holobiont	143
3.3. Nitrogen assimilation and transfer in the Acantharia holobiont.....	145
4. SUMMARY/CONCLUSIONS	145
SUPPLEMENTARY MATERIAL TO CHAPTER IV.3	147
Supplementary Figures	147
CHAPTER IV.4 CHEMICAL IMAGING AND TRANSCRIPTOMICS—CONCLUSIONS	150
ACKNOWLEDGMENTS	152
CHAPTER V CONCLUSIONS AND PERSPECTIVES	153
BIBLIOGRAPHY	160
ANNEX I	177
PUBLIC PRESENTATIONS	178
OCEANOGRAPHIC EXPEDITION	178
AWARDS/GRANTS	178
MIXITIN PROJECT DELIVERABLES	179
ANNEX II OTHER PUBLICATIONS AND COLLABORATIONS	181
A DATASET ON TROPHIC MODES OF AQUATIC PROTISTS	182
MIXOTROPHIC PROTISTS AND A NEW PARADIGM FOR MARINE ECOLOGY:	183
ECO-EVOLUTIONARY PERSPECTIVES ON MIXOPLANKTON	184

Glossary

Items in *italics* are described elsewhere in this glossary. Some terms included here are not strictly required within this manuscript but may help interpreting related published materials.

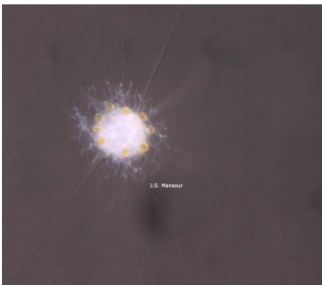
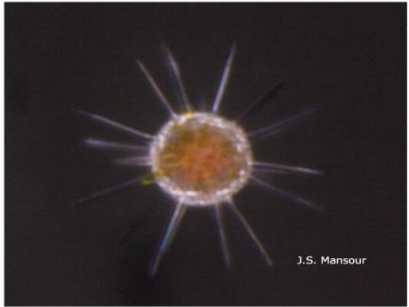
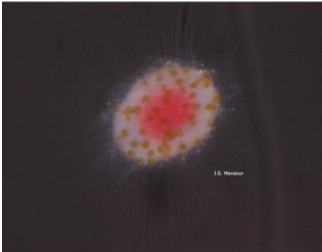
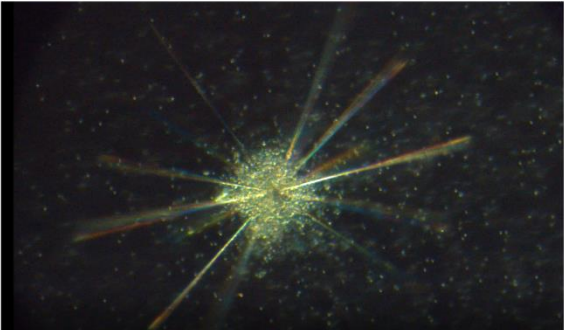
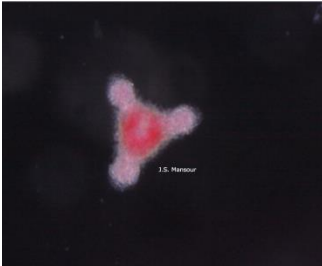
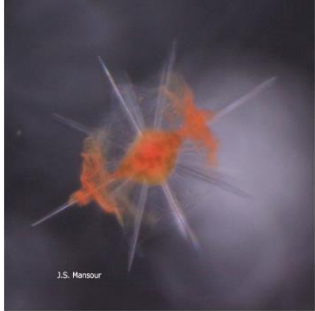
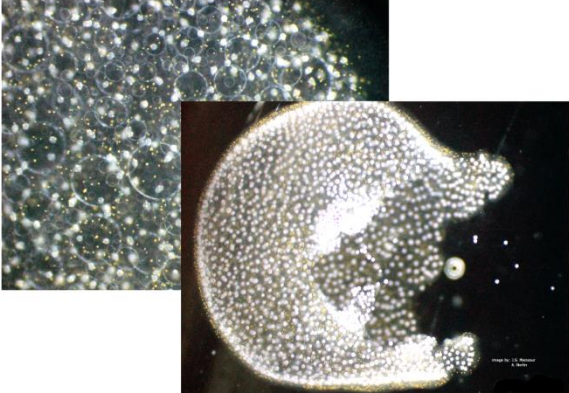
- **Algal:** A non-specific term referring to organisms that are of simple structure (e.g., single-celled 'microalgae') that grow by *phototrophy*.
- **Autotrophy:** Nutrition involving the synthesis of complex organic substances using *photosynthesis* (*phototrophy*) or chemosynthesis. Typically associated with the use of inorganic nutrients, such as CO₂.
- **Commensalism:** A type of *symbiosis* whereby neither species gain clear advantage, nor disadvantage.
- **DIC:** Dissolved inorganic carbon, comprising CO₂ (the substrate for RuBisCO, for photosynthesis), bicarbonate (HCO₃⁻) and carbonate (CO₃⁻).
- **DIN:** dissolved inorganic nitrogen, comprising ammonia (NH₃), ammonium (NH₄⁺), nitrate (NO₃⁻) and nitrite (NO₂⁻). NH₄⁺ and NO₃⁻ are the usual main forms of DIN; NH₄⁺ is the "preferred" N-source in algal physiology but it is toxic at high residual concentrations. Protists isolated from natural (low nutrient) waters may be highly sensitive to even moderate concentrations of ammonium (e.g., > 50 μM), even though ammonium is suspected to be the major DIN source in nature.
- **Dinoflagellates:** A group of common protists belonging to the Alveolata. They have two flagella and half of the species do not have their own chloroplasts.
- **Endosymbiosis:** A symbiosis in which a symbiont lives inside the host cells. Examples include nitrogen-fixing bacteria in plant roots and *photosymbiosis*.
- **Eukaryote:** Eukaryotes correspond to organisms mainly defined by the existence of a nucleus (containing nuclear genomic DNA) surrounded by a cytoplasm containing many organelles, such as mitochondria, or chloroplasts (site for photosynthesis). They can be multicellular (e.g., animals and plants) or unicellular organisms (*i.e.* protists).
- **Ex hospite:** Referring to a symbiont outside of the host, as opposed to *in hospite*.
- **Haptophytes:** a clade of organisms within the phylum Heterokontophyta. Most species have chloroplasts. The cells typically have two slightly unequal flagella, both of which are smooth, together with a unique organelle called a haptonema, which is superficially similar to a flagellum but differs in the arrangement of microtubules and in its use. The mitochondria in this group have tubular cristae (taxonomic aid). Many are suspected *mixoplankton*, feeding on prey ranging from bacteria to prey ca. a third their own size.
- **Heterotrophy:** Nutrition involving the consumption and interconversions of sources of organic carbon (Cf. mixotrophy, osmotrophy, phagotrophy, phototrophy).

- **Holobiont:** A collection of species that are closely associated. Typically composed of a larger entity (*host*) and smaller *symbionts* (bacteria, algae, viruses etc.) that act as a single ecological unit. Further reading: Dittami et al. (2019) and references therein.
- **Horizontal transmission:** Acquisition of associated (endo)*symbionts* from the environment, *i.e.* *symbionts* are not inherited/transferred by the parent (as opposed to *vertical transmission*).
- **Host:** The larger or dominant partner in a *holobiont*.
- **In hospite:** Referring to a *symbiont* inside of the host, as opposed to *ex hospite*.
- **Mature ecosystem:** An ecosystem in which nutrients cycle closely between organisms which are involved in complex food webs. Residual concentrations of inorganic nutrients are minimal, *i.e.* it is mostly organism bound. In planktic ecosystems, this can be typified by temperate summer.
- **Mixoplankton:** *Planktic protists* capable of obtaining nourishment via *photo(auto)trophy* and *phago(hetero)trophy*, as well as via *osmo(hetero)trophy*. See Flynn et al., 2019.
- **Mixotrophy:** Obtaining energy and carbon for growth through a combination of *autotrophy* (usually *phototrophy*) and *heterotrophy*. *Heterotrophy* may be supported by the use of dissolved organics (such as sugar), a process termed *osmotrophy*, and/or by eating (which in microbes is performed by engulfment, *phagotrophy*, or similar).
- **Model:** A simplification of reality, but specifically here referring to a computer model that provides a simulation of real or potentially real events.
- **Mutualism:** A type of symbiosis where the interacting species each gain a net benefit.
- **NanoSIMS:** A nano-scale mass spectroscopy methodology that enables chemical changes (e.g., associated with the movement of nutrients) to be tracked within an individual cell. A primary ion beam (Cs^+ or O^- primary ions) is used for both sputtering and analysis. The high energy of the primary ions causes strong fragmentation of molecules down to single-atomic ions, allowing quantitation of changes in isotopic composition. These secondary ions can then be analysed and are separated by a mass spectrometer according to their mass-to-charge ratios.
- **Osmotrophy:** A mode of *heterotrophy* (*i.e.* *osmo(hetero)trophy*) involving the uptake and consumption of dissolved organic compounds.
- **Parasitism:** A type of symbiosis where one species lives inside another and thereby causes it harm, this could be seen as a form of predation.
- **Phagotrophy:** A mode of *heterotrophy* (*i.e.*, *phago(hetero)trophy*) involving the engulfment of solid particles (often whole organisms) into a phagocytic vacuole in which digestion occurs – phagocytosis.
- **Photosymbiosis:** A kind of symbiosis between a heterotrophic (a predator generally) and a photosynthetic species. The host could be multi- or uni- cellular, their *symbionts* are often unicellular microalgae. These microalgae are generally located inside their host. Examples include corals and sponges, also see Not et al. (2016) for planktic examples.
- **Phototrophy:** A mode of *autotrophy* (*i.e.* *photo(auto)trophy*) involving the fixation of CO_2 using energy derived from light (photosynthesis). Organisms displaying *phototrophy* contains chlorophyll and other pigments that capture light energy.
- **Physiology:** The study of the normal functions and mechanisms of a living organism. From the Greek φύσις (*physis*) 'nature, origin', and -λογία (-logia) 'study of'.

- **Phytoplankton:** Planktonic organisms that use light for the acquisition of energy and the reduction of inorganic carbon (*phototrophy*).
- **Plankton:** Organisms that cannot maintain a fixed location in the water column, and are thus moved by the tides and currents. Plankton vary in size from the microscopic (ca. 1 μm = 0.001 mm) to large sea jellies of many metres in length.
- **Plastid:** A cellular organelle evolutionary derived from an endosymbiosis of a cyanobacterium. It can refer to a variety of homologous organelles, though often more specifically to chloroplast—the organelle for photosynthesis.
- **Predation:** A biological interaction involving killing and eating of an organism by another organism—the predator.
- **Primary production:** The production of new biomass attributed to autotrophy, and as performed by *plankton* linked to *phototrophy* performed by *phytoplankton* and *mixoplankton*.
- **Protist:** Single-celled eukaryote organism.
- **Protozooplankton** microbial (*protist*) members of the *zooplankton*. *Protozooplankton* acquire nutrition via *phagotrophy* and *osmotrophy*
- **Symbiont:** An organisms living in *symbiosis*, this would refer to the smaller partners in a relationship, as opposed to 'host'.
- **Symbiosis:** A close and interaction between species living together. Including *mutualism*, *commensalism*, amensalism and *parasitic* relationships.
- **Vertical transmission:** Transmission of the associated (endo)*symbionts* to a new generation of hosts from the parents (as opposed to *horizontal transmission*).
- **Zooplankton:** *Planktic* organisms that needs to acquire carbon from outside sources (heterotrophy, in *protists* normally *phagotrophy* and/or *osmotrophy*). It cannot produce its own organic carbon.

Chapter I

Introduction



Introduction

1. Planktic protists

The largest ecosystem of our planet is by far the ocean. While most research and documentations highlight the ‘bigger’ ocean life, e.g. fish, turtles, whales, the vast majority of oceanic life is plankton that cannot be seen by the naked eye. The ocean is in fact largely inhabited by microscopic single-celled organisms –eukaryotes (*i.e.* protists) and procaryotes (*i.e.* bacteria and archaea).

“Maer dat deselve swaricheijt maeckten, omme te connen begrijpen de over groote menichte Diertgens, alleen in een droppel water.”

— Antonie Philips van Leeuwenhoek

“Nor do I wonder, they could not well apprehend, how I had been able to observe so vast a number of Animalcules in one drop of water.”

— Antonie Philips van Leeuwenhoek

Protists are both ubiquitous and cosmopolitan, and Earth’s history has been shaped in large by these microscopic organisms. These single celled eukaryotes have long since been recognised as the foundation of many biogeochemical cycles in the ocean. For instance, an important capability of some of these cells, as is familiar to many of us thanks to (land) plants, is photosynthesis—the ability to use light energy to convert carbon-dioxide (CO₂) and water into glucose and oxygen. As the mechanisms for photosynthesis were established over evolutionary time, the gradual increase in gaseous oxygen changed the Earth’s atmosphere to that which is now inhabited by us. Currently, photosynthetic protists are estimated to account for 45% of the Earth’s oxygen production (Field et al., 1998). The impact of these small organisms has been and is undoubtedly disproportionate to their size.

1.1. Trophic modes in microorganisms

Classically, planktic protists are by trophic function considered either “phytoplankton” or “zooplankton”, ‘phototroph’ or ‘heterotroph’, that is, those that can make their own organic carbon or those that need to get carbon through means such as predation. Phytoplankton converts CO₂ directly into organic matter, whereas (proto)zooplankton feeds on other organisms, such as phytoplankton and bacteria, and thereby moves organic matter through the food web to higher trophic levels (*e.g.*, fishes) (**Figure I-1**). Detritus (*e.g.*, feces or dead organic material) of both large and microscopic organisms can sink to the bottom, and is either consumed along the way or by benthic organisms. Unconsumed organic matter is decomposed by bacteria and the waste can again be used by phytoplankton. When photosynthetic protists convert CO₂ into biological matter, they assimilate the atmospheric carbon and export it to the deep sea upon death. This transport from the upper ocean to depth is known as the ‘biological carbon pump’ and is a large part of the carbon cycle (Falkowski et al., 1998; Guidi et al., 2016). It is clear that these single-celled organisms are at the base of biochemical cycles and the oceanic ecosystem. Simulations of ocean ecosystems, *e.g.*, for carbon cycles or climate change, are thus largely based on protists physiology. Such models traditionally define protists by functional group as either phytoplankton or zooplankton.

However, most species do not fit in just one of these functional groups. It has become increasingly evident that mixotrophy—the ability to combine autotrophy and heterotrophy—is commonly found in plankton and seems more rule than exception (Flynn et al., 2013; Caron, 2016; Selosse et al., 2017; Stoecker et al., 2017; Faure et al., 2019). Hence most plankton are better characterized as mixotrophs or mixoplankton; *i.e.* combining both photoautotrophic and phago-heterotrophic activity in a single organism (Annex II: Flynn et al. 2019). In this classification, the role of osmotrophy (the uptake of dissolved organic substances) has been omitted because of its ubiquity in plankton. Combining both photosynthesis and grazing has effects on how we perceive nutrient transfer in the ocean and its food web, enabling primary producers to acquire nutrients directly from prey ingestion. Mixed nutritional behaviour thereby allows energy and biomass to go through the food web at varying trophic levels. Models show, for example, that this enhances biomass transfer efficiency to higher trophic levels, and when taken into account would increase carbon export estimates of biogeochemical models by up to 30% (Ward and Follows, 2016).

Environmental factors, like light and temperature, are highly influential in driving trophic modes (Jeong et al., 2010; Wilken et al., 2013, 2020; Ok et al., 2019). Mixotrophic behaviour is likely to be favoured when conditions are less favourable for either exclusive phototrophy or phagotrophy. As such mixoplankton are often linked to mature ecosystems (Hansen et al., 2019; Schneider et al., 2020b). When inorganic nutrients or light are limiting, mixoplankton can amend their nutritional needs by grazing (Arenovski et al., 1995; Johnson, 2015). On the other hand, when the mixoplankton is primarily heterotrophic, photosynthesis can complement its respiratory carbon needs and improve nutrient assimilation or grazing efficiency (Tittel et al., 2003). Thereby allowing continued maintenance or growth of the algal population.

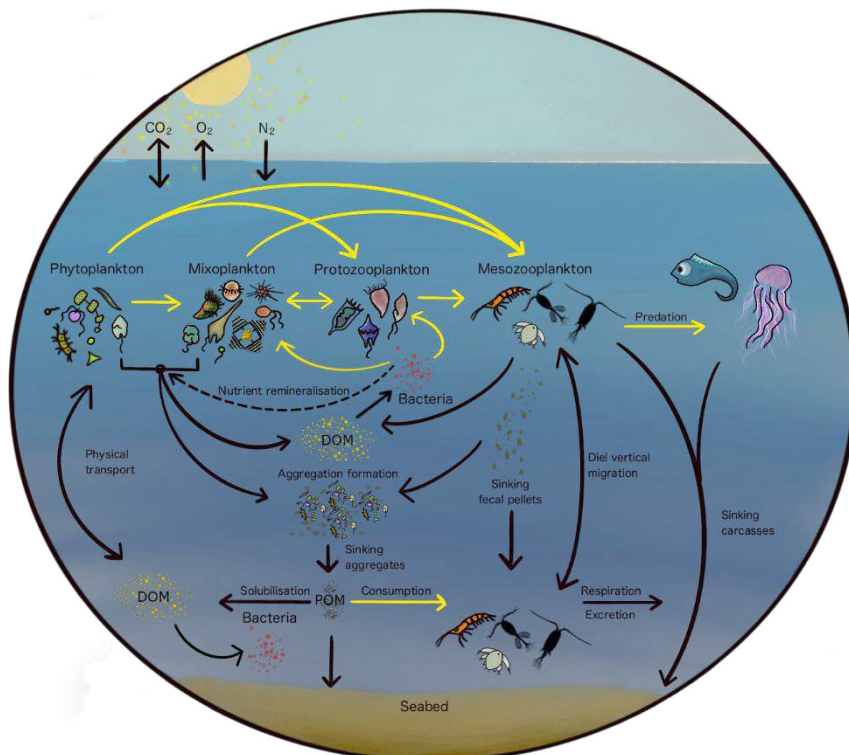


Figure I-1. Schematic of planktonic food web by functional groups. Atmospheric CO_2 is used in the photic zone by phytoplankton and mixoplankton. Grazing or predation processes, indicated with yellow arrows, transports nutrients to higher trophic levels. Respiration releases CO_2 back into the water and atmosphere, and excretion results in dissolved organic matter (DOM) that can again be used by phototrophic organisms or by bacteria using osmotrophy. Bacteria that use DOM contribute to the microbial loop and additionally retain nutrients in the foodweb. Nutrients of sinking detritus (particulate organic matter, POM) might be ‘lost’ in the seabed or re-enter the foodweb after being metabolised by zooplankton or bacteria.

Modified from Steinberg and Landry (2017) with permission from Annual reviews. Redrawing and plankton illustrations courtesy of Claudia Traboni.

Mixoplankton types

The success of mixoplankton can be explained by their high eco-physiological functional diversity. Mixoplankton come in a great range of sizes, and we recognise several functional types of mixoplankton, each achieving mixotrophic behaviour by varying means. Firstly, mixoplankton can be divided between constitutive mixoplankton (CM) or non-constitutive mixoplankton (NCM) (Mitra et al., 2016). CM have an inherent capability for both phototrophy and phagotrophy, but do not necessarily depend on both for growth and/or survival. For example, phagotrophy can be especially active in *Ochromonas* sp. when light, and thus photosynthesis, is limited. In this example the complementary use of phagotrophy allows *Ochromonas* sp. to survive under otherwise inhospitable conditions (Keller et al., 1994; Flöder et al., 2006). Another example is seen in many dinoflagellates for which phagotrophy is particularly induced when major nutrients are limiting. *Tripos furca* (formerly *Ceratium furca*) was found feeding only after weeks of N and P starvation (Smalley et al., 2003), similarly to *Prorocentrum minimum* (Johnson, 2015). This is not restricted to dinoflagellates, but is seen in many diverse groups such as haptophytes and chrysophytes (Chan et al., 2019; González-Olalla et al., 2019).

NCM rely on other organisms to acquire phototrophic potential. NCM that acquire photosynthetic ability by stealing plastids (kleptoplastidy) can be further separated in generalist (GNCM) and plastidic specialist (pSNCM). Generalist species can steal plastids from any prey they phagocytise. GNCM include many oligotrich ciliates like *Strombidium* (**Figure I-2 F**), *Laboea* and *Tontonia*. Whereas those that we classify as pSNCM utilise the sequestered prey nuclei to “farm” and control the sequestered chloroplasts. They can only do this with a limited range of prey types; they are very selective in their choice of prey (e.g. *Mesodinium rubrum* or *Dinophysis* spp. (Hansen et al., 2013). Though we currently make a distinction between GNCM and pSNCM, it is possible that at least some pSNCMs lean more towards GNCM, as often very few data are available to support the GNCM assumption. The basic differences between GNCM and pSNCM protist descriptions rest simply in the rate of failure of acquired plastids (affecting the frequency of “top-up” required) and the specificity of the prey from which plastids can be acquired. Another way to acquire photosynthesis is through photosymbiosis. This involves the internalisation of an ‘intact’ photosynthetic organism, and is a more stable relation than the transient acquisition of kleptoplasts as by GNCM (**Annex II**: Mansour & Anestis 2021). Endosymbiotic specialist non-constitutive mixotrophs (eSNCM) contain photosynthetically active symbionts. This includes most mixotrophic Rhizaria from Acantharia (**Figure I-2 H**), Collodaria (**Figure I-2 I**), and Foraminifera, as well as dinoflagellates such as *Durinskia* spp. (Yamada et al., 2019) and *Noctiluca scintillans* (see also Not et al., 2016 for a review on planktic photosymbiosis).

2. Photosymbiosis - Endosymbiotic mixotrophs

2.1. Symbiosis

The term ‘symbiosis’ was already coined in the 18th century by Heinrich Anton de Bary as the living together of dissimilar organisms- “des Zusammenlebens ungleichnamiger Organismen” (de Bary 1878, English translation in Oulhen, Schulz and Carrier, 2016). The term originally did not have the connotation of mutualism that we nowadays usually associate with symbiosis. Over the century, the exact meaning of the term has been subject of discussion (see Saffo, 1992). The major hurdle with the term involved the

broadness of the definition. As is the current understanding and interpretation here symbiosis is the intimate interaction between species, and can involve all manner of relations, including mutualism, parasitism or commensalism. These interactions are defined based on their effect on the fitness of the host. In mutualistic relation, both involved parties have a fitness increase; parasitism imparts a fitness decrease on the host; commensalism imparts no change in fitness (López-García et al., 2017). Of course, the line between categories is never clear-cut, and is especially thin between parasitism and mutualism (e.g., Lesser et al. 2013). A particular form of symbiosis is endosymbiosis (Greek *endon* “within”, *syn* “together”, and *biosis* “living”), a symbiosis where one of the partners resides inside the other. This is the case for the famous coral-dinoflagellate relationship, but also (human) gut microbes for example. The endosymbiont is the organism that lives inside the host’s body; this can entail any of the aforementioned types of symbiosis, and is thus not necessarily mutually beneficial.

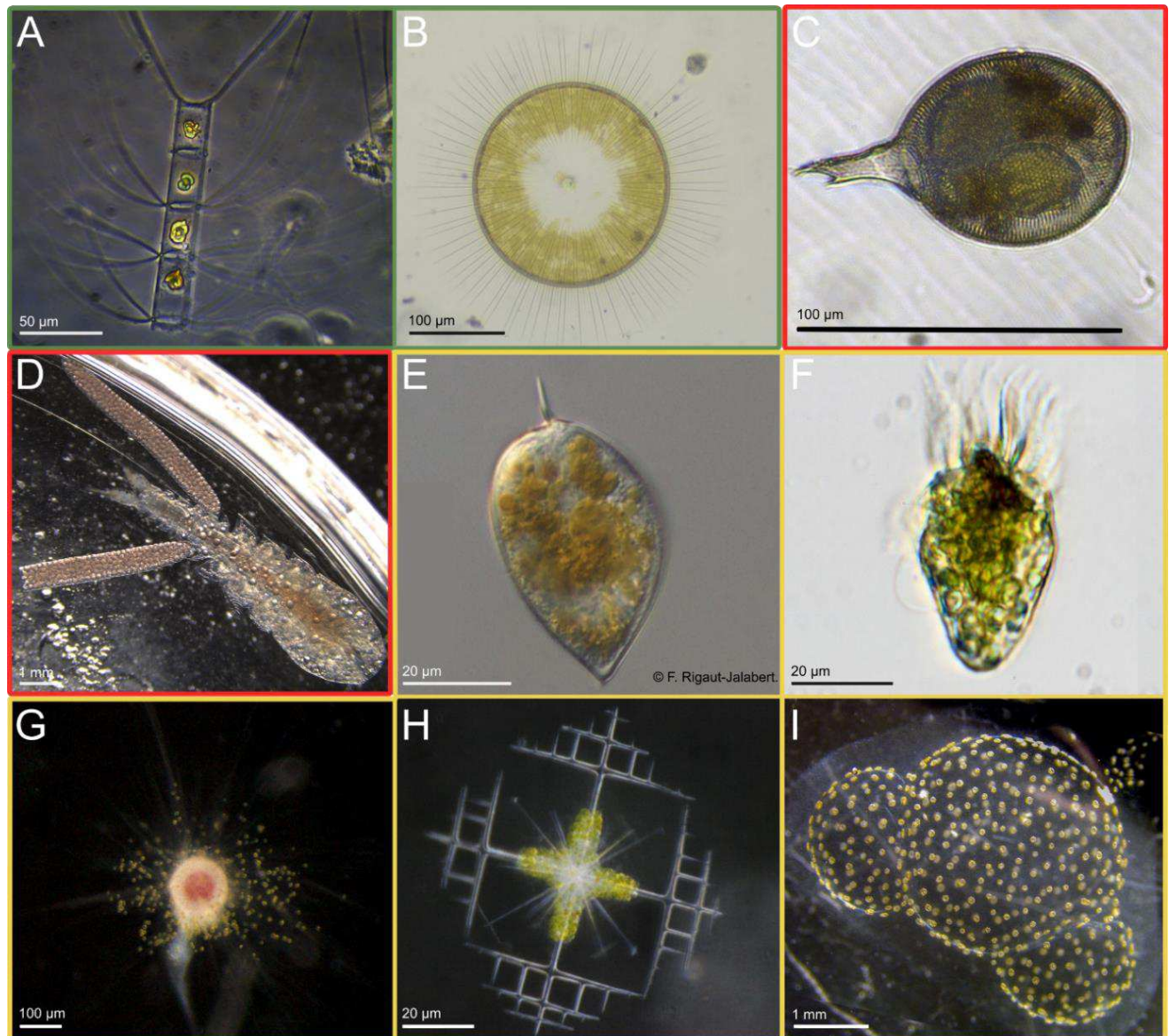


Figure I-2. Example light microscopy photographs of phototrophic (green border), heterotrophic (red border), and mixotrophic (yellow border) plankton: phytoplankton, diatoms (A, B); protozooplankton, *Protocystis tridens* (Phaeodaria) (C); mesozooplankton, copepod (note that this is a multicellular organism) (D); Several mixoplankton, CM *Prorocentrum micans* (E) (© F. Rigaut-Jalabert), GNCM ciliate *Strombidium* sp. (F, Maselli et al. 2020 with permission from Oxford University Press), eSNM Radiolarians, Spumellaria (G), Acantharia (H), and Collodaria (I).

2.2. Photosymbiosis and the relation between the host and algal partners

When the endosymbiont is a photosynthetic microalgae, it is termed photosymbiosis. Photosymbiosis is wide spread in the planktic realm, especially in tropical and subtropical areas, and can have a significant ecological impact on biomass or various biogeochemical cycles (Biard et al., 2016; Guidi et al., 2016; Not et al., 2016; Llopis Monferrer et al., 2020). Such symbioses can involve a wide variety of partners and the diversity of relationships in the oceans is especially large. Although not planktic, an iconic example of photosymbiosis is the one occurring on coral reefs, where dinoflagellates of the family Symbiodiniaceae (*sensu* LaJeunesse *et al.*, 2018) live within benthic invertebrates such as anemones, sponges, upside-down-jellyfish, giant clams, and corals. The photosymbiosis of Symbiodiniaceae with jellyfish (Ohdera et al., 2018), corals (Roth, 2014) and giant clams (Mies, 2019) has been subject to extensive research, mostly in regards to coral reefs in light of its threatened status (Hughes et al., 2003). Yet, photosymbiosis is also common in oceanic plankton (Decelle et al., 2015; Not et al., 2016). In fact, the diversity of planktic host-symbionts relationships is immense (Stoecker et al., 2009; Not et al., 2016).

The combination of low nutrients and low biomass conditions are suggested to favour the presence of photosymbioses (Taylor, 1978). Endosymbiotic algae are subject to a nutrient-rich micro-environment inside the host. Although, this would allow increased growth rates, algal symbiont growth can be limited by the host (Falkowski et al., 1984; Decelle et al., 2019; Uwizeye et al., 2021). In turn the host can supplement its use of phagotrophically acquired nutrients from prey ingestions with photosynthates obtained from the symbiont (Yellowlees et al., 2008). Consequently, both partners benefit from better nutritional conditions, and potentially higher growth rates than non-symbiotic competitors. Nutritional needs drive these long-term symbioses, as the host must preserve the symbiont without fail, or otherwise gain its nutrient in some other way (Lowe et al., 2016; Keeling and McCutcheon, 2017). However, for an endosymbiotic relation to work, the benefits to the host must outweigh the costs. The relation will thus be driven towards exploitation of the symbiont by the host.

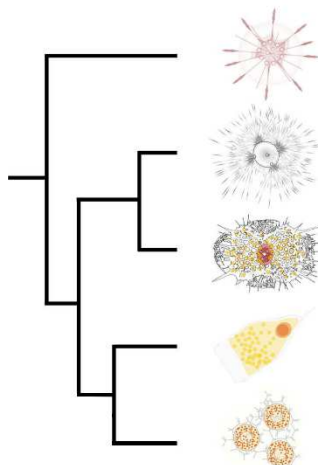
The relation of the host and algal symbiont is usually simply regarded as a relation where the host gets photosynthates from the symbiont; symbiotic algae utilize ammonium from their hosts and are provided habitat (McAuley, 1994; Yellowlees et al., 2008). Though, whether these photosymbioses are mutualistic or not is not always clear-cut and can be a topic of debate (Douglas, 1998; Sachs and Wilcox, 2006; Decelle, 2013; Lesser et al., 2013; Keeling and McCutcheon, 2017). For example, Bishoy Kamel (2016) used genomics to study the metabolic interactions of the coral holobiont as a network. The metabolic network described includes several aspects of the coral holobiont, including the coral with algal and bacterial endosymbionts. Using this network to investigate the support of each 'biont' to the metabolism of the holobiont, unveiled that the interpretation of the coral and algal-symbiont relation can shift from a mutualism to parasitism (by the algae) when the bacteria are also considered. Overall, the study shows a metabolic dependence among all members of the holobiont—together functioning as a whole. Though, when looked at independently could give a skewed view of the nature of the relationship. Additionally, warmer temperatures can cause coral symbionts to use more resources for their own metabolism, shifting the relationship more towards parasitism (Baker et al., 2018). Decelle *et al.* (2012) discussed the nature of the planktic Acantharia–*Phaeocystis* symbiosis. In this symbiosis, it seems clear (like in other photosymbioses) that the host benefits in the form of photosynthates and antioxidant

mechanism like dimethylated sulfur compounds (Michaels, 1991; Gutierrez-Rodriguez et al., 2017; Uwizeye et al., 2021). On the other hand, the *Phaeocystis* symbiont would, like in many endosymbiosis, benefit from the hosts protection. For the symbiont to benefit from endosymbiosis on an evolutionary scale, over several generations, it would need to be released by the host while still being viable. However, in this symbiosis the host exerts a great control over the symbiont, to the extent where the symbiont is heavily modified and restricted in its proliferation (Decelle et al., 2019; Uwizeye et al., 2021). The symbionts *in hospite* are modified in several aspects to affect their physiology, among which are increased plastid volume and more thylakoids, thereby increasing the photosynthetic efficiency. These findings not only have implications for physiological trade-offs of phototrophic versus mixotrophic (when considering the symbiosis as a single organismal entity) life-style, but also on the manor of endosymbiont integration in a non-heritable endosymbiosis. This among others and the fact that the symbiont has not been able to be successfully and viably extracted from the host has Decelle and colleagues suggest that the Acantharia–*Phaeocystis* symbiosis might actually be an alternative or advanced form of kleptoplastidy (Decelle et al., 2019; Uwizeye et al., 2021) (see also **Annex II**: Mansour and Anestis, 2021).

3. Radiolaria

Radiolaria are planktic marine amoeboid protist of the supergroup Rhizaria (Burki and Keeling, 2014). The term Radiolaria has evolved through time. Historically, it referred to marine zooplanktic protists that shared the similar characteristics of a central nucleus and cytoplasm surrounded by pseudopods; and a mineralised skeleton. Three major biologic groups fell under this definition: Polycystina, Acantharia, and Phaeodaria. Taking advantage of advances in single cell molecular techniques, recent studies have focused on systematic taxonomic revision of extant Radiolaria (Decelle et al., 2012c; Biard et al., 2015; Sandin et al., 2019). Both molecular tools and knowledge of skeleton morphology were applied to investigate radiolarian taxonomy and evolution. With increasing knowledge of taxonomic relationships based on these molecular biological analyses, the phylum of “Radiolaria” has been drastically revised in recent years. This makes it that the term “Radiolaria” can encompass quite different meanings, hence it warrants caution when using “Radiolaria” in scientific contributions. As discussed here, Radiolaria include the classes Taxopodia (which are non-photosymbiotic, and not further discussed here), Acantharia, and Polycystina, which entails the orders of Spumellaria, Nassellaria, and Collodaria (**Figure I-3**). Though, Collodaria might in fact taxonomically be a subgroup of the Nassellaria (Sandin, 2019; Nakamura et al., 2021).

The great majority of Radiolaria form elaborate skeletons made of opaline silica ($\text{SiO}_2 \cdot n\text{H}_2\text{O}$, Polycystina, Taxopodida) or strontium sulphate (SrSO_4 , Acantharia) (**Figure I-3**). Their size ranges from tens to several hundreds of micrometres (**Figure I-3**). Colonial Radiolaria (Collodaria) form gelatinous colonies several centimetres in length (up to several meters has been reported in Swanberg 1979). Owing to fact that the shells (also referred to as tests or skeletons) of Radiolaria, specifically of Polycystina, preserve well in the fossil record, Radiolaria have primarily been important in Earth science disciplines. Historically, a lot of research on Radiolaria was in the fields of paleoclimatology, palaeoenvironmental studies, and oil and gas exploration (Wever et al., 2002; Abelmann and Nimmergut, 2005; Boltovskoy



order	body size* (μm)	skeleton type	main skeletal component	colony formation	symbiotic algae
Acantharia	50–1,000	shell**	SrSO ₄	-	+
Taxopodia	200–800	oar-like spines	SiO ₂ <i>n</i> H ₂ O	-	-
Spumellaria	50–2,000	shell**	SiO ₂ <i>n</i> H ₂ O	-	+
Nassellaria	50–300	shell**	SiO ₂ <i>n</i> H ₂ O	-	+
Collodaria	100–1.5 m*	dispersed shell/spicules or naked	SiO ₂ <i>n</i> H ₂ O	+	+

Figure I-3. Topology of extant radiolarian orders and their general characteristics. * Length or diameter of a colony. ** Wholly-covered shell composed of numerous rods forming meshwork. +: reported in some species. -: not reported. Modified from Nakamura et al. 2021 with permission from Elsevier.

et al., 2016). Consequently, morphology, geochemical composition, and evolution of their skeletons are much better understood than their physiology—the normal functions of living organisms. As such, Radiolaria are well used in past-climate reconstructions and ocean conditions, but their underlying biology and ecology responsible for oceanic biochemical fluxes is poorly known (see Boltovskoy et al., 2016 for a review).

3.1. Occurrence/importance

Despite the importance of rhizarian (and radiolarian) fossils in palaeontology, the abundance and importance of extant Radiolaria has long been understudied and underestimated. Among others due to the complexity in their identification that is still largely morphology based; their long complex and largely unknown life cycles (section 3.2); difficulty in preservation, and their fragility during sampling. Especially their fragility and thus the ability to notice them with conventional sampling methods hampered study of their physiology. Living Radiolaria started to be heavily studied by German taxonomists in the second half of the 19th century with Müller laying the foundations by describing several species and genera (Müller, 1858), and Haeckel with his enormous work from the Challenger expedition resulting in his monographs on Radiolaria taxonomy (Haeckel, 1887). Studies during the end of the last century have started showing Radiolaria to be prominently present (Bottazzi, 1978; Swanberg, 1979; Michaels et al., 1995). It was already noted by Ernst Haeckel during the Challenger expedition of 1873 that Radiolaria occur ubiquitously in the oceans. On account of modern techniques such as *in situ* imaging and metabarcoding the interest and acknowledgement of their current importance in the oceans has started to truly manifest.

“Radiolaria occur in all the seas of the world, in all climatic zones and at all depths.”

— Ernst Haeckel, Report on the Radiolaria collected by H.M.S. Challenger, Chapter IX

Radiolaria are ubiquitous and found in high abundance in the marine planktic realm, in numbers sometimes contributing to an approximate of 5.2% of the total oceanic biotic carbon standing stock and 33% of the zooplankton community (Stemmann et al., 2008; De Vargas et al., 2015; Biard et al., 2016; Gutierrez-Rodriguez et al., 2019). Although some species can be found in coastal waters, the majority of

the species is predominantly found in the pelagic realm. In particular areas, such as the California Current, Radiolaria (Rhizaria) can contribute up to 90% of the vertical flux export (Gutierrez-Rodriguez et al., 2019). Acantharia are often the most abundant of the larger protists in oligotrophic oceans and they are also ubiquitously present in oceanic surface waters (Bottazzi, 1978; Michaels, 1991) (**Figure I-4**). Both Acantharia and Collodaria are most prominent in the epipelagic at the surface (Biard and Ohman, 2020), rapidly declining in abundance past 20 m depth (Michaels 1988, 1991). Although, Radiolaria are present in all oceans (Boltovskoy et al., 2016), they are particularly abundant in equatorial and tropical waters, diminishing towards the North (Boltovskoy et al., 2016; Leles et al., 2017) (**Figure I-4**). The number of Acantharia species is noted to be ten times more in equatorial than northern regions (Bottazzi, 1978). Acantharia in the Mediterranean Sea seemed more surface bound from spring to late Autumn and disappear more to depth in the remaining seasons (Bottazzi, 1978). This could be attributed to their photosymbiotic life-style, as might be hypothesised from the observation that *Acanthastaurus purpurascens*, a normally clearly reddish coloured Acantharia (**Supplemental Figure II-4**) was found unpigmented at greater depths (Schewiakoff, 1926; Bottazzi, 1978).

Their surface and tropical distribution can be hypothesized to be related to the presence of photosynthetic symbionts (which require light for photosynthesis) in most Collodaria and many Acantharia. Thus functioning as mixoplankton, these Radiolaria not only contribute to the food web as predators, but also as primary producers. In fact, in the upper 20 meters of the central North Pacific Ocean Acantharia alone may account for up to 4% of the total primary production and as much as 20% of the surface production (Michaels, 1988, 1991). The acantharian contribution to the total carbon flux was estimated at 15.5% in the upper 150 m of the Sargasso Sea (Michaels et al., 1995). Activity by these large protists would thus significantly influence energy transfer, carbon flux (Lampitt et al., 2009; Biard et al., 2016; Guidi et al., 2016), as well as silica flux through their skeletons (Biard et al., 2018; Llopis Monferrer et al., 2020).

3.2. Radiolarian physiology

Understanding radiolarian physiology is the basis for understanding their ecological role and trophic interactions. To be able to study physiology of live Radiolaria is notoriously difficult, as one needs - not unexpectedly - live specimen. But it being that Radiolaria are difficult to culture or even to maintain specimens in the lab for extended periods of time, obtaining live specimens in sufficient quantity is what hinders physiological studies on Radiolaria. Hence, our understanding of this group is far behind in comparison to that of other planktic protists or comparable photosymbiotic benthic eukaryotes (Burki and Keeling, 2014). That is, for example, apparent in the unresolved knowledge of their life-cycle or the (metabolic) interactions of symbiont and host. Most our knowledge on Radiolarian biology is from observational studies in the 1970's, 80's and 90's.

The radiolarian cell

The ultrastructure of radiolarian cells is one of their better understood aspects and has been described and reviewed in amongst others Suzuki and Not, (2015). Common identifying features amongst Radiolaria are a double-layered cytoplasm (consisting of endoplasm and ectoplasm), a central capsule, and pseudopodia. The cytoplasm of the cell is separated by a thin spherical capsular membrane into the endoplasm and the ectoplasm or calymma. The endoplasm with the central capsule hosts the organelles

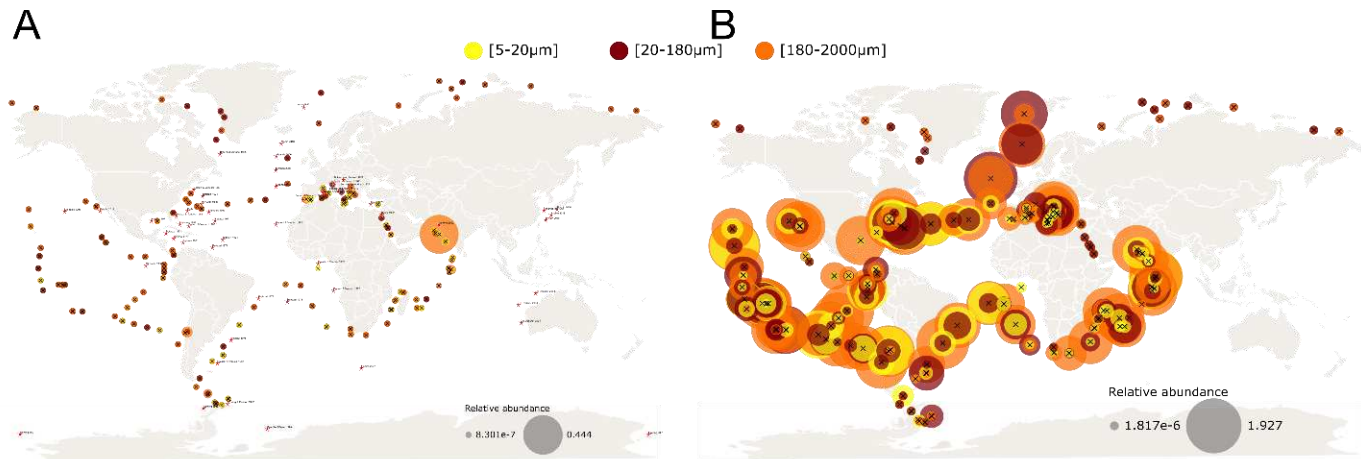


Figure I-4. Biogeography of Acantharia and Collodaria. Abundance and locations of Acantharia (**A**) and Collodaria (**B**) are represented from 18Sv9_V2 data from Tara Ocean environmental metabarcoding data. Metabarcoding map generated using the Ocean Barcode Atlas (Vermette et al. 2020, <http://oba.mio.osupytheas.fr/ocean-atlas>). Each circle represents the abundance of barcode homologous in one environmental sample at the upper layer zone, relative to the maximum and minimum abundance (shown as grey circles) related to the barcode numerical values. For clarity only the 5-20 μm (yellow circles), 20-180 μm (brown circles), and 180-2000 μm (orange circles) size fractions are shown. For Acantharia additional locations from sample collections and microscopy are depicted by a red star.

of the cell, such as the nuclei, ribosomes and mitochondria, as well as algal symbionts in the case of symbiotic Acantharia. This is thus where most biochemical synthesis is carried out. The ectoplasm surrounds the endoplasm and can contain food vacuoles and possibly algal symbionts. The pseudopodia can be of different types, but generally these can be used for feeding and buoyancy control or some form of locomotion by contraction and elongation (Febvre, 1981; Febvre-Chevalier and Febvre, 1986). Colonial Collodaria species have a gelatinous matrix containing numerous central capsules (up to thousands, Chapter II). Under normal conditions Radiolaria float freely in the water with pseudopods radiating in all directions, though creeping/sliding behaviour, by means of their pseudopods, is observed when placed on a Petri dish or similar substrate.

Radiolarian life cycle

Based on seasonal variation in vertical flux, the longevity of Radiolaria can be expected to be up to a few months (Anderson, 1983; Suzuki and Not, 2015). Although generally Radiolaria cannot be properly cultured, some successes in keeping Spumellaria in the lab show survival of, on average, a week and up to 44 days under laboratory conditions (Swanberg and Anderson, 1985; Anderson et al., 1989; Matsuoka, 1992). Swanberg and Anderson (1985) have been able to keep Spumellaria in the lab for almost a month depending on food and light conditions, where fed specimens generally survived longer. Solitary Collodaria (*Thalassicolla nucleata*) was kept in the lab for about 3 weeks when fed (Anderson, 1978). Symbiotic Acantharia tend to only stay alive and well with a full skeleton (acantharian skeletons tend to dissolve under laboratory conditions) in the lab for about a week in filtered seawater (personal experience). These time frames in the lab only represent a specific part of the radiolarian life cycle. Smaller Acantharia will disintegrate whereas bigger, supposedly more mature, Acantharia will produce swimmers (in the case of photosymbiotic clades). Proliferation in the lab has not been observed and our knowledge of the general life cycle of Radiolarian is therefore fractured.

Most protists can reproduce asexually by binary fission, mitosis, as well as sexually. Radiolaria have been seen to release swimmers which are thought to be the gametes of the sexual reproductive mode. During the process of sporogenesis in Acantharia we observed shedding of the pseudopodia and ectoplasm, and the endoplasm noticeable changes colour and appearance. Inside the cytoplasm thousands of cells can be seen to start moving. Upon release of the small swimmers ($< 5 \mu\text{m}$) the test and skeleton become entirely empty, and signals the end of the adult organism's life cycle (personal observations, see 10.5281/zenodo.5105584 for swimmer videos). Spumellarian and nassellarian sporogenesis was described to occur in a similar manner, though the cytoplasmic colour, axopodia, and symbionts remained (Yuasa and Takahashi, 2016). Collodarian swimmers are notably bigger ($8\text{-}10 \mu\text{m}$) than those of other Radiolaria (Yuasa and Takahashi, 2014). The fate, nor ploidy, of these supposed 'reproductive swimmers' is not entirely understood, because the next stage in the life cycle has never been observed (Anderson, 1983). Though the fate of the swimmers is unknown, and they could be confused for parasites, they have been positively identified as radiolarian cells (Kimoto et al., 2011; Yuasa and Takahashi, 2016, see also Supplemental Material to Chapter III). All swimmers have been observed to have a SrSO_4 crystal inclusion, not only those of Acantharia that have a SrSO_4 skeleton in their adult stage, but also those of other, silica skeleton bearing, Radiolaria (Anderson, 1978; Yuasa and Takahashi, 2014, 2016). It has been suggested that this SrSO_4 crystal works as a ballast to allow sinking to deeper waters, where possibly the next stage of reproduction occurs (Bottazzi, 1978; Decelle et al., 2013; Yuasa and Takahashi, 2014) (**Figure I-6 A**). Even though, the sexual life cycle of Radiolaria is not fully confirmed, considering that most eukaryotes are by origin sexual with asexual reproduction being a derived trait, it is fair to assume Radiolaria are also sexual. Asexual reproduction by binary fission is not excluded. It has been documented for some colonial Collodaria based on observations both from skeleton fossils and from live colonies (Anderson, 1976a; Anderson and Gupta, 1998; Decelle et al., 2021). The ability of binary fission helps explain sudden population increases of colonial Collodaria (**Figure I-5**). For those Radiolaria like Collodaria for which binary fission is not excluded, the life cycle might thus be even more complex. Several studies have identified molecular sequences of solitary Collodaria as closely related to different colonial species (Biard, 2015; Liu et al., 2019). Solitary Collodaria are thus suggested to be an alternate life stage of the colonial form (Swanberg, 1979; Biard et al., 2015). These solitary forms, though previously described as separate species (*Thalassicolla* sp.), might in fact proliferate vegetatively to form colonies. This makes collodarian life cycle additionally complex, with both solitary and colonial forms. Subsequent proliferation could then occur either through binary fission or through the release of swimmers which sink to depth for the still even more obscure events of their life cycle (**Figure I-6 B**).



Figure I-5. Bloom of Collodaria, photographed from the water surface in the bay of Villefranche-sur-Mer, France. An abundance of Collodaria colonies (and jellyfish) can be seen just below the water surface and extends to several meters depth.

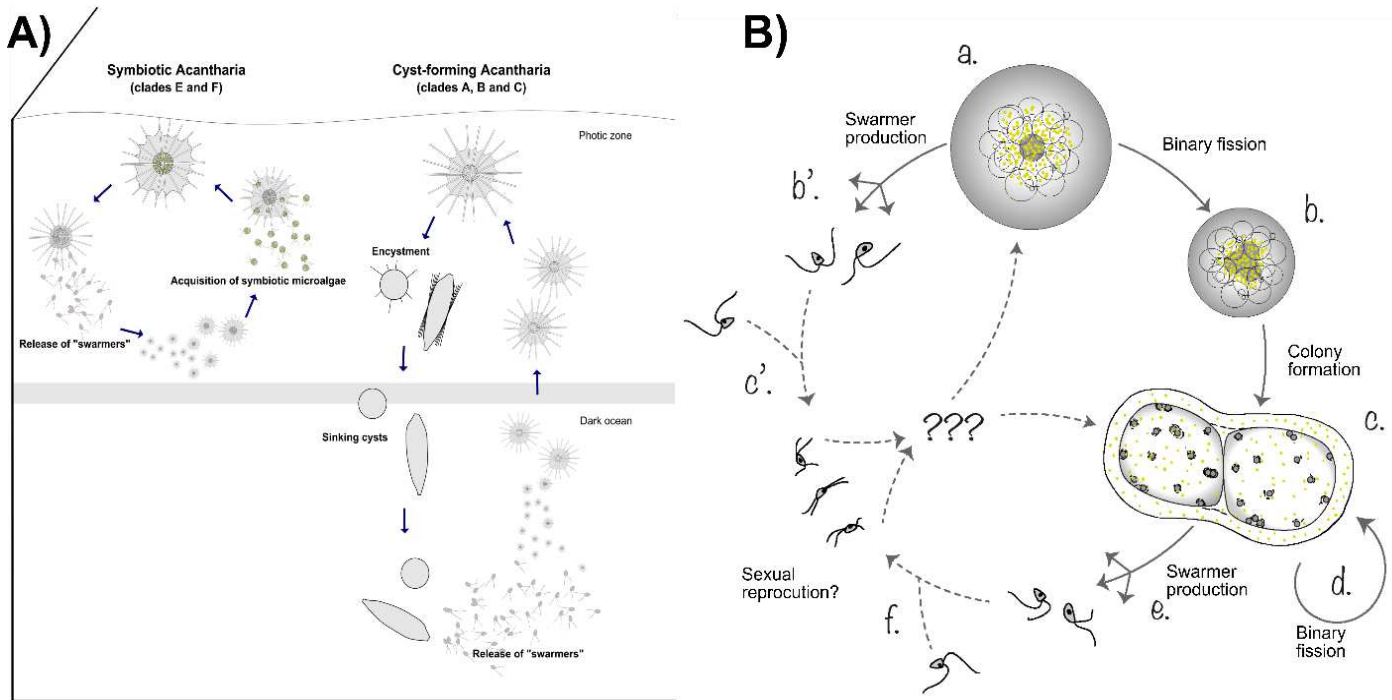


Figure I-6. Hypothetical life cycle for photosymbiotic (non-cyst forming) Acantharia and cyst forming Acantharia (A). Reproduced from Decelle, J., P. Martin, K. Paborstava, and others. 2013. Diversity, Ecology and Biogeochemistry of Cyst-Forming Acantharia (Radiolaria) in the Oceans. PLoS One 8(1): e53598. doi:10.1371/journal.pone.0053598 under CC BY 4.0. Hypothetical life-cycle for Collodaria (B). The asexual cycle follows from a solitary Collodaria (a) growth by binary fission (b), possible colony formation (c) and growth (d). The sexual life cycle (dashed lines) is hypothetical and unobserved, it is defined by production of swarmers (b' or e). The fate of the swarmers is not known, potentially they fuse (c', f) to start the cycle anew. Modified from Biard, T. M. 2015. Diversité, biogéographie et écologie des Collodaires (Radiolaires) dans l'océan mondial. Ph.D. thesis. Université Pierre et Marie Curie.

Intrinsic feeding behaviour - predation

Lacking in motility, Radiolaria are presumed opportunistic and passive predators, intercepting prey that come nearby. Feeding would only be limited by the ability of the Radiolaria to make contact and invade the tissue of potential prey with their pseudopodia (Caron et al., 1995). Despite their lack of 'real' movement, Radiolaria can be great predators actively ensnaring their prey in their pseudopodial network (Swanberg and Caron, 1991). Prey become trapped when they contact the pseudopodia, and are then transported along it towards the cell's body to be phagocytosed. Active feeding behaviour has been described for Nassellaria, where a pseudopod is extended to capture prey and subsequently retracted (Sugiyama et al., 2008). Similarly for Acantharia, pseudopodial extensions with drop-shaped terminal endings have been observed and hypothesized to be part of a predation mechanisms, like a fishing rod, and/or locomotion of the cell (Mars Brisbin, 2020; Mars Brisbin et al., 2020). Matsuoka (2007) reported no active feeding in Collodaria and suggested that they must thus live exclusively of the symbionts. But photosynthetic nutrients will not satisfy the metabolic needs (Swanberg, 1983). More likely, without pseudopodial extension, their feeding is reliant on what chances to get caught in their large extracellular matrix. In fact, a variety of preys have been observed, usually smaller than themselves. Prey of Collodaria and Spumellaria *in situ* and in laboratory conditions range from diatom, ciliates, tintinnids, crustacean larvae to copepods, while Nassellaria have been observed to also consume bacteria (Anderson, 1983; Swanberg and Anderson, 1985; Swanberg et al., 1986). A laboratory study investigating feeding behaviour

of a Spumellaria (*Spongodymus* sp.) with radio-isotopes showed a relative preference for phytoplankton as opposed to zooplankton prey (Anderson et al., 1984). However, this seemingly varies by taxon, as other species showed better survival in the lab when fed with zooplankton or a mixture (Swanberg and Anderson, 1985). Innately consumed preys of Acantharia are in quantity predominantly tintinnids, 'other ciliates' and 'other protozoans'. Prey of Radiolaria (classes Phaeodarea and Polycystinea are still grouped together as Radiolaria in the study of Swanberg and Caron (1991)) are mostly tintinnids and mollusc larvae. When taking into account carbon content, copepods were found to be the dominant carbon food source, that is 48% of all radiolarian consumption, and 40% of acantharian consumption (Swanberg and Caron, 1991). A unique observation showed a Collodaria colony attached to a jellyfish and having it for a third digested after 5 hours (Swanberg, 1979).

Predators of Radiolaria

Currently, the knowledge of predation on Rhizaria is limited. Collodarian remains have been found in the digestive tracts of different organism such as salps, copepods, euphausiids and penaeidae (Boltovskoy et al., 2016). Swanberg (1979) observed no feeding on Collodaria by fish. The best-documented predation is by parasitic juvenile amphipods in colonial Collodaria (Swanberg 1979; Swanberg and Harbison 1980). There is indication, mainly from DNA barcoding, that Radiolaria can be prey items for eel larvae—another organism whose life-cycle and food web links are poorly understood (Watanabe et al., 2021). Gelatinous plankton, which include Collodaria, could be of particular importance for the eel larvae (Riemann et al., 2010; Ayala et al., 2018). Whether this is selective feeding or opportunistically, and thus purely based on abundance and marine snow aggregates is yet unclear.

Living together with algal symbionts - photosynthesis

Radiolarian endosymbionts were indirectly observed by Huxley describing them as 'yellow cells' (Huxley, 1851). Though initially suspected to be for reproduction, the 'yellow cells' were later assigned a nutritional function and classified as 'zooxanthellae', linking them to those symbionts of Cnidaria (Haeckel, 1862; Fulton, 1921). In fact, many Radiolaria host such photosymbionts. Photosymbionts have been reported in all Collodaria and the majority of Acantharia, as well as many Spumellaria (Gast and Caron, 2001; Takahashi et al., 2003; Yuasa et al., 2019). Commonly found in Collodaria are distinct dinoflagellate symbionts related to the *Scrippsiella* genus (*i.e.* *Brandtodinium*), but haptophytes and prasinophytes symbionts have also been reported (Stoecker et al., 2009; Probert et al., 2014; Not et al., 2016). The symbiosis of Collodaria is likely a mutualistic nutritional symbiosis, where both partners take advantage of nutritional gains from one another. In the case of Acantharia symbionts have been predominantly identified as haptophytes from the genus *Phaeocystis*. (Decelle et al., 2012a, 2012b; Balzano et al., 2015; Mars Brisbin et al., 2018). Acantharia can also live in symbiosis with representatives from other haptophyte lineages, simultaneously within the same hosts, such as *Chrysochromulina* (Mars Brisbin et al., 2018; Yuasa et al., 2019). Symbionts are acquired through horizontal transmission, but it has been shown that acantharian symbiont communities can be dissimilar to environmental communities, indicating the symbionts are maintained for extended periods of time (Mars Brisbin et al., 2018). Furthermore, the morphology and gene expression of the symbionts is heavily altered to facilitate photosynthesis and limit growth.

Radiolarian photosymbiosis has been shown to be an obligatory symbiosis where the hosts cannot properly survive without the symbiont (Swanberg and Anderson 1985), though this might not be the case for some Radiolaria like *Physematium muelleri* (Collodaria) (Swanberg et al., 1986). The fact that the host can rarely be kept in culture, indicative of an obligate relation, while the symbiont can, as well as that the symbionts can be free-living, argues that the same cannot be said for the symbiont.

The photosymbionts of Radiolaria, like in most photosymbioses, are suggested to transfer photosynthates to the host organism (Anderson et al., 1983). In an experimental study by Swanberg and Anderson (1985) illuminance was found to be enough for survival, independent of diet, with the exception of the Spumellaria *Physematium muelleri*. *P. muelleri* was in fact shown to grow better with the addition of food, though it still obtained more than half of its carbon diet from photosynthesis (Swanberg et al., 1986). Caron et al. (1995) estimated carbon fixation through photosynthesis to be able to contribute 9 and 19% of the carbon budget for Acantharia and Collodaria respectively. For some colonial Radiolaria (Collodaria), Swanberg (1983) had previously hypothesised that photosynthesis would not be important for growth, but rather merely for subsistence, whereas nutrients for growth would need to be obtained by predation. This based on that net hourly photosynthesis constituted at a maximum only 0.4% of the radiolarian's carbon content for *Acrosphaera spinose* and *Collozoum radiosum*. Considering the modification of the acantharian symbiont, the acantharian host exploits the algal symbionts for their photosynthetic capabilities and likely not digests it (Mars Brisbin et al., 2018; Decelle et al., 2019).

Novel single-cell analyses have been able to investigate the metabolic interactions of symbiont and host on new levels. Gene expression analysis of a Collodaria holobionts by Liu et al., 2019 shines some light on possible nutrient exchange mechanisms between the host and its *Brandtodinium* symbiont. Due to a lack of expression of sugar, glycerol or fatty acid biosynthesis pathways it was hypothesised that amino acids could be one of the predominant forms of translocated compounds of organic carbon. This was also corroborated by patterns of change in ammonium uptake genes, indicating it as an important source of nitrogen for the symbionts. However, chemical imaging of newly-fixed carbon in Collodaria has shown it to be rapidly assimilated into starch granules of the symbiont, and transferred to the host through the Golgi system (Decelle et al., 2021). Considering the function of the Golgi system in carbohydrate synthesis, this could imply carbon is translocated to the host and incorporated as proteins or lipids.

Nonetheless, Rhizaria remain one of least studied groups (Burki and Keeling, 2014).

Objectives

The perceived relevance of mixoplankton to the marine food web and nutrient cycles has been increasing in the last years, owing to more studies on the ecophysiology of mixoplanktic organisms. Among mixoplankton, endosymbiotic mixoplankton such as Radiolaria are ubiquitous, but like most mixoplankton their ecophysiology is understudied.

The pioneering works on Radiolaria by Anderson, Swanberg and colleagues demonstrate most of our current knowledge on extant Radiolaria and at the same time how little we still know about most of them. Despite the ubiquitous presence and importance of Radiolaria both ecological and evolutionary, research focusing on physiology and photosynthesis of this planktic photosymbiosis has lagged behind in comparison to our understanding of the similar endosymbiotic mixotrophic relationship of benthic invertebrates, like corals (Muscatine and Porter 1977; Stoecker et al. 2009). Likely because of their fragility and that the host-symbiont complex cannot be maintained in culture. Our understanding and elucidation of the biology of these protists is further hindered by the technical challenges inherent to the study of single-celled fragile and uncultured microorganisms. The functioning of this key planktic symbiosis, such as the biochemical link and nutrient fluxes between symbionts and their hosts, remains largely unexplored. Many physiological questions remain, for example:

Can the host itself assimilate external nitrogen sources such as nitrate or ammonium?

Does it strictly need to feed? What is the metabolic contribution of phototrophy and phagotrophy?
And what are the uptake rates?

How are nutrients like carbon and nitrogen used in the Radiolarian holobiont and how is it translocated between host and symbiont?

Physiological information for these organisms depends on novel cultivation-independent approaches. Thereby single-cell techniques including single-cell genomics (Labarre et al., 2020), transcriptomics (Cooney et al., 2020) and chemical imaging (Decelle et al., 2020) allow us to study the biological role of individual cells. The potential of such techniques will reinforce the study of these unculturable NCMs, such as Radiolaria. This includes the elucidation of the nutrient dynamics of the radiolarian holobiont, on both metabolic and molecular level. Not only will this be important to understand photosymbiosis in protists, but understanding the nutrient uptake capabilities will also help to predict plankton dynamics by improving and providing data for model input. Our objectives are therefore aimed at elucidating physiology of photosymbiotic (mixotrophic) Radiolaria, and mostly Acantharia, which will inform parameters used in system dynamics models.

- 1) What is the metabolic budget of Acantharia? Their carbon and nitrogen uptake? Photosynthesis and phagotrophy balance?
 - Firstly, I aimed for quantification of inorganic carbon and nitrogen uptake rates for Acantharia using stable and radio isotopes to characterise symbiont photosynthesis, and link symbiont free-living physiology and *in hospite* physiology.
 - Secondly, I aimed for quantification of organic nutrient uptake through feeding, and measurements of ingestion rates of prey by Acantharia.

- Thereby additionally elucidating the carbon and nitrogen content, and the mass to biovolume relationships of several Rhizaria, as these parameters are important in models.
- 2) How is carbon and nitrogen used in the acantharian holobiont and how is it translocated between host and symbiont?
- I visualised the nutrient translocation in the holobiont on a subcellular level by single-cell chemical imaging methods, and assessed the influence of nutrient addition (eutrophication) on carbon uptake and the general interplay between radiolarian host and symbionts.
- 3) What is driving the physiology under different nutrient condition?
- In conjunction with the previous objective I performed a single-cell transcriptomic approach to investigate gene expression of Acantharia under those different treatments of nutrient additions and time.

Chapter II

Carbon and nitrogen content to biovolume relationships for marine protist of the Rhizaria lineage (Radiolaria and Phaeodaria)



“The data may not contain the answer. The combination of some data and an aching desire for an answer does not ensure that a reasonable answer can be extracted from a given body of data”

—Tukey 1986, *The American Statistician*

Brief Context

Rhizaria are ubiquitous in oceanic waters. Their contribution and roles in oceanic ecosystems have previously been underestimated due to their large size range and fragility. Yet, recent studies show that they are major components of the planktic community contributing greatly to, among others, the carbon and silica flux. The difficulties inherent to the study of live Rhizaria make it that very limited data is available on their biomass and volume relationship. While cellular carbon and nitrogen biomass to volume relationships of protists are quite well defined, current conversion factors are not calibrated for larger protists, like Rhizaria. Determination of carbon to volume relation of these larger protists is necessary separately from smaller protists. Single biovolume carbon conversion factors for Collodaria were established by Michaels et al., (1995). Thanks to these conversion factors the biomass and importance of Collodaria has been estimated in other studies. However, it is not possible to account for the large variation in biovolume with these estimations, limiting accurate estimations and their use in models. This study provides key empirical data on the carbon and nitrogen content of several Rhizaria taxa and their relation to cell volume. Over several years we have collected Radiolaria specimens and measured their carbon and nitrogen content, as well as estimated their biovolume. This is pivotal information for studies of ocean ecology and for modelling biomass fluxes being it biogeographically or smaller-scale system dynamics.

Carbon and nitrogen content to biovolume relationships for marine protist of the Rhizaria lineage (Radiolaria and Phaeodaria)

Joost Samir Mansour¹, Andreas Norlin^{2,3}, Natalia Llopis Monferrer^{1,4}, Stéphane L'Helguen⁴, Fabrice Not¹

¹ Sorbonne University, CNRS, UMR7144 Adaptation and Diversity in Marine Environment (AD2M) laboratory, Ecology of Marine Plankton team, Station Biologique de Roscoff, Place Georges Teissier, 29680 Roscoff, France

² School of Earth and Ocean Sciences, Cardiff University, Cardiff CF10 3AT, United Kingdom

³ Université Libre de Bruxelles, Boulevard du Triomphe, B-1050, Belgium

⁴ Université de Bretagne Occidentale - Brest, CNRS, IFREMER, IRD, UMR 6539 Laboratoire des Sciences de l'Environnement Marin (LEMAR), IUEM, 29280 Plouzané, France

Published in: *Limnology and Oceanography* — doi: 10.1002/lno.11714

1. Abstract

Rhizaria are large protistan cells that have been shown to be a major component of the planktic community in the oceans and contribute significantly to major biogeochemical cycles such as carbon or silicon. However, unlike for many other protists, limited data is available on rhizarian cellular carbon (C) and nitrogen (N) content and cell volume. Here we present novel C and N mass to volume equations and ratios for nine Rhizaria taxa belonging to Radiolaria (*i.e.* *Collozoum*, *Sphaerouzoum*, *Collosphaeridae*, *Acantharia*, *Nassellaria*, and *Spumellaria*) and Phaeodaria (*i.e.* *Aulacantha*, *Protocystis* and *Challengeria*). The C and N content of collodarian cells was significantly correlated to cell volume as expressed by the mass:vol equations $\text{ng C cell}^{-1} = -13.51 + 0.1524 \times \text{biovolume } (\mu\text{m}^3)$ or $\text{ng N cell}^{-1} = -4.33 + 0.0249 \times \text{biovolume } (\mu\text{m}^3)$. Significant C and N content to volume correlations were also identified, and corresponding equations are proposed, for C:vol and N:vol of collodarian colonies (Radiolaria), and C:vol of the genus *Protocystis* (Phaeodaria). Furthermore, average C and N densities (mass per volume) are given for all studied Rhizaria. The densities and mass:vol equations established here could show that, with the exception of *Aulacantha*, biomass of most Rhizaria would have been underestimated using previously published generic protist C:vol ratios. We measured up to 35 times more C content for *Acantharia* than otherwise estimated, and between 1.4 and 21.5 times more for other taxa. Our mass:vol data will prove critical for model input and quantitative ecological studies of oceanic ecosystems.

2. Introduction

Rhizaria are single-celled eukaryotes (*i.e.* protists) that are a key component of planktic communities in the ocean (Not et al., 2007; Amacher et al., 2009; Xu et al., 2018). Traditionally, the phylum Radiolaria (Rhizaria) included the orders Acantharia, Nassellaria, Spumellaria, and Phaeodaria (Haeckel, 1887). However, Phaeodaria are now considered Cercozoa of the supergroup Rhizaria (Polet et al., 2004). Marine Rhizaria can represent up to 33% of large zooplankton community (>600 μm) in the upper water column (Biard et al., 2016), and are also abundant in deeper layers (Biard and Ohman, 2020). Rhizaria are fundamental to many biogeochemical cycles, including silicon (Biard et al., 2018; Llopis Monferrer et al., 2020), strontium (Bernstein et al., 1987), carbon through calcification (Erez, 2003), and the sinking of particulate organic matter known as the biological carbon pump process (Lampitt et al., 2009; Stukel et al., 2018; Gutierrez-Rodriguez et al., 2019). The lack of success in culturing Rhizaria and their poor preservation when using conventional sampling methods (Anderson, 1983; Suzuki and Not, 2015) have limited our basic knowledge about ecology and physiology of these organisms. Their role in the food web is still unclear, but Rhizaria have been shown to consume a variety of prey (Gowing, 1989; Swanberg and Caron, 1991). Among Rhizaria, many Retaria (e.g., Radiolaria, Foraminifera) harbour algal symbionts to supplement their metabolic needs (Stoecker et al., 2009).

Carbon (C) and nitrogen (N) content and C:N ratios of planktic organisms are fundamental information for constraints of oceanic ecosystem dynamics or biogeochemical models (Flynn and Mitra, 2009; Flynn et al., 2019), as well as performing quantitative ecological studies of plankton (e.g. Biard et al. 2016; Stukel et al. 2018). Biovolume is often used for the calculation and estimation of C mass of planktic organisms, or in the estimation of relative (primary) production (Caron et al., 1995). These parameters are needed to accurately estimate nutrient and C and N fluxes in ecosystems (Fasham et al., 1990; Franks, 2002). However, current biogeochemical models often neglect larger protists such as Rhizaria (Hood et al., 2006). In large part, this omission occurs because the parameters controlling such predictive models are difficult to evaluate, since quantitative physiological information (e.g. regarding the position in the food web; the functional classification, and the occurrence of mixotrophy) is extremely limited.

Regarding C to volume (C:vol) conversions, in contrast to smaller sized planktic groups (estimated spherical diameter, ESD <17 μm , 3000 μm^3), no published measurements of C:vol specific to larger protists are available (Menden-Deuer and Lessard, 2000). The use of more general values for conversion of biovolume to cellular C and N content (e.g. Michaels 1991; Biard et al. 2016; Stukel et al. 2018) could yield inaccurate or overestimated biomass estimations (Stukel et al., 2018; Ikenoue et al., 2019). For instance, data collected by Menden-Deuer and Lessard (2000) showed that the large dinoflagellate *Noctiluca scintillans* (ESD >250 μm) is an outlier in regards to C:vol among dinoflagellates, likely due to its aberrant size. Ikenoue et al. (2019) thus directly measured cellular C of >1 mm Phaeodaria, showing that the actual measured C content of their Phaeodaria specimen was several orders of magnitude lower than when estimated with available C:vol conversions for protists. Carbon or N content of Radiolaria has to our knowledge only been directly measured on two occasions, by Michaels et al. (1995) and Swanberg (1983), though no relationship to volume has been resolved. It is clear that future plankton studies and ecosystem modeling will benefit from improved data for protists such as Rhizaria.

The goal of this study is to fill the gap of biovolume to cellular carbon and nitrogen content data for marine Rhizaria. We focused on single-cell isolations of colonial Collodaria, as well as solitary Rhizaria (*i.e.* Collodaria, Acantharia, Nassellaria, Spumellaria, *Aulacantha*, *Protocystis* and *Challengeria*) no larger than 1 mm. We provide empirical data on C and N content and biovolume for conversion of measured sizes to cellular mass, as well as a set of constants for the equations describing these conversions.

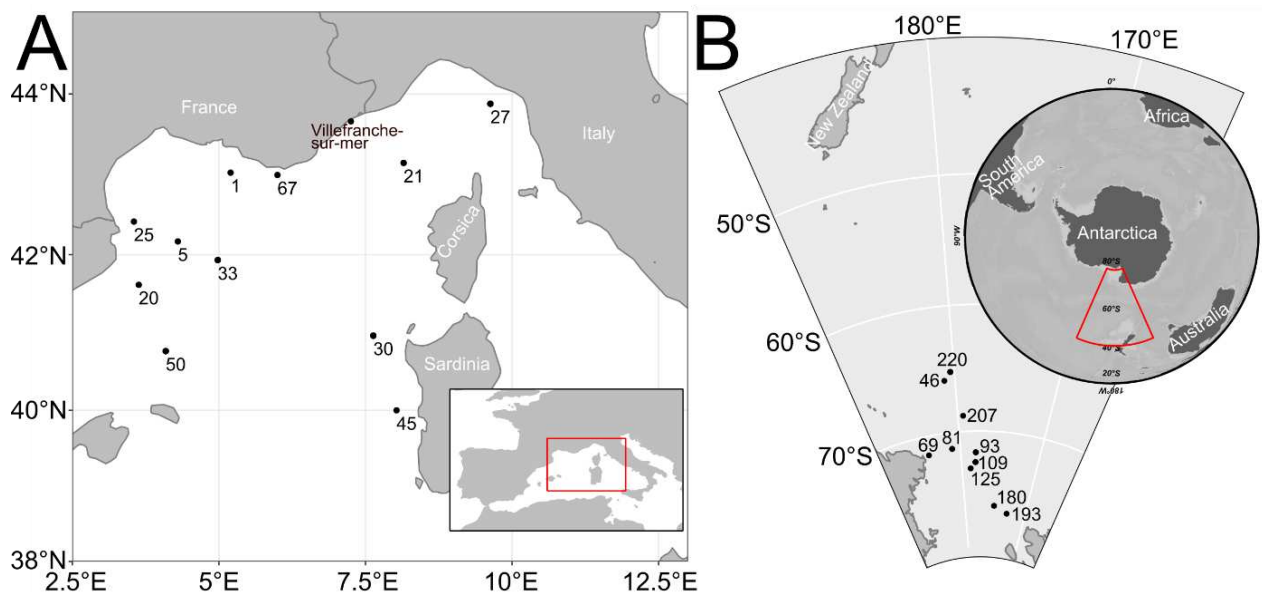


Figure II-1. Sampling sites of the MOOSE-GE cruises, and the sampling location of Villefranche-sur-Mer, with an inlay of the Mediterranean Sea (A), modified from Llopis Monferrer et al., 2020. Estimating Biogenic Silica Production of Rhizaria in the Global Ocean. *Global Biogeochem. Cycles* 34. doi:10.1029/2019GB006286 (CC BY-NC 4.0). Sample sites of the TAN1901 cruise; inlay shows the South Polar Region (B). Not shown are the samples of the AMT cruise that were collected at 3.69°S 24.98°W at depths between 0 and 200 m. Numbers correspond to the sampling station of each sample as indicated in the raw data table <http://dx.doi.org/10.17632/j9262jxgt8.1>.

3. Methodology

3.1. Study sites and Sampling

The study sites encompassed environmentally diverse oceanic ecosystems. We collected symbiotic Collodaria and Acantharia in the bay of Villefranche-sur-Mer (France, 43°41'10" N, 7°18'50" E) (**Figure II-1**) during September 2018, April 2019 and October 2019. This bay is characterised by a steep decline and upwelling from deep water from 1 km offshore, this allows the sampling of these oceanic protists near the shore. Collodaria colonies (**Figure II-2 GHJK**) were collected using a plankton net of 2 mm mesh size, Acantharia (**Figure II-2 F**) with nets of 64 and 150 μm mesh size, by slowly towing the nets at the sub-surface. Phaeodaria (**Figure II-2 ABCD**) were collected at numerous study sites during three different cruises (**Figure II-1**), using a triple net (mesh size of 64, 120 and 200 μm). The genera *Aulacantha* (primarily *Aulacantha scolymantha*, **Figure II-2 D**) and *Challengeria* (primarily *Challengeria xiphodon*, **Figure II-2 C**) were collected in the Western Mediterranean basin during the Mediterranean Ocean Observing System on Environment - Grande Echelle (MOOSE-GE) 2017 cruise. Carbon data on these specimen were previously reported in Llopis Monferrer et al. (2020), but have been recalculated to be consistent with the

biovolume calculations in this study (e.g. using the same geometric shape formulas for the same groups). *Protocystis* species *P. tridens* (PhaeoA, **Figure II-2 A**), *P. harstoni*, and *P. triangularis* (PhaeoC, **Figure II-2 B**) were collected during the TAN1901 expedition along the Pacific sector of the Southern Ocean during the austral summer (January and February 2019). Polycystine Radiolaria of the orders Spumellaria (**Figure II-2 I**) and Nassellaria (**Figure II-2 E**) were collected during both cruises. Spumellaria were further collected during the Atlantic Meridional Transect (AMT28) in October 2018 at 3.69°S 24.98°W from depths between 0 and 200 m.

Collected samples were immediately diluted in buckets with fresh surface seawater. Specimens were handpicked and transferred into filter-sterilized seawater (FSW, 0.2- μ m-pore-size). Collected and isolated specimens were incubated minimally one hour in FSW, after which they were transferred again to fresh FSW. This washing process was repeated at least three times, allowing the self-cleaning of particles attached to the specimen and dilution to extinction of any organisms accidentally taken with (see single-cell isolation procedure: [dx.doi.org/10.17504/protocols.io.bqvrnw56](https://doi.org/10.17504/protocols.io.bqvrnw56)).

Even though Phaeodaria were identifiable during sampling, Rhizaria taxonomy is largely based on skeletal characteristics that are difficult to observe accurately under low magnification when individuals still contain tissue. Consequently, Radiolaria were grouped by overall shape characteristics and specimen were identified solely on the order level, *i.e.* Acantharia, Nassellaria, Spumellaria, or on the genus level for Collodaria. Acantharia and Collodaria identification was verified and complemented with molecular data comparison.

3.2. Elemental analysis

Carbon and nitrogen content was measured from bulk samples or entire Collodaria colonies. Specimens were filtered onto pre-combusted (450 °C, 4 h) Whatman GF/F filters. For colonial Collodaria one or two colonies were used per filter. Samples of solitary specimen were composed of multiple cells, *i.e.* 30 Acantharia, a mean (range) of 18 (1-44) *Aulacantha*, 40 (30-46) Nassellaria, 35 (25-40) *Protocystis*, 24 (22-26) *Challengeria*, 33 (25-40) Spumellaria. A mix of taxa were combined on a single filter for Acantharia, Spumellaria and Nassellaria out of necessity to acquire sufficient biomass, though care was taken to use same-sized specimen. Blank filters were prepared for each sample by filtering a volume of FSW, similar to that used for the sample, onto a pre-combusted GF/F filter. Filters were dried at 60 °C for a minimum of 24 h and subsequently kept in sealed containers in the dark for transport and subsequent analysis.

Filters were dried at 55 °C for a minimum duration of 24 h shortly before the analysis. Analysis of particulate C and N content of Collodaria and Acantharia were done at the METABOMER facility at the Station Biologique de Roscoff, France. All other specimens were analysed at the LEMAR laboratory in Brest, France. The C and N content of entire filters was determined as CO₂ and N₂ released by flash combustion using a Flash 1112 series EA (Thermo Fisher). Samples of acetanilide (in Roscoff) or atropine (in Brest) of different mass were used to calibrate the analyser and determine C and N content of the samples. Standard deviations were 0.11 and 0.06 μ g for C and N, respectively. Carbon and N signal of the samples was corrected by subtracting the signal of the related blank sample. The detection limit was thus at the blank level, plus 10 times the standard deviation in order to avoid false positives. Data was processed in ISODAT 2.0 software and Microsoft Excel.

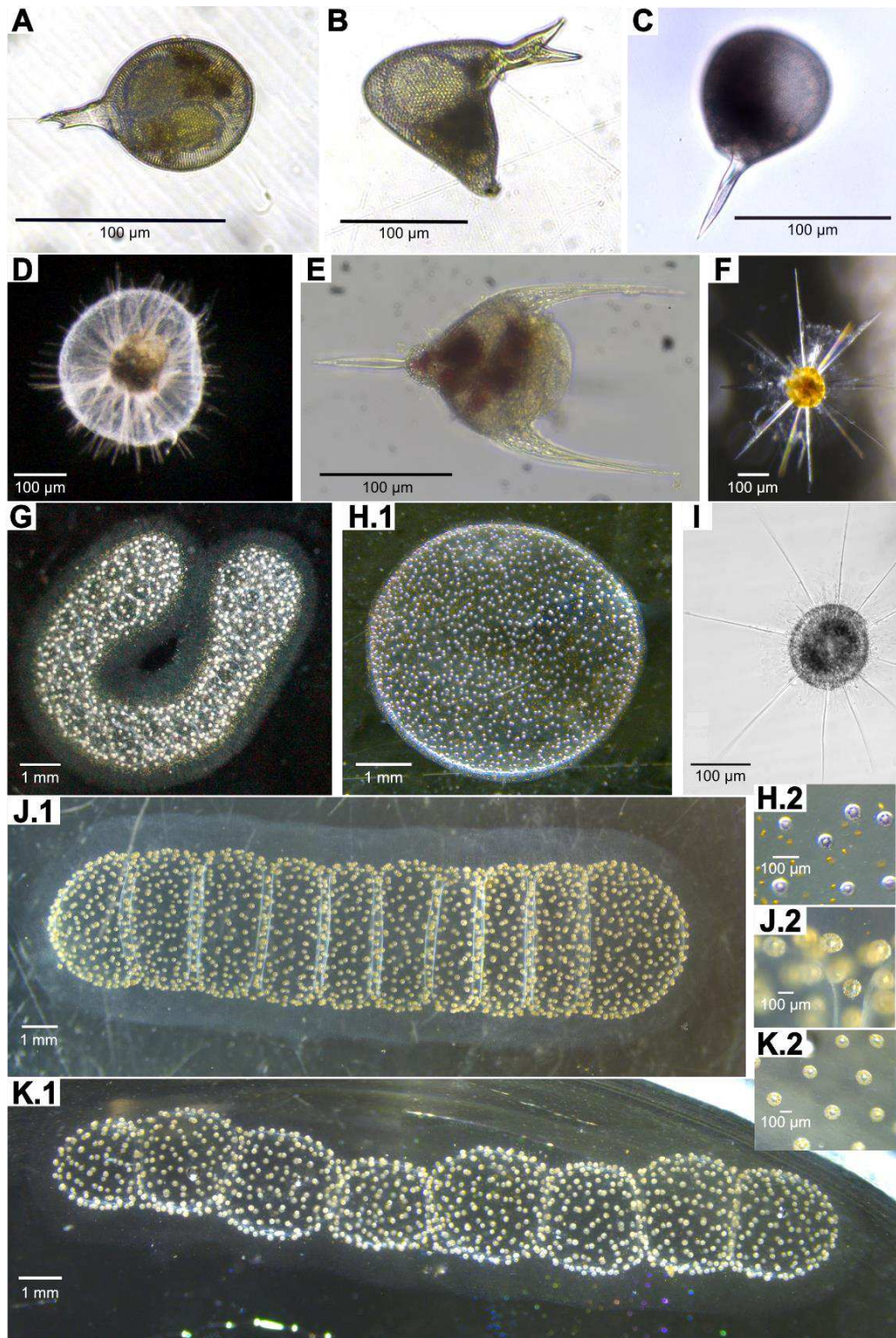


Figure II-2. Light microscopy image examples of the Rhizaria studied. **A** *Protocystis tridens*; **B** *Protocystis triangularis*; **C** *Challengeria xiphodon*; **D** *Aulacantha scolymantha*; **E** Nassellaria (stack of four images); **F** Acantharia; **G** *Sphaerozoum* sp.; **H** Collosphaeridae; **I** Spumellaria (black & white image); **J** & **K** two *Collozoum pelagicum* colonial morphologies. Collodarian colonies (**HJK.1**) are shown alongside a higher magnification image (**HJK.2**), zooming in on the central capsules. The dinoflagellate symbionts can clearly be seen as the golden cells. A scale is indicated separately in each image, note the different units for Collodaria colonies.

3.3. Image analyses

Pictures of specimen were taken after sampling for size inference, cell counts, and biovolume estimates (Zeiss Stemi SV11 stereoscope with Olympus DP21 camera in 2018 and a Leica S8AP0 with a Leica MC170HD camera in 2017 and 2019). Total volume of Collodaria colonies and individual cells were estimated from pictures of live cells. The diameter of at least 20 collodarian cells (*i.e.* central capsules, from here on also referred to as cells) was measured per colony and were assumed a spherical shape for biovolume calculations. Colony volume was measured excluding the outer edges of the gelatinous matrix of the colony (**Supplemental Table II-1**), because this material is variable with physiological state (Swanberg, 1979). Colonies were assigned a simple standardized shape for these calculations: either sphere, prolate spheroid, or cylinder with two half spheres (**Supplementary Methodology 2**). Biovolume of other Rhizaria was calculated in similar fashion using the closest geometric shape (e.g. truncated cone for Nassellaria, prolate spheroid for *Protocystis*, *Challengeria* and Spumellaria, and sphere for *Aulacantha*). For Spumellaria and *Aulacantha* biovolume calculations, the radiate spines were not considered in the calculations, only the central body shape, as suggested by Stukel et al. (2018) and Ikenoue et al. (2019). Additionally, the number of collodarian cells (the central capsules, **Figure II-2 HJK.2**) per Collodaria colony was estimated from images, either counting all cells or counting an area with a minimum of 200 cells and extrapolating this to the surface area (excluding outer gelatinous matrix). All image analysis was done using ImageJ 1.52a for Windows (Abràmoff et al., 2004).

3.4. Molecular identification

Collodaria colonies of identical morphology as the ones used for elemental analyses were used for genetic identification. They were collected and photographed in Villefranche-sur-Mer in 2016. For Acantharia similarly, representative specimen were preserved in 96% EtOH for molecular identification. Ribosomal gene sequences of the Collodaria were retrieved from transcriptome data. DNA of Acantharia, and one Collodaria, was extracted and ribosomal 18S was amplified and sequenced. Subsequently, phylogenetic trees were constructed using the maximum likelihood method for molecular identification (further details in **Supplemental Methodology 1**). Amplified 18S ribosomal sequences are deposited under Bioproject PRJNA658429, and sequences extracted from transcriptome data under accession numbers MT985517-MT985527.

Acantharia and Collodaria used for elemental analysis were identified by 18S rDNA phylogenetic placement, in combination with photographic comparison of our specimens to those linked to reference sequences in the works of Decelle et al. (2012) and Biard (2015).

3.5. Data analysis

Measured C and N content was normalized to cell count for bulk samples and central capsule counts for colonies. Linear least squares regression analysis was used to determine the C or N content to biovolume relationships using JMP for Windows (Version 1.19.4; SAS Institute Inc., Cary, NC, 1989-2019). The residuals were analysed to examine deviations from normality and equal variance. Data regarding total Collodaria colonies were \log_{10} transformed to fit the assumptions of the linear regression analysis. The regression coefficients (slope, *b*) were consistently found to be different from zero as tested with a t-test. Cellular mass estimations can be made following the standard regression equation (Eq 1). When

regression was performed on transformed data, the regression parameters are shown in \log_{10} format, and cell mass can be estimated from Eq 2 for non-logarithmic results. Where b is the slope, and a the y-intercept of the regression equation. Statistics are shown as mean with standard deviation.

$$\text{Eq 1} \quad \text{mass} = a + b \times \text{biovolume}$$

$$\text{Eq 2} \quad \text{mass} = 10^a \times \text{biovolume}^b$$

3.6. Validation of prediction equations

The regression equations for collodarian biovolume to C content were validated on elemental data from samples of two types of Collodaria colonies not included in the regression analysis (April 2019 samples, data available at <http://dx.doi.org/10.17632/j9262jxgt8.1>). Predictions of the total C content of the colony acquired by using our regression equations was compared to C content predictions acquired using the mean C density, and per cell C content. Mean Absolute Percentage Error (MAPE) was subsequently calculated for the different prediction methods according to Eq 3, where Obs_i is the observed mass, and Pre_i the predicted mass.

$$\text{Eq 3} \quad \text{MAPE} = \text{mean} \left(\frac{|Obs_i - Pre_i|}{|Obs_i|} \right) \times 100$$

4. Results

4.1. Colonial Radiolaria

Colonies collected during October 2019 (**Figure II-2 JK**) were identified as *Collozoum pelagicum* (**Supplemental Figure II-2 and 4**). Blue/violet colonies (**Figure II-2 H**) were verified as Collosphaeridae (**Supplemental Figure II-2 and 4**), which form blue pigments in reproductive stages (Swanberg, 1979). The identification of *Sphaerozoum* sp. (**Figure II-2 G**) was not confirmed by molecular data, but was based on the morphological features including the vacuoles and segmentation of the colonies, as compared to images of previous studies (Biard, 2015).

4.1.1 Carbon and nitrogen content and C:N ratios

The C content of Collosphaeridae cells ranged from 32.73 to 251.49 ng C cell⁻¹ (75.43 ± 74.12 ng C cell⁻¹; mean \pm s.d.; n = 8), and N content from 4.17 to 24.54 ng N cell⁻¹ (9.10 ± 7.68 ng N cell⁻¹, n = 6). *Sphaerozoum* and *Collozoum* had a higher C and N content per cell with a range of 15.74 to 597.91 ng C cell⁻¹ (152.90 ± 130.46 , n = 22) and 9.56 to 100.84 ng N cell⁻¹ (29.66 ± 22.0 , n = 20) for *Sphaerozoum*, and a range of 90.31 to 215.85 ng C cell⁻¹ (148.01 ± 37.29 , n = 16) and 8.49 to 22.73 ng N cell⁻¹ (15.35 ± 4.07 , n = 16) for *Collozoum* (**Table II-1**). The average C:N ratio for Collosphaeridae was close to Redfield ratio (6.6) with an average of 6.3 (± 1.7) (**Table II-1**). C:N ratio of *Sphaerozoum* was lower with a mean of 5.9 and *Collozoum* samples were higher with a mean C:N of 9.7, similar to Michaels et al. (1995). Carbon and N content and biovolume was also measured for a sample of *Thalassicolla* sp., a solitary Collodaria (**Table II-1**). Total biomass was not always sufficient to measure N hence the C:N ratio could not be calculated for all samples.

The cellular C content for all Collodaria taxa combined ranged from 15.73 to 597.89 ng C cell⁻¹ (137.73 ± 100.50 ng C cell⁻¹; n = 46). Nitrogen content showed a similar wide range from 4.17 to 100.84 ng N cell⁻¹ (21.27 ± 17.83 ng C cell⁻¹; n = 42). The C:N ratio averaged 7.4 (± 2.5).

Table II-1. Cell volume and carbon (C) and nitrogen (N) data for Rhizaria from this study and from the literature. Carbon or N per volume (i.e. mass density) of Collodaria (i.e. Collosphaeridae, *Collozoum* and *Sphaerozoum*) is indicated both per colony (in $\mu\text{g mm}^{-3}$) and per cell (central capsule) (in pg mm^{-3}). Data of Collodaria are also separately shown as combined for all Collodaria. C content indicated per cell, implies central capsules for Collodaria. The total number of samples analysed (n) differs for N and C content, because N mass was not always above the detection limit. Additionally, the total number of cells of all samples is given. Data of this study is highlighted in bold. Data is given \pm standard deviation. Further data on central capsules per colony, volume measurements, as well as data ranges are summarised in **Supplemental Table II-1**. Full raw data and photographs are accessible at <http://dx.doi.org/10.17632/j9262jxgt8.1>.

Taxa	Carbon				Nitrogen				C:N	reference	
	cells	n	ng C cell ⁻¹	pg C μm^{-3} , or $\mu\text{g C mm}^{-3}$ for colonies	n	ng N cell ⁻¹	pg N μm^{-3} , or $\mu\text{g N mm}^{-3}$ for colonies	n			
Colonial Collodaria											
Collosphaeridae	15034	8	75.43 \pm 74.12	7	0.168 \pm 0.083	6	9.1 \pm 7.68	5	0.0348 \pm 0.0253	6.3 \pm 1.73	This study
<i>Acrosphaera spinosa</i>	2456	6	172 \pm 94	-	-	-	-	-	-	7.7 \pm 0.3	Michaels 1995
<i>Acrosphaera spinosa</i>	480	13	100	-	-	-	-	-	-	8.3 \pm 1.7	Swanberg 1983
<i>Collosphaera Huxleyi</i>	340	1	172	-	-	-	-	-	-	-	Michaels 1995
Sphaerozoum	13874	22	152.9 \pm 130.46	17	0.139 \pm 0.042	20	29.66 \pm 22	15	0.0278 \pm 0.011	5.89 \pm 2.13	This study
<i>Sphaerozoum punctatum</i>	2210	5	146 \pm 31	-	-	-	-	-	-	6.7 \pm 1.1	Michaels 1995
<i>Sphaerozoum punctatum</i>	500	3	64	-	-	-	-	-	-	9.8 \pm 0.98	Swanberg 1983
Collozoum	23396	16	148.01 \pm 37.29	16	0.139 \pm 0.035	16	15.35 \pm 4.07	16	0.0144 \pm 0.0037	9.72 \pm 0.98	This study
<i>Collozoum pelagicum</i>	5224	5	131 \pm 104	-	-	-	-	-	-	8.5 \pm 1.2	Michaels 1995
<i>Collozoum pelagicum</i>	1500	4	107	-	-	-	-	-	-	13 \pm 1.7	Swanberg 1983
<i>Collozoum radiosum</i>	350	13	200	-	-	-	-	-	-	8.4 \pm 0.76	Swanberg 1983
<i>Collozoum longiforme</i>	-	3	67 to 96	-	-	-	-	-	-	8,6	Swanberg and Harbison 1980
<i>Collozoum inerme</i>	7700	3	51 \pm 10	-	-	-	-	-	-	9,7	Michaels 1995
<i>Collozoum inerme</i>	2500	11	50	-	-	-	-	-	-	11 \pm 3.2	Swanberg 1983
<i>Rhaphidozoum acuferum</i>	2230	5	115 \pm 28	-	-	-	-	-	-	9.4 \pm 1.7	Michaels 1995
All colonial Collodaria	52304	46	137.73 \pm 100.5	40	0.144 \pm 0.049	42	21.27 \pm 17.53	36	0.0228 \pm 0.0138	7.41 \pm 2.49	This study
All colonial Collodaria	20160	25	133 \pm 73	-	-	-	-	-	-	8.2 \pm 1.5	Michaels 1995
Collosphaeridae (colony)	15034		NA	8	0.629 \pm 0.413		NA	8	0.0836 \pm 0.0568		This study
Collozoum (colony)	23396		NA	16	1.21 \pm 0.516		NA	16	0.1254 \pm 0.0572		This study
Sphaerozoum (colony)	13874		NA	22	1.423 \pm 0.94		NA	20	0.2637 \pm 0.1179		This study
all colonial Collodaria (colony)	52304		NA	46	1.211 \pm 0.781		NA	42	0.1853 \pm 0.1181		This study
Solitary Collodaria											
<i>Thalassicolla sp.</i>	16	1	21577,46	1	0,189		3723,60	1	0,03	5,79	This study
<i>Thalassicolla melanogaster</i>	1	1	-	-	0,01		-	-	-	4,70	Michaels 1995
<i>Thalassicolla nucleata</i>	15	11	-	-	0.28 \pm 0.25		-	-	-	6.4 \pm 2.1	Michaels 1995
Spumellaria	74	2	799.38 \pm 345.79	2	0.328 \pm 0.127	2	94.96 \pm 5.54	2	0.0456 \pm 0.0325	8.33 \pm 3.16	This study
<i>Physematium muelleri</i>	17	12	-	-	0.009 \pm 0.003		-	-	-	4.8 \pm 0.06	Michaels 1995
Nassellaria	241	6	458.45 \pm 249.26	6	1.472 \pm 0.73	6	52.97 \pm 27.64	6	0.1713 \pm 0.0853	8.79 \pm 1.43	This study
Acantharia (clade F3)	540	18	168.59 \pm 151.15		0.04 to 0.939*		-		-		This study
Acantharia mix	370	12	-	-	0.0026 \pm 0.0036 [^]		-		-		Michaels 1995
Foraminifera											
<i>Orbulina universa (spherical chambers)</i>	36	12	-	-	0.018 \pm 0.008		-		-	6.1 \pm 1.7	Michaels 1995
<i>Orbulina universa (trochospiral chambers)</i>	19	2	-	-	0.18 \pm 0.13		-		-	6,6	Michaels 1995
<i>Hasugerina pelagica</i>	0	0	-	-	0.092 \pm 0.014		-		-	5.7 \pm 1.4	Michaels 1995
<i>Globigerinoides ruber</i>	8	1	-	-	0,06		-		-	-	Michaels 1995
Mixed assemblage	24	4	-	-	0.045 \pm 0.007		-		-	-	Michaels 1995
All foraminifera (excl. spherical O. universa)	112	22	-	-	0.089 \pm 0.055		-		-	5.8 \pm 1.3	Michaels 1995
Phaeodaria											
Phaeodaria (size >1 mm)			7200 to 25000								Ikenoue et al., 2019
<i>Aulacantha</i>	302	17	3075.48 \pm 1559.57	17	0.018 \pm 0.015	17	305.7 \pm 174.83	17	0.0018 \pm 0.0016	10.61 \pm 2	This study
<i>Protocystis</i>	414	12	721.92 \pm 450.34	12	2.224 \pm 1.283	12	82.8 \pm 42.45	12	0.2593 \pm 0.1314	8.61 \pm 1.76	This study
<i>Challengeria</i>	48	2	1226.84 \pm 1360.87	2	0.24 \pm 0.113	2	64.89 \pm 61.29	2	0.0146 \pm 0.0017	16.25 \pm 5.62	This study

*estimated assuming a cell size of 200 and 70 μm for min and max, see results for further explanation.

[^] note that these values are based on biovolume calculated from the spicule extremes.

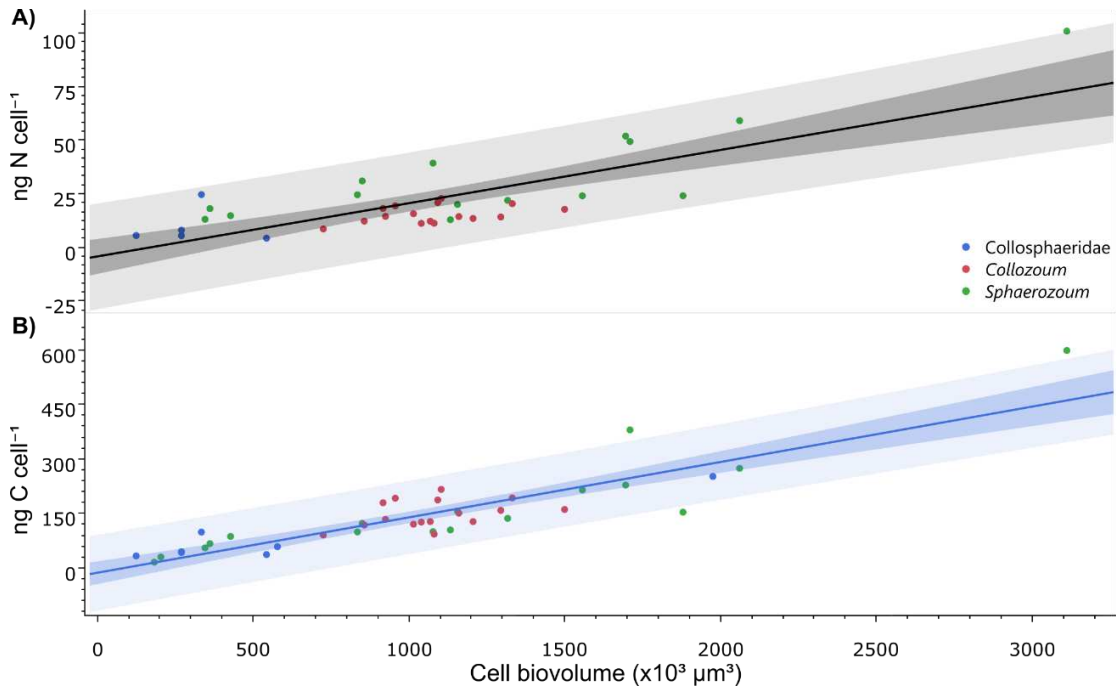


Figure II-3. Relationships between cell volume (μm^3) and (A) nitrogen (ng) per cell, and (B) carbon (ng) per cell for central capsules of colonial Collodaria. The different Collodaria genera investigated in this study are indicated by colour, Collosphaeridae (blue), *Collozoum* (red), and *Sphaerozoum* (green). The line of best fit is shown as a solid black/blue line with the 95% confidence interval of the fit in dark grey/blue shading and 95% prediction interval in lighter grey/blue shading. Regression parameters are shown in **Table II-2**.

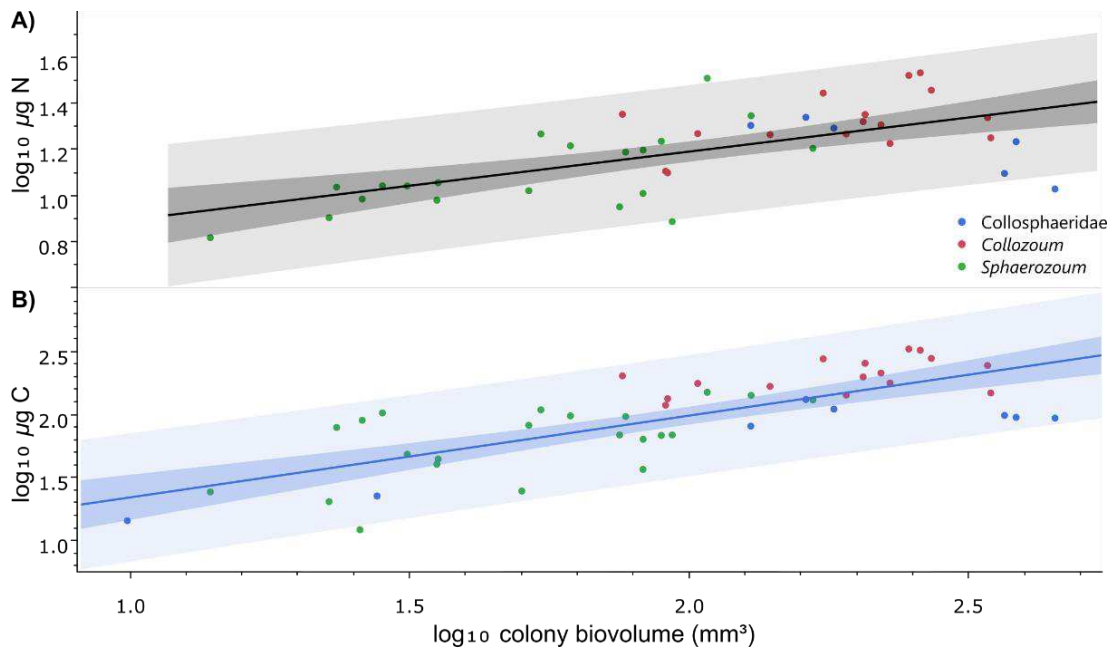


Figure II-4. Relationships between total colony volume (mm³) and (A) nitrogen (μg) per colony, and (B) carbon (μg) per colony for colonial Collodaria. Graphs show log₁₀-transformed data. The different Collodaria genera investigated in this study are indicated by colour, Collosphaeridae (blue), *Collozoum* (red), and *Sphaerozoum* (green). The line of best fit is shown as a solid black/blue line with the 95% confidence interval of the fit in dark grey/blue shading and 95% prediction interval in lighter grey/blue shading. Regression parameters are shown in **Table II-2**. The conversion of the log₁₀ expressed regression equation is outlined in the Methods.

4.1.2 Carbon and nitrogen to biovolume relationships

To allow for extrapolation and usability in modelling and ecological (in situ) studies, we determined C:vol and N:vol relationships of all Collodaria taxa clustered. The strong correlation of C content per cell to the average cell volume in a colony ($\text{ng C cell}^{-1} = -13.51 + 0.0001524 \times \text{volume } (\mu\text{m}^3)$, $F_{1,38} = 139.70$, $R^2 = 0.79$, $p < 0.0001$, **Figure II-3 B, Table II-2**) largely explains the variation among C content. Yet, N content is only moderately correlated with the average cell volume by the regression equation $\text{ng N cell}^{-1} = -4.33 + 0.000249 \times \text{volume } (\mu\text{m}^3)$ ($F_{1,34} = 56.44$, $R^2 = 0.62$, $p < 0.0001$, **Figure II-3 A, Table II-2**).

Assessing the relationship of entire colony C (or N) content with biovolume showed a similar significant positive correlation by the regression equations $\log_{10} \mu\text{g C colony}^{-1} = 0.692 + 0.649 \times \log_{10} \text{volume } (\text{mm}^3)$, and $\log_{10} \mu\text{g N colony}^{-1} = 0.597 + 0.297 \times \log_{10} \text{volume } (\text{mm}^3)$ ($F_{1,44} = 58.76$, $R^2 = 0.57$, $p < 0.0001$, and $F_{1,40} = 26.73$, $R^2 = 0.40$, $p < 0.0001$, for C and N respectively, **Figure II-4, Table II-2**), though this correlation was less strong than on the cell level. Further analysis shows a significant negative correlation of C and N density (mass per biovolume) with colonial volume ($F_{1,44} = 17.15$, $R^2 = 0.28$, $p < 0.0002$, and $F_{1,40} = 149.74$, $R^2 = 0.79$, $p < 0.0001$, respectively) (**Supplemental Figure II-5**). Carbon and N density per colony and per cell are given in **Table II-1**.

4.1.3 Validation of Collodaria biovolume to carbon content equations

We compared the total colonial Collodaria C content results from four different prediction methods, to identify the most accurate approach.

(1) Colony C content (ng C) was predicted using the average C content per cell of $137.73 \text{ ng C cell}^{-1}$ ($\text{C content}_{\text{cell}}$), and multiplied by the total number of cells counted in the colony (No_{cells}) of which C content was to be predicted (Eq 4).

$$\text{Eq 4} \quad \text{predicted colonial C content} = \text{average}(\text{C content}_{\text{cell}}) \times \text{No}_{\text{cells}}$$

(2) Colony C content ($\mu\text{g C}$) was predicted based on the average colonial C density of $1.21 \mu\text{g C mm}^{-3}$ ($\text{C density}_{\text{colony}}$), and multiplied by the colony's volume (V , mm^3) (Eq 5).

$$\text{Eq 5} \quad \text{predicted colonial C content} = \text{average}(\text{C density}_{\text{colony}}) \times V$$

(3) Colony C content (ng C) was estimated using our collodarian cell biovolume to C content equation (**Figure II-3 B; Table II-2**) with V (μm^3) being the average biovolume of the cells. The predicted C content per cell was multiplied by the total number of cells counted in the colony (No_{cells}) to acquire colony C content (Eq 6).

$$\text{Eq 6} \quad \text{predicted colonial C content} = (-13.51 + 0.0001524 \times V) \times \text{No}_{\text{cells}}$$

(4) Lastly, our equation for colonies was used to predict colony C content ($\mu\text{g C}$) with V in mm^3 (**Figure II-4 B; Eq 7**), thereby not having to account for cell biovolume and quantity.

$$\text{Eq 7} \quad \text{predicted colonial C content} = 10^{(0.6922)} \times V^{(0.6492)}$$

In order of lowest to highest Mean Absolute Percentage Error (MAPE) we found: method 3 (MAPE = 37.12), method 4 (MAPE = 45.17), method 2 (MAPE = 55.69), and method 1 (MAPE = 64.16) (**Supplemental Table II-2**).

Table II-2. Results of significant least-squares regression analyses of C and N to biovolume. Presented are the slope (regression coefficient, b) and y-intercept (a) of the regression equations; the standard deviation (s.d.); the square of the correlation coefficient r (R^2), and the number of data points (n). All slopes are significantly different from zero ($p < 0.05$). For collodarian colonies the data was \log_{10} -transformed. The cellular C (or N) content is thus determined as $\mu\text{g C (or } \mu\text{g N) colony}^{-1} = 10^a \times (\text{volume (mm}^3))^b$, Eq 2. All other data is untransformed, and mass is thus determined by linear regression as $\text{ng C (or ng N) cell}^{-1} = a + b \times \text{volume } (\mu\text{m}^3)$, Eq 1.

Data	Intercept (a)	s.d.	Slope (b)	s.d.	R^2	n
Collodaria central capsule C	-13.51	15.40	0.0001524	0.0000129	0.786	40
Collodaria central capsule N	-4.33	4.01	0.0000249	0.0000033	0.624	36
Collodaria colony C*	0.692	0.17	0.649	0.0847	0.572	46
Collodaria colony N*	0.597	0.118	0.297	0.0575	0.401	42
<i>Protocystis</i> C	128.31	278.8	0.00176	0.000759	0.349	12

* Data was \log_{10} transformed

4.2. Nassellaria and Spumellaria

Carbon content of Nassellaria varied between 178.40 and 876.27 ng C cell⁻¹ (458.44 ± 249.25 ng C cell⁻¹; $n = 6$), and N content ranged from 22.39 to 88.61 ng N cell⁻¹ (52.97 ± 27.64 ng N cell⁻¹; s.d.; $n = 6$), with an average C:N ratio of 8.8 (Table II-1). The C:vol relationships for Nassellaria cells showed no significant correlations ($F_{1,4} = 0.54$, $p = 0.5022$), nor did it for N:vol ($F_{1,4} = 0.30$, $p = 0.6108$) (**Supplemental Figure II-6**). Hence, the best mass estimates can only be made by the average C (or N) density, 1.47 ± 0.73 pg C μm^{-3} (or 0.17 ± 0.09 pg N μm^{-3} , **Table II-1**).

For Spumellaria we measured C content of 554.87 and 1043.89 ng C cell⁻¹ ($n = 2$), and N content of 91.04 and 98.87 ng N cell⁻¹. Average carbon and nitrogen density was 0.33 ± 0.13 pg C μm^{-3} and 0.046 ± 0.033 pg N μm^{-3} (**Table II-1**). Since we had only two samples, no regression analysis could be made.

4.3. Acantharia

Phylogenetic placement of the sequences identified the Acantharia specimen as belonging to sub-group F3b (**Supplemental Figure II-3 and 4**). Sub-group F3 lacks molecular resolution (Decelle et al., 2012c), therefore the genera of the samples could not be distinguished molecularly between the closely related taxa of clade F3. Photographic comparison show the samples Ac-6 and Ac-16 to be most similar to *Acanthostaurus*, possibly *Acanthostaurus purpurascens*, which is commonly found at the sampling location (**Supplemental Figure II-4**). Ac-17 is likely *Amphistaurus complanatus* (**Supplemental Figure II-4**). Because acantharian taxonomy is usually determined by skeletal features, it was not possible to be certain of the identification. Nonetheless, considering the specimens were molecularly clearly a mix of sub-group F3b Acantharia, this was deemed sufficient.

Overall, Acantharia had an average C content of 168.59 ± 151.15 ng C cell⁻¹ ($n = 18$). Unfortunately, no pictures were taken for these samples, hence average size and biovolume could not be determined *a posteriori*. However, based on the Acantharia observed during the cell isolation process, the diameter of the central capsule was estimated between the limits of 70 to 200 μm . Using those as the upper and lower limits of size range, and assuming a spheroid shape, we can calculate the C:vol ratio to be between 0.94 ± 0.85 and 0.04 ± 0.03 pg C μm^{-3} (**Table II-1**). A tentative estimate of Acantharia size from the spicule

extremes would range from 200 to 500 μm for a C:vol ratio between 0.04 ± 0.03 and 0.0026 ± 0.002 $\text{pg C } \mu\text{m}^{-3}$. Elemental analysis of *Acantharia* was hampered by a lack of total biomass. Consequently, we were unable to measure N content, and in some cases, neither C content, resulting in a loss of samples.

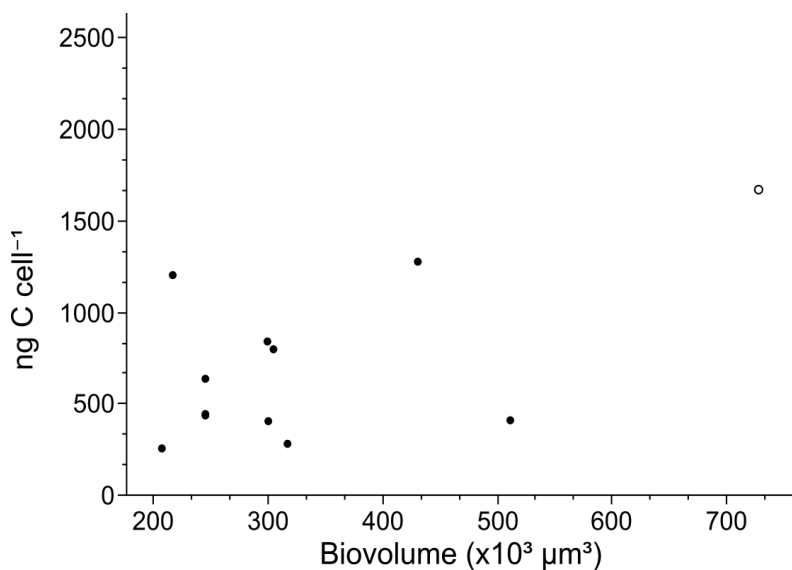


Figure II-5. *Protocystis* carbon to cell volume relationship. The outlier dictating the carbon:volume relationship is shown as an open circle. The regression statistics are shown in Table II-2.

4.4. Phaeodaria

The C content of the genera *Aulacantha* and *Protocystis* ranged from 943.03 to 6003.69 and 256.87 to 1670.20 ng C cell^{-1} respectively. Nitrogen content ranged from 66.70 to 700.34 and 26.95 to 158.09 ng N cell^{-1} for *Aulacantha* and *Protocystis*, respectively. No significant correlation of C:vol nor N:vol was found for *Aulacantha* (respectively: $F_{1,15} = 0.90$, $p = 0.357$; $F_{1,15} = 0.86$, $p = 0.368$, **Supplemental Figure II-6**). *Aulacantha* C and N density is significantly negatively correlated to biovolume ($F_{1,15} = 15.04$, $R^2 = 0.501$, $p < 0.0015$ and $F_{1,15} = 12.98$, $R^2 = 0.464$, $p < 0.0026$ for C and N density respectively, **Supplemental Figure II-7 A**). Additionally, for *Aulacantha* a wide range of cells (1-44) was used per sample, this could have influenced C and N content measurements. Concordantly, we find C and N density weakly but significantly negatively correlated to the number of cells per samples ($F_{1,15} = 4.99$, $R^2 = 0.250$, $p < 0.0412$ and $F_{1,15} = 4.87$, $R^2 = 0.245$, $p < 0.0433$ for C and N density respectively, **Supplemental Figure II-7 B**). When a low number of cells were used per sample a higher density seems to be measured and vice-versa. A significant weak correlation was found for *Protocystis* C:vol by the equation $\text{ng C cell}^{-1} = 128.31 + 0.000176 \times \text{volume } (\mu\text{m}^3)$ ($F_{1,10} = 5.37$, $R^2 = 0.349$; $p = 0.0430$; **Table II-2** and **Supplemental Figure II-6**), but not for N:vol ($F_{1,10} = 3.72$, $p = 0.083$, **Supplemental Figure II-6**). The correlation was heavily influenced by one outlier with a high biovolume, without this sample there would be no correlation (**Figure II-5**). More samples of higher biovolume could possibly resolve this. Thus, average C and N densities, as given in Table 1, might be better estimates for prediction.

Only three samples containing the genus *Challengeria* were procured, and for one sample the C and N content data was aberrant and thus excluded. The two samples considered had 264.56 and 2189.12 ng C cell^{-1} , and 21.55 and 108.23 ng N cell^{-1} (**Table II-1**).

5. Discussion

5.1. Mean Rhizaria carbon and nitrogen densities and mass estimations

Carbon or N content and biovolume data on Rhizaria are extremely scarce, with only one study with C and N measurements for Acantharia and Phaeodaria known to us (see **Table II-1**). While the rest of the available data are for the Collodaria taxa. The measured Collodaria C and N density and relatively high variation in C and N content of all our samples was similar to that reported in previous studies (**Table II-1**). Here we have measured C and N density of several not previously investigated Rhizaria taxa, in addition to establishing new mass to biovolume relationships (**Table II-1; Figure II-6**).

For both Radiolaria and Phaeodaria it is not the bigger cell that is most C dense. Nassellaria (Radiolaria) and *Protocystis* (Phaeodaria), on average the smallest of their representative taxa, have a C and N density an order of magnitude higher than the other taxa (**Figure II-6**). Nearly all Rhizaria species have elaborate skeletal structures, with the extracapsulum making up most of the soft body, yet most of the biological material is likely centrally located, in the central capsule (Haeckel, 1887; Suzuki and Not, 2015). Thus from the total inferred size only a small fraction would contain plenty organic matter, and the total C (and N) density would be lower than expected from the volume of the entire body. The central capsule of these smaller taxa might be relatively bigger in relation to the total structure as compared to other Rhizaria.

Acantharia were previously reported with a very low C:vol ratio (Michaels et al. 1995, **Table II-1**). This has been attributed to a lack of the acantharian ectoplasm outer membrane in their samples, and to biovolume measurements estimated of the spicule extremes, whereas most C would be expected in the central capsule. We did not observe lack of this outer membrane in our samples. Using the C:vol ratio of $0.0026 \text{ pg C } \mu\text{m}^{-3}$, as reported by Michaels et al. (1995), a cell of half a millimetre (from the spicule extremes) would on average have a C content of $170.2 \text{ ng C cell}^{-1}$, which is near our average cellular carbon content for Acantharia ($168.59 \text{ ng C cell}^{-1}$). This C density of $0.0026 \text{ pg C } \mu\text{m}^{-3}$ falls below our lowest estimate for acantharian C density, assuming the biggest cell analysed (*i.e.* $200 \mu\text{m}$). Our data thus suggest average C density is more likely to be higher than the previously reported $0.0026 \text{ pg C } \mu\text{m}^{-3}$. In agreement with the previous measurement, we find highly variable C and N content, likely caused by both intraspecific and interspecific variation as attributed to the bulk analysis on low taxonomic resolution.

It has been suggested that the C:vol conversion factors for protists reported by Menden-Deuer and Lessard (2000) overestimates biomass of larger protists considerably (Stukel et al., 2018; Ikenoue et al., 2019). The C (and N) density of the largest protist here studied (*Aulacantha*) is one to two orders of magnitude lower than that of the other studied Rhizaria taxa. If we take *Aulacantha* as an example (mean biovolume = 0.241 mm^3), the general protist plankton C:vol equation (*i.e.* $\log \text{ pg C cell}^{-1} = -0.665 + 0.939 \times \log (\mu\text{m}^3)$, Menden-Deuer and Lessard 2000) would give a cellular C content of $16.04 \mu\text{g C cell}^{-1}$. This is around five times more than the average C content that we found for *Aulacantha*, *i.e.* $3.08 \mu\text{g C cell}^{-1}$. Indeed, as has been suggested by Stukel et al. (2018) (for Phaeodaria $>200 \mu\text{m}$) and Ikenoue et al. (2019) (for Phaeodaria $>1 \text{ mm}$), global biomass of Phaeodaria would have been overestimated due to the use of inappropriate C:vol conversions. However, this only holds for a single genus considered here. The genus *Protocystis* has the highest C density ($2.22 \text{ pg C mm}^{-3}$) of our study. Using the mean biovolume of

0.000338 mm³, and the same equation would give a large underestimation of C content, namely 33.60 ng C cell⁻¹ instead of the actually measured mean of 721.92 ng C cell⁻¹. Based on our measurements, it turns out that C mass for all Rhizaria taxa with a size range from 0.69 to 236 μm would be underestimated, whereas *Aulacantha* (size range 529 to 860 μm) would indeed be overestimated with previously published generic protist C:vol equation (**Table II-3**). Our data shows that global Rhizaria biomass might have thus in fact still been underestimated, by up to a factor of 35 (**Table II-3**). Most notable is the difference between the estimate and our measurement for Acantharia (35.8 factor of change), whereas the factor of change for Collodaria is less pronounced with C content only differing a factor of 1.4. Thereby underlining the need for direct C and N content measurements of different plankton groups and sizes, to be able to make more accurate biomass estimations. Specifically for large sized protists like Rhizaria, taxa-specific mass:vol conversions as presented here can increase the estimation accuracy.

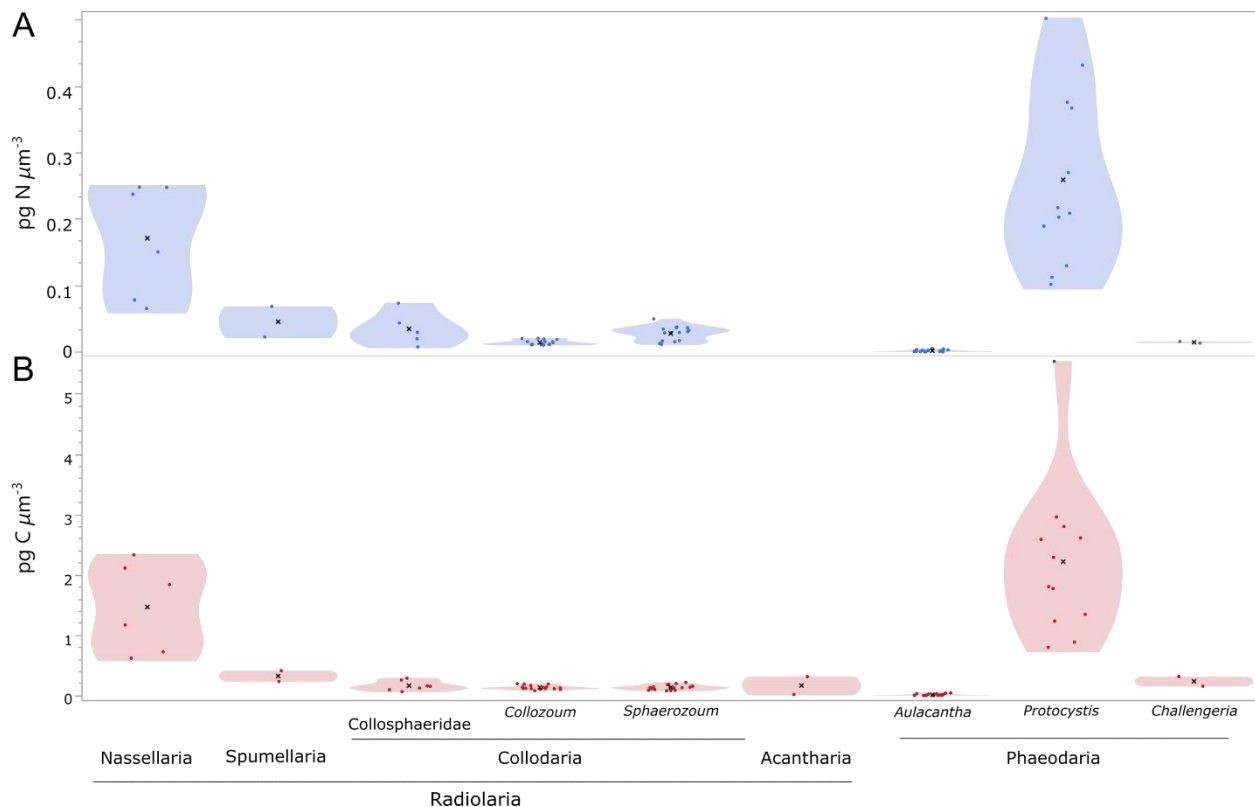


Figure II-6. Violin plot for (A) C and (B) N density of Rhizaria. The mean is shown as an 'x', the individual datapoints of pg N μm⁻³ or pg C μm⁻³, and the distribution of the data is shown with respectively blue dots and shading or red dots and shading. All values are shown by cell and for Collodaria per central capsules. The range of C content for Acantharia has been estimated based on a suspected size of 100 to 200 μm.

5.2. C:vol relationship of Collodaria - comparison of prediction methods

Carbon content of several Collodaria taxa have previously been measured and normalised based on central capsule quantity, but these values did not account for biovolume (Swanberg, 1983; Michaels et al., 1995). Accordingly, C mass estimations of collodarian colonies have previously been based entirely on

the average C content per central capsule (Dennett et al., 2002; Villar et al., 2018). We compared the error in cellular C content estimates of four different prediction methods, illustrating that factoring in biovolume for C (or N) estimation greatly reduce the prediction error. Comparison of the prediction errors showed that C content of collodarian colonies is best predicted when taking into account the central capsule quantity and biovolume, and thus using Eq 6 (**Supplemental Table II-2**).

Though previous studies report C content values of Rhizaria on the species level, we opted for a lower taxonomic resolution. This not only assured higher sample quantity, it aims at being more pragmatic in future studies where it is often not possible to identify Rhizaria to species level. The regression analysis combining genera of colonial Collodaria shows a regression without extreme outliers, consenting for the analysis of Collodaria on this taxonomic level.

Furthermore, C and N measurements normalised to central capsule quantity would not always allow easy and accurate extrapolation to ecologically relevant colonies. Microscopic measurement and accurate counts of central capsules are not always practical for in situ monitoring of Collodaria. Therefore, we have additionally shown C and N content in relation to colony volume. It will be particularly useful for mass estimates in situations where three dimensionally layered central capsules cannot be accurately determined (e.g. in situ optics based technologies, like Underwater Vision Profilers or similar plankton recorders (Nakamura et al., 2017; Biard and Ohman, 2020)). In these cases, despite showing weaker correlations, possibly due to the size and quantity variation of the central capsules in the colony, the equations for C:vol (or N:vol) of colonies (Eq 7, **Table II-3**) can still give a more accurate prediction than other mass estimation methods for these Collodaria colonies (**Supplemental Table II-2**).

Using the data presented here, collodarian cellular C and N content can be relatively accurately predicted, though these predictions remain subject to high variation inherent to the organism. This is also reflected in the C to biovolume relationship that has an R^2 of 0.782, whereas for other protists the R^2 mostly lies above 0.9 (Menden-Deuer and Lessard, 2000). Nitrogen to biovolume relationships are less strong than those of C content, hence, cellular N content might be alternatively estimated by C:N ratio.

However, life history stages could influence the cell's C:N stoichiometry, as has been shown in animals and metazoans that undergo significant morphological changes, like copepods (Sterner and Elser, 2002). The blue pigmented Collosphaeridae samples were likely all reproductive stages (Swanberg, 1979). We do not have sufficient data to compare different Collosphaeridae life stage stoichiometry, though we find no reason in our Collodaria mass:vol regression analysis to consider them as outliers. The central capsules of the Collosphaeridae specimen are smaller in diameter in comparison to those of Sphaerozoum and Collozoum with average diameters of $100.5 \pm 2.8 \mu\text{m}$, 122.6 ± 3.2 and 125.6 ± 0.8 , respectively. However, the C content per central capsule is not different between these species, and the smaller size of Collosphaeridae cells likely explains their lower C content per cell. It should also be noted that solitary Collodaria, which are likely an alternative life stage of colonial forms (Swanberg, 1979; Biard et al., 2015), show a C and N density two orders of magnitude higher than colonies (average of 0.0012 vs $0.189 \text{ pg C } \mu\text{m}^{-3}$, and 0.000185 vs $0.03 \text{ pg N } \mu\text{m}^{-3}$), as well as a lower C:N ratio (7.41 vs 5.79). Though the radiolarian life cycle is not fully understood, such high densities could allow vegetative growth and colony formation when nutrients are otherwise limited.

Table II-3. Comparison of carbon estimates by protist plankton formula of Menden-Deuer and Lessard (2000) to carbon as measured in this study. Carbon content estimates are based on the mean cell volumes found in our samples, for Acantharia a volume associated with a 100- μm cell was used instead. Collodaria carbon content is per central capsule. A green highlight indicates that the actual measurement is higher than the prediction; red highlight indicates the opposite. Furthermore, the average diameter of our samples and the factor of change between the estimated and measured mass is given.

	Average size (diameter, μm)	C estimate using protist plankton formula (ng C cell^{-1})	Mean C measured (ng C cell^{-1})	Factor of change
Collosphearidae	94.93	63.19	75.43	1.19
<i>Collozoum</i>	125.57	100.04	148.01	1.48
<i>Sphaerouzoum</i>	122.65	107.97	152.90	1.42
all colonial Collodaria	118.97	97.91	137.73	1.41
Spumellaria	158.00	249.21	799.38	3.21
Nassellaria	83.67	31.47	458.45	14.57
Acantharia (F3)	70-200*	4.71	168.59	35.83
<i>Aulacantha</i>	733.35	16036.31	3075.48	0.19
<i>Protocystis</i>	97.83	33.60	721.92	21.49
<i>Challengeria</i>	184.00	362.00	1226.84	3.39

*estimated based on visual observations, see results for further explanation

Furthermore, the effect of physiological status is shown to affect cellular C and N content. For example, Tada et al. (2000) showed the C and N content and C:N ratio of *Noctiluca scintillans* cells to increase for fed cells and *vice-versa* for starved cell. Nutritional status can subsequently affect C:N ratio, as a decrease is often observed with increased particulate (prey) and/or dissolved inorganic N (exemplified in symbiotic jellyfish (Djeghri et al., 2020), symbiotic Foraminifera (Uthicke and Altenrath, 2010), and symbiotic corals (Muscatine et al., 1989)). We thus expect the C:N ratio to fluctuate to the relative prevalence of autotrophy vs heterotrophy, which will especially be influential in mixotrophic specimens like Collodaria and Acantharia. Unfortunately, it is not well known to what proportion they rely on which trophic mode for nutrition, nor about the environmental influences on switching between trophic modes.

6. Conclusion

We report for the first time carbon and nitrogen to biovolume relations for several groups of Rhizaria and summarised similar available data from the literature. Rhizaria are widely distributed in the world oceans (Biard et al., 2016). Symbiont bearing Rhizaria, like Collodaria and Acantharia, are most abundant in the upper epipelagic zone, whereas Phaeodaria are predominantly found in deeper water layers (Michaels, 1988; Biard and Ohman, 2020). Phaeodaria and Radiolaria have shown especially high abundance in locations where the efficiency of the biological carbon pump is high, but also in oligotrophic regions such as the North Pacific and California Current Ecosystem (Stukel et al., 2018; Gutierrez-

Rodriguez et al., 2019). Accordingly, knowledge and quantification of cellular C and N content of these abundant organisms is paramount in characterising oceanic ecosystems and C and N fluxes.

The empirically measured C and N densities of Rhizaria can be used to estimate their cellular C and N content in observational or modelling studies. For Collodaria we showed biovolume to mass equations that can give more accurate predictions than mean C or N density or previously available central capsule normalised values. These novel data will be invaluable for further studies involving these large protistan plankton (>100 μm). With the data presented here, improved incorporation of these larger protists into (biomass-based) eco-physiological and ecosystem models is expected, in conjunction with improved estimates. The focus on single cell isolated specimens, of different sizes and life stages, further permits the usage of the data in Individual-based models, also known as Agent-based models. Such studies will allow us to formulate hypotheses on the role of these important organisms in the ecosystem and elucidate their contribution to global biogeochemical cycles.

7. Acknowledgements

This work was carried in conjunction with the European Marine Biological Resource Centre (EMBRC-ERIC), EMBRC-France, and the METABOMER platform in Roscoff, France. The authors thank Fabien Lombard and the Observatoire d'Océanologie de Villefranche sur Mer for hosting us, and Guillaume de Liege and David Luquet for their help with sampling. We greatly appreciate Sarah Romac for the 18S sequencing, and Charles Bachy and Miguel Mendez Sandin for help with the transcriptomic and phylogenetic analyses. The authors are grateful to the MOOSE observation national network (funded by CNRS-INSU and Research Infrastructure ILICO) which sustain the annual ship-based hydrographic sections in the northwestern Mediterranean Sea (MOOSE-GE). Furthermore, the authors acknowledge the captain and crew of RV Tangaroa for their efforts in facilitating the sampling during TAN1901. This study is a contribution to the international IMBER project and was supported by the UK Natural Environment Research Council National Capability funding. French state funds are managed by the ANR within the Investments of the Future program under reference ANR-10-INSB-02. This work was funded by the 'Agence Nationale de la Recherche' grants ISblue (ANR-17-EURE-0015 and ANR IMPEKAB), LabexMER (ANR-10-LABX-19) and EC MSCA-ITN 2019 funding to the project MixITiN (grant 766327). We thank Tristan Biard, as well as three anonymous reviewers for critical comments.

Supplementary Material to Chapter II

Carbon and nitrogen to volume relationships for marine protist of the Rhizaria lineage (Radiolaria and Phaeodaria)

Joost Samir Mansour, Andreas Norlin, Natalia Llopis Monferrer, Stéphane L'Helguen, and Fabrice Not

Supplementary Methodology 1

Collodaria transcriptome 18S extraction

RNA extraction, cDNA synthesis and sequencing were performed by Genoscope, Paris. RNA reads obtained from Illumina HiSeq2500 sequencing of three Collodaria specimens, were trimmed using SortMeRna to retrieve ribosomal sequences, at GENOSCOPE, Paris. The reads were further cleaned using PrinSeq (SLIDINGWINDOW:4:5; MINQUALITY:5; TRIM-POLYA/T:40; MINLEN:25), and assembled using Trinity. Contigs were matched using NHMMER against a custom HMMR profile for Collodaria. The best NHMMER contig hits were extracted and verified using NCBI blast to be of Collodaria origin. Contig sequences were deposited under Genbank accession numbers MT985517-MT985527.

Acantharia / Collodaria DNA extraction, amplification and sequencing

Acantharia and Collodaria specimen for DNA extraction were collected in 96% EtOH. DNA extraction and purification were done using a Masterpure DNA purification kit (Epicentre-Illumina) following the manufacturers protocol. Single-cell Polymerase Chain Reaction (PCR) was done to amplify the 18S ribosomal DNA gene with specific primers for Acantharia, 'SA' and 'S879' as described in Decelle et al., 2012, and for Collodaria 'S81Col' and 'V9R' as in Biard et al., 2015. The 18S gene for Acantharia was amplified in a total volume of 25 µL with: 0.35 µM of each primer, MgCL2 1.5 mM, dNTPs mix 0.4 µM, buffer GoTaq 1x and 0.625u of GoTaq Flexi polymerase G2 (Promega). The reaction proceeded with the following PCR parameters: 5 min at 95 °C, followed by 35 cycles of 30 s denaturation at 95 °C, 30 s annealing at 53-55 °C, 2 min extension at 72 °C, with a final elongation step of 10 minutes at 72 °C. For the Collodaria sample the reaction mix was as follows in a total volume of 25 µL: 0.35 µM of each primer, 0.35 µM of each primer, DMSO 3%, and Mastermix Phusion GC (ref F532L, Finnzymes). PCR parameters for Collodaria were: 30 sec at 98 °C, followed by 35 cycles of 10 s denaturation at 98 °C, 30 s annealing at 55 °C and 30 s extension at 72 °C, with a final elongation step of 10 min at 72 °C. All positive amplification products have been purified using the kit Nucleospin PCR Clean-Up (Macherey-Nagel) and eluted with 22 µL of NE buffer. Sequencing was done using Big Dye Terminator Cycle Sequencing Kit (Life Technologies) by Macrogen. Sequence were cleaned using ChromasPro software, contig construction was only possible for one Acantharia sample (*i.e.* Ac-16). Sequences were deposited under Bioproject PRJNA658429.

Phylogenetic analyses

Sequences from published and single cell identified Acantharia (Decelle et al., 2012a, 2012c) and Collodaria (Biard et al., 2015) were retrieved from NCBI Genbank for reference tree construction.

Reference trees were built with both 18S and 28S rRNA sequences for a concatenated alignment tree representing the phylogenetic diversity as depicted in Decelle et al. 2012b (Acantharia) or Biard et al., 2015 (Collodaria). For Acantharia phylogenetic identification 12 Spumellaria sequence were used as outgroup and for Collodaria 6 Nassellaria sequences.

Sequences were aligned using MAFFT (Katoh et al., 2005) in AliView (Larsson, 2014). Positions with $\geq 20\%$ gaps in Acantharia and $\geq 30\%$ gaps in Collodaria sequences were removed using TrimAl v1.2 (Capella-Gutiérrez et al., 2009). The Acantharia concatenated sequence alignment consisted of 1629 nucleotides of the 18S region, and 561 nucleotides of the 28S region. For Collodaria the alignment was 1614 and 528 nucleotides of respectively the 18S and 28S regions. The concatenated alignments were analysed using the Maximum Likelihood (ML) methods (under the GTR+ Γ model and 4 rate categories) with RaxML v8.2.4 (Stamatakis, 2014). Node support was computed with 1000 bootstraps. Final tree was visualized and edited with FigTree version 1.4.4.

Supplementary Methodology 2

Equations from Hillebrand et al. (1999) were used for volume calculation of rhizarian samples. Rhizaria were assigned the standardized shapes as follows: truncated cone for Nassellaria; prolate spheroid for *Protocystis*, *Challengeria* and Spumellaria, and sphere for Aulacantha. Collodaria were assigned either sphere, spheroid or cylinder with two half spheres depending on the colony shape. The equations used are given below. All sample data and photographs are available at <http://dx.doi.org/10.17632/j9262jxgt8.1>

Truncated cone:

$$\frac{\pi}{12} \times h \times (r^2 + R \times r + R^2) = V$$

Sphere:

$$\frac{4}{3} \times \pi \times r^3 = V$$

$$4 \times \pi \times r^2 = A$$

Prolate Spheroid:

$$\frac{4}{3} \times \pi \times r^2 \times R = V$$

$$\frac{\pi \times 2r}{2} \times \left(2r + \frac{R^2}{\sqrt{R^2 - (2r)^2}} \operatorname{asin}\left(\frac{\sqrt{R^2 - (2r)^2}}{R}\right) \right) = A$$

Cylinder + two half spheres:

$$\left(\frac{4}{3} \times \pi \times r^3 \right) + (\pi \times r^2 \times (L - 2r)) = V$$

$$(4 \times \pi \times r^2) + (2\pi r \times (L - 2r)) = A$$

r = short radius (or top radius of a cone)

h = cone height

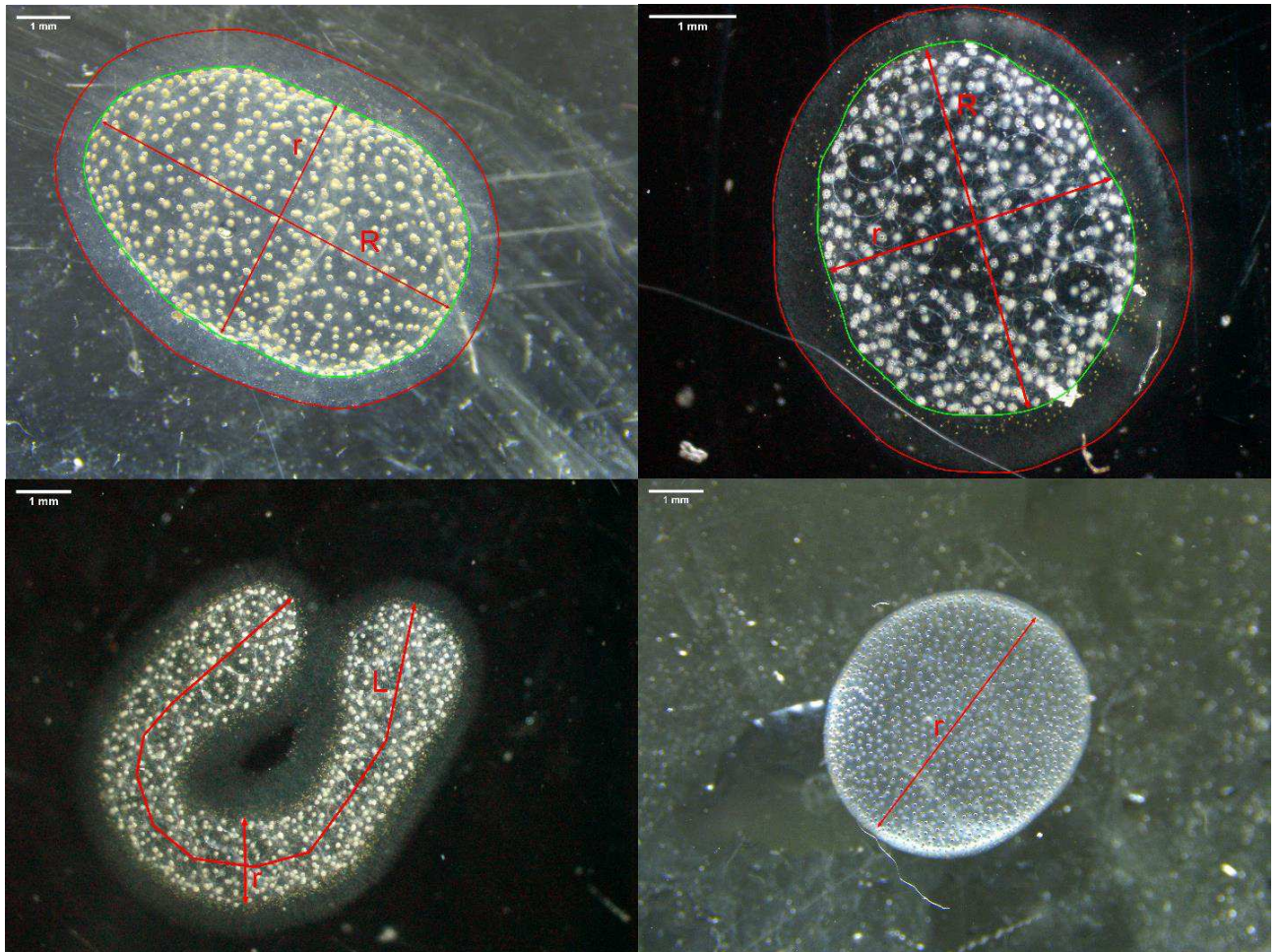
R = long radius (or base radius of a cone)

L = length of colony (used for cylinder + two half spheres, L = R)

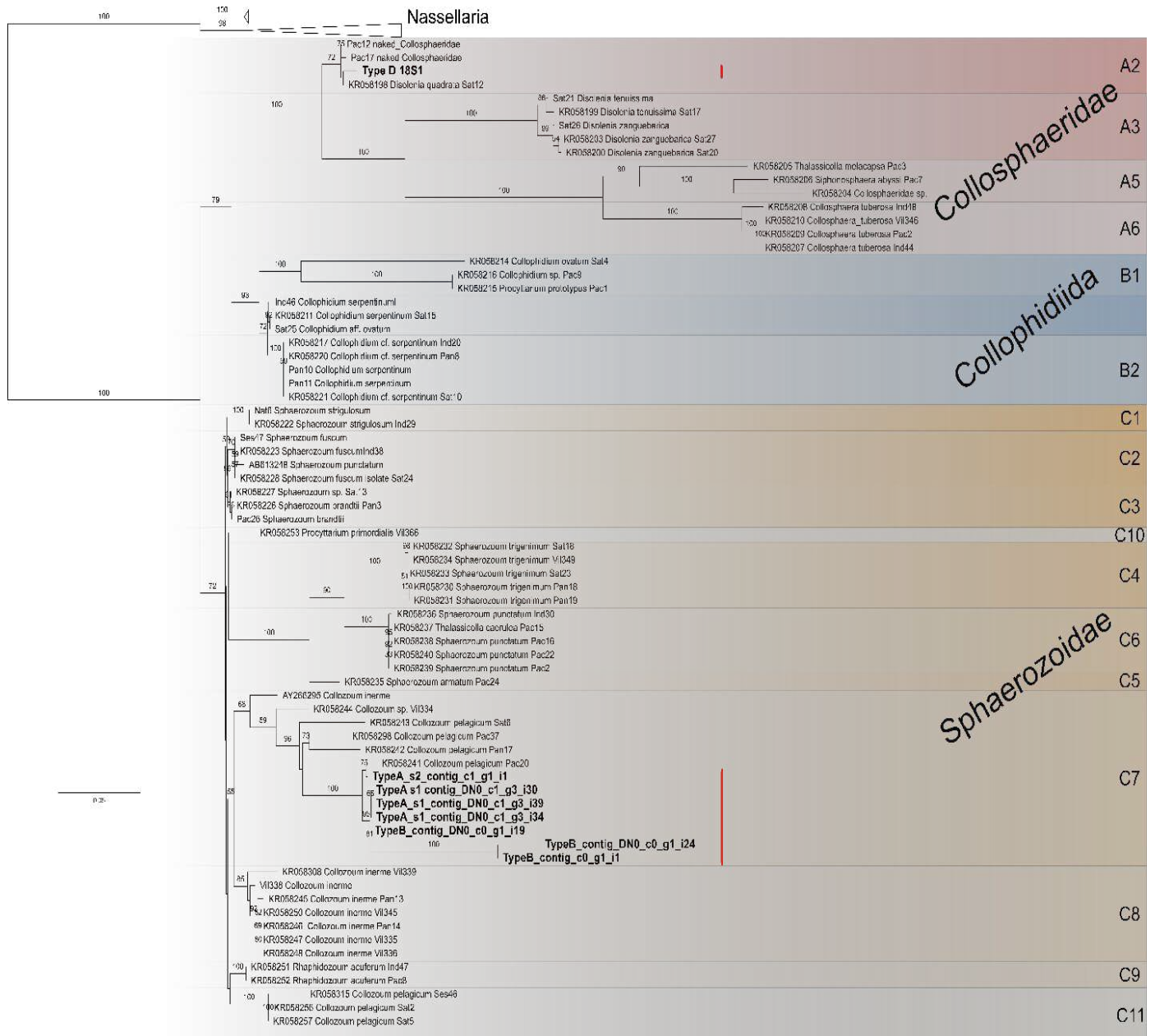
V = Volume

A = Surface area

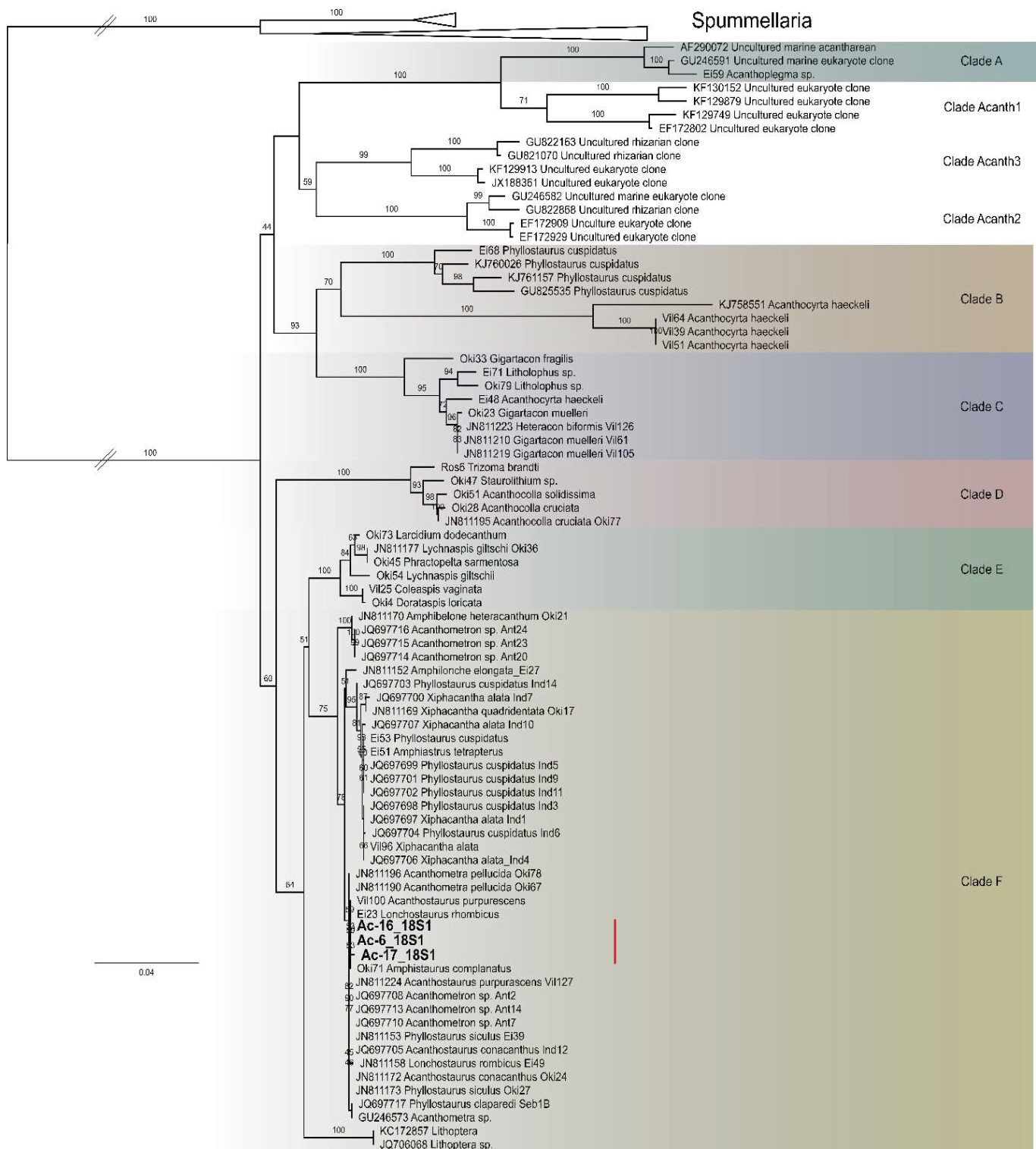
Supplementary Figures and Tables



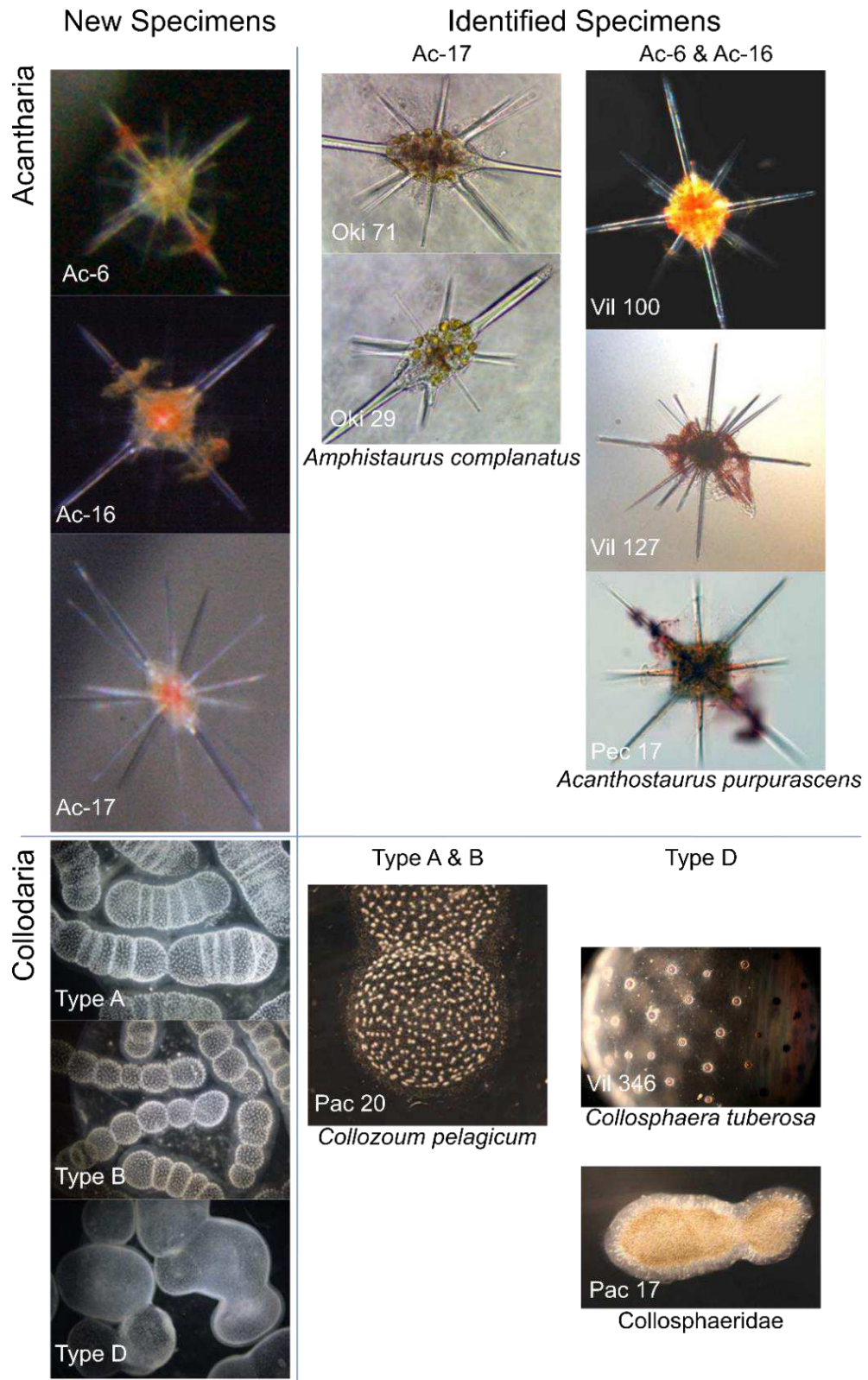
Supplemental Figure II-1. Selection of light microscopy photographs of Collodaria to illustrate the methodology for colonial volume measurements from images. The measurements done for use with the equations of **Supplementary Methodology 2** are illustrated with a red arrowed line. These lines are examples for illustrative purpose and do not consist of actual measurements, actual measurements were done of multiple lines to acquire an average and thus more accurate estimate. For Collodaria colonies these measurements thus omit the extracellular matrix, and will allow calculation of the colonial volume as within the green outline (top pictures). The extracellular matrix of the Collodaria is indicated between red and green outlines (top photos). Note that the extracellular matrix can be variable with physiological state, and is also not captured using in-situ photography like UVP5 (Biard and Ohman, 2020).



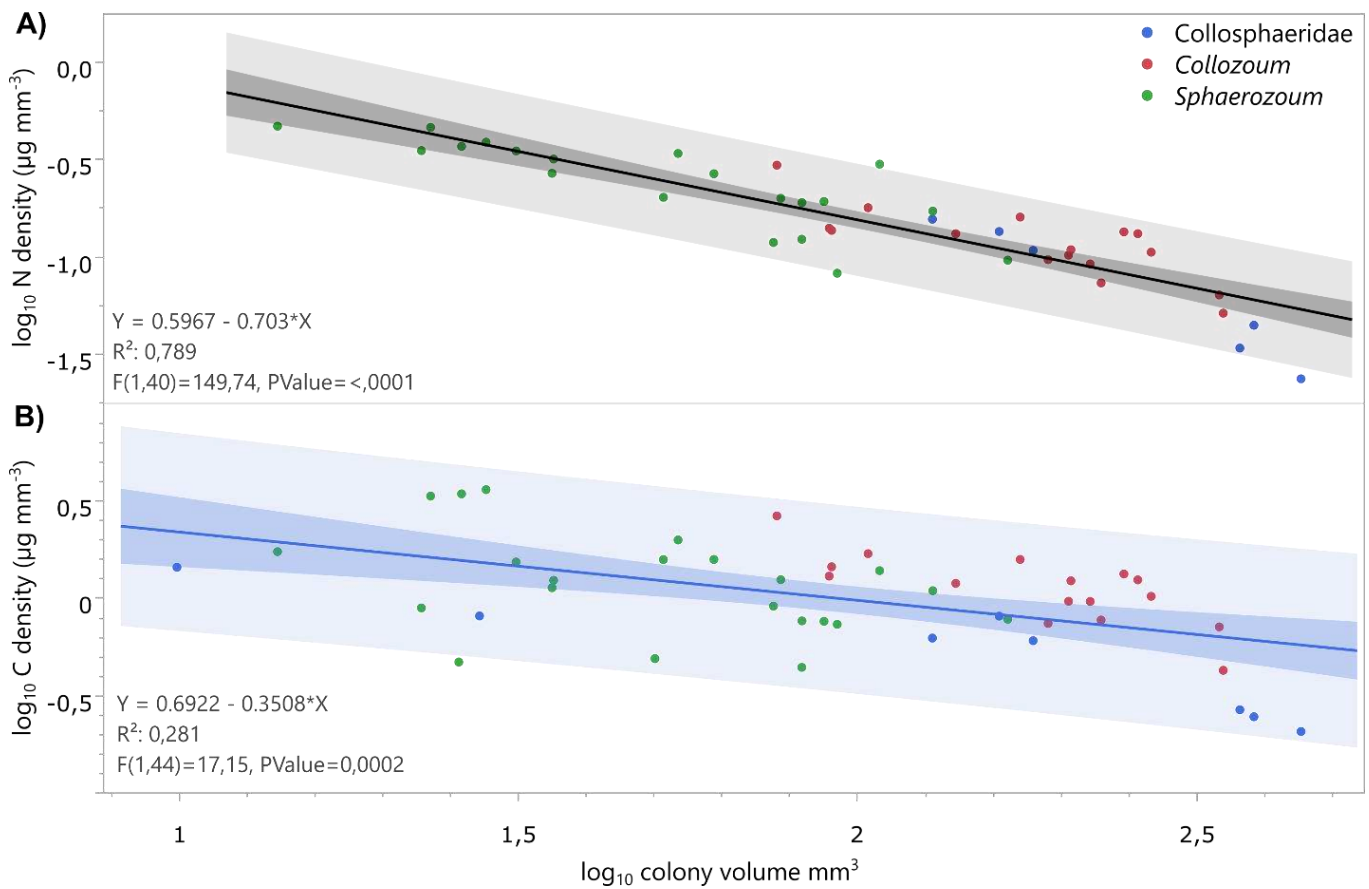
Supplemental Figure II-2. Phylogenetic tree for Collozaria identification. The molecular phylogeny of Collozaria was inferred by concatenation of 18S and 28S rRNA genes, and obtained by a Maximum Likelihood reconstruction method using the GTR + Γ model of sequence evolution on an alignment of 81 sequences and 2140 aligned nucleotide positions. Only RAxML bootstrap values (1000 replicates) higher than 50% are shown. The new barcode and contig sequences extracted from our transcriptome data are highlighted in bold and indicated by red lines on the right of them. The clade and sub-clade naming and collaring follow the nomenclature system as in Biard et al. 2015. The tree has been rooted using *Nassellaria* sequences.



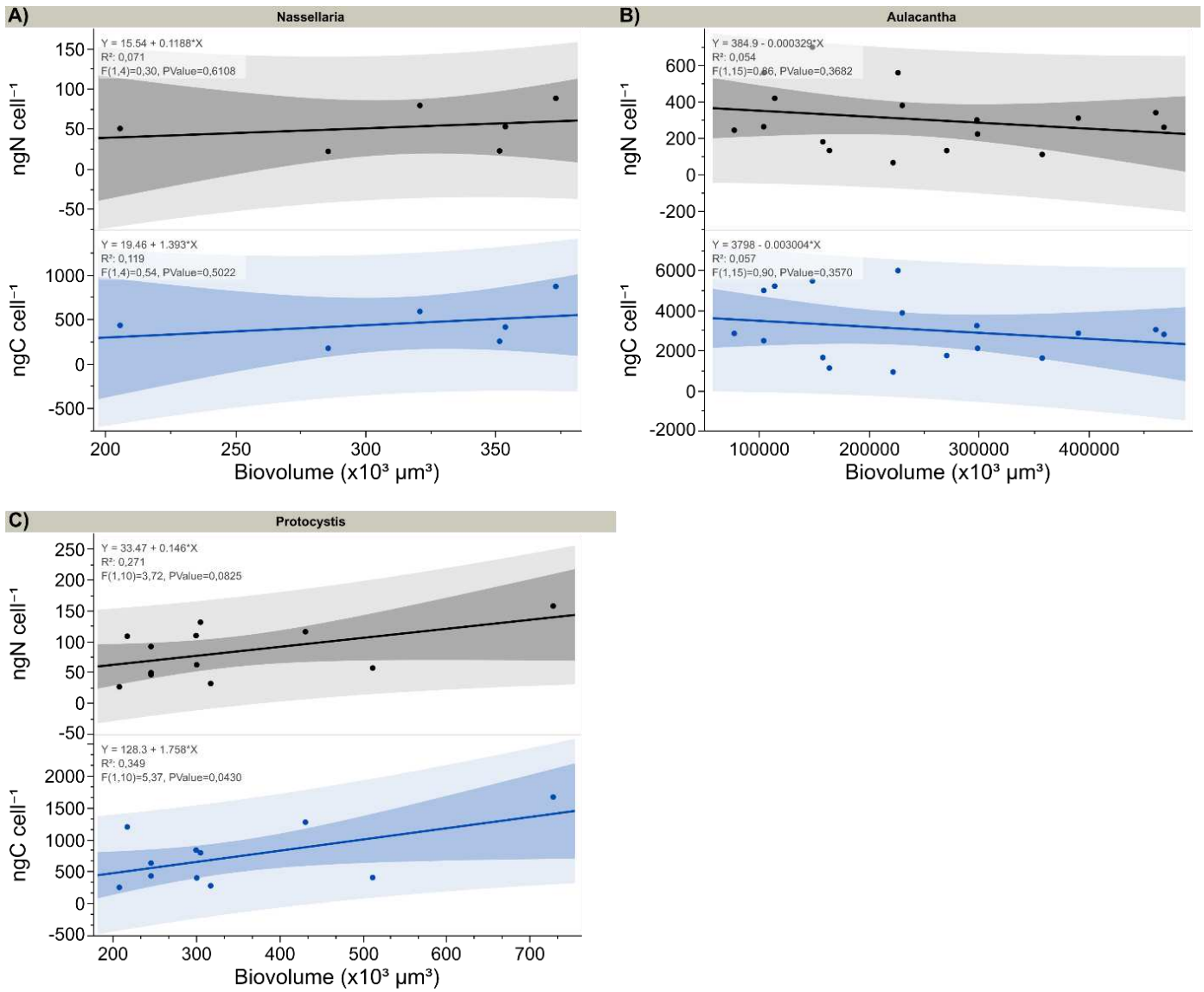
Supplemental Figure II-3. Phylogenetic tree for the Acantharia identification. The molecular phylogeny of Acantharia was inferred by concatenation of 18S and 28S rRNA genes, and constructed by a Maximum Likelihood reconstruction method using the GTR + Γ model on an alignment of 94 sequences with 2190 positions. Only RAxML bootstrap values (1000 replicates) higher than 40% are shown. Our new 18S barcode sequences are highlighted in bold and indicated with a red line on the right of them. The clade and sub-clade naming and colouring are as in Decelle et al. 2012. The tree has been rooted using Spumellaria sequences. Branches with a double barred symbol have been reduced in length for clarity.



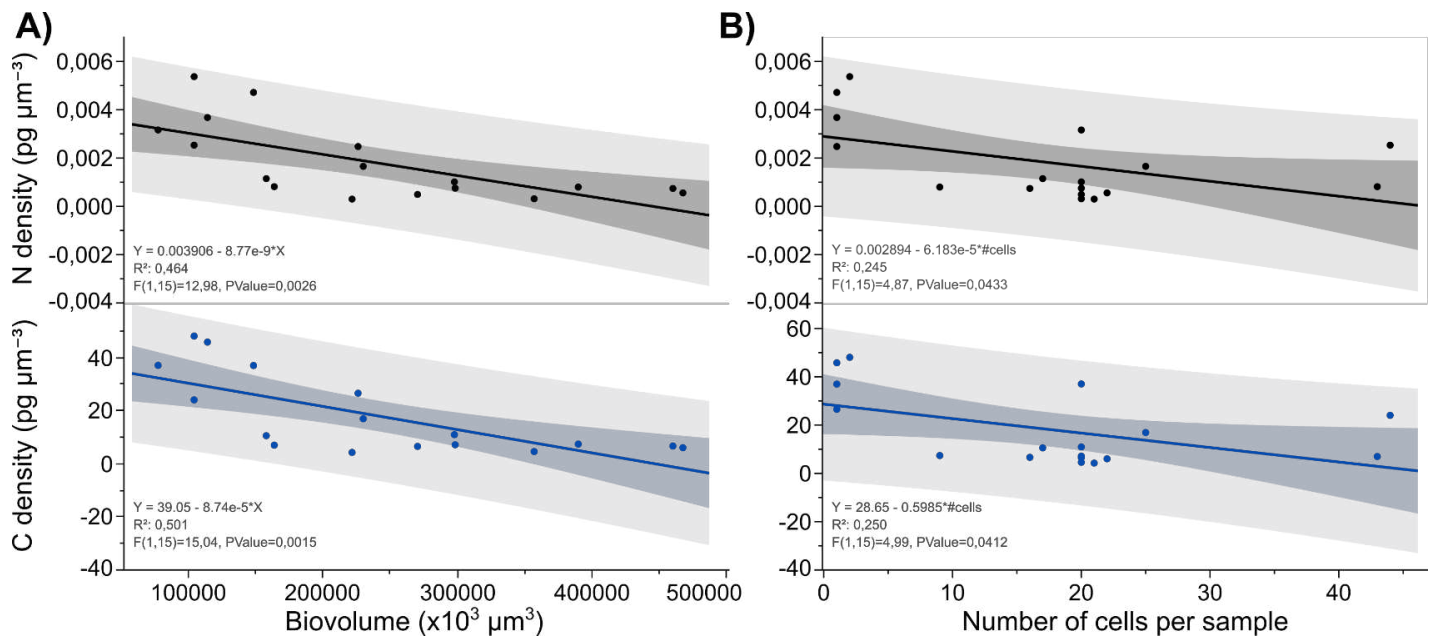
Supplemental Figure II-4. Light microscopy photographs of Acantharia and Collodaria samples (left), compared to photographs of phylogenetically closely related and previously identified specimens (right) with location number as in the original study and available at <http://renkan.sb-roscoff.fr>.



Supplemental Figure II-5. Collodaria nitrogen and carbon density to colony volume. Graphs show \log_{10} transformed data, \log_{10} (volume) in mm^3 to \log_{10} (biomass) in $\mu\text{g N mm}^{-3}$ (A) or $\mu\text{g C mm}^{-3}$ (B). The different Collodaria genera investigated in this study are indicated by colour, Collosphaeridae (blue), *Collozoum* (red), and *Sphaerozoum* (green). The line of best fit is shown as a solid black/blue line with the 95% confidence interval of the fit in dark grey/blue shading and 95% prediction interval in lighter grey/blue shading. Furthermore, the regression statistics are shown for each graph. The conversion of the in \log_{10} expressed regression equation is outlined in the Methodology.



Supplemental Figure II-6. Nassellaria (A), *Aulacantha* (B) and *Protocystis* (C) nitrogen and carbon content to biovolume. The line of best fit is shown as a solid black/blue line with the 95% confidence interval of the fit in dark grey/blue shading and 95% prediction interval in lighter grey/blue shading. The regression statistics are shown for each graph.



Supplemental Figure II-7. *Aulacantha* nitrogen and carbon density to biovolume (A), and to number of cells per sample (B). The line of best fit is shown as a solid black/blue line with the 95% confidence interval of the fit in dark grey/blue shading and 95% prediction interval in lighter grey/blue shading. The regression statistics are shown for each graph.

Supplemental Table II-1. Extended table summarising carbon, nitrogen and volume data of the studied Rhizaria taxa. The total number of samples analysed (n) differs for nitrogen and carbon content because nitrogen mass was not always sufficient to analyse. The table is cut in width to fit the page, the first column is repeated for the second part of the table. Full raw data table is accessible at <http://dx.doi.org/10.17632/j9262jxgt8.1>.

	total # cells or cc	Colony carbon density ($\mu\text{g C mm}^{-3}$)					central capsules density (cc mm^{-3})		Carbon density per cell or central capsule ($\mu\text{g C mm}^{-3}$)					Nitrogen density per cell or central capsule ($\mu\text{g N mm}^{-3}$)				
		n	mean	sd	min	max	mean	sd	n	mean	sd	min	max	n	mean	sd	min	max
Collosphearidae	15034	8	0,63	0,41	0,21	1,45	10,35	6,81	7	0,17	0,08	0,07	0,29	5	0,03	0,03	0,01	0,07
<i>Collozoum</i>	23396	16	1,21	0,52	0,43	2,66	8,26	3,17	16	0,14	0,03	0,09	0,20	16	0,01	0,00	0,01	0,02
<i>Sphaerozoum</i>	13873	22	1,42	0,94	0,44	3,63	13,77	10,01	17	0,14	0,04	0,08	0,22	15	0,03	0,01	0,01	0,05
all colonial Collodaria	52303	46	1,21	0,78	0,21	3,63	11,26	7,98	39	0,14	0,05	0,07	0,29	35	0,02	0,01	0,01	0,07
<i>Thalassicolla</i>	16								1	0,19				1	0,03			
Spumellaria	74								2	0,33	0,13	0,24	0,42	2	0,05	0,03	0,02	0,07
Nassellaria	241								6	1,47	0,73	0,62	2,34	6	0,17	0,09	0,07	0,25
Acantharia (F3)	540								18			0,04*	0,94*					
<i>Aulacantha</i>	302								17	0,02	0,02	0,00	0,05	17	0,00	0,00	0,00	0,01
<i>Protocystis</i>	414								12	2,22	1,28	0,80	5,54	12	0,26	0,13	0,10	0,50
<i>Challengeria</i>	48								2	0,24	0,11	0,16	0,32	2	0,01	0,00	0,01	0,02

	cell or central capsule diameter			volume (mm^3)			Carbon (ng C cell^{-1})					Nitrogen (ng N cell^{-1})					C:N			
	n	mean	sd	n	mean	sd	n	mean	sd	min	max	n	mean	sd	min	max	mean	sd	min	max
Collosphearidae	7	0,09	0,03	6	0,000662	0,000657	8	75,43	74,12	32,73	251,40	6	9,10	7,68	4,17	24,54	6,30	1,73	4,00	8,77
<i>Collozoum</i>	16	0,13	0,01	16	0,001079	0,000193	16	148,01	37,29	90,31	215,85	16	15,35	4,07	8,49	22,73	9,72	0,98	7,69	11,33
<i>Sphaerozoum</i>	17	0,12	0,03	17	0,001171	0,000783	22	152,90	130,46	15,74	597,91	20	29,66	22,00	9,56	100,84	5,89	2,13	2,54	9,33
all colonial Collodaria	40	0,12	0,03	40	0,001032	0,000611	46	137,73	100,50	15,74	597,91	42	21,27	17,53	4,17	100,84	7,41	2,49	2,54	11,33
<i>Thalassicolla</i>	16	572,63	131,01	16	0,114242	0,079488	1	21577,46					3723,60				5,79			
Spumellaria		0,16	0,04	2	0,002853	0,002157	2	799,38	345,79	554,87	1043,89	2	94,96	5,54	91,04	98,87	8,33	3,16	6,09	10,56
Nassellaria		0,08	0,01	6	0,000315	0,000062	6	458,45	249,26	178,40	872,41	6	52,97	27,64	22,39	88,61	8,79	1,43	7,43	11,16
Acantharia (F3)							18	168,59	151,15	46,368	684,06									
<i>Aulacantha</i>		0,73	0,12	17	0,240640	0,123726	17	3075,48	1559,57	943,03	6003,69	17	305,70	174,83	66,70	700,34	10,61	2,00	7,84	14,59
<i>Protocystis</i>		0,10	0,01	12	0,000338	0,000151	12	721,92	450,34	256,87	1670,20	12	82,80	42,45	26,95	158,09	8,61	1,76	6,06	11,03
<i>Challengeria</i>		0,18	0,07	2	0,004246	0,003728	2	1226,84	1360,87	264,56	2189,12	2	64,89	61,29	21,55	108,23	16,25	5,62	12,28	20,23

*estimated assuming a cell size of 70 and 200 μm for min and max, see text for further explanation

Supplemental Table II-2. Comparison of prediction estimates for total colony C content. Four prediction methods are compared by calculations of the Mean Absolute Percentage Error (MAPE). The first prediction is based on the average carbon content being 137.73 ng per cell (central capsule). The second prediction is based on the product of the mean colonial C density of 1.21 $\mu\text{g C mm}^{-3}$ and the colony's total volume. Thirdly, the carbon to central capsule biovolume equation as proposed in this study (Eq 6 of the main text) is used in combination with central capsule counts to estimate colonial C content. The last prediction is based on the carbon to colonial volume equation as proposed in this study (Eq 7 of the main text). Samples used here were not used in the regression analysis to establish the C:vol equations.

Sample ID	Measurements						Method 1: Prediction using mean C cc^{-1}				Method 2: Prediction using mean colony C biomass density				Method 3: Prediction using cc equation (eq6) and cc counts				Method 4: Prediction using colony equation (eq7)						
	total colony C	cc count	cc vol (μm^3)	log10 vol	colony volume (mm^3)	log10 colony volume	Total $\mu\text{g C}$		MAPE		Total $\mu\text{g C}$		MAPE		Total $\mu\text{g C}$		MAPE		Total $\mu\text{g C}$		MAPE				
	(μg)						predicted	obs-pred	calc			predicted	obs-pred	calc			predicted	obs-pred	calc			predicted	obs-pred	calc	
200l	27,90	193	1081069,02	6,03	11,48	1,06	26,58	1,32	0,05	RMSE	13,89	14,01	0,50	RMSE	29,19	-1,29	0,046	RMSE	24,00	3,90	0,14	RMSE			
201l	43,66	287	1002841,67	6,00	18,53	1,27	39,53	4,14	0,09	14,04	22,42	21,24	0,49	17,04	39,99	3,68	0,084	7,90	32,76	10,91	0,25	12,07			
202l	29,39	215	753520,53	5,88	15,64	1,19	29,61	-0,23	0,01	MAPE	18,92	10,46	0,36	MAPE	21,79	7,60	0,259	MAPE	29,34	0,05	0,00	MAPE			
203d	44,28	174	1862684,08	6,27	8,44	0,93	23,97	20,32	0,46	64,16	10,21	34,07	0,77	55,69	47,04	-2,76	0,062	37,12	19,66	24,62	0,56	45,17			
204d	27,36	180	668848,74	5,83	3,54	0,55	24,79	2,57	0,09		4,28	23,09	0,84		15,92	11,45	0,418		11,18	16,19	0,59				
205d	24,21	130	635807,04	5,80	5,47	0,74	17,90	6,31	0,26		6,62	17,59	0,73		10,84	13,37	0,552		14,84	9,37	0,39				
209l	9,47	118	306213,39	5,49	1,08	0,03	16,25	-6,78	0,72		1,31	8,16	0,86		3,91	5,56	0,587		5,18	4,29	0,45				
210l	11,35	220	192534,94	5,28	17,04	1,23	30,30	-18,95	1,67		20,62	-9,27	0,82		3,48	7,87	0,693		31,02	-19,67	1,73				
211l	16,33	219	318800,52	5,50	3,96	0,60	30,16	-13,83	0,85		4,80	11,54	0,71		7,68	8,65	0,530		12,03	4,30	0,26				
212d	8,29	155	319180,42	5,50	6,82	0,83	21,35	-13,06	1,57		8,25	0,04	0,00		5,45	2,85	0,343		17,12	-8,83	1,06				
213d	8,97	137	249499,35	5,40	5,25	0,72	18,87	-9,90	1,10		6,35	2,61	0,29		3,36	5,61	0,625		14,45	-5,48	0,61				
214d	10,78	169	186106,74	5,27	3,30	0,52	23,28	-12,50	1,16		3,99	6,79	0,63		2,51	8,27	0,767		10,69	0,09	0,01				
57n	40,50	393	847385,45	5,93	40,65	1,61	54,13	-13,62	0,34		49,19	-8,68	0,21		45,44	-4,94	0,122		54,55	-14,05	0,35				
58n	34,80	374	823592,47	5,92	11,61	1,06	51,51	-16,71	0,48		14,05	20,75	0,60		41,89	-7,09	0,204		24,19	10,61	0,30				
59n	43,16	484	511782,60	5,71	10,91	1,04	66,66	-23,51	0,54		13,20	29,95	0,69		31,21	11,95	0,277		23,23	19,93	0,46				
60n	28,99	394	393107,15	5,59	14,10	1,15	54,27	-25,27	0,87		17,06	11,93	0,41		18,28	10,71	0,369		27,44	1,56	0,05				

RMSE = Root Mean Square Error

MAPE = Mean Absolute Percentage Error

Chapter III

Carbon and nitrogen uptake through photosynthesis and feeding by photosymbiotic Acantharia

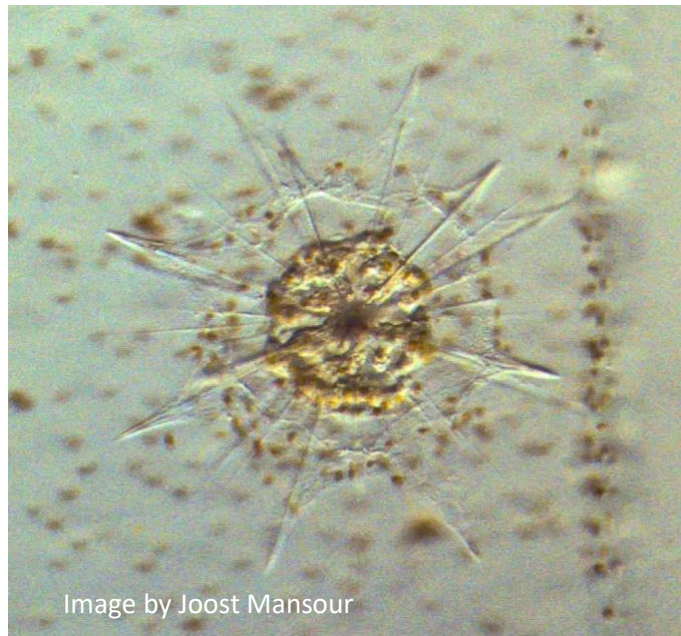


Image by Joost Mansour

“We cannot get round photosynthesis. We cannot say I am not going to give a damn about plankton. All these tiny mechanisms provide the preconditions of our planetary life. To say we do not care is to say in the most literal sense that “we choose death.”

—Barbera Ward

Brief Context

Mixoplankton are found to be major components of the oceanic ecosystem. This trophic mode combining both phototrophy and phagotrophy might be proposed to be the norm among protists, instead of the exception. The combination of both producer and consumer in a single organism changes biogeochemical and trophic dynamics involving these organisms at the base of the food chain, thereby it changes the way that we understand and thus simulate and model processes from harmful algal blooms, fisheries or global climate change. To be able to reflect this in simulations and models there is a need for numerical data of rates of processes involving the nutrient flow in these mixoplankton, and their reliance on each trophic mode. Yet, the significance of most mixoplankton activity and indeed their physiology is not known. A major hurdle hereby are the difficulties in culturing them. Acantharia (Radiolaria) are ubiquitous oceanic protists, many of which are mixoplankton by endosymbiotic relation. Here we aimed to produce such numerical data of phototrophy and phagotrophy for unculturable endosymbiotic mixoplanktic Acantharia (Radiolaria). Like for many mixoplankton, to study trophic reliances for these endosymbiotic Acantharia it is mandatory to work with freshly isolated specimens. We achieved rate measurements for Acantharia by using isotopic incubations, as well as used traditional techniques and fluorescent labelling to qualitatively assess prey uptake.

Carbon and nitrogen uptake through photosynthesis and feeding by photosymbiotic Acantharia

JS Mansour¹, C Leroux², PJ Hansen³, F Not¹

¹ CNRS and Sorbonne University, UMR7144, Adaptation and Diversity in Marine Environment (AD2M) Laboratory, Ecology of Marine Plankton Team, Station Biologique de Roscoff, Place Georges Teissier, Roscoff, France

² CNRS and Sorbonne University, FR2424, Corsaire/Metabomer core facility, Station Biologique de Roscoff, Place Georges Teissier, Roscoff, France

³ Marine Biological Section, University of Copenhagen, Helsingør, Denmark

1. Introduction

Mixotrophy is a widespread trophic mode that combines heterotrophy and autotrophy in order to acquire nutrients and energy (Selosse et al., 2017). Mixoplanktivory in planktic protists is specifically defined as a nutritional strategy that combines phagotrophy and phototrophy (Flynn et al., 2019). The perceived relevance of mixoplanktivory to the marine food web and nutrient cycles has been increasing in the last years, owing to more studies on the ecophysiology of mixoplanktic organisms. It is now recognised that mixoplankton are a common occurrence (Leles et al., 2017; Faure et al., 2019; Schneider et al., 2020a). Mixoplankton could provide new evolutionary insights as intermediates of permanent plastids (Sibbald and Archibald, 2020; Mansour and Anestis, 2021). Ecologically, mixoplankton can form an important (alternative) path for nutrient transfer at the base of the food web (Caron, 2016). To improve predictive models, mixoplanktic organisms have explicitly been incorporated into ecosystem models of aquatic environments (Ward and Follows, 2016; Ghyoot et al., 2017a, 2017b).

Mixoplanktonic organisms have been categorized by Mitra et al., (2016) as (1) constitutive mixoplankton (CM) that have innate photosynthetic machinery, and (2) non-constitutive mixoplankton (NCM) that use photosynthetic machinery from other photosynthetic organisms. Non-constitutive mixoplankton can be subdivided into: 1) generalist non-constitutive mixoplankton (GNCM) that can acquire their photosynthetic machinery from different prey sources; 2) plastidic-specialist non-constitutive mixoplankton (pSNCM) that can only use the plastids (and sometimes also other cell organelles) from a specific species or genera of prey, and 3) endosymbiont-containing specialist non-constitutive mixoplankton (eSNCM) that harbour entire photosynthetic algae as endosymbionts to account for their photosynthetic ability. Their symbiotic partner exploits light and carbon dioxide to produce photosynthates, and these photosynthates might be transferred and used by the host, as is seen in many photosymbiotic systems (Trench, 1979; Yellowlees et al., 2008).

The acquired ability to photosynthesise can give all NCM a competitive advantage over pure phototrophs or heterotrophs since they can supplement their metabolic needs with either nutritional mode. This will be of particular relevance when, for example, prey concentrations are low (Schoener and McManus, 2017). The increase in gross growth efficiency gained from photosynthesis by NCM will be reflected on higher trophic levels and is therefore crucial in the parametrisation of carbon budgets in planktonic ecosystem models.

Non-constitutive mixoplankton includes many different taxa with diverse ecophysologies. Hence, the various physiological characteristics representing this diversity have to be taken into consideration. The contribution of each nutritional mode to the total metabolism is likely subject to great variation within 'mixoplankton', but our knowledge of the metabolic budgets of NCM is limited. The pSNCM typically receives a substantial amount of carbon through photosynthesis. For example, the pSNCM ciliate, *Mesodinium rubrum* has been shown to obtain up to 94% of its daily carbon uptake through photosynthesis and can live as a complete autotroph for approximately 4 generations in the absence of prey (Smith and Hansen, 2007). Oppositely, the GNCM ciliate *Strombidium* spp. cannot sustain itself on photosynthesis alone, but obtains at most ~20–50% of total carbon uptake through photosynthesis, under prey depleted conditions (Schoener and McManus, 2017; Maselli et al., 2020; Hughes et al., 2021). However, very little is known about the role of endosymbionts in eSNCM. Some eSNCM colonial Radiolaria (Collodaria) have previously been hypothesized to use photosynthesis merely for subsistence, whereas nutrients for growth would be obtained through predation; net hourly photosynthesis would constitute at a maximum only 0.4% of the radiolarian's carbon content (Swanberg, 1983). In stark contrast, the spumellarian Radiolaria *Physematium muelleri* was estimated to obtain more than half of its carbon by photosynthesis (Swanberg et al., 1986). Likewise, for green *Noctiluca* photosynthesis has been shown to contribute ~50% of the carbon uptake used for growth in the light (Hansen et al., 2004).

Endosymbiotic Acantharia (Radiolaria) are prominent planktic members of the epipelagic surface community (Michaels, 1988; Biard and Ohman, 2020). In the upper 20 meters (where Acantharia are most abundant) of the central North Pacific Ocean, Acantharia have been estimated to account for up to 4 % of the total primary production or even 20% of the surface production by virtue of their endosymbionts (Michaels, 1988, 1991). However, like for most NCM, very little data on the contribution of photosynthesis to the carbon budgets of endosymbiotic Acantharia is available in the literature and even less (to none) related to prey uptake. Likewise, little is known about how the availability of dissolved inorganic nutrients influences acantharian physiology. A recent gene expression study of a solitary Collodaria (Radiolaria) suggests that they cannot take up nitrate (they lack the transporters to do so), but can use ammonium (Liu et al., 2019). One of the main reasons for this lack of quantitative data is the inability in keeping laboratory cultures.

A study by Swanberg and Caron (1991) microscopically investigated the prey content of Acantharia and other Radiolaria. Although most (60%) of collected Acantharia had no detectable prey; the identifiable presumed prey consisted (numerically) mostly of tintinnids, other (*i.e.* non-oligotrich) ciliates, and other protozoa including smaller Radiolaria. If accounting for an estimate of carbon biomass, then copepods contributed to 40% of the acantharian consumption. Further qualitative accounts of radiolarian feeding behaviour show a general preference for zooplankton over algal prey (Anderson et al., 1984 and

references therein). *Spongodymus* sp., a large 800 µm Spumellaria (Radiolaria), was shown to be able to consume 791 cells of *Isochrysis galbana* (haptophyte), 466 cells of *Amphidinium carterae* (dinoflagellate), or 0.5 *Artemia* spp nauplius larvae (crustacean) per hour in the laboratory (Anderson et al., 1984). Quantitative estimates of acantharian grazing rate are, however, not available.

To gain insights into the reliance of Acantharia on prey ingestion versus symbiotic photosynthesis we measured photosynthetic carbon uptake using stable isotopes under different conditions of nitrogen availability (nitrate (NO₃⁻) or ammonium (NH₄⁺)). Coupled with this, we estimated feeding rates on potential prey using calculations based on prey disappearance, as well as tested this with (stable isotopic and fluorescent) labelled prey. To qualitatively explore acantharian feeding, potential prey was fluorescently labelled. Additionally, photosynthetic carbon uptake of free-living symbionts was also measured, to compare the change in physiological rates between *in-hospite* and *ex-hospite* symbionts.

2. Methodology

2.1. Experimental designs for photosynthesis and grazing

2.1.1 Study specimens

Symbiotic Acantharia (molecular clade F, see Supplemental Material) were collected daily around 9 AM, by gentle plankton net tows along the sub-surface in the bay of Villefranche (Mediterranean Sea, Villefranche-sur-Mer, 43°41'10" N, 7°18'50" E, France) as described previously (Mansour et al., 2021c). Acantharia specimens for photosynthesis and feeding experiments were collected during April and May 2020. For both instances, specimens have been prepared as described in (Mansour and Not, 2021: [dx.doi.org/10.17504/protocols.io.bqvrnw56](https://doi.org/10.17504/protocols.io.bqvrnw56)). Briefly, following collection, individual cells were promptly isolated under a microscope and deposited in 0.22 µm-filtered seawater (FSW). Isolated specimen were incubated for an hour and transferred again to fresh filtered seawater, this was repeated three times before experimental incubations. This procedure allows for self-cleaning of particles attached to the cells and dilution to achieve extinction of any organisms accidentally taken with during isolation.

Cultures of *Isochrysis galbana* (RCC178), *Phaeocystis cordata* (RCC1383), *Synechococcus* sp. (RCC307), and *Effrenium voratum* (formerly *Symbiodinium voratum*, RCC1521) were obtained from the Roscoff Culture Collection, France (**Supplemental Table III-1**). *Synechococcus* was maintained in 'Red Sea medium' as described in <https://www.protocols.io/view/pcr-s11-red-sea-medium-sz3ef8n>. The other species were grown in K/5 medium consisting of 0.22 µm filter-sterilised and pasteurised aged natural seawater with a salinity of 35‰, and a dissolved inorganic carbon (DIC) concentration of 24.65 µg C mL⁻¹. Seawater was obtained offshore near Roscoff (Lat 48°46'18" N, Long 3°58'6" W). Added macronutrients consisted of 288 µM NO₃; 5 µM NH₄ and 18 µM PO₄ (K-medium preparation is described in <https://dx.doi.org/10.17504/protocols.io.7bxhipn>; full K medium composition in **Supplemental Table III-2**). Stock cultures were maintained in light of 125 µmol photons m⁻² s⁻¹ with a light-dark cycle of 16:8 h and grown at 20 °C. Aliquots of dense algal stock culture were diluted in FSW, with no addition of nutrients, before being used as prey for Acantharia.

2.1.2 Acantharian photosynthesis

Experiments were designed to determine rates of photosynthetic assimilation of inorganic carbon and nitrogen in symbiotic Acantharia (see a conceptual drawing of the experiment in **Figure III-1**). The used specimens all harbour intact photosynthetic symbionts which provide the hosts with photosynthates (Anderson, 1983; Yellowlees et al., 2008; Decelle et al., 2012b; Probert et al., 2014). Seawater was collected from the bay of Villefranche-sur-Mer and filtered (0.22 μm) for experimental incubations. The concentration and isotopic ratio of dissolved inorganic carbon in the seawater was measured using Delta V Plus mass spectrometer and Gas Bench II at the IRMS platform in Brest, France.

Acantharia were transferred to 6-well plates containing 10 mL FSW enriched with $\text{NaH}^{13}\text{CO}_3$ (99 % ^{13}C , Eurisotop) and either $^{15}\text{NH}_4\text{Cl}$ (99 % ^{15}N , Eurisotop) or $\text{Na}^{15}\text{NO}_3$ (98 % ^{15}N , Eurisotop). Each treatment was accompanied by a control incubation containing non-enriched nutrients in the same concentrations (natural medium incubations). The experimental treatments were as follows:

- Treatment 1 used $\text{NaH}^{13}\text{CO}_3$ at 10 μM ;
- Treatment 2 used $\text{NaH}^{13}\text{CO}_3$ at 10 μM and $^{15}\text{NH}_4\text{Cl}$ at 0.3 μM ;
- Treatment 3 used $\text{NaH}^{13}\text{CO}_3$ at 10 μM and $\text{Na}^{15}\text{NO}_3$ at 0.5 μM ;
- Treatment 4 was performed in complete darkness with $\text{NaH}^{13}\text{CO}_3$ at 10 μM and $^{15}\text{NH}_4\text{Cl}$ at 0.3 μM , this treatment was not accompanied by a similar incubation using non-enriched nutrients.

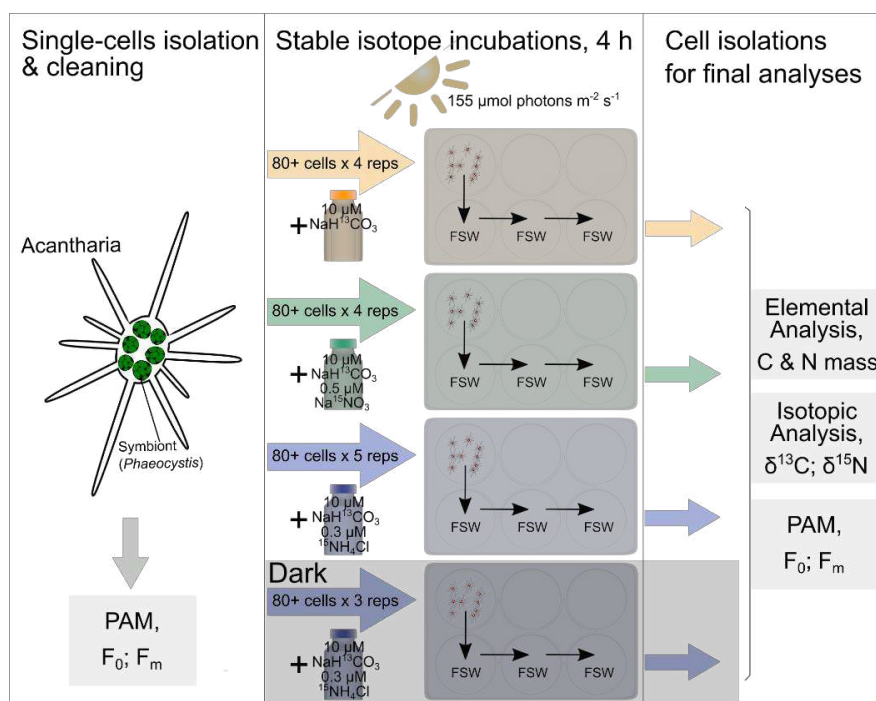


Figure III-1. Conceptual drawing of experiments to assess carbon and nitrogen uptake rates. Pulse Amplitude Modulated (PAM) fluorometer measurements were performed on several Acantharia each day before incubations. Each illuminated treatment was accompanied by a similar incubation using non-enriched nutrients, which is not depicted.

Specimens were incubated for 4 h in an incubator set at seawater temperature (16.5 °C, April 2021), with a 16:8 h light:dark cycle at 150-160 $\mu\text{mol photons m}^{-2} \text{s}^{-1}$. After the incubation 60 to 100 cells were manually transferred through three series of clean filtered seawater and finally deposited one by one on a pre-combusted (450 °C for 4 h) GF/F filter (25 mm, Whatman). The volumes of medium used to transfer all Acantharia were kept track of, and analytical blanks were made by wetting a separate GF/F filter with an equal amount of seawater leftover from the incubation. All filters were dried at 60 °C for a minimum of 24 h and subsequently kept in sealed containers in the dark before isotopic analysis. Experiments were

always initiated at the same time of day (*i.e.*, between 15:00 and 16:00) to avoid any confounding effects owing to circadian rhythms.

Additionally, several Acantharia were reserved for measurements of photochemical efficiency before and after incubation. This provided us an indication of the symbionts, and thereby presumably the holobionts, their general health, and allowed insights into the treatments where photosynthetic efficiency was determined.

2.1.3 Symbiont (Phaeocystis) photosynthesis

Photosynthetic rates of the free-living state (*i.e.* in algal culture, not in symbiosis) of *Phaeocystis cordata* (RCC1383) were measured from cultures. Prior to the experiments cultures were grown in 50 mL flasks, partially submerged in an aquarium with a water temperature of 20 °C, a light:dark cycle 14:10 h at a photon irradiance of 150-170 $\mu\text{mol photons m}^{-2} \text{s}^{-1}$ as measured in the water. The aquarium with culture flasks was placed on a glass table with light provided from below. Light was provided by cool white fluorescent tubes (OSRAM 58W, 840) and photon irradiance was measured using a light meter equipped with a spherical quantum sensor (ULM & US-SQS/L, Walz GmbH, Germany).

Cultures in exponential growth phase (as estimated by daily flowcytometric cell counts) were used for photosynthesis measurements employing the ^{14}C methodology, see details below. Different incubations were performed for a duration of 0, 3, 6, 8 and 24 h. For each incubation-time, one set of triplicates was incubated in the light, while the other was kept in complete darkness to compensate for passive incorporation of the radioisotope.

Simultaneous with the ^{14}C experimental procedure aliquots of the culture were taken for cell enumeration and algal chlorophyll *a* (Chl*a*) content measurements. Total dissolved inorganic carbon concentrations were measured on 25 mL of the medium used for the experiments using a Shimadzu TOC-L analyser.

2.1.4 Acantharian grazing

To measure the contribution of prey ingestion to the acantharian metabolism, experiments were set up with different potential prey algal cultures (see a conceptual drawing of the experiment in **Figure III-2**). In triplicate, Acantharia (15 to 25 cells) were transferred to 6-well plates prefilled with 1 mL FSW after which 10 ml of algal culture (from the same culture flask) was added. Control monocultures of each algal culture (xenic) were also set up in triplicates allowing for the calculation of prey ingestion rate as the reduction in prey concentration in grazing treatments compared to control treatments with the prey algae alone. Incubations were done under the same conditions as for Acantharian photosynthesis measurements *i.e.*, at seawater temperature (16.5 °C, April 2021), with a 16:8 h light:dark cycle at 150-160 $\mu\text{mol photons m}^{-2} \text{s}^{-1}$. At 4 h and 24 h triplicate 1 mL samples were taken (avoiding the Acantharia specimens), fixed in 0.25% (final concentration) glutaraldehyde, and frozen at -20 °C for flow-cytometry cell counts.

Additionally, in order to qualitatively observe ingested prey, a similar incubation was performed, though with beforehand staining of *I. galbana* cell using the fluorochrome CellTracker Blue CMAC (7-amino-4-chloromethylcoumarin, ThermoFisher), a vital cytoplasmic stain, as described by Martínez et al. (2014). Cells were stained for 4-6 h with the CellTracker at a final concentration of 10 μM . To reduce

the carryover of stain that could enter Acantharia, excess stain was removed from the medium after the staining period by washing three times. This was performed by centrifugation of the live fluorescently labelled algae (LFLA) at 2000 g for 5 min; the supernatant was discarded and the cells were re-suspended in FSW. Acantharia were incubated with the labelled prey as before, triplicate Acantharia were individually isolated after 0, 30, 60, and 240 min; transferred to 0.5 mL tubes; fixed in a final concentration of 0.25% glutaraldehyde (Sigma, ref. G5882-100ML) and 1% paraformaldehyde (Electron Microscopy Sciences, ref. 15714, diluted in phosphate-buffered saline); and stored at 4 °C for fluorescence microscopy.

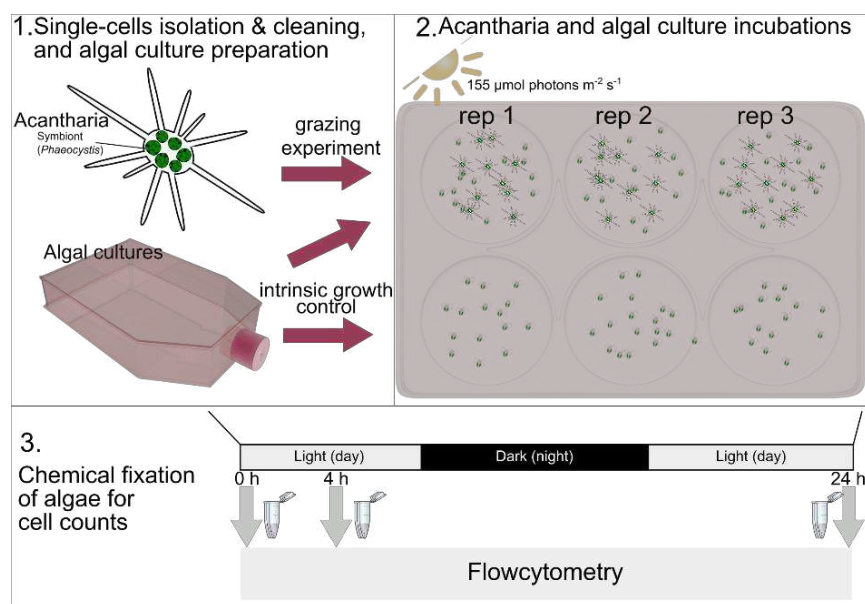


Figure III-2 Conceptual drawing of experiments for assessment of acantharian grazing rates estimation by cell counts (prey disappearance, as performed on each algal culture. Samples for algal cell density at 0 h were taken from the initial culture at step 1.

2.2. Isotopic analysis

Isotopic analysis was done at the “Metabomer” core facility, at Station Biologique de Roscoff. The C and N isotopic composition and content of the particulate organic matter was determined as CO₂ and N₂ released by flash combustion using an elemental analyser (EA Isolink CN/OH, Thermo Fisher) coupled to an isotope ratio mass spectrometer (IRMS, Delta V Advantage, Thermo Fisher) *via* an open split and dilution controlled interface (ConFlow IV, Thermo Fisher) with a continuous flow of helium at 180 mL min⁻¹. In addition to the samples, each run contained international isotopic standards from IAEA (these were IAEA-600 (caffeine), and CH6 (sucrose) for C; N2 (Ammonium Sulfate) and USGS34 (Potassium Nitrate) for N). IAEA standards were used for manual normalization of the δ-unit to the Vienna Pee Dee Belemnite-limestone (VPDP) or atmospheric N₂ scale, for carbon and nitrogen respectively, using a linear calibration curve (Coplen et al., 2006; Paul et al., 2007). An isotopic laboratory working standard (casein, certified Elemental Microanalysis) was run every 15 samples for verification of system stability. Though it was not needed in our case, a correction for linearity could be performed using the casein standard. A laboratory weight standard (acetanilide, certified Elemental Microanalysis) of different masses were used to calibrate the analyser and determine C and N content of the samples. Standard deviations were 0.11 and 0.06 μg for C and N content respectively, and 0.1 ‰, and 0.05 ‰ for δ¹³C and δ¹⁵N respectively. Additionally, a quality check (urea, certified Elemental Microanalysis) for isotopic ratios and weight (urea, certified Elemental Microanalysis) was run randomly to validate the quality of analysis. Isotopic Ratio Mass

Spectrometry data was processed in ISODAT 3.0 software and Microsoft Excel for the output of values expressed in delta notation (δ) in units of per mil (‰).

Carbon and nitrogen signal of the samples was corrected by accounting for the related analytical blank. The blank correction was performed for the normalized δ -values using the following equation:

$$\delta_{blkcorr} = \frac{(\delta_{meas} \times Area_{meas}) - (\delta_{blk} \times Area_{blk})}{Area_{meas} - Area_{blk}}$$

$\delta_{blkcorr}$ = blank corrected δ -value of the sample

δ_{meas} = δ -value of the sample

δ_{blk} = δ -value of the blank (*i.e.* medium the specimen was kept in)

$Area_{mea}$ = area of the sample peak

$Area_{blk}$ = area of the blank peak

For qualitative measurements of isotope uptake, or the calculation of excess, ^{13}C and ^{15}N of each sample relative to natural abundance $\delta^{13}\text{C}$ and $\delta^{15}\text{N}$ were converted to fractional abundances (F) using the following equations (Moodley et al., 2005; Fry, 2006):

$$R = \left(\frac{\delta X}{1000} + 1 \right) \times R_{VPDP}$$

$$F = \frac{R}{R+1}$$

Where R is the ratio of either $^{13}\text{C}/^{12}\text{C}$ or $^{15}\text{N}/^{14}\text{N}$; δX is the normalised-blank-corrected- δ -value of the sample, either $\delta^{13}\text{C}$ or $\delta^{15}\text{N}$; $R_{vpdp} = 0.0112372$, for nitrogen this is substituted with $R_{air} = 0.0036765$, and F is the fractional abundance. Finally, total uptake (I) of the heavier isotope in $\mu\text{g C cell}^{-1} \text{h}^{-1}$ or $\mu\text{g N cell}^{-1} \text{h}^{-1}$ was calculated as:

$$I = (F_{sample} - F_{control}) \times m_{sample} / t / n$$

Here F_{sample} is the fractional abundance of the sample after incubation and $F_{control}$ the non-enriched samples. m_{sample} is the total C or N mass of the sample in μg and t is the incubation time in hours. The ^{13}C uptake was further normalised per acantharian cell by division with the total number of Acantharia in the sample (n).

The total uptake of carbon ($^{12}\text{C} + ^{13}\text{C}$) was calculated by division of the total ^{13}C uptake (I) by the fractional abundance of total ^{13}C of dissolved inorganic carbon in the incubation. The dissolved inorganic carbon concentration of the seawater was measured to average $5900 \mu\text{M}$, with a natural abundance of ^{13}C of 1.08%. The total fraction of ^{13}C in the experimental incubations was thus 1.9%. For total uptake of nitrogen, the concentrations of nitrite, nitrate, and ammonium at the sampling location were considered (<https://www.somlit.fr/visualisation-des-donnees>). With an assumed natural ^{15}N fraction of 0.368%, we estimated the total fraction of ^{15}N as 43.95 and 32.53% for the nitrate and ammonium treatments respectively.

2.3. Microscopy chlorophyll fluorescence measurements

Chlorophyll fluorescence parameters of single Acantharia cells were measured using a Pulse Amplitude Modulated (PAM) fluorometer coupled to a microscope (MICROSCOPY-PAM; Walz, Effeltrich, Germany), equipped with a 10X objective lens. After a minimum of 5 min dark incubation, the basal level of fluorescence (F_0) was measured under modulated light (9 $\mu\text{mol photons m}^{-2} \text{s}^{-1}$, frequency: 8 Hz at 625 nm), after which the maximum fluorescence level (F_m) was determined with a saturating light pulse (1719 $\mu\text{mol photons m}^{-2} \text{s}^{-1}$, during 8×60 ms at 625 nm). Dark-adapted maximal quantum yield (F_v/F_m) of photosystem II (PSII) was calculated as follows: $F_v/F_m = (F_m - F_0)/F_m$.

ImageWin (v2.46) software was used to determine areas of interest (AOI) that encompass the entire Acantharia cell. Due to the patchiness of the photosynthetic activity, only pixels for which $F_v/F_m > 0$ were used to calculate fluorescence parameters, hence non-photosynthetically active regions (such as those of the host cell) are not taken into consideration.

2.4. Growth and ingestion rate calculations

Algal culture growth rates (μ , d^{-1}) were measured as change in cell concentrations over time and calculated assuming exponential growth.

$$\mu = \ln(N_x/N_0) / (t_x - t_0)$$

Where N_x and N_0 are the cell concentrations in cells mL^{-1} at time point t_x and time t_0 respectively.

The ingestion rates ($U = \text{prey predator}^{-1} \text{h}^{-1}$) were calculated by Frost (1972) equations as modified by Heinbokel et al. (1978):

$$U = C \times F$$

Where C is the average prey concentration in the experimental incubations with prey and grazer, calculated as:

$$C = (X_{t_x} - X_{t_0}) / (\ln(X_{t_x}) - \ln(X_{t_0}))$$

With X_{t_x} being the prey concentration at the end of the incubation and X_{t_0} at the start.

F is the clearance rate ($\text{mL grazer}^{-1} \text{h}^{-1}$) calculated as:

$$F = (k - g)/P$$

k is the intrinsic growth rate of prey in monoculture incubations, calculated as:

$$k = (\ln(X_{t_2}) - \ln(X_{t_1})) / (t_2 - t_1)$$

g is the grazing coefficient, calculated as the growth rate of prey in the experimental incubations with prey and grazer:

$$g = (\ln(X_{t_2}) - \ln(X_{t_1})) / (t_2 - t_1)$$

X_{t_2} and X_{t_1} being the prey concentrations at t_2 and t_1 respectively.

P is the average grazer concentration in the experimental incubations with prey and grazer. Considering that Acantharia do not proliferate during the experiments (only death might be observed), P is simply:

$$P = A/V$$

Where A is the Acantharia count at the end of the incubation and V the volume of the incubation.

2.5. Fluorescence Microscopy

Microscopy to visualise fluorescently labelled algal cells was conducted using an inverted Leica SP8 confocal laser scanning microscope (Leica Microsystems, Germany) equipped with a compact supply unit that integrates a LIAchroic scan head and several laser lines (405 nm, 488 nm, 552 nm, 638 nm), and either an HC PL APO CS2 63 × 1.40 OIL objective or an HC PL APO CS2 40 × 1.1 WATER objective, according to specimen size. Single cells were isolated from the fixative solution and placed on LabTek II chambered coverglass (Nunc 155382; Thermo Fisher Scientific, MA, USA). To visualise the membrane and skeletal structures, the cells were additionally stained with 50 µM Poly-L-lysine conjugated with Alexa Fluor 546 for 15 min (Colin et al., 2017), and then washed by means of cell transfer through FSW. This stain binds among others strontium sulfate, protein, and polysaccharide materials (Colin et al., 2017).

Imaging was performed with excitation using the 405 nm, and 552 nm lasers, and signal collection at emission wavelengths 460-472 nm, 603-635 nm, and 693-782 nm to capture fluorescence of the Celltracker blue stain, carotenoids/Alexa Fluor 546 stain, and chlorophyll respectively. Image processing and 3D rendering from z-stacks was performed using the software Imaris (Bitplane AG, Zurich, Switzerland), following guidelines of (Schmied and Jambor, 2020).

2.6. Algal cell enumeration

Fixed algal culture cells (glutaraldehyde 0.25% final concentration) were enumerated on an Agilent NovoCyto Advanteon flowcytometer in most cases. For cells < 1.5 µm (*Synechococcus* sp.), cells were enumerated on a Guava Easycyte Ht flowcytometer. Free-living stages of the algal symbionts (*Phaeocystis*) for the symbiont photosynthesis experiments, were enumerated on a Cytoflex flowcytometer (Beckman Coulter, USA) with threshold on red fluorescence, based on fluorescence patterns and cell size from side scatter (Olson et al., 1991).

2.7. Chlorophyll content

Samples for Chl a measurements from algal suspensions were filtered or deposited on a GF/F filter and Chl a was extracted by adding an equal amount of 96% ethanol (*i.e.* 2 mL sample with 2 mL 96% ethanol). Samples were stored at 4 °C for 24 h in darkness. Fluorescence and Chl a concentrations were measured using a bench-top fluorometer (Trilogy, Turner designs, CA) equipped with a manufacturer's Chl a non-acidification insert for Chl a determination. The fluorometer was calibrated against a pure Chl a standard (2.13 mg Chl a L $^{-1}$) of cyanobacterial origin (DHI, Hørsholm, Denmark).

2.8. Algal photosynthetic rates measurements

Photosynthetic rates were measured using the ^{14}C technique by Rivkin and Seliger (1981) and previously described by Skovgaard et al. (2000) and Hansen et al. (2016). Sample aliquots of 2 mL from

algae suspensions were taken in two sets of triplicates. To each sample 20 μL of $\text{NaH}^{14}\text{CO}_3$ stock solution (specific activity = 100 $\mu\text{Ci mL}^{-1}$; Carbon-14 Centralen, Denmark) was added for a final concentration 1 $\mu\text{Ci mL}^{-1}$. For each experimental incubation, one set of triplicates was incubated in the light, while the other was kept in complete darkness to compensate for passive incorporation of the isotope. After incubation, a 100 μL sub-sample was transferred to a new vial containing 200 μL phenylethylamine for determination of specific activity. The remaining 1.9 mL were acidified with 2 mL 10% glacial acetic acid in methanol and evaporated overnight at 60 $^\circ\text{C}$ to remove inorganic carbon. The residue was then re-dissolved in 1.5 mL Milli-Q water. All vials were treated with 10 mL Ultima Gold XR scintillation cocktail, and disintegrations per minute were measured using a Perkin Elmer, Tri-Carb 2910TR liquid scintillation analyzer with 10-minute acquisition time. As per Skovgaard et al. (2000), new caps (Packard poly screw caps) were mounted after adding the scintillation cocktail.

Photosynthetic activity (PA in $\text{pg C cells}^{-1} \text{h}^{-1}$) was calculated from the disintegration per minute using the following equation.

$$PA = \frac{(\text{lightDPM} - \text{darkDPM}) \times [\text{DIC}]}{\text{DPMspecific activity} \times h \times N}$$

Where DPM is disintegrations $\text{min}^{-1} \text{mL}^{-1}$, either in the 'light', 'dark' or 'specific activity' vial; h is the incubation time; N is cells mL^{-1} and [DIC] is the concentration of dissolved inorganic carbon (pg C mL^{-1}) in the medium. Total dissolved inorganic carbon concentrations [DIC] were measured on 25 mL of the medium used for the experiments using a TOC-L analyser, Shimadzu.

2.9. Statistical analyses

Mean $\delta^{13}\text{C}$ (or $\delta^{15}\text{N}$) differences between treatments were tested by comparing means with an ANOVA and Tukey-Kramer HSD post-hoc test. Effects of Acantharia grazing were tested by comparing the grazing coefficient with the intrinsic growth rate using a Student's t-test. The software JMP Pro 15.0 (SAS Institute, Inc) was used for all analyses, and results are presented as mean \pm standard deviation.

3. Results

Acantharia used in these experiments all belong to clade F3b, and are molecularly determined as *Acanthostaurus* sp. or *Acanthometra* sp. (see **Supplementary Methodology and Results**).

Average maximal quantum yield (F_v/F_m) of Acantharia cells after isolation and cleaning over all days was 0.7 ± 0.08 ($n = 86$) and was similar for Acantharia after 4 h incubation with an average 0.7 ± 0.07 ($n = 90$) (**Supplemental Figure III-1**). Physical cues, such as extended cytoplasm and pseudopodal extension, further indicate the Acantharia were in a healthy state during the experimental incubations (**Supplemental Figure III-2**).

Elemental content of Acantharia measured for an average carbon content of $122.8 \pm 25.1 \mu\text{g cell}^{-1}$ and average nitrogen content of $14.9 \pm 5.0 \mu\text{g cell}^{-1}$, for a ratio of 9.0 ± 1.7 . The C:N ratio did not significantly change with nutrient addition (ANOVA $F_{2,19} = 0.323$, $p = 0.8$), and the previously given average values are thus for all samples combined ($n = 27$).

3.1. Inorganic nutrient uptake rates—photosynthesis

Carbon uptake rates by Acantharia holobiont

Acantharia in control incubations with natural medium averaged a $\delta^{13}\text{C}$ value of $-22.5 \pm 2.3\text{‰}$ ($n = 11$) over all control treatments. After 4 h incubation with ^{13}C -bicarbonate, all treatments showed significant ^{13}C enrichment compared to the relevant control incubation (ANOVA $F_{2,19} = 23.55$, $p < 0.01$; **Figure III-3 A**, **Supplemental Table III-3**

Incubations in complete darkness do not differ significantly in $\delta^{13}\text{C}$ from incubations in natural medium, implying that ^{13}C uptake requires light (photosynthesis) and thus excludes passive ^{13}C uptake. Nutrient additions of ammonium or nitrate did not statistically significantly affect acantharian ^{13}C uptake as compared to without their addition. There, however, seems to be a significantly higher carbon enrichment with the nitrate treatment than with the ammonium treatment (**Supplemental Table III-3**).

To determine quantitative uptake rates of total C per Acantharia cell the relative abundance of naturally occurring ^{13}C (1.1%) was combined with the relative abundance of added ^{13}C tracer. Hence, the total ^{13}C (1.9%) in our incubations was used to calculate total carbon uptake. **Table III-1** shows the C uptake rates for each enrichment treatment. Considering an average of 50 symbionts per Acantharia cell, the total carbon uptake rate per symbiont would total $22.3 \pm 1.6 \text{ pg C h}^{-1} \text{ symbiont cell}^{-1}$.

Nitrogen uptake rates by Acantharia holobiont

Isotopic ratios of nitrogen in Acantharia were only measurable for a fraction of the samples due to insufficient sample biomass, and the ratios were best measured when isotopic enrichment was high. Thus, most measurements came from the labelled ammonium treatment, where there is highest ^{15}N enrichment (**Figure III-3 B**). There is indication that nitrate is also taken up, as there is an increase of $\delta^{15}\text{N}$ by 31.8‰ (**Table III-2**). No nitrogen enrichment by ammonium can be observed in the dark, though it is unclear whether this is due to biological or technical effects. A rough estimate of total nitrogen uptake is made by accounting for the fractional abundance of ^{15}N in the respective treatments (**Table III-2**).

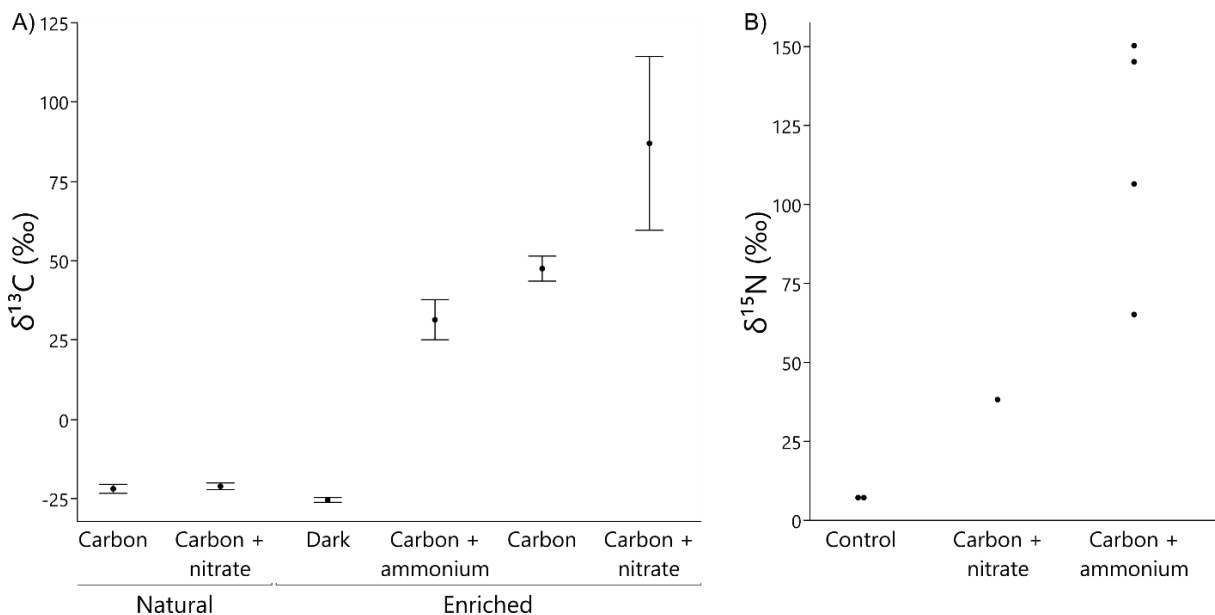


Figure III-3. Carbon (A) and nitrogen (B) isotopic composition of Acantharia in delta (‰) notation for each treatment and control treatment. The dark treatment involved incubation with labelled carbon and ammonium. For $\delta^{15}\text{N}$, control is both values from the natural nitrate and ammonium treatments. Values are means and standard deviations for $\delta^{13}\text{C}$, and individual sample data for $\delta^{15}\text{N}$; n for each treatment is indicated in **Table III-1** for carbon and in **Table III-2** for nitrogen.

Photosynthesis by free-living *Phaeocystis*

Phaeocystis cordata is the dominant symbiont in the acantharian photosymbiosis in the Mediterranean Sea. We measured the C uptake of free-living *P. cordata* cultures to average 0.38 ± 0.043 pg C cell⁻¹ h⁻¹ or 2.2 ± 0.2 pg C Chl_a⁻¹ h⁻¹, with Chl_a ranging between 0.094 and 0.18 pg Chl_a cell⁻¹ (n = 21). With an estimated cell diameter of 4 μm the carbon content of a *Phaeocystis* cell estimates as 5.8 pg C, according to the protist volume to carbon content conversion by Menden-Deuer and Lessard (2000). Thereby carbon-specific photosynthesis rate for *Phaeocystis* is 0.065 pg C C⁻¹ h⁻¹.

Table III-1 Carbon isotopic ratio and uptake data for Acantharia. Data shown are the δ¹³C (‰) for each treatment, and the uptake rates of labelled and total carbon for enriched samples. Data are presented as means and standard deviations.

	Treatment	δ ¹³ C (‰)	pg ¹³ C h ⁻¹ cell ⁻¹	pg C h ⁻¹ cell ⁻¹
Controls	Carbon (n = 4)	-21.9 ± 2.8	NA	NA
	Carbon + ammonium (n = 4)	-24.2 ± 1.0	NA	NA
	Carbon + nitrate (n = 3)	-21.1 ± 1.8	NA	NA
Enriched	Carbon (n = 4)	47.5 ± 7.9	21.2 ± 1.6	111769 ± 82.1
	Carbon + ammonium, Dark (n = 3)	-25.4 ± 1.3	-1.1 ± 0.3	-59.3 ± 15.0
	Carbon + ammonium (n = 5)	31.4 ± 14.1	20.5 ± 3.9	1075.6 ± 203.2
	Carbon + nitrate (n = 3)	87.0 ± 27.4	32.5 ± 12.8	1706.5 ± 671.1

Table III-2. Nitrogen isotopic ratio and uptake data for Acantharia. Data shown are the δ¹⁵N (‰) for each nitrogen treatment, and the uptake rates of labelled and total nitrogen for enriched samples. Data are presented as means and standard deviations.

	Treatment	δ ¹⁵ N (‰)	pg ¹⁵ N h ⁻¹ cell ⁻¹	pg N h ⁻¹ cell ⁻¹
Controls	Carbon + ammonium (n = 1)	7.8	NA	NA
	Carbon + nitrate (n = 1)	6.4	NA	NA
Enriched	Carbon + ammonium (n = 4)	116.9 ± 39.6	12.8 ± 8.0	39.5 ± 24.5
	Carbon + nitrate (n = 1)	39.2	20.7	47.1

3.2. Organic nutrient uptake—predation

Calculated grazing rates of Acantharia on different prey were in most cases not different from zero (**Table III-3**). Incubations with *Synechococcus* sp. (RCC307), and *Isochrysis galbana* (RCC178) were performed with different initial concentrations, but that did not change the significance of the ingestion rates. Incubation of 4 h with *Effrenium voratum* (RCC1521) led to a significant ingestion rate of 728 ± 89 prey per Acantharia per hour. Incubation for 24 h however did not show significant grazing (**Table III-3**).

Incubation of Acantharia with LFLA *I. galbana* does indicate prey ingestion (**Figure III-5** and **Figure III-6**). Control Acantharia experiments that were not subjected to LFLA gave a baseline (auto)fluorescence for the cells. Acantharia show inherent autofluorescence independent of symbionts as is seen when observing fixed cells, as well as live cells (not shown), and is likewise the case for non-symbiotic species (**Supplemental Figure III-3**). The ingestion of LFLA in these non-symbiotic cells appears initially faster, *i.e.*, after already 30 min. Signals of LFLA in symbiotic Acantharia were best observed after 60 min, and apparently declined after 4 h of incubation. Fluorescence of LFLA cells was observed inside of the central capsule membrane (**Figure III-5**).

Table III-3. Ingestion rates for each incubation of Acantharia with algal culture, as well as the incubation time point, and the average Acantharia to algal culture ratio over the incubation time. The 24 h incubations are the same incubations following the respective 4 h incubations. A negative ingestion rate implies a higher growth rate of algal prey with Acantharia than in monoculture. Shown is the p-value for the Student's t-test testing the hypothesis that incubations with and without Acantharia do not differ in algal growth rate, rejection of the hypothesis is indicated in bold. Data are presented as mean \pm standard deviation, $n = 3$.

Algal species	Time point (h)	Acantharia to prey ratio	Ingestion rate (prey Acantharia ⁻¹ hour ⁻¹)	p-value
<i>Isochrysis galbana</i> *	4	7.23E+04	3681 \pm 4468	0.198
<i>Isochrysis galbana</i>	4	3.50E+04	2. \pm 112.	0.994
<i>Isochrysis galbana</i>	24	4.03E+04	319 \pm 189	0.157
<i>Isochrysis galbana</i>	4	1.33E+04	51 \pm 100	0.350
<i>Isochrysis galbana</i>	24	1.64E+04	9 \pm 25	0.583
<i>Synechococcus</i> sp.	4	7.16E+06	246577 \pm 156953	0.068
<i>Synechococcus</i> sp.	24	4.49E+06	-14105 \pm 37361	0.454
<i>Synechococcus</i> sp.	4	8.24E+05	-8837 \pm 9905	0.165
<i>Synechococcus</i> sp.	24	9.52E+05	490 \pm 2255	0.865
<i>Synechococcus</i> sp.	4	3.69E+05	-4276 \pm 5215	0.618
<i>Synechococcus</i> sp.	24	2.01E+05	2088 \pm 2476	0.167
<i>Synechococcus</i> sp.	4	3.90E+03	36 \pm 0.01	0.318
<i>Synechococcus</i> sp.	24	3.52E+03	-0.59 \pm 5.9	0.973
<i>Effrenium voratum</i>	4	1.06E+04	728 \pm 89	0.000
<i>Effrenium voratum</i>	24	1.17E+04	-137 \pm 109	0.089

* incubation performed using live fluorescent labelled algae, samples only taken at 4 h

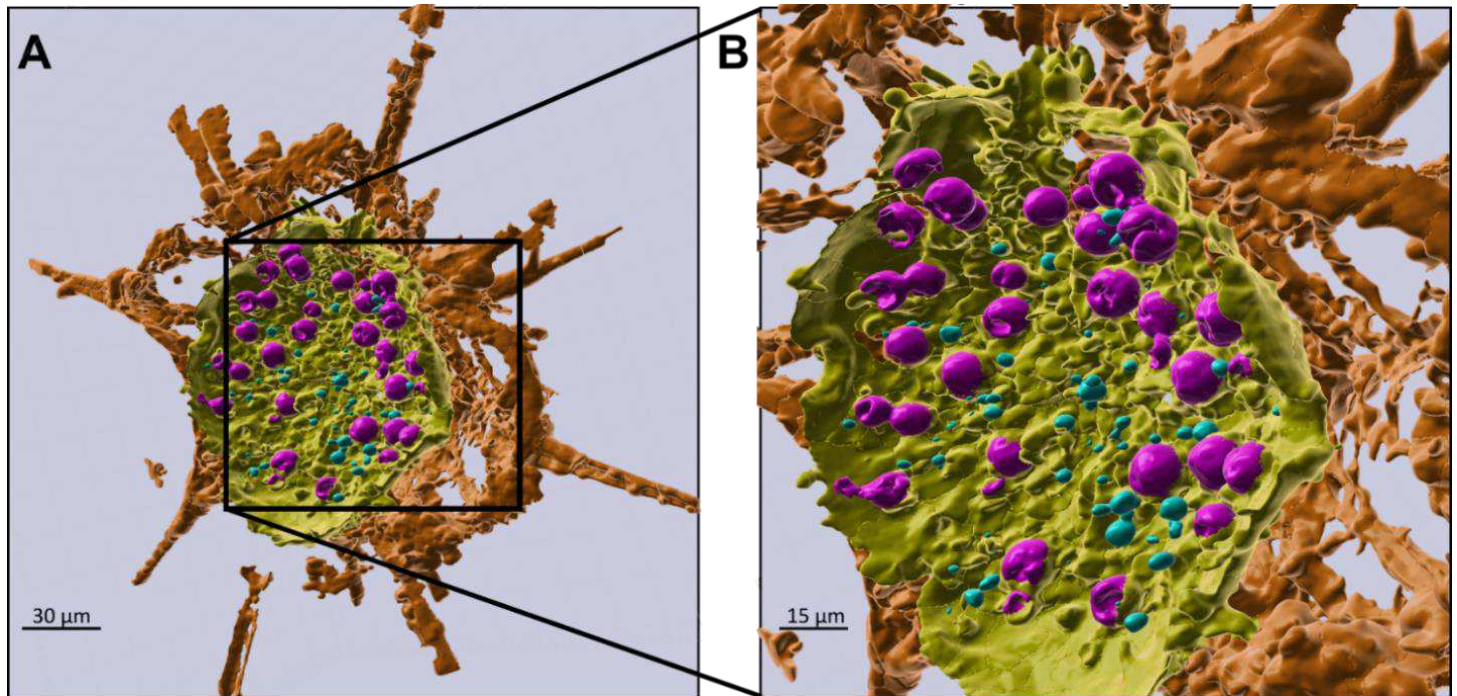
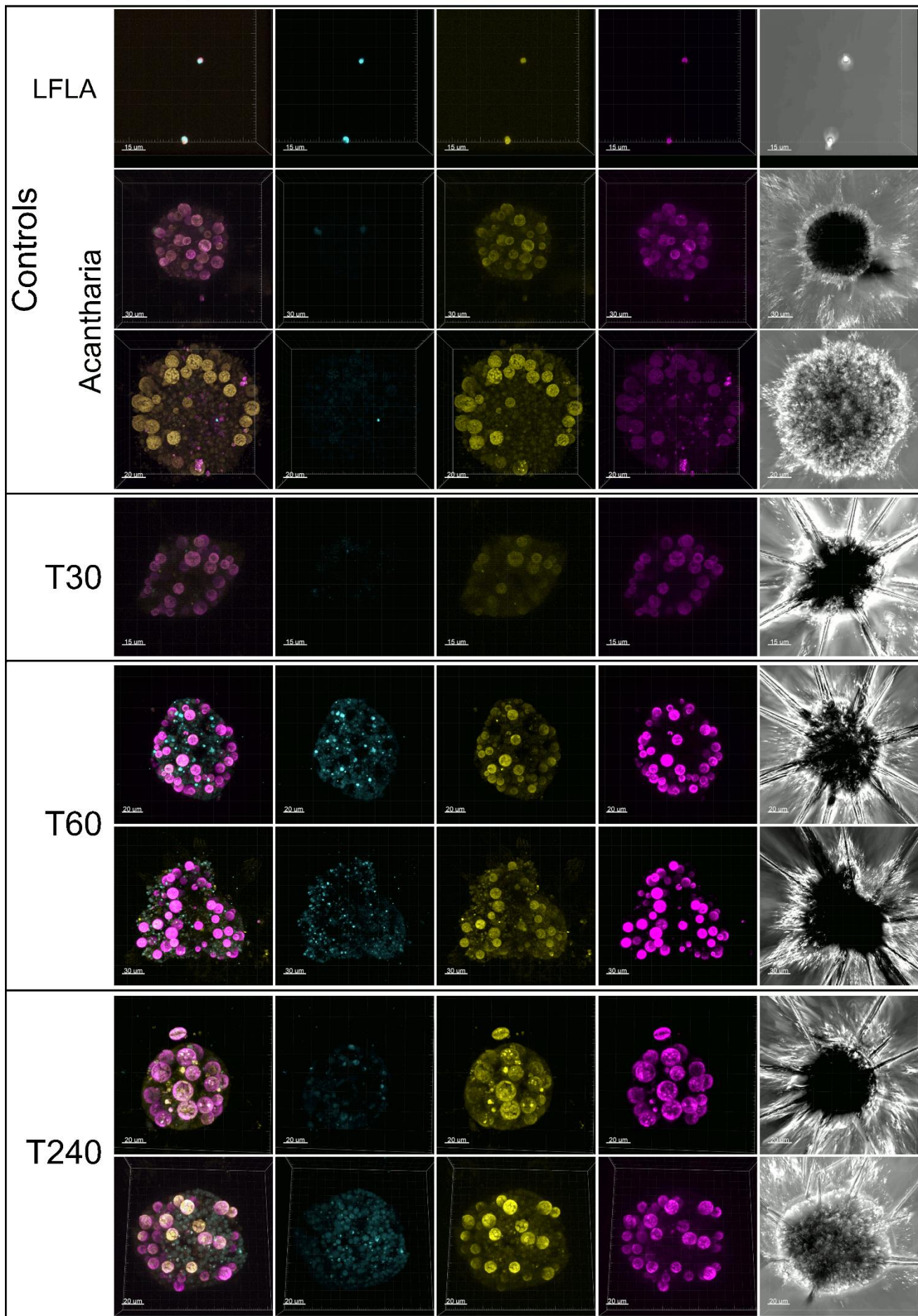


Figure III-5. 3-D reconstruction of (half) an Acantharia after 60-minute incubation with LFLA *I. galbana* imaged using confocal microscopy. Membranes and skeletons have been stained using Poly-L-lysine Alexa Fluor 546. **A)** Cyan indicates captured emission wavelengths at 460-472 nm (Celltracker Blue fluorescence), yellow and maroon at 603-635 nm (Alexa Fluor 546, masking the cell's autofluorescence), and magenta at 693 782 nm (chlorophyll autofluorescence). The signal of the Alexa Fluor has been coloured maroon to indicate the outer membrane and spicules whereas the central capsule membrane is shown in yellow. **B)** Zoomed and angled frame of the same cell. LFLA and symbiont chlorophyll signal is found inside the central capsule membrane. Z-stack images were three-dimensionally reconstructed with Imaris software.

Composite Channel 1 Channel 2 Channel 3 Channel 4



Caption on next page →

Figure III-6. Acantharia after incubation with LFLA *I. galbana* at different time points imaged using confocal microscopy. Panels show the snapshots of different time points (30, 60, and 240 min) with 3-D projections of separate channels and a composite of channels 1 through 3. Channel 1 (cyan) is for emission wavelengths 460-472 nm (Celltracker Blue fluorescence), and channel 2 (yellow) for 603-635 nm (unknown autofluorescence, likely carotenoids), and channel 3 (magenta) for 693-782 nm (chlorophyll autofluorescence). Channel 4 represents transmission light images. The first row represents stained *I. galbana* (LFLA). The Acantharia controls show a lack of spicules, as seen in the channel 4 panels, due to it being cells that have been stored longer in fixative and spicules appear to be dissolved. Lower fluorescence intensity is observed with control and T30 panel images, due to those having been imaged using an oil immersion objective, whereas the other images were made using a water immersion objective. Z-stack images were three-dimensionally reconstructed with Imaris software. The fluorescence signal assumed to be of prey (Channel 1) is observed in Acantharia after 60 minutes. Subsequent hours show a loss of this signal indicating a higher rate of digestion than uptake.

4. Discussion

Although Acantharia are a dominant and ubiquitous component of marine pelagic systems, quantification of their photosynthetic and phagotrophic nutrient fluxes remains an experimental challenge. We here present one of the first attempts to use the ^{13}C and ^{15}N tracer in Radiolaria to assess the uptake rates of carbon and near-natural ammonium concentrations. Acantharia indeed live in waters that contain low levels of nutrients. The ^{15}N technique would allow the avoidance of a big change in natural nitrogen concentrations because low enrichments can be used.

4.1. Photosynthetic carbon uptake by Acantharia

Results obtained in this study showed that carbon uptake rates do not significantly vary according to the nitrogen source. We established the total carbon uptake rate as $1112.7 \pm 82.1 \text{ pg C h}^{-1} \text{ Acantharia}^{-1}$ (based on results without extra nitrogen addition). This acantharian primary productivity measurement is more precise compared to previous research in the central North Pacific Ocean ($816.7 \pm 875 \text{ pg C Acantharia}^{-1} \text{ h}^{-1}$, Michaels, 1991). Though they used ^{14}C methodology and here we used ^{13}C , these methodologies should indeed give comparable results (López-Sandoval et al., 2018). The data of Michaels et al. (1991) were highly variable (high standard deviations), due to a small number of Acantharia per sample, specimen size, and symbiont number differences, making direct comparisons difficult. Here we used stable laboratory light and temperature conditions, as well as, more specimens per sample that were isolated for specific species. Hence, the variation in our data is much less.

4.1.1 Free-living versus in hospite symbiont carbon uptake

When assuming an average of 50 *Phaeocystis* symbionts per Acantharia, the primary productivity of one acantharian symbiont, as measured here, averages $22.3 \pm 1.6 \text{ pg C symbiont}^{-1} \text{ h}^{-1}$. Whereas the free-living algae (*Phaeocystis*) have a primary productivity rate ~ 55 times lower (*i.e.* $0.38 \pm 0.04 \text{ pg C cell}^{-1} \text{ h}^{-1}$). The number of symbionts here chosen for comparison is rather conservative, between 30 and 50 symbionts are often observed (see also **Figure III-6**). Though for different species and sizes of Acantharia symbiont numbers can vary from 10 to > 65 (Michaels, 1991). Consistent with this increase of *in hospite* carbon uptake and fixation, *Phaeocystis* has been shown to be heavily modified *in hospite* (Decelle et al., 2019; Uwizeye et al., 2021); with an increased number of chloroplasts; a several-fold increase in thylakoid density, and likewise photosynthetic efficiency is increased (Decelle et al., 2019). Concurrently, carbon fixation genes, like genes for Calvin Benson cycle enzymes, are found to be upregulated in symbiotic *Phaeocystis* as compared to free-living (Uwizeye et al., 2021).

However, accounting for an increase in the size of *Phaeocystis in hospite*, one could compare the carbon-specific uptake rates. Doing so, a cell diameter of 10 μm can be assumed for enlarged symbiotic cells (Decelle et al., 2019, see also **Figure III-5** and **Figure III-6**), which would, by estimation, account for a carbon content of 77.3 $\mu\text{g C}$ per symbiont cell. The carbon-specific primary productivity per acantharian symbiont cell would then be $0.29 \pm 0.02 \mu\text{g C C}^{-1} \text{ h}^{-1}$. Which is less than 5 times more than the free-living symbiont's carbon-specific uptake rate ($0.065 \mu\text{g C C}^{-1} \text{ h}^{-1}$). The symbiont's cellular composition and structural changes, like the increased number of plastids (up to 60, Uwizeye et al., 2021, and see also Chapter IV.2), are not accounted for in this estimation. The carbon-specific photosynthetic rates might thus not be so different between *in hospite* and *ex hospite Phaeocystis* (only a ~ 5 times higher rate), nonetheless *Phaeocystis* does not achieve the same carbon uptake rates in its free-living state.

4.1.2 Influence of nitrogen on inorganic carbon uptake

Ammonium has been suggested to increase the rate at which carbon is fixed by dinoflagellate coral symbionts in darkness (Cook et al., 1992; Ezzat et al., 2015), although this was not seen in *Cassiopea* sp. (Lyndby et al., 2020). Possibly this can proceed through both host and symbiont pathways in a photosynthesis-independent manner in the urea cycle where ammonium is combined with bicarbonate (e.g., Allen et al., 2011; Burns et al., 2020). Under the conditions described here, we do not see statistically significant differences in C uptake with nitrogen additions. Though, it seems C uptake might be lower in the treatment with ammonium addition and higher with nitrate addition, as compared to without the addition of these N-sources. We might note that in this endo-photosymbiosis internal recycling of N is expected, and symbionts would thus not be N-limited. It has been shown that with increasing ammonium assimilation, catabolic process and stored carbon (e.g., starch, sucrose) may be used to fulfil the extra carbon demands (Elrifi and Turpin, 1986; Turpin, 1991; Huppe and Turpin, 1994). This might explain a lower $\delta^{13}\text{C}$ ratio. Whereas nitrate would demand more photosynthetic activity to satisfy the energetic demands for its reduction, it was however still taken up at a lower rate than ammonium (section 4.3).

Even though carbon assimilation in the dark could be significant in some photosymbiotic associations (Röthig et al., 2021), under the current experimental conditions no photosynthesis-independent (in the dark) carbon fixation was measured. In a separate experiment we have measured photosynthetic (inorganic) carbon uptake under low light conditions, see **Supplemental Figure III-4**. Uptake of carbon was in that experiment only seen in the treatments with ammonium addition, though at a low rate, suggesting there could be a role for ammonium in affecting carbon uptake.

4.2. Nitrogen uptake by Acantharia

Both ammonium and nitrate are significantly taken up by the Acantharia. Though ammonium is taken up at a higher rate, as might be expected due to its lower energetic demands (von Wirén et al., 2000), and is similar in planktic photosymbiotic Foraminifera (LeKieffre et al., 2020). Lower nitrate uptake could also be attributed to the sufficient presence of ammonium available through host waste products (e.g. in photosymbiotic corals, Grover et al., 2002; Ezzat et al., 2015). The nitrogen uptake rate from ammonium sources is, however, rather low (39.5 ± 24.5). For the ammonium treatment, the ratio of carbon to nitrogen uptake is 27; other sources of nitrogen (inorganic or organic) must thus be used to constitute a cellular C/N ratio of 8.9 for Acantharia.

We were not able to measure ammonium uptake in the dark. This could be due to technical limitations, seeing as no isotopic ratio for nitrogen could be established in the dark. However, considering that it was possible to measure ammonium uptake in the light, there is a chance that technical limitations were not of influence here. In which case we would need to assume that there is indeed no ammonium uptake in the dark. Whereas photosynthesis-independent processes for ammonium assimilation might be possible, the fact that we do not see a significant uptake of ammonium in complete darkness could mean that the energy needed for its assimilation might need to come from symbiont processes (photosynthesis); assimilation of ammonium in complete darkness might thus not be possible or efficient. For the radiolarian Collodaria, we did see ammonium uptake in the dark (**Supplemental Figure III-6**). An important difference here between the Acantharia and Collodaria is that Acantharia host haptophyte symbionts, whereas Collodaria host dinoflagellates. Indeed, at least some dinoflagellates have been reported to be able to use ammonium in the dark (Dagenais-Bellefeuille and Morse, 2013). Ammonium uptake in the dark by dinoflagellate bearing photosymbioses has been demonstrated in several studies. For example, corals efficiently take up ammonium in the dark (Grover et al., 2002). Photosymbiotic planktic Foraminifera and the photosymbiotic jellyfish *Cassiopea* are likewise shown to take up ammonium in the dark (LeKieffre et al., 2020; Lyndby et al., 2020). Nitrate uptake in the dark has also been shown in *Cassiopea*, as well as in corals (Kopp et al., 2013; Freeman et al., 2016).

4.3. Grazing by Acantharia

The grazing experiments likely suffer from low or not significant grazing rates. Possibly the ratios between Acantharia and prey were too low at the chosen prey densities. In our grazing experiments, statistically significant grazing could only be established on *E. voratum*, and with a grazing rate of 729 prey Acantharia⁻¹ hour⁻¹ (i.e. 56.3 ng C h⁻¹ assuming a C content of 77.3 pg C prey). Such an ingestion rate could potentially provide enough C for acantharian growth. However, the cell densities tested upon here are unlikely to occur naturally. After 24 h incubation with *E. voratum* significant grazing by Acantharia was no longer observed. Oppositely, it seemed more death of Acantharia was observed, and dinoflagellates accumulated around and circled near-dead Acantharia cells. It is unclear if this was a form of predation by the dinoflagellates. Despite being unable to establish significant Acantharia ingestion rates on *I. galbana*, indication of prey ingestion has been observed using LFLA (**Figure III-6**) and stable isotope labelled algae (**Supplemental Figure III-5**). The LFLA fluorescent signal did not coincide with a chlorophyll signal of the algae, possibly due to rapid digestion of algal pigments upon ingestion and internalisation (Moore and Gelder, 1983; Mayzaud and Razouls, 1992). Staining visible in the Acantharia might be labelled food vacuoles, as the size is already smaller than that of the original LFLA, as well as, stain that has dissipated into the Acantharia. Dispersal of stain to the predator has been observed previously, but it is more commonly an issue with other feeding mechanisms such as peduncle feeding (Ferreira et al., 2021). Continuous fluorescent monitoring of algal cells during grazing could better elucidate the digestion process and could be possible considering the stability of the Celltracker Blue stain that experiences minimal bleaching (Ferreira et al., 2021).

4.4. Natural isotopic ratios to investigate trophic of Radiolaria

Isotopic ratios are widely used to analyse food webs and define trophic levels of organisms. The $\delta^{13}\text{C}$ trophic fractionation over trophic levels is close to zero i.e. 0.4‰ (SD = 1.3) (Post, 2002), thus $\delta^{13}\text{C}$ change

with trophic level is not large, though slightly more negative values are expected with more heterotrophy. The $\delta^{13}\text{C}$ can, however, shift more substantially based on autotrophy. For plants, generally, those with a CO_2 concentrating mechanism (like C4, CAM) have a higher $\delta^{13}\text{C}$, around -7‰ than those without (C3 plants), around -22‰ (Beardall, 1989). In contrast to $\delta^{13}\text{C}$, the $\delta^{15}\text{N}$ value increase due to predation typically increases approximately 3 to 4.5‰ with each trophic level; $\delta^{15}\text{N}$ can thus be used to help define the trophic level of an organism (Post, 2002; Fry, 2006). Whereas $\delta^{13}\text{C}$ would rather give clues on the source of the nutrients (Fry and Sherr, 1989). The issue with mixotrophic organisms is that both the photosynthetic and phagotrophic metabolism influence nutrient assimilation and thus isotopic ratios will reflect a mix between the organic and inorganic food sources, making it difficult to assess the original nutrient source (Ferrier-Pagès and Leal, 2018). Both the $\delta^{13}\text{C}$ (-22.5‰) and $\delta^{15}\text{N}$ (7.1‰) ratios of Acantharia might imply a trophic level similar to Mediterranean zooplankton (Vizzini and Mazzola, 2006; Bănaru et al., 2014). The natural isotopic ratios of carbon and nitrogen of Acantharia might suggest a higher contribution of organic (grazing) than inorganic (photosynthesis) nutrition. This is, however, better compared locally, as nutritional status and nutrient sources can differ seasonally and geographically, affecting C/N and delta ratios (Dobberfuhl and Elser, 2000; Bănaru et al., 2014). As an example: for Collodaria we measured an average $\delta^{13}\text{C}$ of $-14.9 \pm 4.1\text{‰}$ ($n = 18$) in autumn (September) 2018, and $-20.9 \pm 1.5\text{‰}$ ($n = 4$) during spring (April) 2019. This could imply seasonal differences in nutrient sources, for example, leading to spring collodarian trophic mode could live more on heterotrophy than autotrophy, and vice versa towards autumn. In spring, a phytoplankton bloom would allow subsequently heterotrophic organisms to increase due to the abundance of biomass to graze on (Hansen et al., 2019). Thus resulting in more heterotrophy and a lower $\delta^{13}\text{C}$ for the Collodaria. During the following summer period of high light and low nutrients, the Collodaria could resort to a more autotrophic lifestyle, which would explain the higher $\delta^{13}\text{C}$ values we measured nearing autumn. Such a trend in changing isotopic ratios throughout the seasons has also been observed in corals (Ferrier-Pagés et al., 2011), and seasonal dependency on differing trophic modes has also been predicted by model simulations (Mitra et al., 2014; Gonçalves Leles et al., 2021). The difference in $\delta^{13}\text{C}$ was over seasons was not as pronounced as for Collodaria, with for Acantharia a $\delta^{13}\text{C}$ of $-19.7 \pm 6.6\text{‰}$ ($n = 10$) in autumn (September) 2018 and $-22.5 \pm 2.29\text{‰}$ ($n = 11$) during spring (May) 2021. Overall, it might suggest that these mixotrophic Radiolaria rely more on heterotrophy and external (organic) food sources around spring, whereas summer and autumn would be a period where phototrophy is exploited.

Additionally, we note a lower $\delta^{13}\text{C}$ for Acantharia than for Collodaria. As noted, $\delta^{13}\text{C}$ tends to increase with autotrophy and decrease with heterotrophy, which might suggest a more heterotrophic role in the food web for Acantharia than for Collodaria. Symbiont differences likely play a major role in the isotopic difference between these Radiolaria. The relevant β -carboxylase for dinoflagellates and haptophytes (major symbionts for Collodaria and Acantharia respectively) are different (Raven, 1997). This is not only relevant for possible carbon isotopic discrimination differences, but also for the fact that in the marine environment two inorganic carbon sources are available for photosynthesis: CO_2 and HCO_3^- . Dissolved CO_2 in seawater has a ^{13}C value of around -7‰ whilst that of HCO_3^- is more enriched in ^{13}C and close to 0‰. When the activity of the photosynthetic carbon reduction cycle is reduced then fixation of HCO_3^- by β -carboxylase becomes more important. Additionally, compared to haptophytes, dinoflagellates generally have higher dark respiration (Geider and Osborne, 1989), where the utilisation of HCO_3^- might be of more

importance. Rost and colleagues (2006) estimated that HCO_3^- uptake accounted for > 80% of photosynthetic carbon fixation for three species of marine dinoflagellates. Hence using HCO_3^- (*i.e.* the product with the higher $\delta^{13}\text{C}$ value) could presumably increase the overall $\delta^{13}\text{C}$ of the collodarian holobiont. A lower $\delta^{13}\text{C}$ could also imply a heterotrophic food source; big Collodaria colonies are more likely to consume larger zooplanktic organisms. This can all result in a higher $\delta^{13}\text{C}$ value for Collodaria compared to Acantharia. Using natural isotopic ratios of these Radiolaria in comparison to other organisms in the local food web might thereby further help identify their reliance on either phototrophy or phagotrophy.

4.5. Inorganic and organic nutrient uptake balance of Acantharia

Photosynthesis should be a major part of the acantharian metabolism since modifications are made on the photosynthetic system in symbiont cells. Though we do not have data on daily respiration, photosynthesis (assuming net photosynthesis rates) would contribute 17.8 ng C on a 16 h light period per day, thereby constituting 14.5% of total Acantharia carbon content (122.8 ng C), suggesting that photosynthesis is a small part of the carbon budget. Photosynthesis has been shown to be a requirement for survival for the Spumellaria (Radiolaria) (Swanberg and Anderson, 1985). The variety of food items utilised by the Radiolaria is wide. Still, food in absence of light could not extend the survival of the cells, thus light is required for growth and survival. Symbiont photosynthesis would thus fulfil an important role in radiolarian metabolism. It has also been hypothesised that photosynthesis in some mixotrophic organisms predominately provides energy (Wilken et al., 2014; Terrado et al., 2017).

Results obtained in this study could suggest that the uptake of inorganic nutrients in this symbiotic association depends on the symbiont. Photosynthetic carbon assimilation is, however, only a fraction of the total holobiont carbon content. Photosynthesis would thus likely need to be supplemented with food uptake, as has been suggested for spumellarian and collodarian Radiolaria (Swanberg, 1983; Swanberg et al., 1986). How both symbiont and host benefit from phototrophic or phagotrophic nutrient sources might be further investigated by comparison of natural isotopic ratios of the symbiont and host (symbiont would need to be separated from the host). The uptake of inorganic nitrogen has not been entirely resolved with our results. The current bulk sample methodology is limited by biomass requirements. An increased amount of cell material would be needed to consistently quantify nitrogen uptake for these unculturable protists. Thereby the feasibility for such an analysis is low because of the need for sufficient replicates. The next step of this work will be to verify and assess how the assimilated nitrogen is partitioned between algae and host. We suggest that by elucidating the primary location of nitrogen assimilation, and the genetical/transcriptional capability of host and symbiont for processes involved in nitrogen metabolism (*e.g.* urea cycle), the role of the symbiont and host in nitrogen uptake and assimilation can be addressed.

5. Acknowledgements

This work benefited from access to the Observatoire Océanologique de Villefranche sur Mer, an EMBRC-FR and EMBRC-ERIC Site. We thank the Corsaire/Metabomer core facility (Biogenouest) for facilitating isotope analysis, the Roscoff Culture Collection for providing algal strains, as well as the MERIMAGE platform. We are grateful to Marie Walde, and Ioannis Theodorou, for assistance with confocal microscopy; to Andreas Norlin for help with preliminary stable isotope experiments; to Sarah Romac for the 28S sequencing; and Guillaume de Liege and David Luquet for their help with boat sampling. This work was supported by the European Union's Horizon 2020 research and innovation programme under grant agreement No. 766327 (project MixITiN).

Supplementary Material to Chapter III

Carbon and nitrogen uptake through photosynthesis and feeding by photosymbiotic Acantharia

Supplementary Tables and Figures

Supplemental Table III-1. Information on RCC cultures used in this study.

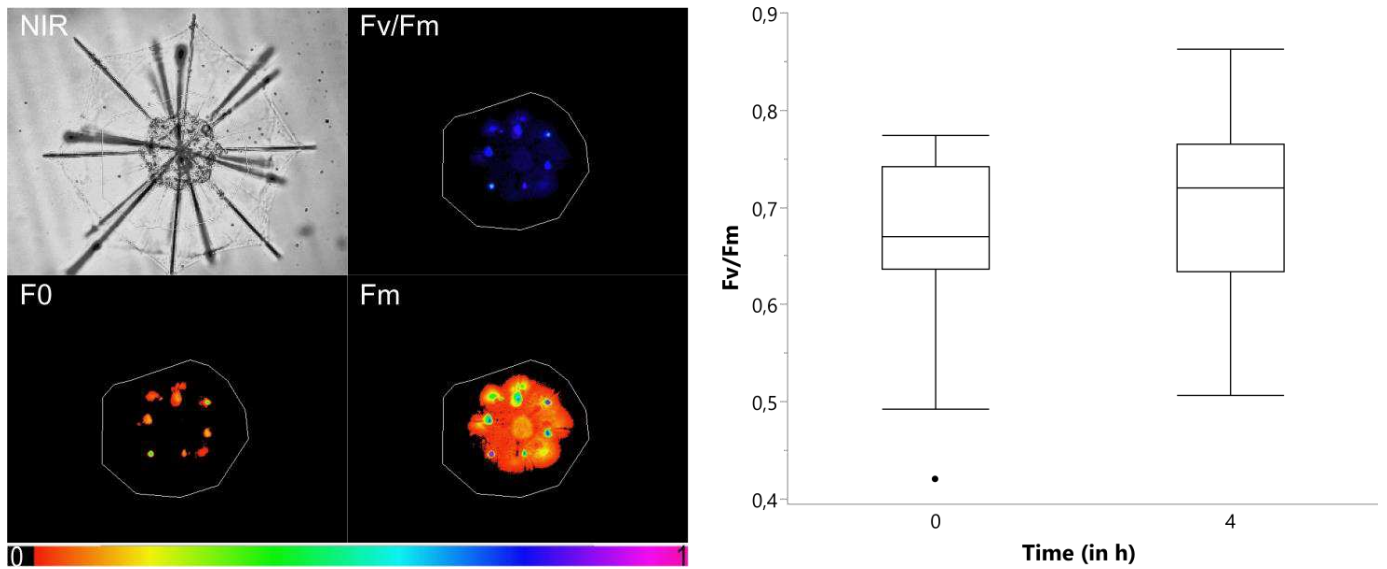
Algal strain:	RCC 178	RCC 1383 / CCMP2495	RCC 1521	RCC 372	RCC 307
Species	<i>Isochrysis galbana</i> *	<i>Phaeocystis cordata</i>	<i>Effrenium voratum</i> (<i>Symbiodinium voratum</i>)	<i>Micromonas commoda</i>	<i>Synechococcus</i> sp.
Class	Prymnesiophyceae	Prymnesiophyceae	Dinophyceae	Mamiellophyceae	Cyanophyceae
Division	Haptophyta	Haptophyta	Alveolata	Chlorophyta	Cyanophyta
ESD	5 µm	4 µm			1 µm
Ocean	Atlantic Ocean	Mediterranean Sea	Mediterranean Sea	Mediterranean Sea	Mediterranean Sea
Sampling site	Britanny coast - Caen	Gulf of Naples	Gulf of Naples	Gulf of Naples	lat:39.17; long:6.17
Original isolation date	12/02/1988	15/03/1991	Unknown	01/01/1986	Unknown
Growth temperature	19.5 °C	19.5 °C	19.5 °C	19.5 °C	19.5 °C

* Strain has recently been re-identified as *Tisochrysis lutea*.

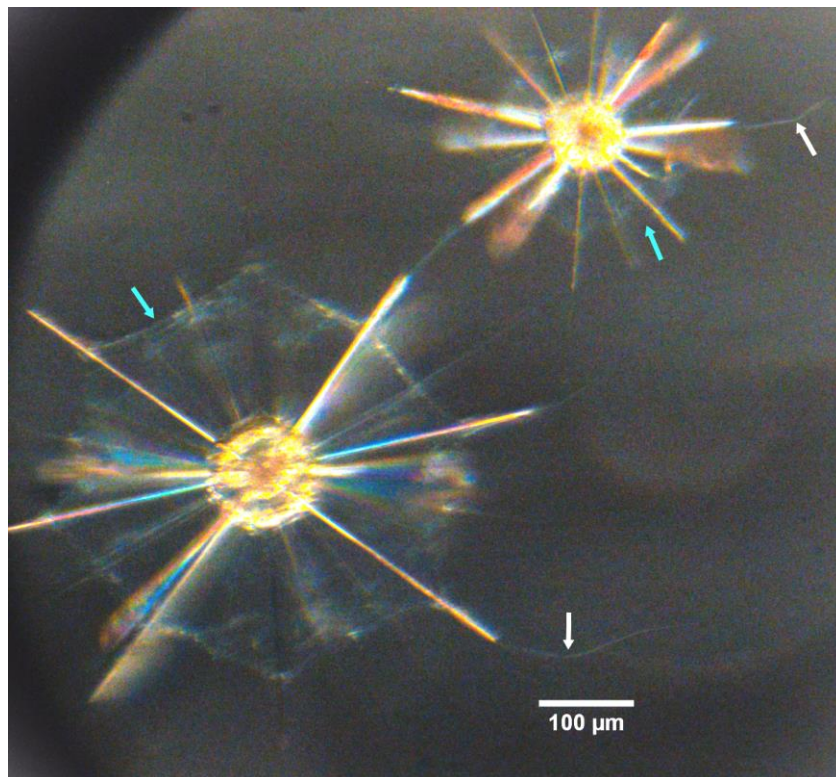
Supplemental Table III-2 Nutrient conditions of growth medium and in the surface waters of the Mediterranean Sea. Concentrations are in µM unless otherwise indicated. For natural seawater, the data for macronutrients correspond to an average over three years at the sampling site of our study (at Villefranche-sur-Mer available at <https://www.somlit.fr/>).

Compound	K/2 growth medium	K/5-6 growth medium	Med. Sea water *		
			min	max	
Macro nutrients	NaNO ₃	288	100	4.38 x10 ⁻²	1.02
	NH ₄ Cl	5	5	2.01 x10 ⁻³	1.12 x10 ⁻¹
	NaH ₂ PO ₄	18	6.25	7.92 x10 ⁻²	3.03 x10 ⁻¹
	(Na)FeEDTA	5.85	5.85		
Trace metal solution	Na ₂ EDTA.2H ₂ O	50	50		
	Na ₂ MoO ₄ .2H ₂ O	0.0026	0.0026		
	ZnSO ₄ .7H ₂ O	0.04	0.04	4.21 x10 ⁻⁴	5.27 x10 ⁻³
	CoCl ₂ .6H ₂ O	0.025	0.025	1.7371 x10 ⁻⁵	3.78 x10 ⁻⁴
	MnCl ₂ .4H ₂ O	0.45	0.45		
	H ₂ SeO ₃	0.005	0.005		
Vitamin solution	NiCl ₂ .6H ₂ O	0.00314	0.00314	1.00 x10 ⁻⁵	1.51 x10 ⁻⁴
	Vit. B12	0.37 nM	0.37 nM		
	Biotin	2.0 nM	2.0 nM		
Thiamine HCL	0.3	0.3			

* CoSO₄.6H₂O instead of CoCl₂.6H₂O and NiCl₂ instead of NiCl₂.6H₂O



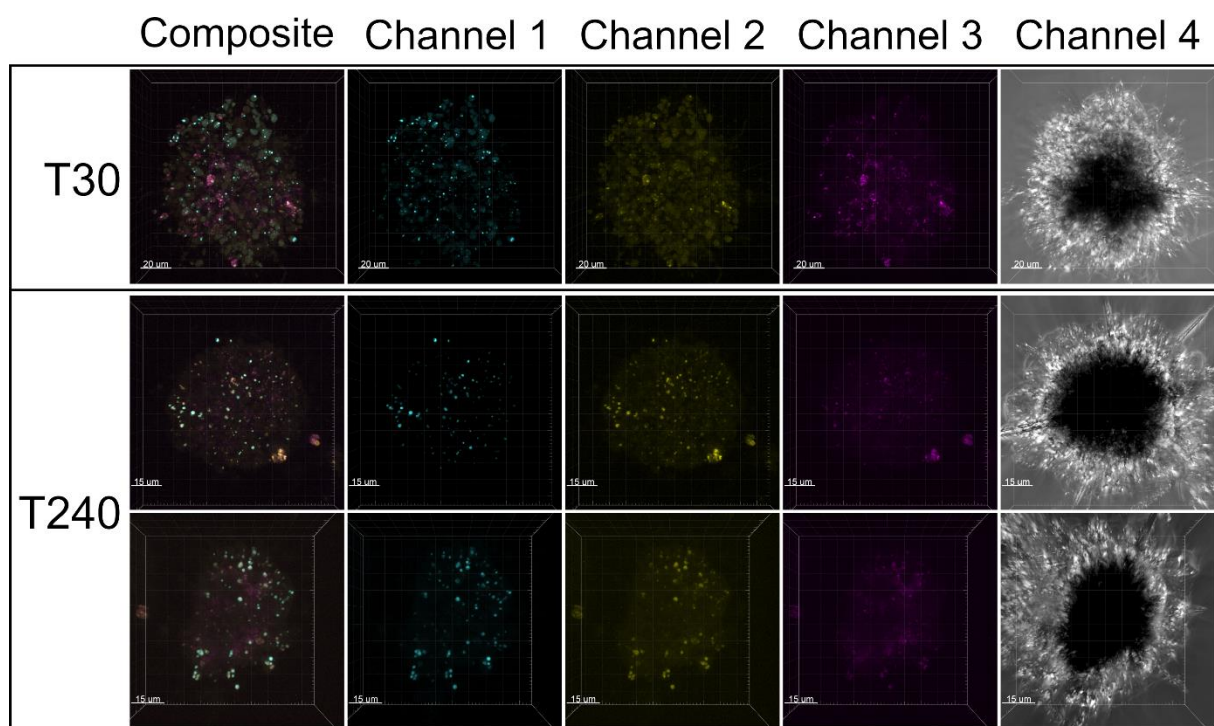
Supplemental Figure III-1. Example images made using a CCD camera for Microscopy Pulse-Amplitude-Modulation fluorescence analysis and ImagingWIN software, and a boxplot showing maximal quantum yield (F_v/F_m) of Acantharia measured before incubation (0 h, $n = 86$) and after incubation (4 h, $n = 90$). The colour scale applies for the F_0 and F_m images to indicate fluorescence signal intensity. The F_v/F_m image is scaled to F_m to give a 3-D impression and better show out of focus objects. A near infrared (NIR) image take under minimal light illumination is shown to illustrate the entire cell. The region of interest of which fluorescence values were obtained is encircled in each image (*i.e.* the central capsule).



Supplemental Figure III-2. Light (Rottermann Contrast) microscopy photographs taken after an experimental incubation. White arrows indicate a pseudopodal extension of each cell, and cyan arrows the limitations of the Acantharia ectoplasm

Supplemental Table III-3. Results of Tukey Kramer HSD post-hoc test for all possible comparisons of $\delta^{13}\text{C}$ in Acantharia incubations with inorganic nutrients. The most relevant comparisons are highlighted in bold, these entail the comparisons of each treatment with its natural control and the comparisons between the enrichment treatments.

Treatment	vs	Treatment	Difference	Std Err Dif	Lower CL	Upper CL	p-Value	Conclusion
15NO3		Dark	112.40	13.92	66.67	158.13	<.0001	Significant difference
15NO3		14NH4 control	111.19	13.02	68.41	153.97	<.0001	Significant difference
15NO3		12C control	108.88	13.02	66.10	151.66	<.0001	Significant difference
15NO3		14NO3 control	108.11	13.92	62.38	153.84	<.0001	Significant difference
13C		Dark	72.93	13.02	30.15	115.70	0.0004	Significant difference
13C		14NH4 control	71.72	12.06	32.11	111.32	0.0002	Significant difference
13C		12C control	69.41	12.06	29.80	109.01	0.0003	Significant difference
13C		14NO3 control	68.64	13.02	25.86	111.42	0.0007	Significant difference
15NH4		Dark	56.81	12.45	15.91	97.72	0.0033	Significant difference
15NH4		14NH4 control	55.60	11.44	18.03	93.18	0.0018	Significant difference
15NO3		15NH4	55.59	12.45	14.68	96.49	0.0041	Significant difference
15NH4		12C control	53.29	11.44	15.72	90.87	0.0027	Significant difference
15NH4		14NO3 control	52.52	12.45	11.62	93.43	0.0071	Significant difference
15NO3		13C	39.47	13.02	-3.31	82.25	0.0824	No Significant difference
13C		15NH4	16.12	11.44	-21.46	53.69	0.7908	No Significant difference
14NO3 control		Dark	4.29	13.92	-41.45	50.02	0.9999	No Significant difference
12C control		Dark	3.52	13.02	-39.26	46.30	1	No Significant difference
14NO3 control		14NH4 control	3.08	13.02	-39.70	45.86	1	No Significant difference
12C control		14NH4 control	2.31	12.06	-37.30	41.92	1	No Significant difference
14NH4 control		Dark	1.21	13.02	-41.57	43.99	1	No Significant difference
14NO3 control		12C control	0.77	13.02	-42.01	43.55	1	No Significant difference



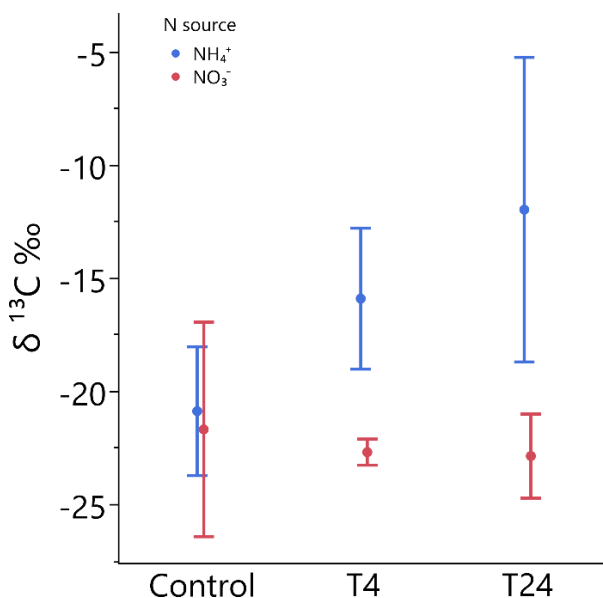
Supplemental Figure III-3. Non-symbiotic Acantharia after incubation with LFLA *I. galbana* at different time points imaged using confocal microscopy. Panels show the snapshots of different time points (30 and 240 min) with 3-D projections of separate channels and a composite of channels 1 through 3. Channel 1 (cyan) is for emission wavelengths 460-472 nm (Celltracker Blue fluorescence), and channel 2 (yellow) for 603-635 nm (unknown autofluorescence, likely carotenoids), and channel 3 (magenta) for 693-782 nm (chlorophyll autofluorescence). Channel 4 represents transmission light images. Z-stack images were three-dimensionally reconstructed with Imaris software.

Supplementary Methodology and Results

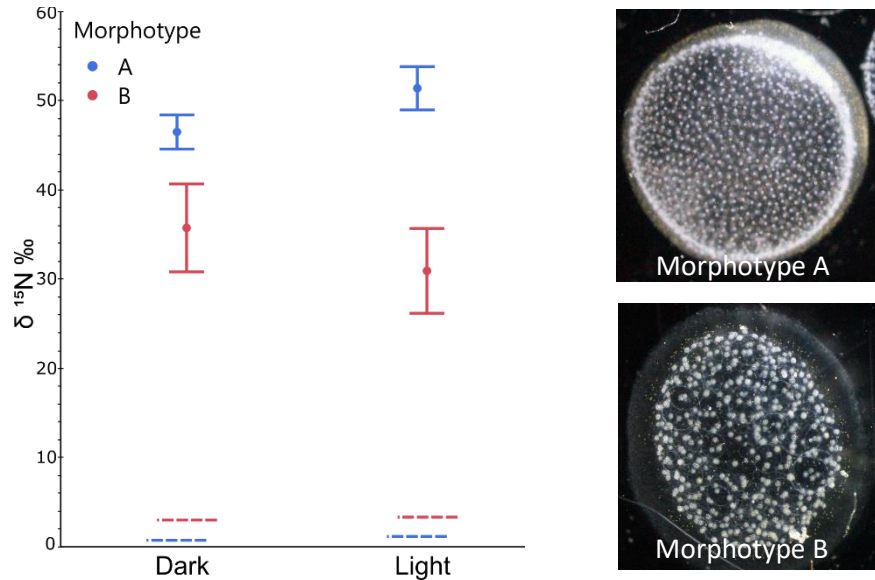
Acantharia and acantharian swarmer barcoding

Five single-cell Acantharia samples, as well as in triplicate acantharian swarmer were collected in 98% EtOH for barcoding. DNA extraction and purification were done using a Masterpure DNA purification kit (Epicentre-Illumina) following the manufacturer's protocol. Single-cell Polymerase Chain Reaction (PCR) was done to amplify the 28S ribosomal DNA gene with specific primers for Acantharia, '28S_Rad2' (5'-TAA GCG GAG GAA AAG AAA-3') and 'ITS a3' (5'-TCA CCA TCT TTC GGG TCC CAA CA-3') as described in Decelle et al., 2012. The 28S gene for Acantharia was amplified in a total volume of 25 μ L with: 0.35 μ M of each primer, MgCL2 1.5 mM, dNTPs mix 0.4 μ M, buffer GoTaq 1x and 0.625u of GoTaq Flexi polymerase G2 (Promega). The reaction proceeded with the following PCR parameters: 5 min at 95 $^{\circ}$ C, followed by 35 cycles of 30 s denaturation at 95 $^{\circ}$ C, 30 s annealing at 53-55 $^{\circ}$ C, 2 min extension at 72 $^{\circ}$ C, with a final elongation step of 10 minutes at 72 $^{\circ}$ C. All amplification products have been purified using the kit Nucleospin PCR Clean-Up (Macherey-Nagel) and eluted with 22 μ L of NE buffer. Sequencing was done using Big Dye Terminator Cycle Sequencing Kit (Life Technologies) by Macrogen. Sequences were cleaned and contigs constructed using ChromasPro software. Contig sequences were deposited under Genbank accession numbers OK157864-OK157871.

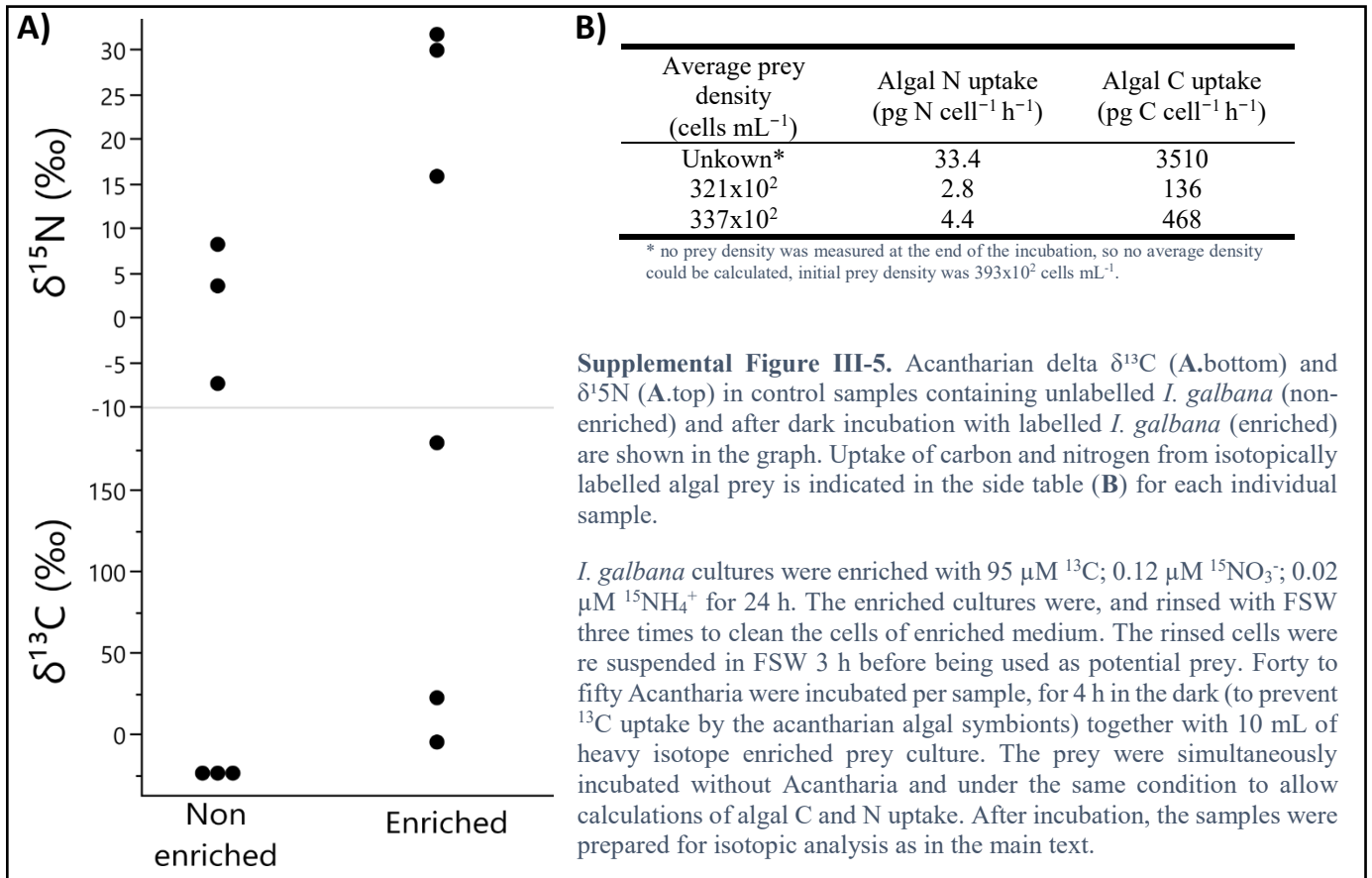
All resulting 28S contig sequences constituted the same sequence, with the best NCBI blast result identified as *Acanthostaurus* sp. or *Acanthometra* sp..



Supplemental Figure III-4. Evolution of isotopic carbon composition of Acantharia at different sampling times (4 h; 24 h) with two N sources treatment (blue: NH_4^+ ; red NO_3^-) (n = 3 each). Controls (n = 7 each) are the combination of the control (non-enriched) treatments at all the time points (0 h; 4 h; 24 h). Incubations were performed in 0.025 μ M $^{15}\text{NH}_4\text{Cl}$ or 0.12 μ M $\text{Na}^{15}\text{NO}_3$ and 10 μ M $\text{NaH}^{13}\text{CO}_3$, with Acantharia specimens obtained in September 2018 from the bay of Villefranche-sur-Mer. Further methodology is as described in the main text, except that incubations were performed in glass bottles in 50 ml volume, and under low (room level) illumination (undetermined, estimated at 20 to 35 photons $\text{m}^{-2}\text{s}^{-1}$ by reference). Shown are mean $\delta^{13}\text{C}$ values \pm SE. Isotope ratios suggests more carbon fixation in the presence of NH_4^+ .



Supplemental Figure III-6. Isotopic nitrogen composition for two Collodaria morphotypes after 5 hours of incubation in either the light or dark with dissolved $\text{NaH}^{13}\text{CO}_3$ ($30 \mu\text{M}$) and $^{15}\text{NH}_4\text{Cl}$ ($0.2 \mu\text{M}$). Specimens were obtained in April 2019 from the bay of Villefranche-sur-Mer using the methodology as described in the main text. Shown are mean $\delta^{15}\text{N}$ values \pm SE in ‰. The $\delta^{15}\text{N}$ of control incubations (incubated with non-enriched solutions) is indicated with dashed lines. Oneway-ANOVA with Tukey-Kramer post hoc test was conducted to compare the $\delta^{15}\text{N}$ among treatments, for this the natural samples (both dark and light) were combined. For morphotype A the combined samples of natural incubation average $0.97 \pm 0.26\text{‰}$ and is significantly different from $\delta^{15}\text{N}$ after incubation with enriched nutrients in both light ($51.41 \pm 2.43\text{‰}$) and dark ($46.51 \pm 1.92\text{‰}$) incubations ($F_{2,5} = 151.6$, $p < 0.0001$). In the case of morphotype B a similar trend is seen but with a smaller change in $\delta^{15}\text{N}$. After 5 hours both dark ($35.76 \pm 4.93\text{‰}$) and light incubation ($30.94 \pm 4.75\text{‰}$), $\delta^{15}\text{N}$ has increased significantly from the natural situation ($3.18 \pm 0.19\text{‰}$, $F_{2,5} = 12.45$, $p = 0.011$). This shows nitrogen uptake is significant in both morphotype A and B independent of light or dark conditions.

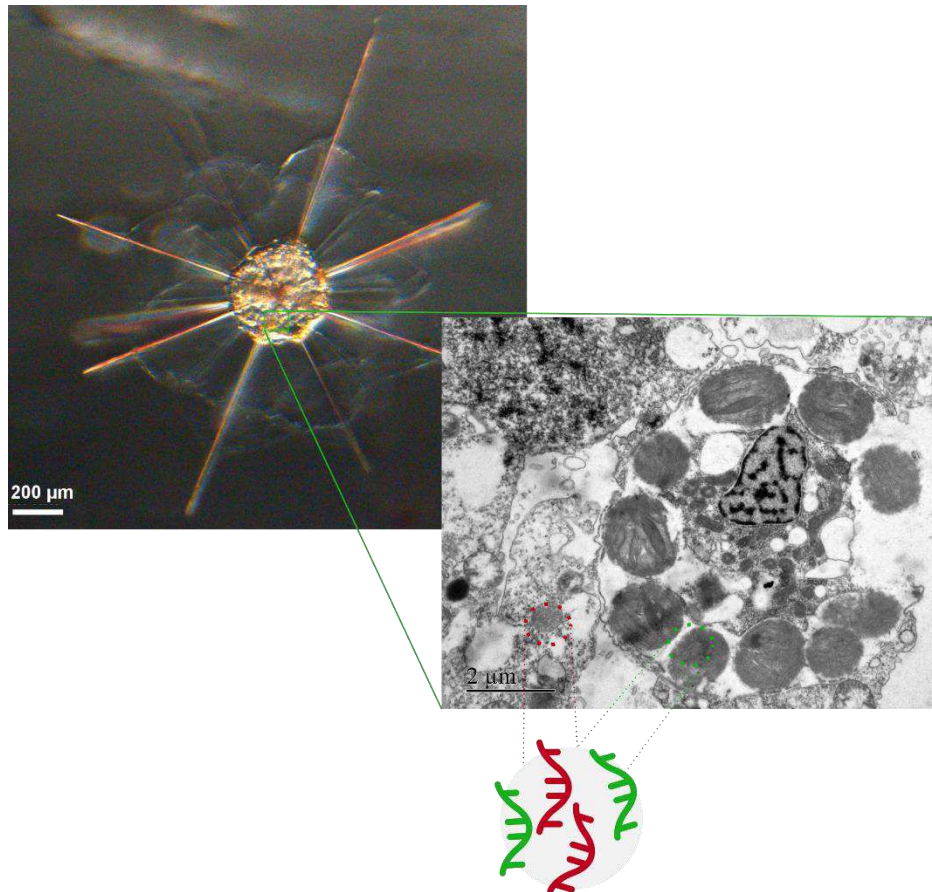


Supplemental Figure III-5. Acantharian delta $\delta^{13}\text{C}$ (A.bottom) and $\delta^{15}\text{N}$ (A.top) in control samples containing unlabelled *I. galbana* (non-enriched) and after dark incubation with labelled *I. galbana* (enriched) are shown in the graph. Uptake of carbon and nitrogen from isotopically labelled algal prey is indicated in the side table (B) for each individual sample.

I. galbana cultures were enriched with $95 \mu\text{M } ^{13}\text{C}$; $0.12 \mu\text{M } ^{15}\text{NO}_3^-$; $0.02 \mu\text{M } ^{15}\text{NH}_4^+$ for 24 h. The enriched cultures were, and rinsed with FSW three times to clean the cells of enriched medium. The rinsed cells were re suspended in FSW 3 h before being used as potential prey. Forty to fifty Acantharia were incubated per sample, for 4 h in the dark (to prevent ^{13}C uptake by the acantharian algal symbionts) together with 10 mL of heavy isotope enriched prey culture. The prey were simultaneously incubated without Acantharia and under the same condition to allow calculations of algal C and N uptake. After incubation, the samples were prepared for isotopic analysis as in the main text.

Chapter IV

The Acantharian holobiont—nutrient uptake capabilities investigated by chemical imaging and transcriptomics



“Je n’ai fait celle-ci plus longue que parce que je n’ai pas eu le loisir de la faire plus courte.”

— Blaise Pascal

“I apologize for such a long letter - I didn't have time to write a short one.”

— Mark Twain

Chapter overview

Acantharia are ubiquitous, heterotrophic single-celled plankton in oceanic waters. Their contribution and roles in ecosystems have previously been underestimated, being elusive due to their broad size range and fragility. Yet, recent studies show that they are major components of the planktic community contributing greatly to, among others, the carbon flux. The difficulties inherent to the study of live Acantharia, as for all Radiolaria, make it that very little is known about their physiology. Acantharia are known to form a photosymbiosis with the microalgae *Phaeocystis* sp.. It has recently been demonstrated that the photosymbionts are heavily modified in the acantharian host. These modifications seem to aim to exploit photosynthetic capabilities. Yet, how much the Acantharia relies on photosynthesis *versus* feeding is not well understood, nor are the metabolic interactions of host and symbiont. Here we aimed at elucidating the metabolic dialogue between these endosymbiotic partners. Therefore, we used single-cell isolations of Acantharia specimens incubated with carbon and nitrogen stable isotopes. We then used single-cell gene expression analyses (*i.e.* transcriptomics) to investigate the regulation, metabolic process, and their dependency of the nutrient uptake capabilities of the photosymbiont and host, and used chemical imaging to visualise and track the dynamics of carbon and nitrogen (nitrate and ammonium) assimilation and translocation between symbionts and host over time. With this, we aim to understand how and where carbon and nitrogen are assimilated and translocated in the holobiont. Furthermore, this combinatory approach could illustrate if the host itself has the capabilities to directly take up nitrate or ammonium, as well as how increased extraneous nitrogen concentrations affect the carbon assimilation.

This chapter starts with a general introduction and overview of the experimental design. The next part of the chapter details the single-cell transcriptomic approach, followed by the single-cell chemical imaging approach, and last part of the chapter attempts to bring it together.

Chapter IV.1

The Acantharian holobiont—nutrient uptake capabilities investigated by chemical imaging and transcriptomics

1. Introduction

Radiolaria are amoeboid planktic protists that are widespread throughout pelagic oceanic ecosystems (e.g., Dennett et al., 2002; De Vargas et al., 2015; Biard et al., 2016). They are characterised by their large size, from tens of micrometres to millimetres, and complex protoplasmic pseudopodal networks, as well as (when present) skeletons composed of either strontium sulfate (Acantharia) or silica (other Radiolaria) (Suzuki and Not, 2015). Radiolaria are inherently heterotrophic, and feed by means of their pseudopods, though many species are also photosymbiotic. Akin to corals, it is a symbiosis in which symbionts provide photosynthesis-derived products (photosynthates) to the host, which in turn provides an enclosed and relatively nutrient-rich microhabitat for their microalgal symbiont. The symbiont's photosynthates could be an important nutrient source for the Radiolaria (see Chapter III; Caron et al., 1995). The symbiosis could thus provide an advantage in nutritionally demanding habitats, such as oligotrophic oceanic waters where nutrients (such as nitrogen) are limited in availability.

Despite the ubiquitous presence of photosymbiotic Radiolaria in the sunlit layers of the oceans, metabarcoding approaches have shown contrasting biogeographies among the radiolarian classes of Collodaria and Acantharia, both being endosymbiotic (Faure et al., 2019). Big gelatinous colonies of Collodaria are predominantly inhabiting oligotrophic open ocean waters, whereas photosymbiotic Acantharia seem more prevalent in warmer shallow waters (Faure et al., 2019; Sandin, 2019). The studies of Faure et al., (2019) and Sandin (2019), however, show contrasting general trends toward depth for Collodaria, and there is likely still interspecificity to be taken into account. Photosymbiotic Acantharia can locally be of the most abundant large protists (Bottazzi, 1978; Michaels, 1991), and in the central North Pacific Ocean, they have been found to contribute up to 4% of the total primary production and as much as 20% of the surface production (Michaels, 1988, 1991). The significant contribution of Acantharia to primary production as well as vertical flux (Michaels et al., 1995; Gutierrez-Rodriguez et al., 2019) makes them important contributors of carbon fluxes in oceanic waters.

To explain their ecological success, it is critical to better understand the photosymbiotic relation and dependency that is of physiological importance to many Radiolaria. However, many aspects of the metabolism and physiology of this planktic symbiosis are still unknown. Fundamental aspects such as nutrient (e.g., carbon and nitrogen) uptake rates and capability have only minimally been studied (e.g., Michaels, 1991; Caron et al., 1995; Chapter III). The obligatory and inseparable nature of the Acantharia-*Phaeocystis* endosymbiosis, combined with the inability to culture the symbiosis, nor the symbiont from its symbiotic state, makes the quantifications of relative contributions of symbiont and host metabolic

process extremely challenging. Though unnatural, investigations of other endosymbioses, such as those involving dinoflagellates and Cnidaria, at least allow the separation of symbiont and host, and thereby allowing the investigation of their separated physiology (Yellowlees et al., 2008). Short-term maintenance experiments and single-cell methods have been proven to partially circumvent this problem (e.g., in Collodaria: Villar et al., 2018; Decelle et al., 2021, and Chapter III). In the context of the planktic Acantharia endosymbiosis, direct chemical imaging and quantification of metabolic exchanges (using NanoSIMS) in an intact symbiosis poses one of the few outcomes. Such chemical imaging techniques combined with stable isotope probing have already been successfully used to trace fixation of labelled carbon and nitrogen in several endosymbiotic systems, such as corals (Pernice et al., 2012); sponges (Achlati et al., 2018); foraminifera (LeKieffre et al., 2018), and even Radiolaria (Decelle et al., 2021; Uwizeye et al., 2021).

Decelle et al. (2021) used multimodal subcellular imaging (electron microscopy, and mass spectrometry imaging) to show that carbon assimilation is initially fixed in starch grains of collodarian symbionts. Subsequently, newly-fixed carbon was detected in the host's Golgi apparatus and is thus likely assimilated in the host cell as lipids or proteins through the Golgi. This is unlike other photosymbioses (e.g., corals (Kopp et al., 2015a), and foraminifera (LeKieffre et al., 2018) where newly-fixed carbon is firstly detected in lipid droplets before elsewhere in the host cell. In these colonial Radiolaria nitrogen from up taken ammonium is predominantly fixed in the symbiont compartments (Decelle et al., 2021). This is corroborated by single-cell transcriptomics (though on a different Collodaria species), where the presence of ammonium metabolism genes indicates ammonium as a major source of nitrogen for the symbionts (Liu et al., 2019). In the acantharian symbiosis, the symbiont *Phaeocystis sp.*, is shown to be transformed into a 'photosynthesis factory', as compared to a normal free-living *Phaeocystis* cell (Decelle et al., 2019; Uwizeye et al., 2021). Specifically, there is a multiplication and enlargement of the plastids and pyrenoids, as well as an increase in trace metals in the more voluminous vacuoles (Decelle et al., 2019). Enlarged pyrenoids could suggest further facilitation of carbon concentration for more efficient CO₂ supply to the Rubisco molecules and thus CO₂ fixation (Badger et al., 1998; Kaplan and Reinhold, 1999; Izumo et al., 2007). Transcriptome analysis also implied that the symbionts fix more carbon *in hospite* than *ex hospite*. Such extra carbon, as confirmed by chemical imaging, is transferred to the host cell (Uwizeye et al., 2021).

In the oceanic regions that these Acantharia inhabit, dissolved inorganic nitrogen (e.g. ammonium or nitrate) is scarce and can limit biological productivity (Vitousek and Howarth, 1991). In addition to nitrogen from feeding, the Acantharia-*Phaeocystis* symbiosis is able to take up dissolved inorganic nitrogen sources, which is an advantage when organic sources of nitrogen might be limited. In Chapter III I have shown the holobiont's capability for ammonium uptake, though nitrate uptake is not yet clear. In most instances, ammonium is the preferred source for nitrogen, due to its more energy-efficient assimilation (reviewed in Glibert et al., 2016). Indeed, free-living *Phaeocystis* are shown to increase ammonium uptake in lieu of nitrate when it is available. Contrastingly, it has been shown that nitrate better supports their growth (Wang et al., 2011). However, the metabolic and regulative pathways present in the host Acantharia are not known. *Thalassicolla nucleata* (Radiolaria), a solitary collodarian Radiolaria, lacks nitrate reductase genes, but the presence of nitrogen metabolism genes like glutamate dehydrogenases, ammonium transporters, and glutamine synthase indicate its capability of ammonium

uptake and assimilation (Liu et al., 2019). However, it remains unclear whether ammonium fixation proceeds predominately through the host or symbiont system, and likewise for nitrate.

In this chapter, the overarching objective is to elucidate the metabolic dialogue between symbiotic partners of the ubiquitous photosymbiotic Acantharia. Building off the information obtained in Chapter III, we here employ a pulse-chase experiment followed by single-cell mass spectrometry imaging and transcriptomics to investigate the carbon and nitrogen flux between both partners of the Acantharia-*Phaeocystis* photosymbiosis.

An experiment was set up to combine these both approaches and examine single cells under the exact same physiological conditions:

Chapter IV.1) A single-cell RNA-seq transcriptomic approach was utilised to assess gene expressional difference over time and between nitrogen treatments (nitrate or ammonium addition). Thereby separately investigating the genetic capability in regulative and metabolic processes of host and symbiont underlying observed physiology in nitrogen and carbon uptake, along with transcriptional difference, adaptability/plasticity of nutrient uptake when increased nutrients are present (eutrophication). The holobiont transcriptome will allow investigation of genetic pathways attributed to the host or symbiont.

Chapter IV.2) I further aimed to investigate the metabolic interactions of host and symbiont by tracing carbon and nitrogen fixation, localisation, and translocation using stable isotopes and NanoSIMS. Thereby, we visualized carbon fixation, and carbon translocation between symbionts and host over time, and the effect of nitrogen source (nitrate or ammonium) thereon.

2. Experimental setup

2.1. Sampling

Sampling was performed in the bay of Villefranche-sur-Mer (France, 43°41'10" N, 7°18'50" E) in October 2019. Plankton was collected each morning by gentle horizontal plankton net tows using a 150 µm plankton net. Collected samples were immediately diluted in buckets with freshly collected surface seawater. Acantharia specimen were manually sorted under Zeiss Stemi SV11 stereoscope in a 23 °C climate-controlled room and transferred into filter-sterilised seawater (FSW, 0.22-µm-pore-size). Isolated Acantharia were incubated minimally for one hour in FSW, after which they were transferred to fresh FSW. This washing process was repeated at least 3 times and allowed the self-cleaning of particles attached to the specimen and dilution to extinction of any organisms accidentally taken with (as described in Mansour & Not (2021), <https://dx.doi.org/10.17504/protocols.io.bqvrnw56>).

2.2. Isotopic Pulse-Chase Experiment

After the last specimen-cleaning step, as per the sampling procedure, samples were transferred to the experimental conditions. **Figure III-7** shows a conceptual drawing of the experimental design. Experimental treatments consisted of specimens incubated in FSW enriched with ¹³C (NaH¹³CO₃, 99% ¹³C, Eurisotop) and/or ¹⁵N (either nitrate (Na¹⁵NO₃, 98 % ¹⁵N, Eurisotop) or ammonium (¹⁵NH₄Cl, 99 % ¹⁵N, Eurisotop)). The nutrient treatments are thus as follows: 1) 1 mM NaH¹³CO₃ ; 2) 1 mM NaH¹³CO₃ + 1 µM ¹⁵NO₃⁻ or 3) 1 mM NaH¹³CO₃ + 0.4 µM ¹⁵NH₄⁺. Acantharia were incubated for five different durations, *i.e.*, 0 h, 2 h, 4 h, 16 h, 24 h, each timepoint consisting of a separate incubation. Additional individuals

were maintained in unspiked FSW to serve as unlabeled control specimens for NanoSIMS analyses. Incubations were done at 23 °C under a normal day-night cycle (light at $\pm 190 \mu\text{mol photons m}^{-2} \text{s}^{-1}$), as well as in complete darkness to assess photosynthesis-independent processes. For each treatment and timepoint 30 cells were incubated in 6-well plates. At T4 the cells were transferred to fresh FSW, through an intermediate transfer step in FSW (by means of rinsing), for the chase incubation period. At each timepoint 7 Acantharia (in max 5 μL volume of SW) were individually deposited in 0.2 mL micro-centrifuge tubes pre-filled with 100 μL lysis buffer (RNAqueous kit); immediately flash-frozen in liquid nitrogen, and stored at -80 °C for transcriptomic analyses (**Chapter IV.1**). Simultaneously, between 13 and 21 Acantharia in 30 μL FSW were chemically fixed at each timepoint in phosphate-buffered saline with a final concentration of 1% glutaraldehyde (Sigma) and 2% paraformaldehyde (Electron Microscopy Sciences), and stored at 4 °C for subsequent imaging analyses (**Chapter IV.2**). The current status of processing of all samples is outlined in **Table III-4**.

Table III-4. Overview of acantharian single-cell samples acquired for both chemical imaging (NanoSIMS) and transcriptomics (RNA) analyses for each treatment (rows) and timepoint (columns). Unprocessed samples are indicated without shading, and by a number that indicates the number of cells/samples still available. Samples indicated with a green shading are completed (*i.e.*, NanoSIMS chemical images or sequencing have been done); blue shading if samples have been prepared for and imaged with electron microscopy; red if samples have failed at an intermediate step (e.g., electron microscopy step or RNA extraction). All processed transcriptomic samples are indicated with green shading and the number of cell/samples for which cDNA libraries have been sequenced, with between brackets the additional number of technical replicates if applicable. Grey shaded cells are timepoints and treatments that were not collected.

		T0		T2		T4		T16		T24	
		NanoSIMS	RNA	NanoSIMS	RNA	NanoSIMS	RNA	NanoSIMS	RNA	NanoSIMS	RNA
Light	^{13}C	17	6	26	8	16	6	11	7	13	7
	$^{13}\text{C} + ^{15}\text{NO}_3$	21	2	17	2(2)	21		18	3(2)	19	4(1)
	$^{13}\text{C} + ^{15}\text{NH}_4$	19	4	23	4(1)	19	4(1)	16	5	19	4(1)
Dark	^{13}C (dark)			19	7	18	7	16	7		
	$^{13}\text{C} + ^{15}\text{NO}_3$ (dark)			13	4(1)	12	5	13	3(2)		
	$^{13}\text{C} + ^{15}\text{NH}_4$ (dark)			17	5	12	4(1)	14	4(1)		
Unlabelled	^{12}C	20	7			15		14			
	$^{12}\text{C} + ^{14}\text{NO}_3$	20	7			15		14			
	$^{12}\text{C} + ^{14}\text{NH}_4$	20	7			15		16			

complete in progress lost/failed

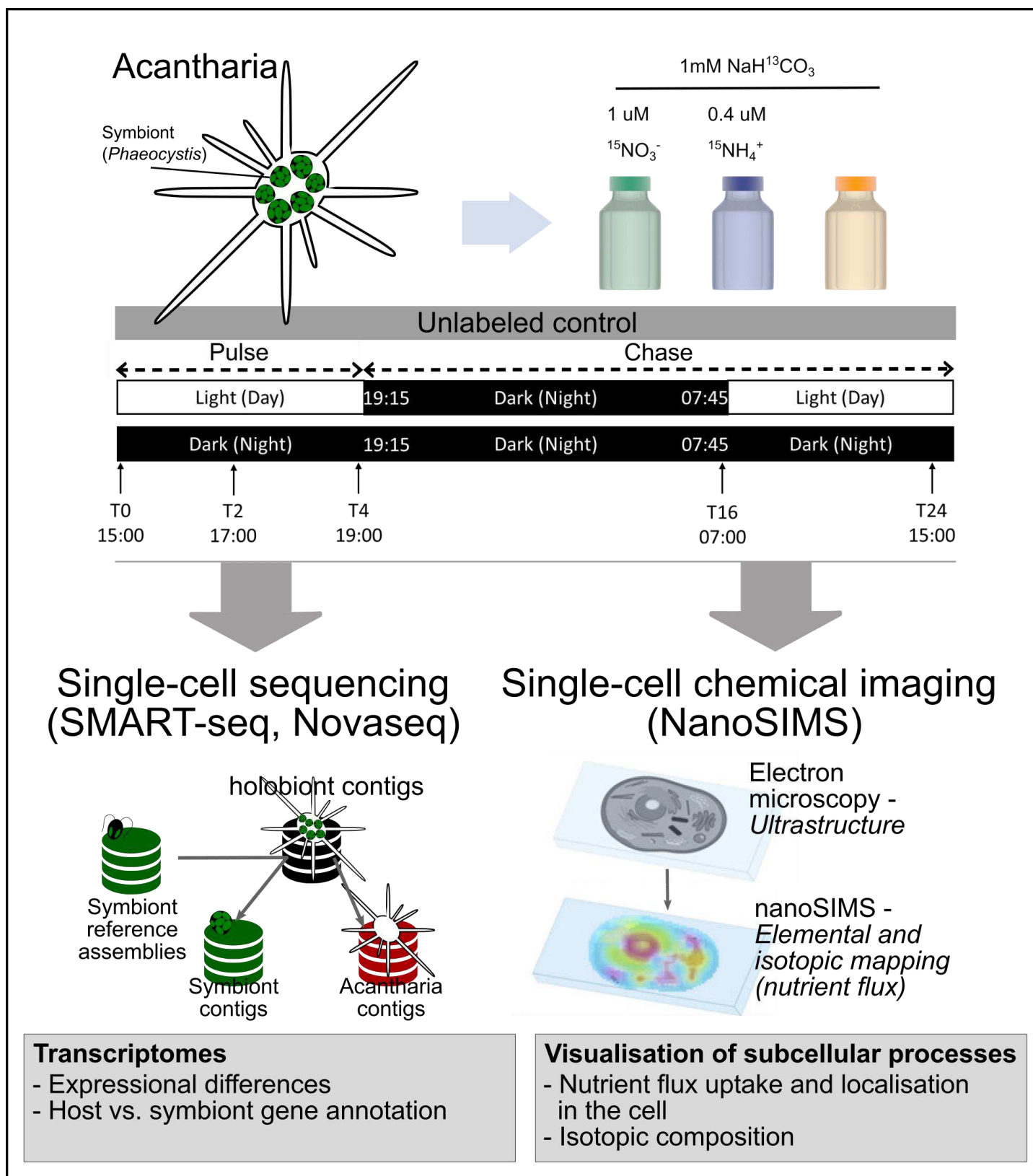


Figure III-7. Experimental design and analyses. The collected and isolated single cells were subjected to three different treatments under a normal day-night cycle and under complete darkness. Samples were subsequently taken for the indicated analyses at each timepoint. Electron microscopy, and NanoSIMS cell drawings reproduced from Decelle et al., 2020 with permission from Elsevier.

Chapter IV.2

Novel transcriptome of photosymbiotic *Acantharia* and an investigation of nutrient uptake capabilities of both symbiont and host

J.S. Mansour¹, E. Corre², U. John^{3,4}, F. Not¹

¹ CNRS and Sorbonne University, UMR7144, Adaptation and Diversity in Marine Environment (AD2M) Laboratory, Ecology of Marine Plankton Team, Station Biologique de Roscoff, Place Georges Teissier, Roscoff, France

² CNRS and Sorbonne University, FR2424, ABiMS team, Station Biologique de Roscoff, Place Georges Teissier, Roscoff, France

³ Alfred-Wegener-Institut, Helmholtz-Zentrum für Polar- und Meeresforschung, Bremerhaven, Germany.

⁴ Helmholtz Institute for Functional Marine Biodiversity (HIFMB), Oldenburg, Germany.

Keywords: symbiosis, single-cell transcriptomics, photosynthesis, oceanic plankton

In preparation

1. Methodology

1.1. RNA extraction, cDNA library preparation and sequencing

Total RNA was extracted directly from thawed specimen in lysis buffer using the RNAaquaous -Micro Total RNA Isolation kit (ThermoFisher #AM1912). A sub-sample of total RNA was analysed for successful extraction on an Agilent 2100 Bioanalyzer with a RNA 6000 Pico kit (Agilent #5067-1513) (for the detailed RNA extraction protocol see Mansour et al., 2021b). cDNA synthesis and amplification was performed following the manufacturer's protocol for the SMART-Seq V4 Ultra Low Input RNA kit (Takara #634890), using 50% extracted total RNA with 18 cycles in the polymerase chain reaction. Purified cDNA was quality checked and quantified with an Agilent 2100 Bioanalyzer using a High Sensitivity DNA Kit (Agilent #5067-4626) (for the detailed cDNA library preparation protocol see Mansour et al., 2021a). When less than five RNA samples were successfully extracted, a technical replicate for cDNA amplification was instead made from a successful RNA extract. Subsequently, cDNA that was deemed of sufficient quality was tagged (fragmented and tagged), indexed, and bead cleaned following the manufacturer's protocol for the Nextera XT DNA library prep kit (Illumina, FC-131-1096), using Nextera XT Index Kit v2 Set (Illumina # FC-131-2001) with 150 pg input cDNA. If less than five libraries of biological replicates were successfully

prepared, a technical replicate was prepared instead (total biological replicates (*i.e.* cells) = 57, with 13 technical replicates for a total of 70 samples). The indexed cDNA libraries were quantified and quality checked on an Agilent 2100 Bioanalyzer using a High Sensitivity DNA Kit (Agilent #5067-4626) and pooled in equal Molar of 2.25 nM, based on calculation of the cDNA concentration and average fragment size of each sample (concentration $\times 10^6$ divided by fragment size $\times 660$). Two pools were made, one with an average size range from 380 – 499 bp (average 451 bp) and one pool with a range from 500 – 779 bp (average 557 bp). Library pools were again bead cleaned with a ratio of 0.7x bead to eliminate primer influences. Library pools were pre-run on MiSeq (Bremerhaven, Germany) to quality check the libraries and assess the total reads per sample. Final sequencing was done on a Novaseq S1 flowcell (Jena, Germany), and a total of 2.1 billion reads were generated. Raw de-multiplexed reads have been deposited to NCBI SRA under BioProject [PRJNA763349](https://www.ncbi.nlm.nih.gov/bioproject/PRJNA763349).

1.2. Acantharia transcriptome assembly and binning

Raw reads were de-multiplexed using Illumina bcl2fastq2. Sequencing data quality was assessed using FastQC v. 0.72 (Andrews, 2010) and visualized using MultiQC (Ewels et al., 2016) before and after each trimming step. All reads were quality trimmed and filtered using Trimmomatic v. 0.38 (Bolger et al., 2014), with ILLUMINACLIP: 2:30:10 and the parameters: SLIDINGWINDOW:4:5 LEADING:5 TRAILING:5 MINLEN:25. Quality trimmed paired-end reads were filtered for rRNA using SortMeRNA v. 2.1b.4 (Kopylova et al., 2012) matching the reads versus SILVA 16S bacteria, 23S bacteria, 18S eukarya, and 28S eukarya databases. Matched reads were regarded as rRNA and removed for subsequent transcriptome assembly. The remaining supposed mRNA transcripts from all samples ($n = 70$) were assembled using RNAspades (see **Supplementary Material 1** for assembly comparison with a Trinity v2.11.0 (Grabherr et al., 2011) assembly). The assembly was annotated following the Trinotate pipeline (Bryant et al., 2017), as well as GhostKoala (Kanehisa et al., 2016) for functional annotation of the transcripts with Kyoto Encyclopedia of Genes and Genomes (KEGG) orthologs.

The *de-novo* assembly was searched against a custom database, containing four *Phaeocystis* transcriptome assemblies (*i.e.* METDB_00327, METDB_00333, METDB_00329 from <http://metdb.sb-roscoff.fr/metdb>, and the *Phaeocystis* assembly from Mars Brisbin 2020: https://github.com/maggimars/PcordataSymbiosisDGE/blob/2b7836d2f6ebf9a5d80cbcce22988f161428e459/pc_euk_seqs.fasta), using MegaBLAST. All hits with bitscores > 90 were considered *Phaeocystis* transcripts. Additionally, a two-component Gaussian Mixture Model (GMM) was fitted to the GC-content distribution of the assembly. Transcripts that were predicated with $> 99\%$ confidence to belong to high GC-content component were deemed *Phaeocystis* transcripts (Liu et al., 2019). The *Phaeocystis* transcripts identified with the BLAST hits and the GMM analysis were separated out of our assembly into a “*Phaeocystis* bin”.

Transcriptome “completeness” was evaluated by determining the percentage of eukaryotic Benchmarking Universal Single-Copy Orthologs (BUSCO v5, Manni et al., 2021) that were complete, fragmented, or missing in the transcriptomes. BUSCOs provide a method to quantitatively assess the quality of a transcriptome in terms of gene content; more complete transcriptomes contain more full-length BUSCOs, which are well-conserved genes for the representative genomes of each BUSCO group. All code and data analysis pipelines are available in **Online Supplementary Material 1**.

1.3. Differential gene expression analysis

Quality trimmed reads were mapped back to the assembly and read counts were calculated using RSEM v. 1.2.29 (Li and Dewey, 2011) with bowtie2 v.2.4.1 (Langmead and Salzberg, 2012) in the Trinity package. Counts of read mapping were analysed in the R statistical environment (R Core Team 2013). Counts of transcripts were kept when counts per million was more than one in at least two samples (smallest group size), transcripts not passing this criteria were filtered out from the analysis. Normalisation, statistical analyses, and differential gene expression comparisons were done using the EdgeR (Robinson et al., 2009) and limma (Law et al., 2014) packages. Genes with adjusted $p < 0.01$ and \log_2 fold-change $> |1|$ were considered significantly differentially expressed. Likewise, KEGG (Kyoto Encyclopedia of Genes and Genomes) pathways were considered significantly enriched among enriched or depleted genes when $p\text{-adj} < 0.01$. Detailed procedures are shown in **Supplementary Material 2**, and all code and data analysis pipelines are available in Online Supplementary Material 2.

2. Results

2.1. Transcriptome assembly, assessment, and binning

A total of 2.1 billion 2x100bp paired-end reads were generated by Novaseq S1 flowcell sequencing; 19.4 to 116.2 million sequence reads per sample. Quality filtering with Trimmomatic removed only 0.003% read pairs, SortmeRNA filtered out 328 million reads (15%) leaving 1.8 billion prospected paired mRNA reads, 4.8 – 70.2 million read per sample. *De novo* assembly was performed with both Trinity and rnaSPAdes, though the rnaSPAdes assembly achieved overall better metrics and read mapping, and was thus used for further analyses (**Supplementary Material 1**). The *de novo* assembly generated 2,108,782 transcripts totalling 2,649,628,289 bp, with a N50 of 2073 and an Ex90N50 of 3200. The GC content of the transcripts exhibited a bimodal distribution (**Figure III-8**). The low GC% transcripts are suspected to be Acantharia transcripts, and the high GC% transcripts from symbionts (Liu et al., 2019). The holobiont transcriptome assembly includes complete sequences for 96.9% of searched eukaryotic BUSCOs.

Only using the BLAST results to filter out the symbiont of the holobiont transcriptome results in a GC-content profile for the presumed host transcripts that still contained a high-GC-content tail. For that reason, we additionally used a Gaussian Mixed Model (GMM) to filter out those contigs, *i.e.* contigs with 99% certainty of belonging to the high GC-content model. In this manner, 15% of the assembly was designated as from the symbiont, *Phaeocystis*. The remaining 85% of the transcripts are treated as Acantharia host transcripts. The split assembly had 91% and 89% complete eukaryotic BUSCOs for the contigs assigned to *Phaeocystis* and those assigned to Acantharia respectively. Summary statistics of the holobiont transcriptome and the splitting are listed in **Table III-5**. Further details, scripts, and analyses for assembly assessment and splitting are found in **Supplementary Material 1**.

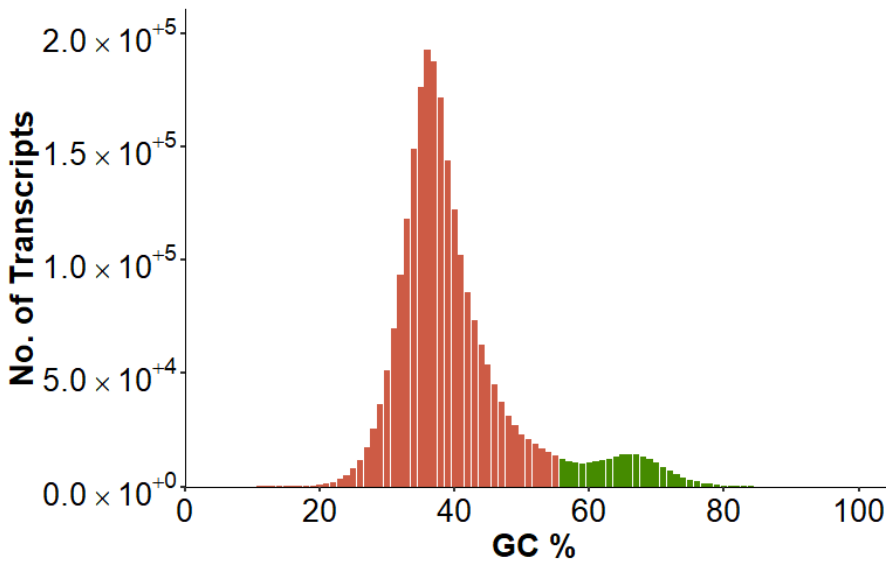


Figure III-8. GC-content distribution of all assembled transcripts. Colours indicate an arbitrary cut-off for the low GC% transcripts (red) suspected to be of acantharian origin and high GC% transcripts (green) suspected to be of symbiont origin.

Table III-5. Summary metrics of assembled transcripts of *Acantharia* holobiont after quality filtering of reads, and sorting into symbiont and host partitions. Read alignment has been performed using RSEM bowtie2.

	Holobiont Assembly	<i>Phaeocystis</i> bin	Non- <i>Phaeocystis</i> bin
Number of contigs (transcripts)	2,108,782	305,580	1,803,202
Sum base pairs	2,649,628,289	397,066,192	2,252,562,097
max contig length	85,738	85,738	60,511
min contig length	54	56	54
median contig length	760	762	759
average contig length	1256.47	1299.39	1249.2
GC%	41.08	56.65	38.34
N50	2,073	2,161	2,059
Average alignment rate %	88.63	18.07	78.15
Ex90N50	3,200	2,266	3,051
Ex90N50 (RSEM) #number of genes	145,802	2,993	144,604
Transcripts with ≥ 1 TPM	1,114,262	252,848	996,055

2.2. Transcript annotations

Transcripts assigned to the *Phaeocystis* symbionts accounted for only 12.5% of the holobiont transcriptome, yet were better annotated than the presumed host transcripts (**Table III-6**). Within annotated pathways for nitrogen metabolism both transcriptome partitions contained transcripts for all annotated paths, including nitrate reductase, and genes for ammonium uptake including glutamate synthase, as well as carbamoyl-phosphate synthase involved in the urea pathway by catalysing a reaction involving ammonia. Urea carboxylase, which is also involved in the urea excretion pathway was only found in presumed host transcripts. More than 450 transcripts related to carbonic anhydrase transcripts were found in the presumed host transcriptome, whereas less than 40 were identified in the *Phaeocystis* transcriptome bin. Photosynthesis pathway-related transcripts remained present in the presumed host transcriptome bin, these included transcripts for photosystems I and II (**Supplemental Figure III-20, Online Supplementary Material 1**).

Table III-6. Annotation metrics for the *Acantharia* holobiont assembly, and after sorting into symbiont and host partitions. The Trinotate pipeline was followed for annotation, as well as Transdecoder to predict total proteins, protein predictions were used to assign KEGG annotations using GhostKoala.

	Holobiont Assembly	<i>Phaeocystis</i> bin	Non- <i>Phaeocystis</i> bin
Number of contigs (transcripts)	2,108,782	305,580	1,803,202
Transdecoder: Number of predicted proteins	975,424	241,874	33,550
Trinotate			
Contigs with GO annotations	212,493 (10%)	88,345 (37%)	124,148 (17%)
with eggnoG annotation	106,231	32,900	73,331
with Kegg annotation	282,245	103,242	179,003
GhostKOALA			
Predicted proteins with KO annotation	249,439 (26%)	84,468 (35%)	164,971 (22%)
Contigs with KO annotation	187,094 (9%)	60,592 (25%)	126,502 (17%)
Contigs with also KEGG pathway annotation	154,460	56,217	98,243

2.3. Differential expression exploration

Initial data exploration revealed four samples (from several treatments) to be outliers amongst the other samples (**Supplemental Material 2**). These samples showed expressional differences unlike the relevant biological replicates. It is noted that concurrently these samples showed abnormal Bioanalyser profiles, and GC-content profiles consisting of high GC-content (**Supplemental Figure III-26**). Analyses were thus redone without these samples.

2.3.1 *Phaeocystis* bin

Differential expression in the symbiont is mostly observed within the first 2 hours. With a difference between the nitrate and ammonium treatment apparent for incubations in complete darkness, this difference fades after 16 hours (**Online Supplementary Material 2.1**). Under normal day/night conditions there does not seem to be a difference between the ammonium and nitrate treatments (**Online Supplementary Material 2.1**). At each condition, the strongest differential expression is indeed observed after 2 hours with no or limited further changes observed from 2 to 4 hours (**Supplemental Figure III-28, 26**). Expressional differences are then again observed from 4 to 16 hours, which includes the night, so likely circadian rhythm related expression would be expected indifferent from the treatment since this is observed under both normal light cycles as well as dark treatment (with the exemption of the nitrate treatment under a normal day-night cycle). Comparisons of dark and light treatments indicate differential expression only with the ammonium treatment (**Online Supplementary Material 2.1**).

Compared to the 0 h control timepoint, there is a decrease in expression in the TCA cycle of the *Phaeocystis* bin after 16 h (night) with ammonium under a normal light cycle. However, at 2 h in the dark this was upregulated. Fatty acid biosynthesis is consistently downregulated in ammonium treatments, *i.e.* at 2 h in the dark and light, as well as after 16 h with a normal light cycle (**Online Supplementary Material 2.1**).

2.3.2 Non-*Phaeocystis* bin

Very few transcripts are differentially expressed under nitrate treatments in the non-*Phaeocystis* bin (**Online Supplementary Material 2.2**). Under ammonium treatments in the dark differential expression is, like for the *Phaeocystis* transcriptome bin, apparent after 2 hours with no further changes at later timepoints. The differential expression under a normal light cycle with ammonium shows downregulation of transcripts after 2 h hour, but this changes to mostly upregulation at 16 h (encompassing the night), and changes back to downregulation at 24 h (the subsequent morning) (**Supplemental Figure III-30**).

Compared to the 0 h control timepoint, the non-*Phaeocystis* (host) pathway for fatty acid biosynthesis is downregulated at 2 h in the dark and in the light with ammonium, it is however highly upregulated at 16 h with ammonium under a normal light cycle. Likewise, nitrogen metabolism and arginine biosynthesis (including aspects of the urea cycle) are also downregulated at 2 h in the dark and in the light with ammonium. After 16 h at a normal light cycle, these pathways become upregulated (**Online Supplementary Material 2.2**). Seeing as pathways for, e.g., nitrogen metabolism, arginine biosynthesis, and fatty acid biosynthesis show similar expression at 2 h independent of light, but changes at 16 h (at night), suggests the expression might be mediated by circadian rhythm patterns.

3. Discussion

3.1. Dataset features

We constructed an assembly from multiple (70) single-cell holobiont samples resulting in a large assembly of 2 million contigs, with a high N50 (Ex90N50) (N50 > 500 bp considered high quality) as compared to other holobiont transcriptomes (e.g., coral-dinoflagellate an N50 of ± 1332 bp; Colodaria-dinoflagellate an N50 of ± 300 bp, Meng et al., 2018). The holobiont transcriptome is found to be very complete, as assessed with BUSCOs (96.9%). However, as might be expected considering the holobiont nature of this assembly the duplication rate is also quite high with 69.8%. Splitting of this assembly into our *Phaeocystis* and non-*Phaeocystis* bins reduced the BUSCO duplications for both bins to around 50%. The still high duplication rate in these assembly bins might imply there are still other contaminating sequences that might need to be discarded in their entirety. For example, there might be other symbiont identities to consider (see next paragraph) for filtering out from the transcriptome. Read mapping remapping rate is another crucial aspect for a high-quality *de novo* assembly, the Acantharia holobiont assembly has good read remapping with mapping rates > 80% for the great majority of samples. The *Phaeocystis* assembly bin maps on average 10% of the reads and is considerably higher than for previous Acantharia holobiont samples (Mars Brisbin 2020), likewise, annotation rate is higher.

3.2. Identifying holobiont taxonomy and possible prey items

The single-cell reads generated could be further exploited to study the acantharian holobiont. The rRNA reads separated with SortMeRNA have been assembled using Trinity for each sample. Barrnap and Seqkit were further used to select for rRNA sequences of at least 850 bp in length. Such rRNA transcriptome contigs may additionally be used to explore the identity of other holobiont constituents such as bacteria and microalgae using metagenomics classifications. Our initial BLAST analysis of this rRNA already finds sequences matching haptophytes of the genus *Phaeocystis*, as well as *Chrysochromulina*. *Phaeocystis* is perceived as the common symbiont of Acantharia (Decelle et al., 2012a), though

Chrysochromulina has also been identified as a possible photosymbiont of Acantharia (Mars Brisbin et al., 2018). Additionally, hits of ciliates—presumed prey items—often show up among the samples, specifically, *Parafavella*, *Tintinnopsis*, and *Strombidium*. Congruent with this, tintinnids and other ciliates have previously been identified as the main prey source of Acantharia (Swanberg and Caron, 1991). Other potential prey sequence hits are among others, Diplonemidae, *Colponema*, *Emiliana huxleyi*, *Neobodo*, *Cafeteria burkhardae*, a single sample also contained rRNA sequence of the copepod *Calanus*. However, current analyses do not exclude any of the sequences as contamination, nonetheless, give an indication of possible relations by consistency in their presence.

3.3. Symbiont and host pathways

To identify gene annotations for both symbiont and host, an attempt was made to computationally separate (*in silico*) the holobiont transcriptome into symbiont and host transcripts. KEGG pathway annotations identified pathways involving nitrate reduction and ammonium transport in both host and symbiont transcriptome bins (**Supplemental Figure III-23**) indicating that also the host might directly benefit from these nitrogen sources. Nitrate reduction genes are not commonly found in the (heterotrophic) host animal transcriptome/genome, and are, for example, not found in a Collodaria transcriptome (Liu et al., 2017). Likewise, mixotrophic *Dinophysis* does not use nitrate (García-Portela et al., 2020). Urea pathway-related genes in the host might allow the host to independently from photosynthesis fix carbon, through the reduction of ammonium using bicarbonate. How these genes are expressed in dark treatments could shed further light on the role of the host in carbon fixation in a photosynthesis-independent manner.

Carbonic anhydrase-related transcripts are mainly found in the presumed host transcripts (**Supplemental Figure III-23**) and would imply the Acantharia facilitates rapid interconversion of carbon dioxide into bicarbonate ions that might be used during photosynthesis by the symbionts. It can also be expected that the host supplies its symbionts with CO₂ for carbon fixation since the symbionts are not directly connected to the outside environment (Furla et al., 2011). In collodarian symbionts, carbonic anhydrase is downregulated as compared to the free-living algae, which was suggested to be due to a lessened need for a carbon-concentrating mechanism (CCM) as this role might be fulfilled by the host's respiration (Liu et al., 2019). Additionally, like the transcriptome in this study, the Collodaria transcriptome also contained several carbonic anhydrase transcripts. It is likely that in photosymbiotic systems the host also fulfils a role in the CCMs, as might be evidenced by this Acantharia transcriptome, and was previously suggested for cnidarian photosymbioses (Davy et al., 2012).

Oddly, photosynthesis pathway-related transcripts are also identified in the presumed host transcripts. The Acantharia-*Phaeocystis* symbiosis has been shown to be a symbiosis where the symbiont is heavily altered (Decelle et al., 2019), and host and symbiont might be further intertwined through symbiosome invagination (Uwizeye et al., 2021). Considering this entangled nature of the symbiosis it is not unlikely that endosymbiont gene transfers might have occurred.

Though, these observations should be taken cautiously as the observation might still be biased by mistaken transcriptome separation or sample contamination, and would require more evidence and further investigation into the Acantharia transcriptome. The separated transcriptome bins might be further verified for their taxonomy to exclude contaminating, or bacterial microbiome sequences.

Supplementary Material to Chapter IV.2

Novel transcriptome of photosymbiotic Acantharia and an investigation of nutrient uptake capabilities of both symbiont and host

Supplementary Material 1:

Methods and analyses on Acantharia holobiont transcriptome assembly and annotation

An online version containing all scripts and code underlying the analyses, as well as interactive graphics, can be found online at <https://doi.org/10.5281/zenodo.5105584> (Online Supplementary Material 1).

1. Conclusion/Summary on de-novo assembly analyses

- Quality trimming, cleaning and rRNA filtering of raw reads removed 15.3% of all reads leaving a total of 1,818,532,330 paired mRNA reads (**Supplemental Table III-5**).
- BUSCOs of the assemblies show high percentage of duplicate BUSCOs, missing BUSCOs are few. Complete BUSCOs of the rnaSPAdes assembly are 96.9% of the searched eukaryotic database.
- GC content of the assembled transcript show a bimodal distribution, similar to the reads used in the assembly (**Supplemental Figure III-7**, and **Supplemental Figure III-8**). The low GC% transcripts could be suspected to be Acantharia transcripts, and the high GC% transcripts of the symbiont.
- Remapping on the assemblies is good, but better for the rnaSPAdes assembly (**Supplemental Figure III-10**).
- Mapping rates are better with RSEM than kallisto.
- Stats of the rnaSPAdes (hard filtered) assembly are generally better and this assembly is decided to be the preferred assembly (**Supplemental Table III-6**).
- Splitting the assemblies by mapping reads to a *Phaeocystis* reference selects most of the high percent GC contigs, but also some of the low percent GC contigs (**Supplemental Figure III-14, and 11**).
- Both transcriptome bins contain annotated pathways for genes involved in nitrate and ammonium metabolism (**Supplemental Figure III-23**).
- Photosynthesis pathway-related transcripts are present in the Non-*Phaeocystis* transcriptome bins (**Supplemental Figure III-20**).

2. Intro

A total of 2.1 billion 2x100bp paired-end reads were generated. 19.4 to 116.2 million sequence reads per sample. Quality filtering with Trimmomatic removed only 0.003% read pairs, SortmeRNA filtered out 425 million reads leaving 1.7 billion prospected mRNA reads, 4.8 – 70.2 million read per sample.

2.1 Sequence data

Raw reads were de-multiplexed using Illumina's bcl2fastq2. The numbers of a *sample code* are corresponding to the timepoint and treatment as in **Supplemental Table III-4**. Where the first number indicates the treatment and the second number the biological replicate. A letter 'a' or 'b' indicates a 'technical' replicate on the cDNA amplification level from the same sample/specimen. Hence both from an aliquot of the same RNA. A third number, either 1 or 2, indicates an aliquot of the cDNA sample has been used twice for indexing. Hence, that would be a 'technical' replicate on the sequencing level.

Supplemental Table III-4. Samples and SRA repository number

Sample code	Condition	SRA Run Number
23_2	D16NH4_rep1	SRR15902135
23_4_1	D16NH4_rep2	SRR15902134
23_4_2	D16NH4_rep3	SRR15902133
23_5	D16NH4_rep4	SRR15902089
23_6	D16NH4_rep5	SRR15902088
19_2_1	D16NO3_rep1	SRR15902087
19_2_2	D16NO3_rep2	SRR15902086
19_4_1	D16NO3_rep3	SRR15902085
19_4_2	D16NO3_rep4	SRR15902084
19_5	D16NO3_rep5	SRR15902083
21_1	D2NH4_rep1	SRR15902082
21_2	D2NH4_rep2	SRR15902081
21_3	D2NH4_rep3	SRR15902080
21_4	D2NH4_rep4	SRR15902079
21_5	D2NH4_rep5	SRR15902078
17_1_1	D2NO3_rep1	SRR15902077
17_1_2	D2NO3_rep2	SRR15902076
17_2	D2NO3_rep3	SRR15902075
17_3	D2NO3_rep4	SRR15902074
17_5	D2NO3_rep5	SRR15902073
22_1	D4NH4_rep1	SRR15902072
22_5	D4NH4_rep2	SRR15902071
22_6_1	D4NH4_rep3	SRR15902070
22_6_2	D4NH4_rep4	SRR15902069
22_7	D4NH4_rep5	SRR15902068
18_1	D4NO3_rep1	SRR15902067
18_2	D4NO3_rep2	SRR15902066
18_3	D4NO3_rep3	SRR15902132

Supplemental Table III-4. Samples and SRA repository number

Sample code	Condition	SRA Run Number
18_4	D4NO3_rep4	SRR15902131
18_5	D4NO3_rep5	SRR15902130
9_1	L0NH4_rep1	SRR15902129
9_3	L0NH4_rep2	SRR15902128
9_4	L0NH4_rep3	SRR15902127
9_6	L0NH4_rep4	SRR15902126
5_2	L0NO3_rep1	SRR15902125
5_3	L0NO3_rep2	SRR15902124
11_1	L16NH4_rep1	SRR15902123
11_2	L16NH4_rep2	SRR15902122
11_3	L16NH4_rep3	SRR15902121
11_6	L16NH4_rep4	SRR15902120
11_7	L16NH4_rep5	SRR15902119
7_6_1	L16NO3_rep1	SRR15902118
7_6_2	L16NO3_rep2	SRR15902117
7_7a_1	L16NO3_rep3	SRR15902116
7_7a_2	L16NO3_rep4	SRR15902115
7_7b	L16NO3_rep5	SRR15902114
12_1	L24NH4_rep1	SRR15902113
12_2_1	L24NH4_rep2	SRR15902112
12_2_2	L24NH4_rep3	SRR15902111
12_3	L24NH4_rep4	SRR15902110
12_4	L24NH4_rep5	SRR15902109
8_1	L24NO3_rep1	SRR15902108
8_2a	L24NO3_rep2	SRR15902107
8_2b	L24NO3_rep3	SRR15902106
8_3	L24NO3_rep4	SRR15902105
8_6	L24NO3_rep5	SRR15902104
36_2_1	L2NH4_rep1	SRR15902103
36_2_2	L2NH4_rep2	SRR15902102
36_3	L2NH4_rep3	SRR15902101
36_4	L2NH4_rep4	SRR15902100
36_5	L2NH4_rep5	SRR15902099
32_5_1	L2NO3_rep1	SRR15902098
32_5_2	L2NO3_rep2	SRR15902097
32_7_1	L2NO3_rep3	SRR15902096
32_7_2	L2NO3_rep4	SRR15902095
10_1	L4NH4_rep1	SRR15902094
10_2	L4NH4_rep2	SRR15902093
10_3	L4NH4_rep3	SRR15902092
10_5_1	L4NH4_rep4	SRR15902091
10_5_2	L4NH4_rep5	SRR15902090

3. Read cleaning

3.1 Trimmomatic

All reads were quality trimmed and filtered using Trimmomatic v. 0.38 (Bolger, Lohse, and Usadel 2014), with ILLUMINACLIP: 2:30:10 and the parameters: SLIDINGWINDOW:4:5 LEADING:5 TRAILING:5 MINLEN:25. Trimmomatic was run in the Galaxy environment.

3.2 SortmeRNA and read pairing

Quality trimmed paired-end reads were filtered for rRNA using SortMeRNA v. 2.1b.4 (Kopylova, Noé, and Touzet 2012) matching the reads versus SILVA 16S bacteria, 23S bacteria, 18S eukarya, and 28S eukarya databases. SortmeRNA was run in the Galaxy environment. Matched reads were regarded as rRNA and removed for subsequent transcriptome assembly. SortmeRNA filtered reads had to be re-paired using [seqkit pair](#) (Shen et al. 2016).

The resulting change in the number or paired reads before and after each quality trimming and filtering is shown in **Supplemental Table III-5**

Supplemental Table III-5. Table of reads after each trimming and quality filtering step

Sample	Trimmomatic		SortMeRNA		seqkit-pair Surviving paired-end reads
	Input read pairs	Surviving	rRNA	rRNA (%)	
10_1_S21	34,452,140	34,451,430	16,268,530	47.2	26,696,888
10_2_S22	116,230,700	116,229,007	97,037,409	83.5	19,044,289
10_3_S23	27,964,108	27,963,620	20,829,549	74.5	12,333,822
10_5_1_S24	17,183,280	17,182,939	12,340,674	71.8	4,801,521
10_5_2_S25	46,160,267	46,159,361	31,676,139	68.6	14,411,170
11_1_S30	34,588,552	34,587,508	2,043,973	5.9	34,434,578
11_2_S31	41,540,618	41,538,956	1,515,045	3.6	41,468,558
11_3_S32	30,289,940	30,289,072	986,782	3.3	30,247,146
11_6_S33	21,533,654	21,533,071	804,041	3.7	20,491,433
11_7_S34	28,979,691	28,978,535	7,875,263	27.2	20,380,381
12_1_S47	22,044,792	22,044,323	2,272,742	10.3	19,687,627
12_2_1_S48	36,365,604	36,364,687	1,024,131	2.8	35,218,631
12_2_2_S49	29,564,418	29,563,369	864,962	2.9	28,559,629
12_3_S50	24,981,262	24,980,379	1,610,883	6.4	23,189,274
12_4_S51	20,827,085	20,826,497	775,891	3.7	19,986,653
17_1_1_S59	20,781,891	20,781,223	1,243,348	6.0	19,317,117
17_1_2_S60	17,258,347	17,257,718	1,047,980	6.1	17,174,038
17_2_S17	16,147,189	16,146,960	5,954,902	36.9	13,889,672
17_3_S44	48,858,206	48,856,832	5,719,158	11.7	48,131,906
17_5_S52	20,117,458	20,116,469	2,578,281	12.8	17,328,736
18_1_S8	26,549,079	26,548,559	9,451,006	35.6	17,000,399

Supplemental Table III-5. Table of reads after each trimming and quality filtering step

Sample	Trimmomatic		SortMeRNA		seqkit-pair
	Input read pairs	Surviving	rRNA	rRNA (%)	Surviving paired-end reads
18_2_S18	29,228,939	29,227,667	2,696,323	9.2	26,441,177
18_3_S9	24,432,707	24,432,153	2,153,908	8.8	22,160,532
18_4_S19	20,180,983	20,180,621	3,832,874	19.0	16,242,182
18_5_S10	20,381,480	20,380,970	7,050,344	34.6	17,816,464
19_2_1_S27	20,402,230	20,401,611	1,823,528	8.9	18,433,752
19_2_2_S28	36,443,335	36,442,594	3,517,425	9.7	36,059,818
19_4_1_S36	27,532,522	27,531,816	1,433,996	5.2	27,442,392
19_4_2_S37	24,781,530	24,780,763	1,194,967	4.8	23,452,070
19_5_S20	28,317,285	28,316,616	9,133,899	32.3	25,276,340
21_1_S16	22,743,178	22,742,548	5,899,717	25.9	21,143,342
21_2_S26	19,573,685	19,573,106	13,130,819	67.1	10,599,374
21_3_S35	42,629,573	42,628,850	23,153,271	54.3	29,877,050
21_4_S68	23,396,667	23,396,137	4,769,641	20.4	18,529,174
21_5_S7	15,870,285	15,869,951	5,105,627	32.2	10,710,355
22_1_S45	44,867,294	44,866,242	14,448,743	32.2	40,066,222
22_5_S53	27,584,630	27,584,297	6,463,674	23.4	20,906,373
22_6_1_S46	27,635,353	27,634,687	3,121,509	11.3	24,370,550
22_6_2_S29	19,991,461	19,990,901	2,067,300	10.3	17,811,532
22_7_S54	20,093,022	20,092,674	6,330,958	31.5	18,004,636
23_2_S61	20,138,474	20,137,302	488,291	2.4	20,118,348
23_4_1_S69	17,977,468	17,977,017	427,953	2.4	17,463,750
23_4_2_S62	21,691,784	21,691,182	509,125	2.3	21,674,578
23_5_S70	29,860,422	29,859,764	1,039,842	3.5	29,812,396
23_6_S38	23,073,539	23,073,001	498,215	2.2	22,461,246
32_5_1_S55	24,505,418	24,504,681	1,369,191	5.6	23,030,003
32_5_2_S56	42,313,764	42,312,313	2,341,428	5.5	39,807,491
32_7_1_S57	30,236,003	30,235,140	10,983,050	36.3	25,896,228
32_7_2_S58	31,822,132	31,821,284	11,056,139	34.7	27,617,232
36_2_1_S63	36,517,414	36,516,465	1,215,946	3.3	35,207,906
36_2_2_S64	38,989,258	38,987,950	1,214,127	3.1	38,943,382
36_3_S65	32,620,535	32,619,571	3,228,593	9.9	29,269,269
36_4_S66	29,035,119	29,034,058	601,390	2.1	29,019,574
36_5_S67	30,184,882	30,182,934	1,844,209	6.1	30,045,120
5_2_S1	27,585,384	27,584,568	869,840	3.2	27,548,252
5_3_S2	73,262,577	73,259,941	2,995,100	4.1	69,866,357
7_6_1_S39	33,015,915	33,014,909	910,337	2.8	31,967,473
7_6_2_S40	49,693,671	49,692,273	1,446,858	2.9	48,060,403
7_7a_1_S41	25,574,942	25,573,815	1,705,357	6.7	23,654,595
7_7a_2_S42	19,628,158	19,627,940	1,177,054	6.0	19,538,188

Supplemental Table III-5. Table of reads after each trimming and quality filtering step

Sample	Trimmomatic		SortMeRNA		seqkit-pair
	Input read pairs	Surviving	rRNA	rRNA (%)	Surviving paired-end reads
7_7b_S43	20,946,959	20,945,871	1,638,423	7.8	19,034,764
8_1_S11	19,400,380	19,399,542	2,850,634	14.7	18,879,374
8_2a_S12	50,198,738	50,196,823	1,850,422	3.7	48,152,113
8_2b_S13	32,566,755	32,565,375	2,870,581	8.8	29,484,658
8_3_S14	33,800,201	33,798,998	1,220,856	3.6	33,748,194
8_6_S15	47,965,425	47,963,369	7,247,476	15.1	40,527,456
9_1_S3	34,370,305	34,369,443	10,991,564	32.0	22,237,445
9_3_S4	26,765,615	26,765,108	6,390,077	23.9	25,026,958
9_4_S5	36,201,813	36,199,681	1,211,139	3.3	34,710,875
9_6_S6	28,933,807	28,932,597	2,238,311	7.7	26,591,899
SUMMARY STATS					
SUMS	2,147,381,297	2,147,317,634	425,680,740	19.8	1,818,532,330
MIN	15,870,285	15,869,951	427,953	2.1	4,801,521
MAX	116,230,700	116,229,007	97,037,409	83.5	69,866,357
% removed		0.003			15.314

Only forward reads are indicated for clarity

4. Transcriptome assembly and assessment

A Trinity *de-novo* transcriptome assembly was initially tested using a selection of 33 samples (from 70) that showed a similar GC profile with a single peak at GC% 44-46 and a slight tail (metrics in **Supplemental Table III-6**). After the initial exploration rnaSPAdes and Trinity v2.11.0 (Grabherr et al. 2011) were used to make an assembly using all quality trimmed and filtered reads from 70 samples.

4.1 Assembly metrics ([TrinityStats.pl](#))

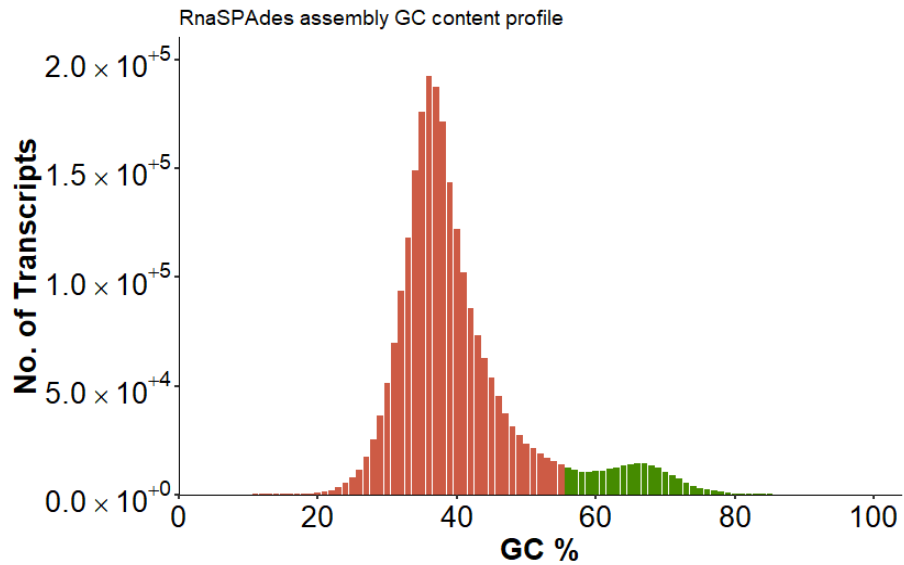
The Trinity assembly showed a greater number of contigs than RNAspades (not a good thing), in addition, the max contig length is lower and the minimum contig length higher (a good thing). The largest contigs of the RNA spades are possibly chimeras as their GC content falls in the middle of the 2 peaks (the GC peaks as seen in **Supplemental Figure III-7**). Additionally, the assembly metrics are shown for the split assemblies, see further details below.

Supplemental Table III-6. Assemblies Summary

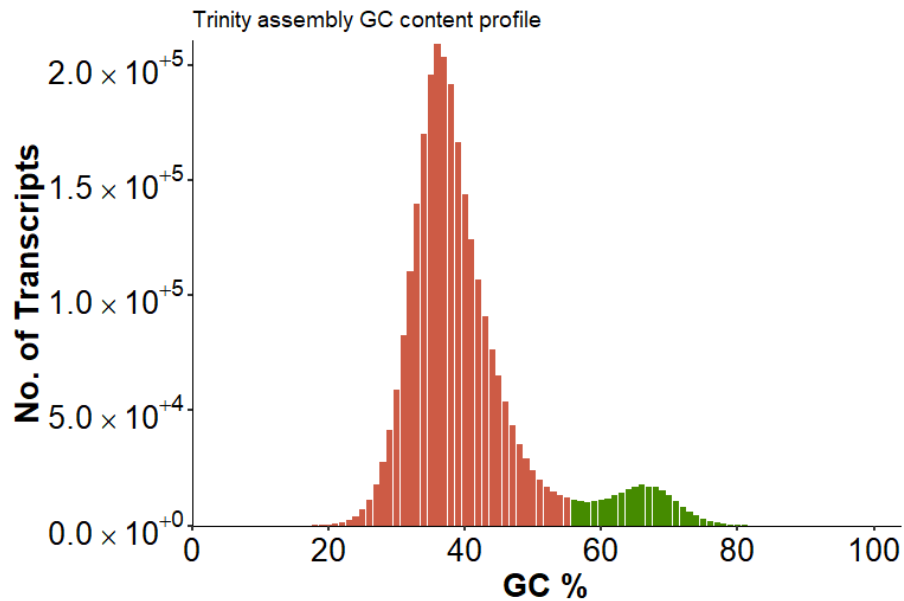
	GC44-46		Trinity All		RnaSPAdes All		Trinity Blastn		Trinity Blastn GMM		RnaSPAdes Blastn GMM	
	All transcripts	Longest isoform per gene	All transcripts	Longest isoform per gene	'normal' assembly	hard-filtered assembly	<i>Phaeocystis</i> bin	Non- <i>Phaeocystis</i> bin	<i>Phaeocystis</i> bin	Non- <i>Phaeocystis</i> bin	<i>Phaeocystis</i> bin	Non- <i>Phaeocystis</i> bin
Number of contigs	1,966,978		2,751,425		2,432,577	2,108,782	221,929	2,529,496	311,193	2,440,232	305,580	1,803,202
Number of trinity 'genes'	1,342,012		1,643,675				131,940	1,517,328	200,949	1,448,572		
Sum bp	1,618,448,250	950,870,983	2,536,403,524	1,303,293,148	2,706,057,449	2,649,628,289	294,342,064	146,784,514	91,758,542	2,144,644,982	397,066,192	2,252,562,097
max contig length			71,048		85,738	85,738					85,738	60,511
min contig length			219		49	54					56	54
median contig length	466	445	537	481	609	760	874	520	784	518	762	759
average contig length	823	709	922	793	1,112	1,256	1,326	886	1258.89	879	1,299	1,249
N50	1,163	914	1,378	1,098	2,025	2,073	1,965	1,299	1,921	1,282	2,161	2,059
Ex90N50 (RSEM)	1,611		1,923			3,200					2,266	3,051
Ex90N50 (RSEM)	135,106		161,615			145,802					2,993	14,460
Transcripts with ≥ 1 TPM			1,176,859			1,114,262					252,848	996,055
GC%	43.06		42.32		41.09	41.08	60.19	39.97	60.62	38.98	56.65	38.34

4.2 Assessing GC content of the Assembly

The GC content of filtered transcripts clearly shows a bimodal distribution. Where the low GC% transcripts are suspected to be acantharian transcripts, and the high GC% transcripts of the symbiont (Liu et al. 2019). GC content of each transcript in the assembly was quantified using `emboss/6.6.0 geecee`.



Supplemental Figure III-7. GC content of the rnaSPAdes Assembly, indicated in red and green, respectively, are presumed Acantharia and symbiont GC% ranges.



Supplemental Figure III-8. GC content of the Trinity Assembly, indicated in red and green, respectively, are presumed Acantharia and symbiont GC range.

4.3 BUSCO

The “completeness” of the transcriptome was evaluated by determining how many Benchmarking Universal Single-Copy Orthologs (BUSCOs) were complete, fragmented, or missing in the transcriptome. The BUSCO software (v4.1.4) was used to calculate BUSCO scores for Eukaryote BUSCOs.

BUSCO results from rnaSPAdes Assembly on dataset eukaryota_odb10

C:96.9%[S:27.1%,D:69.8%],F:1.2%,M:1.9%,n:255

247 Complete BUSCOs (C)
69 Complete and single-copy BUSCOs (S)
178 Complete and duplicated BUSCOs (D)
3 Fragmented BUSCOs (F)
5 Missing BUSCOs (M)
255 Total BUSCO groups searched

BUSCO results from Trinity Assembly on dataset eukaryota_odb10

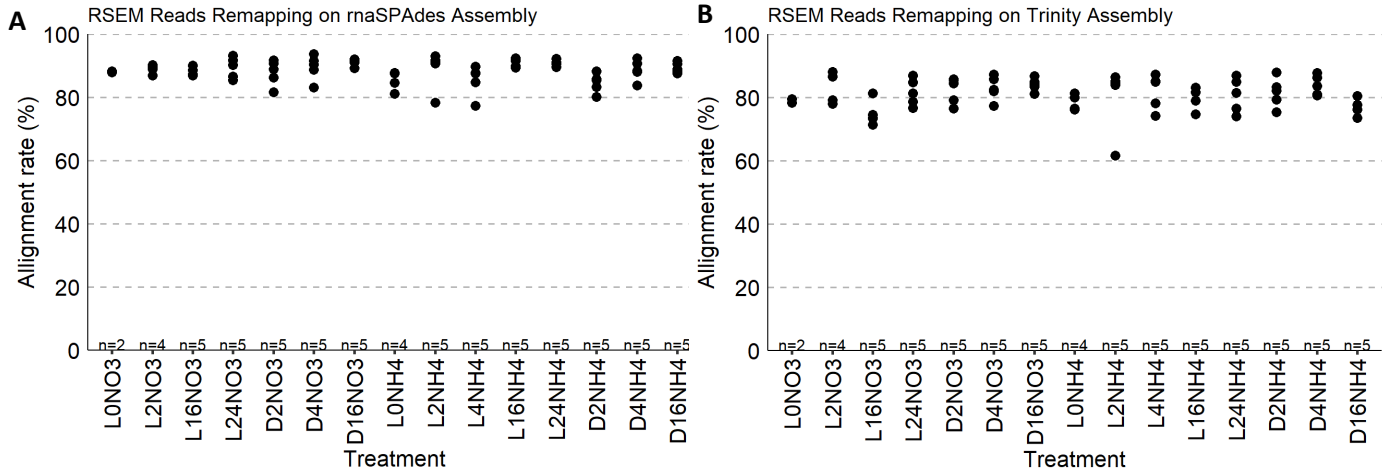
C:97.2%[S:27.8%,D:69.4%],F:0.8%,M:2.0%,n:255

248 Complete BUSCOs (C)
71 Complete and single-copy BUSCOs (S)
177 Complete and duplicated BUSCOs (D)
2 Fragmented BUSCOs (F)
5 Missing BUSCOs (M)
255 Total BUSCO groups searched

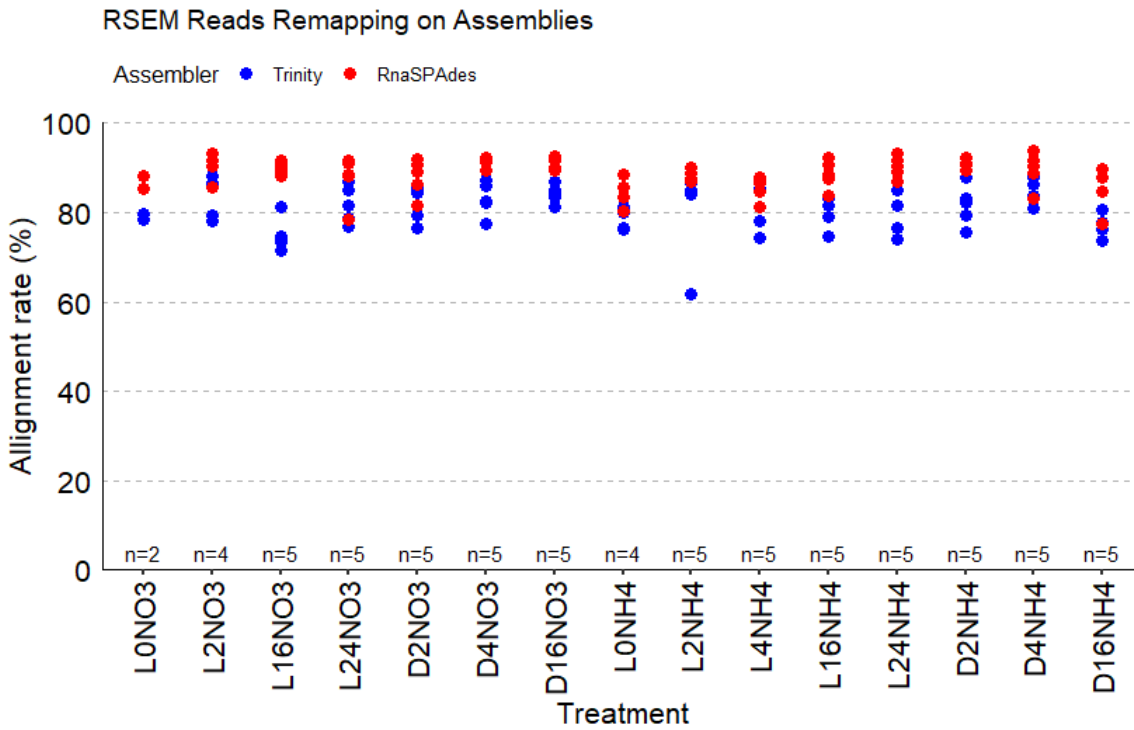
4.5 Read mapping on *de-novo* transcriptomes

Quality filtered reads were re-mapped to the assembly and read counts were calculated using both Kallisto and RSEM v. 1.2.29 (Li and Dewey, 2011) with bowtie2 v.2.4.1 (Langmead and Salzberg, 2012) in the Trinity package. Kallisto was used as the faster preliminary analysis whereas RSEM mapping was better and used for subsequent analyses.

Remapping rates were extracted from the *.err* file and plotted.



Supplemental Figure III-9. RSEM read mapping to the rnaSPAdes assembly (A), and on the Trinity assembly (B).



produced on 2021-09-13 10:29:44

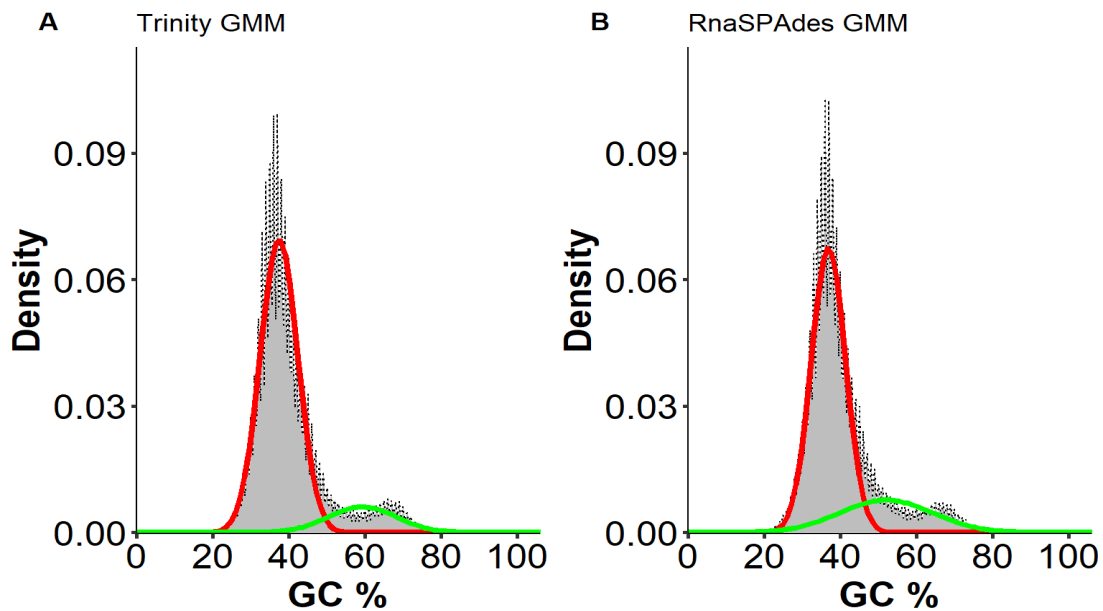
Supplemental Figure III-10. RSEM Read mapping for both Trinity and rnaSPAdes *de-novo* transcriptome assemblies.

5. Assembly binning

5.1 Selection of symbiont contigs by Gaussian Mixed Model on transcript GC-content profile

The GC content of the Trinity Assembly **Supplemental Figure III-8** shows a more defined bimodal model than that of the RNASPADES assembly **Supplemental Figure III-7**, maybe due to less chimeric sequence (80000+bp contigs). This is reflected in better separation of the Gaussian Mixed Models (GMM) based on GC content (**Supplemental Figure III-11**).

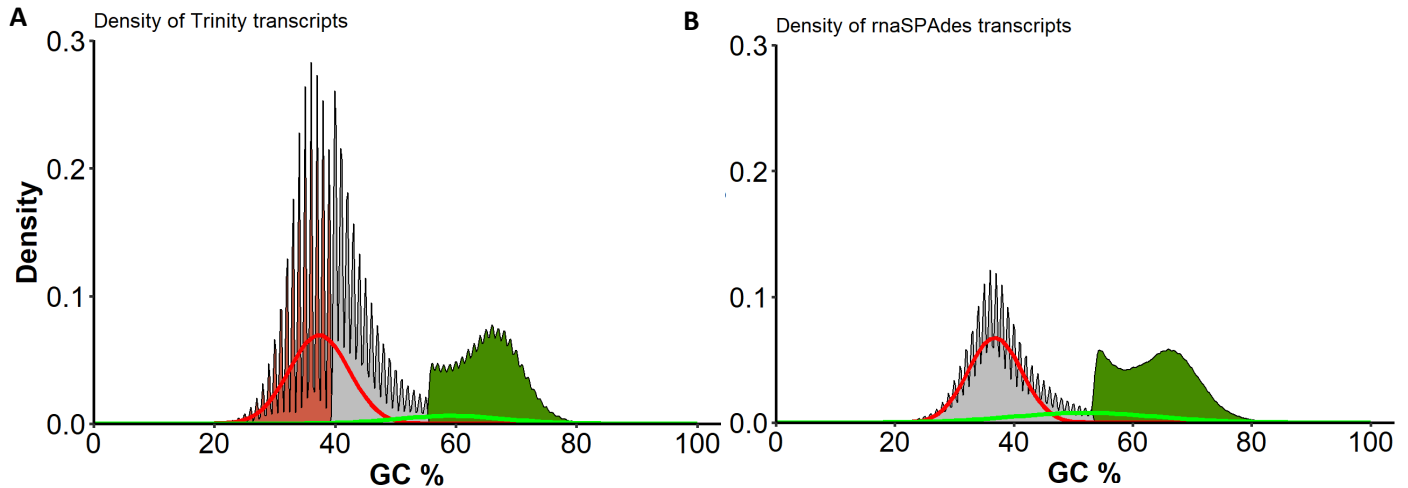
A GMM is done for 2 clusters using the R package mixtools.



Supplemental Figure III-11. Gaussian Mixed Model (GMM) plots for the Trinity assembly (A) and the rnaSPAdes assembly (B). Shown in red and green lines the two components of the model.

The assignment of the second Gaussian model component, the symbiont, does not define well (especially for the RNASPADES assembly). The model ends up with too low a mean and a high standard deviation, causing increasing overlap with the first component—the presumed host. For this reason, only the transcripts with 99% confidence of being assigned to the symbiont component were selected and filtered out from the assembly (*i.e.* only this bin was used for selection).

The transcripts that are predicted to belong to one of the model components with 99% certainty are selected and extracted.



Supplemental Figure III-12. Gaussian Mixed model density plot for the Trinity assembly (A), and the rnaSPAdes assembly (B). With in red and green lines the 2 components of the Gaussian model fit. Shown as red, green and grey bars are the contigs which based on the model have 99% confidence of being assigned to respectively the first low GC-content component (presumed host), the second high GC-content component (presumed symbiont), or to neither (uncertain).

5.2 Selection of symbiont contigs by BLAST

All the assembled sequences were searched against a custom database containing four of the better *Phaeocystis* transcriptomes (i.e. METDB_00327, METDB_00333, METDB_00329 from <http://metdb.sb-roscoff.fr/metdb>, and the *Phaeocystis* assembly from Mars Brisbin 2020: https://github.com/maggimars/PcordataSymbiosisDGE/blob/2b7836d2f6ebf9a5d80cbce22988f161428e459/pc_euk_seqs.fasta) using MegaBLAST. All hits with bitscores >90 were considered *Phaeocystis* transcripts. The hits were separated out of our assembly. The same procedure is followed for both Trinity and rnaSPAdes assemblies, though only the Trinity assembly is exemplified.

The metrics of the separated Trinity transcriptomes based only on the blast results are shown in **Supplemental Table III-6**

BUSCO results from Trinity Assembly selected on *Phaeocystis* Blast hits on dataset eukaryota_odb10
 C: 76.5% [S: 24.7%, D: 51.8%], F: 8.2%, M: 15.3%, n: 255

```

195 Complete BUSCOs (C)
63 Complete and single-copy BUSCOs (S)
132 Complete and duplicated BUSCOs (D)
21 Fragmented BUSCOs (F)
39 Missing BUSCOs (M)
255 Total BUSCO groups searched

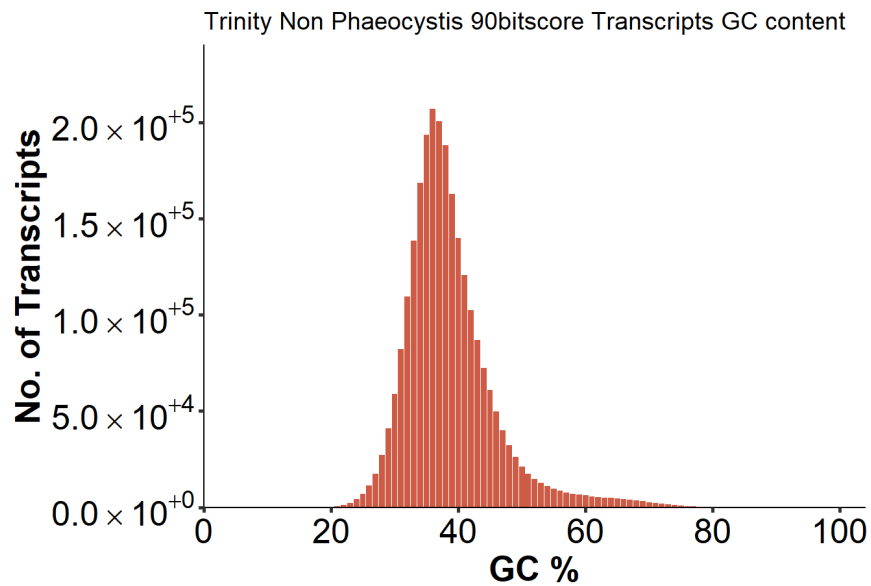
```

BUSCO results from Trinity Assembly selected on Non-*Phaeocystis* Blast hits on dataset eukaryota_odb10

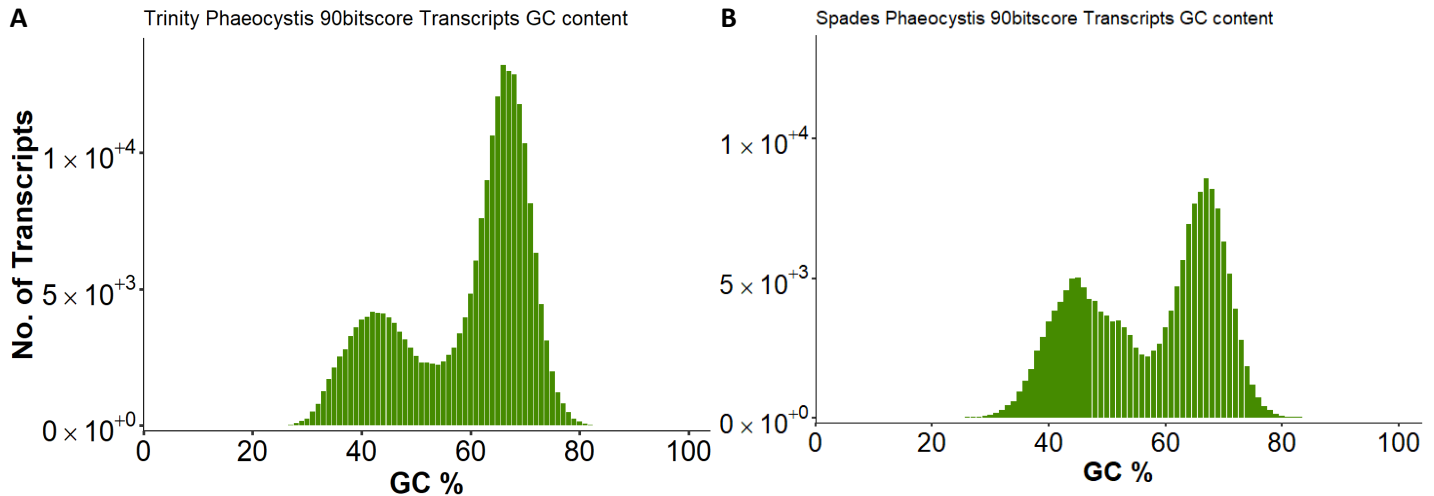
C:94.9%,S:29.8%,D:65.1%,F:1.6%,M:3.5%,n:255

242 Complete BUSCOs (C)
76 Complete and single-copy BUSCOs (S)
166 Complete and duplicated BUSCOs (D)
4 Fragmented BUSCOs (F)
9 Missing BUSCOs (M)
255 Total BUSCO groups searched

The separated individual transcriptome bins are below assessed on GC content.



Supplemental Figure III-13. GC content of the Trinity contigs **not** matched by BLAST against our *Phaeocystis* database.



Supplemental Figure III-14. GC content of the Trinity contigs (A), and the rnaSPAdes contigs (B) that matched by BLAST against our *Phaeocystis* database

The assembly of the contig bin that matched against *Phaeocystis* show an unexpected bimodal GC-content distribution. This might be due to chimeric contig sequences.

5.3 Sort Transcriptome Assembly based on GMM and BLAST results

Only using the Blast results to filter out the symbiont of the holobiont transcriptome results in a GC-content profile for the presumed host transcripts that still contain a small high-GC-content tail. For that reason we additionally used the GMM to filter out those contigs based on the GMM results. *Phaeocystis* symbiont transcripts were selected from the rnaSpades assembly using `seqkit greb`, the non-*Phaeocystis* transcripts were selected by an inverse `seqkit greb`.

The BUSCO results did not change with this step, below are thus only shown the results for the split rnaSPAdes assembly that was not shown before.

BUSCO results from rnaSPAdes Assembly selected on *Phaeocystis* BLAST hits on dataset eukaryota_odb10
C:91.0%[S:35.7%,D:55.3%],F:5.5%,M:3.5%,n:255

```
232 Complete BUSCOs (C)
91 Complete and single-copy BUSCOs (S)
141 Complete and duplicated BUSCOs (D)
14 Fragmented BUSCOs (F)
9 Missing BUSCOs (M)
255 Total BUSCO groups searched
```

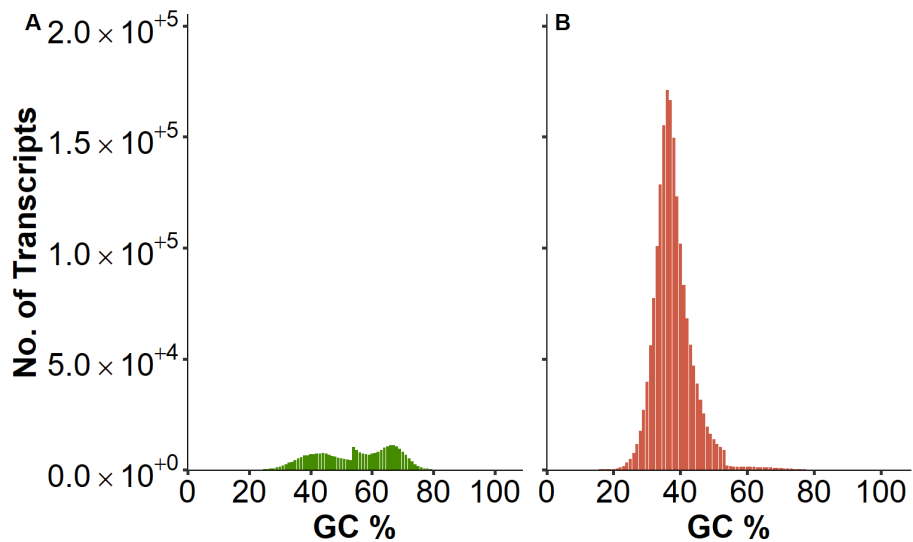
BUSCO results from rnaSPAdes Assembly selected on Non-*Phaeocystis* BLAST hits on dataset eukaryota_odb10

C:89.0%[S:36.1%,D:52.9%],F:2.7%,M:8.3%,n:255

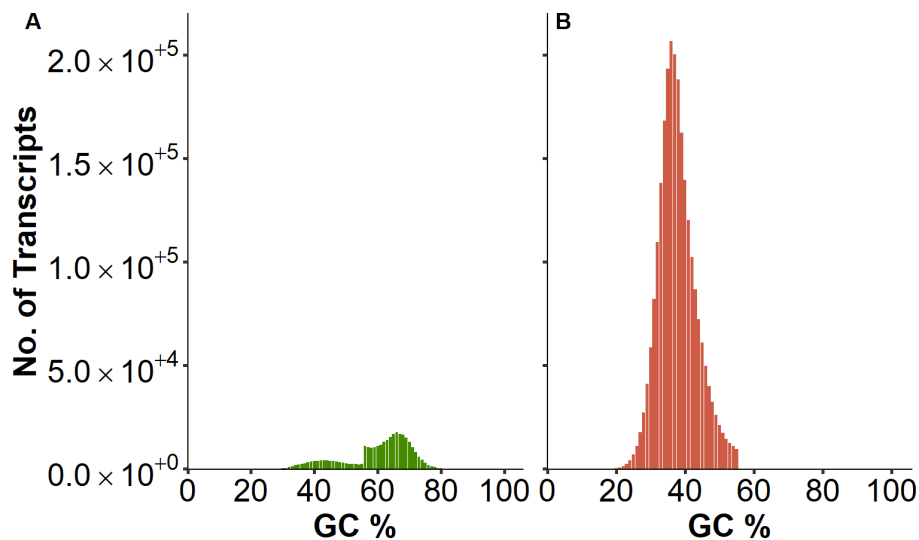
227 Complete BUSCOs (C)
 92 Complete and single-copy BUSCOs (S)
 135 Complete and duplicated BUSCOs (D)
 7 Fragmented BUSCOs (F)
 21 Missing BUSCOs (M)
 255 Total BUSCO groups searched

The metrics of the separated transcriptomes based on the BLAST and GMM results are shown in **Supplemental Table III-6**.

The GC-content of the separated rnaSPAdes and Trinity transcriptomes is shown below.



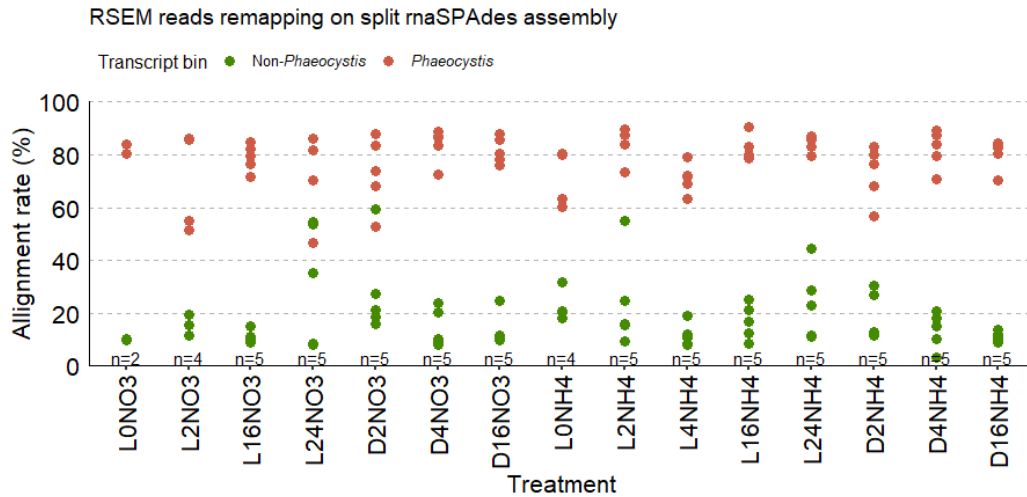
Supplemental Figure III-15. GC content of the rnaSPAdes assembly split into (A) *Phaeocystis* contigs, and (B) Non-*Phaeocystis* (i.e. presumed Acantharia contigs), by means of BLAST and GMM results.



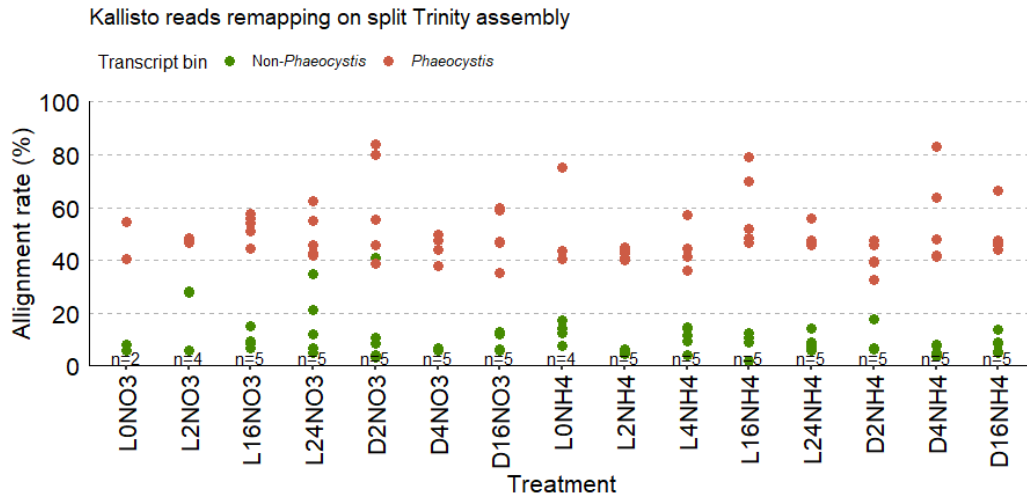
Supplemental Figure III-16. GC content of the Trinity Assembly split into (A) *Phaeocystis* contigs, and (B) Non-*Phaeocystis* (i.e. presumed Acantharia contigs), by means of BLAST and GMM results.

5.4 Read mapping on split transcriptomes

Read mapping was performed as before but on the split transcriptomes. That is thus on the *Phaeocystis* bin of the transcriptome as well as on the non-*Phaeocystis* bin of the transcriptome. RSEM read mapping rates on both these transcriptomes are shown below. Note that for the Trinity assembly kallisto read remapping is shown which is generally lower. RSEM remapping is shown for rnaSPAdes assemblies as this is the remapping data that is subsequently used.



Supplemental Figure III-17. RSEM read mapping to the rnaSPAdes assembly.



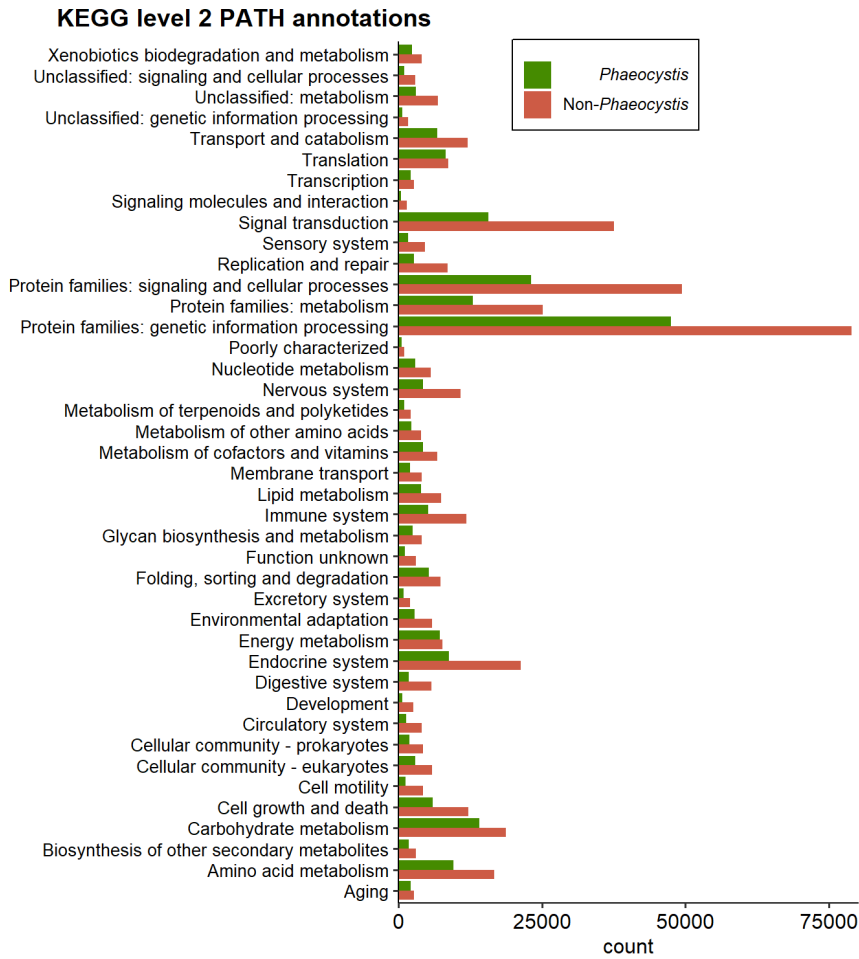
Supplemental Figure III-18. Kallisto read mapping to the Trinity assembly.

6. Assembly annotation

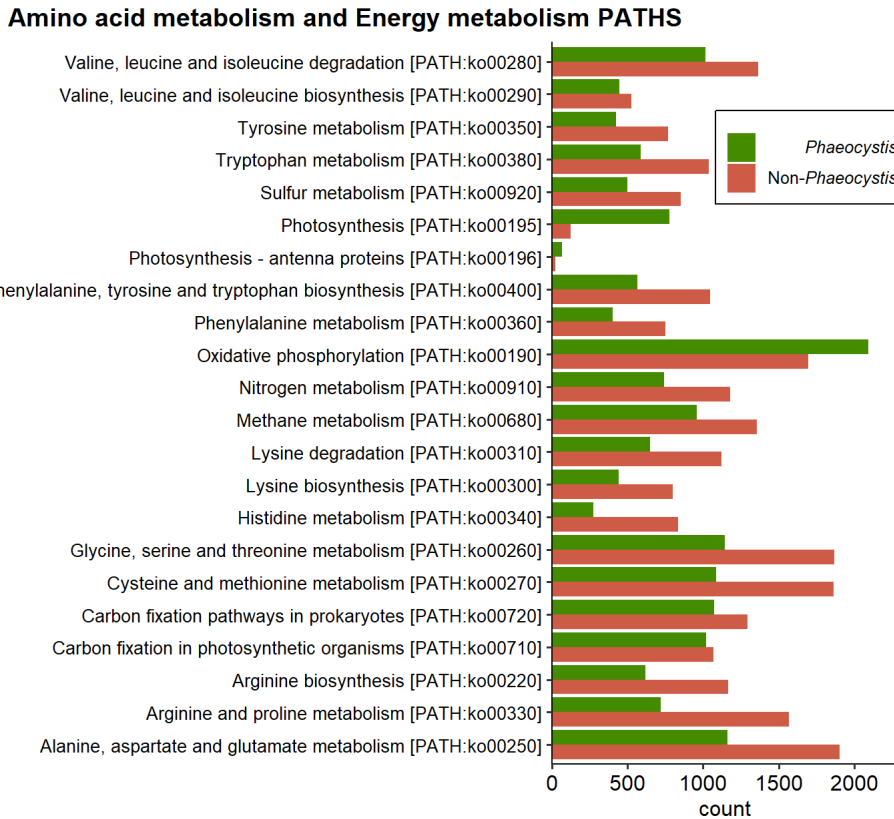
The rnaSPAdes transcriptome was annotated using the Trinotate pipeline (Bryant et al. 2017). The Trinotate annotation report was split into *Phaeocystis* and non-*Phaeocystis* assembly bins to acquire annotation metrics from Trinotate and extract GO terms from both partitions.

KEGG annotations (K numbers) were additionally obtained by splitting the Transdecoder peptide sequence results and submitting it as a GhostKOALA job (Kanehisa et al., 2016), through <https://www.kegg.jp/ghostkoala>, [searching against the full KEGG database](#). Annotation results were downloaded from the GhostKOALA results and combined. The transcripts with annotated K-numbers were split into transcripts belonging to the *Phaeocystis* and non-*Phaeocystis* assembly bins. Subsequently, KO numbers were linked to KEGG pathways. Annotation metrics of both Trinotate and GhostKOALA annotation pipelines have been presented in **Table III-6**

KEGG pathway annotations assigned to the symbiont *Phaeocystis* and the presumed host transcripts (non-*Phaeocystis*) are explored and visualised by category on subsequent pages.

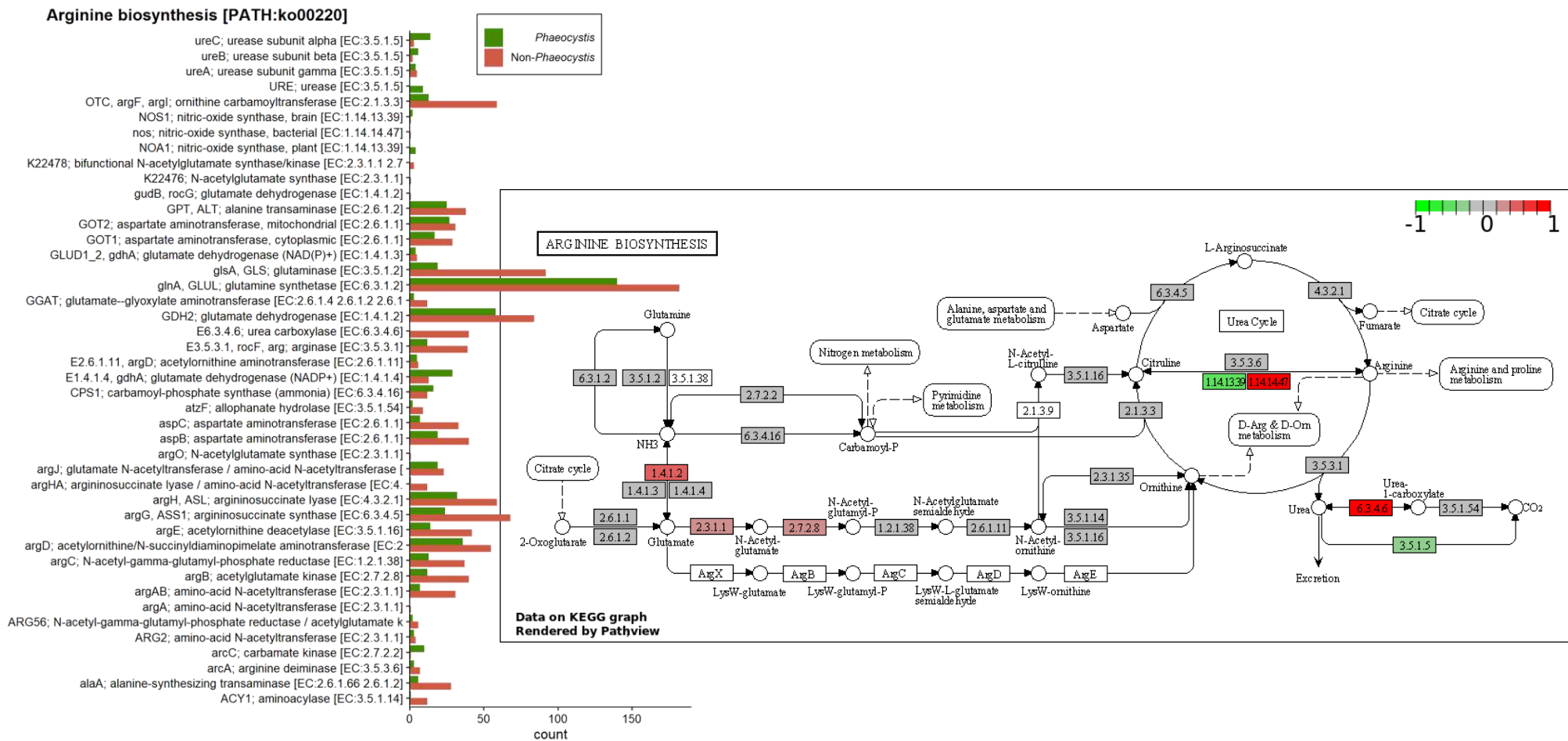


Supplemental Figure III-19. Counts of KEGG pathways for symbiont and host.



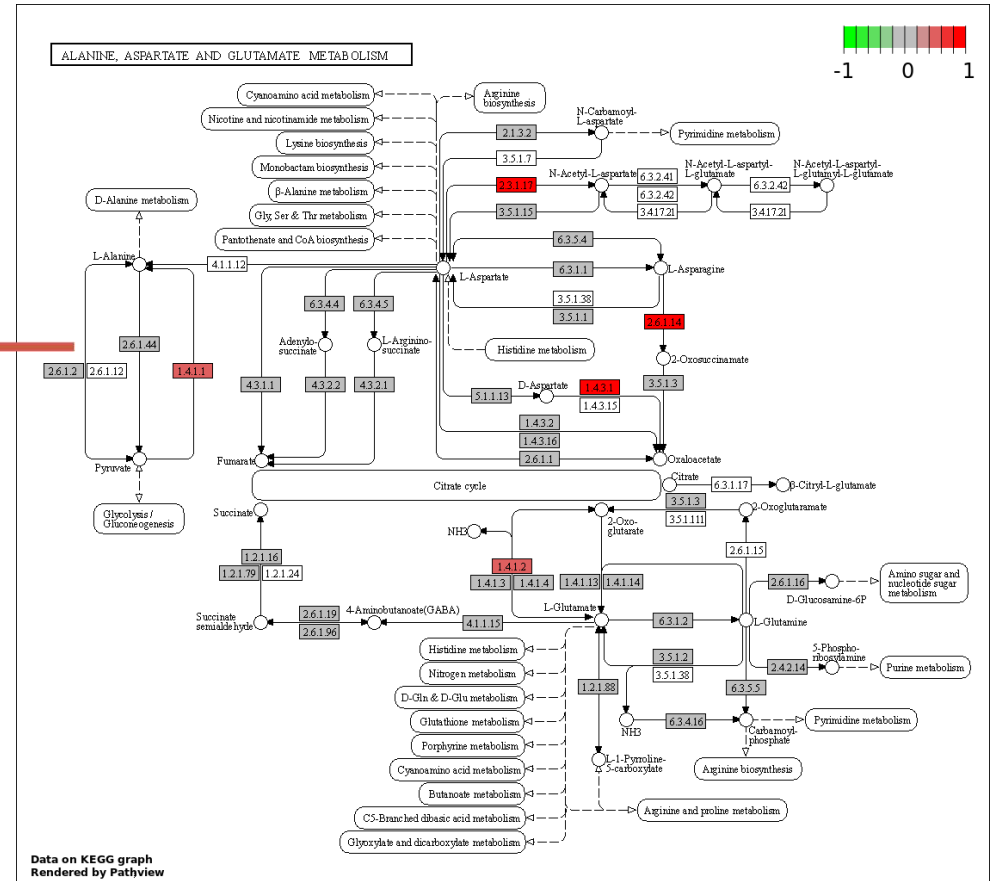
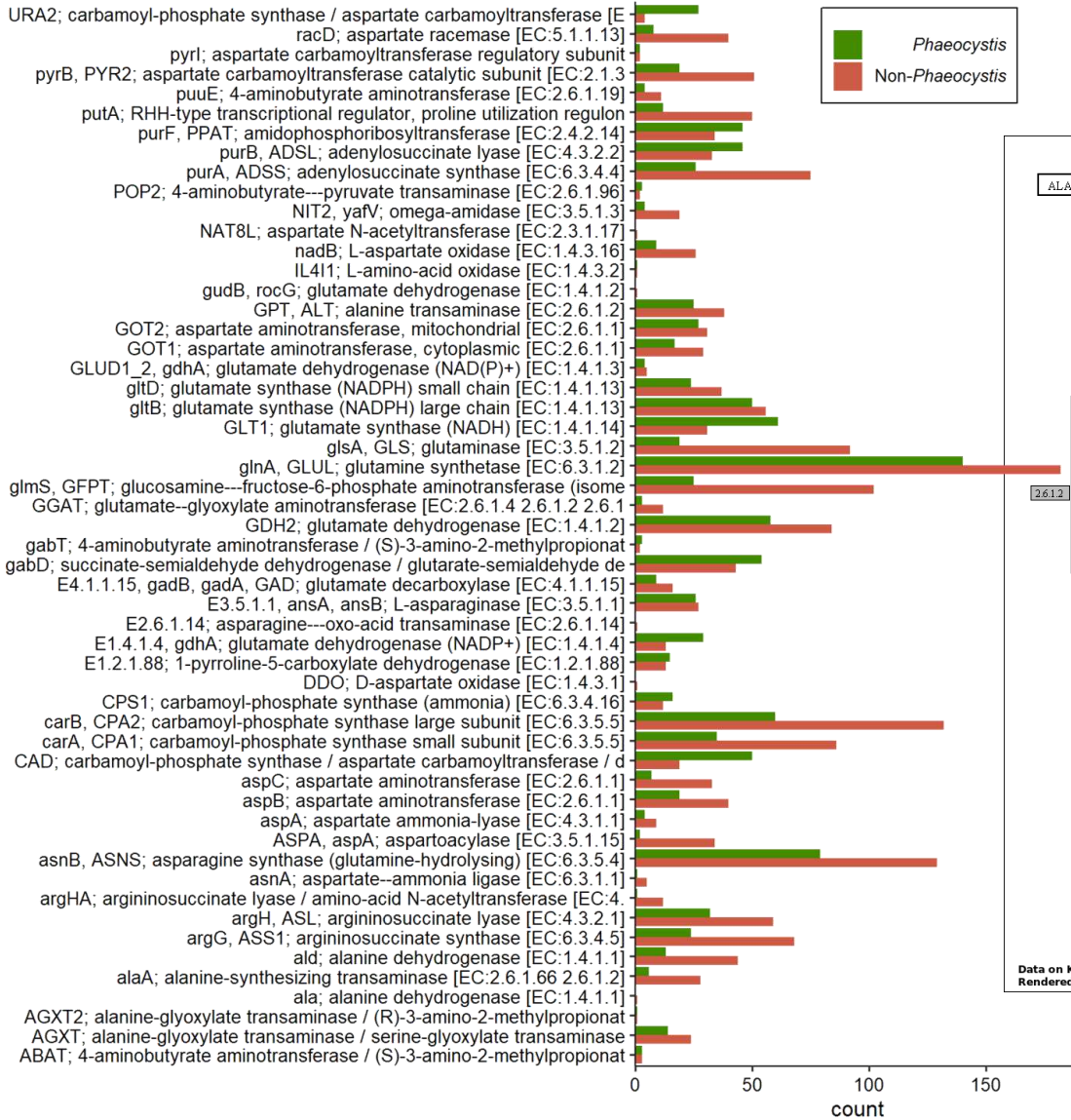
Supplemental Figure III-20. Counts of KEGG pathways within amino acid metabolism and energy metabolism for symbiont and host.

Overview graphs for annotations of specific pathways (i.e. arginine biosynthesis; alanine, aspartate and glutamate metabolism, and nitrogen metabolism) have been plotted.



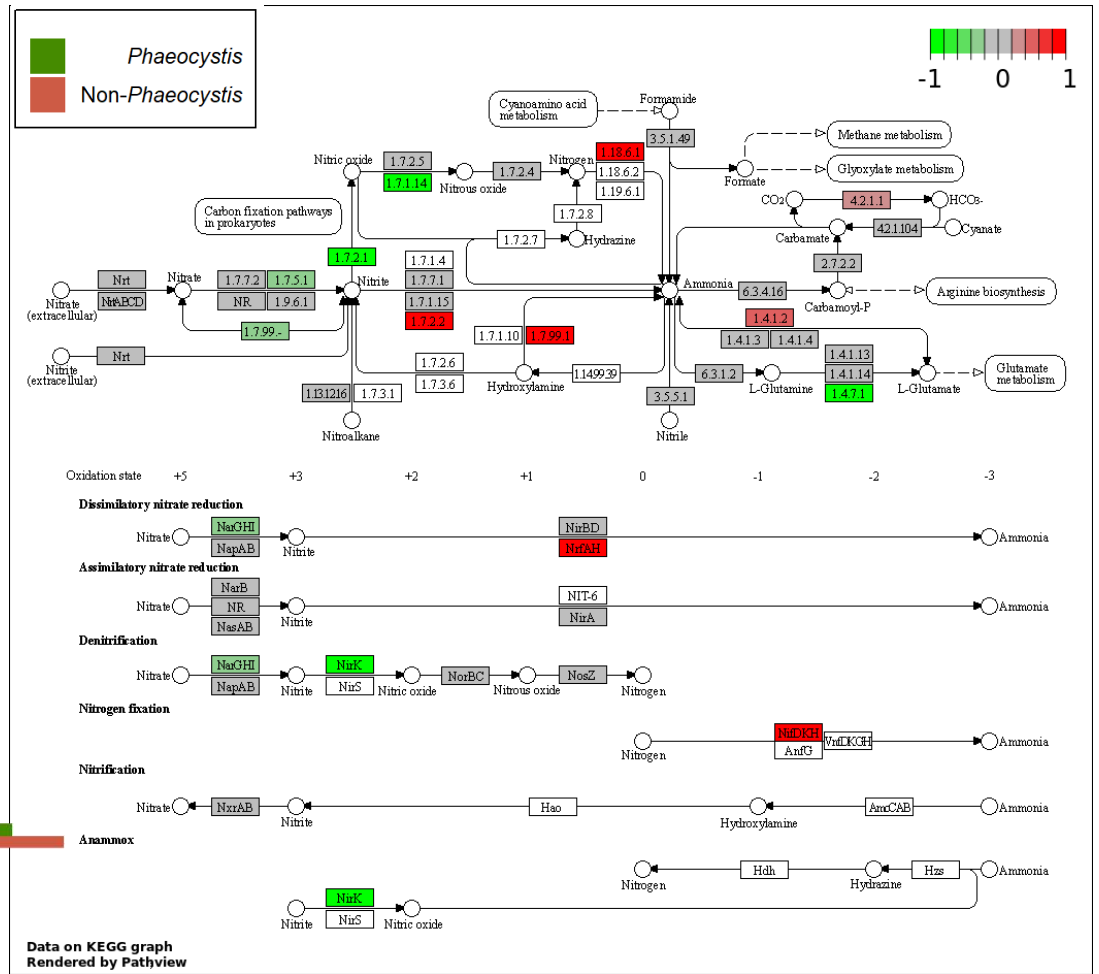
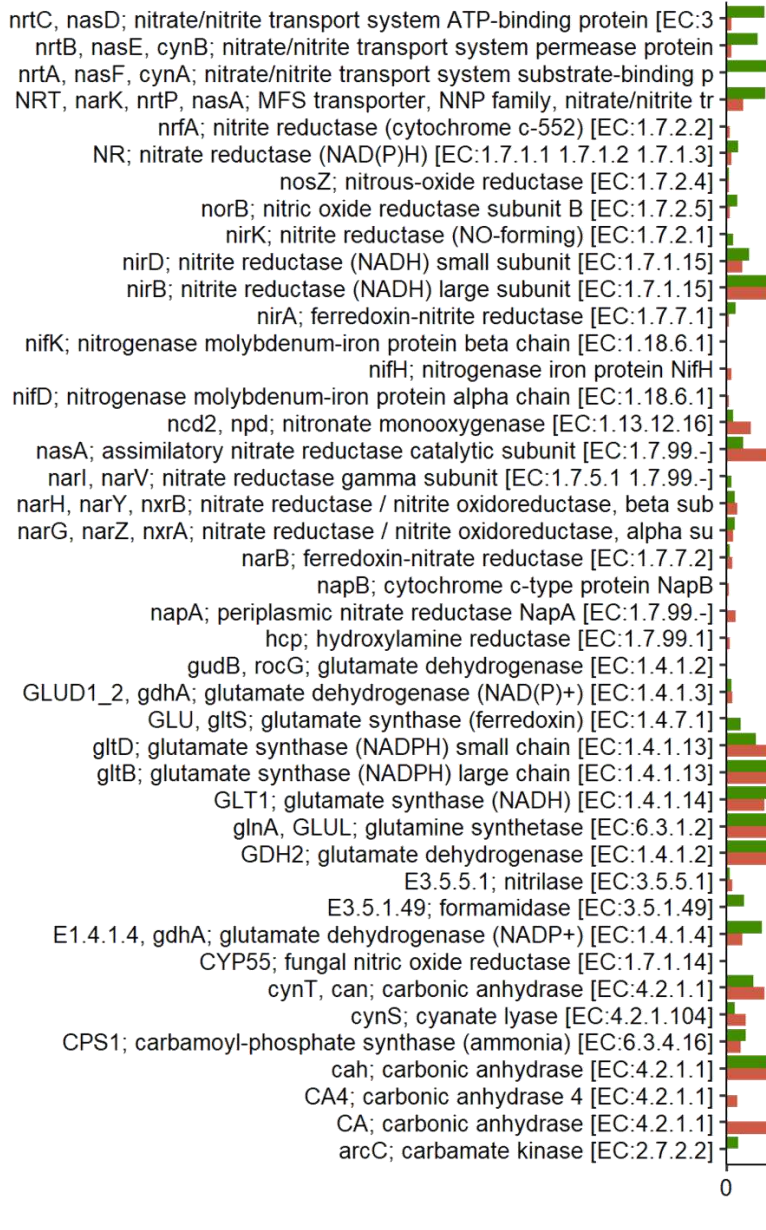
Supplemental Figure III-21. Counts of Arginine biosynthesis specific path descriptors for symbiont and host, and an overview of the pathway with annotated transcripts only present in the symbiont bin in green (-1); those only in the host bin in red (1), and those present in both in grey (0). Given that multiple genes can be mapped to it a node, shaded nodes thus imply that some genes attributing to that node are exclusive to either symbiont or host bin. Open boxes represent genes not annotated in either transcriptome.

Alanine, aspartate and glutamate metabolism [PATH:ko00250]



Supplemental Figure III-22. Counts of Alanine, aspartate and glutamate metabolism specific path descriptors for symbiont and host, and an overview of the pathway with annotated transcripts only present in the symbiont bin in green (-1); those only in the host bin in red (1), and those present in both in grey (0). Given that multiple genes can be mapped to it a node, shaded nodes thus imply that some genes attributing to that node are exclusive to either symbiont or host bin. Open boxes represent genes not annotated in either transcriptome.

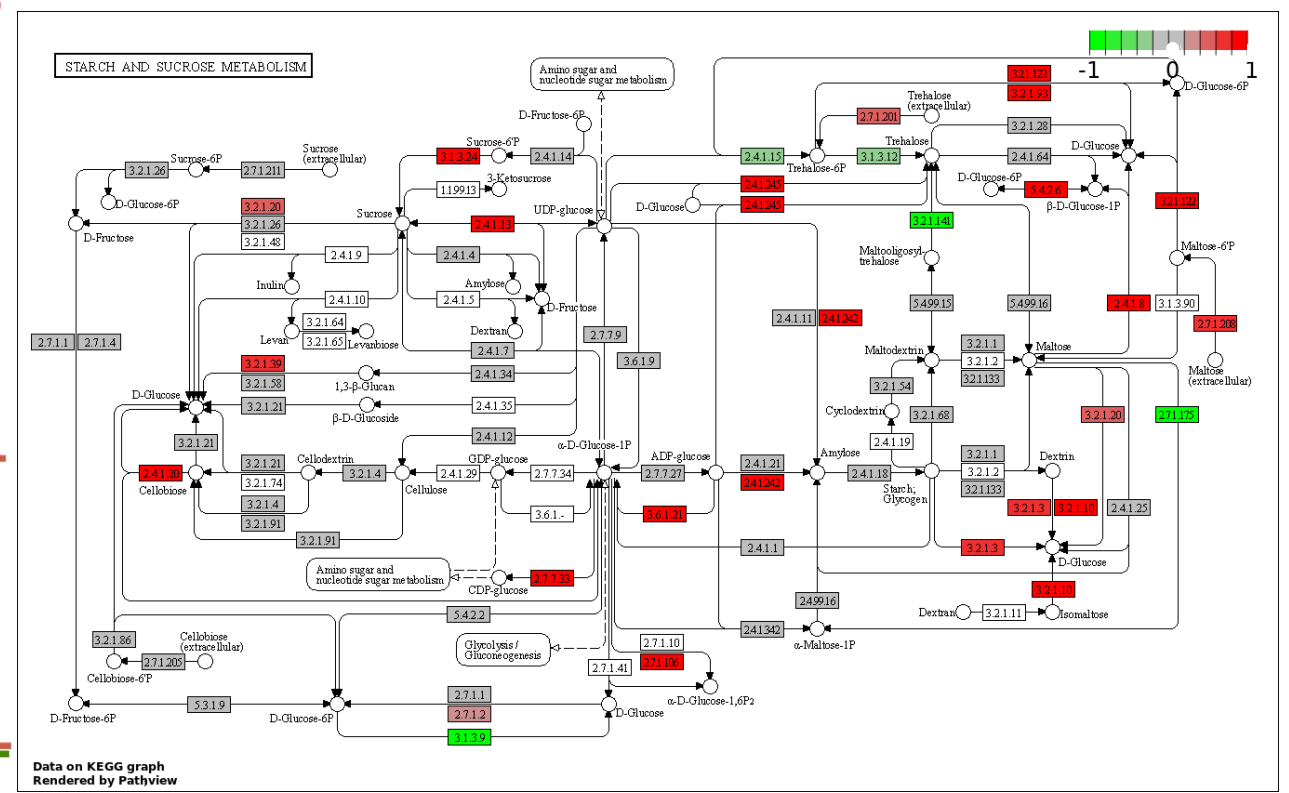
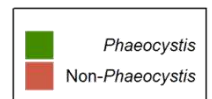
Nitrogen metabolism [PATH:ko00910]



Supplemental Figure III-23. Counts of nitrogen metabolism specific path descriptors for symbiont and host, and an overview of the pathway with annotated transcripts only present in the symbiont bin in green (-1); those only in the host bin in red (1), and those present in both in grey (0). Given that multiple genes can be mapped to it a node, shaded nodes thus imply that some genes attributing to that node are exclusive to either symbiont or host bin. Open boxes represent genes not annotated in either transcriptome.

Starch and sucrose metabolism [PATH:ko00500]

- UGP2, galU, galF, WAXY; granule-bound starch synthase [EC:2.4.1.242]
- TSL1, TPS3; trehalose 6-phosphate synthase complex regulatory subunit [EC:2.7.1.141]
- treZ, glgZ; maltooligosyltrehalose trehalohydrolase [EC:3.2.1.141]
- treY, glgY; (1->4)-alpha-D-glucan 1-alpha-D-glucosylmutase [EC:5.4.99.1]
- treT; trehalose synthase [EC:2.4.1.245]
- treS; maltose alpha-D-glucosyltransferase / alpha-amylase [EC:5.4.99.1]
- TREH, treA, treF; alpha-alpha-trehalase [EC:3.2.1.28]
- treC; trehalose 6-phosphate hydrolase [EC:3.2.1.93]
- TPS; trehalose 6-phosphate synthase/phosphatase [EC:2.4.1.153]
- 3.12
- susB; glucan 1,4-alpha-glucosidase [EC:3.2.1.3]
- SPP; sucrose 6-phosphatase [EC:3.1.3.24]
- SGA1; glucoamylase [EC:3.2.1.3]
- rfbF; glucose-1-phosphate cytidyltransferase [EC:2.7.7.33]
- PYG, glgP; glycogen phosphorylase [EC:2.4.1.1]
- pullA; pullulanase [EC:3.2.1.41]
- PTS-Tre-EIIC, treB; PTS system, trehalose-specific IIC component
- PTS-Scr-EIIC, scrA, sacP, sacX, ptsS; PTS system, sucrose-specific IIC
- PTS-MalGlc-EIIC, malX; PTS system, maltose/glucose-specific IIC compon
- PTS-Mal-EIIC, malT; PTS system, maltose-specific IIC component
- PTS-Glc-EIIA, crr; PTS system, sugar-specific IIA component [EC:2.7.1.1]
- PTS-Cel-EIIC, celB, chbC; PTS system, cellobiose-specific IIC componen
- PTS-Cel-EIIB, celA, chbB; PTS system, cellobiose-specific IIB componen
- PTS-Cel-EIIA, celC, chbA; PTS system, cellobiose-specific IIA componen
- pmm-pgm; phosphomannomutase / phosphoglucomutase [EC:5.4.2.8]
- 5.4.2.2
- pgmB; beta-phosphoglucomutase [EC:5.4.2.6]
- PGM2L1; glucose-1,6-bisphosphate synthase [EC:2.7.1.106]
- PGM2; phosphoglucomutase / phosphopentomutase [EC:5.4.2.2]
- 5.4.2.2
- pgi-pmi; glucose/mannose-6-phosphate isomerase [EC:5.3.1.9]
- 5.3.1.8
- pep2; maltokinase [EC:2.7.1.175]
- otsB; trehalose 6-phosphate phosphatase [EC:3.1.3.12]
- otsA; trehalose 6-phosphate synthase [EC:2.4.1.15]
- 2.4.1.347
- NUDX14; ADP-sugar diphosphatase [EC:2.4.1.20]
- 2.4.1.3
- MGAM; maltase-glucoamylase [EC:3.2.1.20]
- mapA; maltose phosphorylase [EC:2.4.1.8]
- malZ; alpha-glucosidase [EC:3.2.1.20]
- malQ; 4-alpha-glucanotransferase [EC:2.4.1.25]
- ISA, treX; isoamylase [EC:3.2.1.68]
- INV, sacA; beta-fructofuranosidase [EC:3.2.1.26]
- IMA, mall; oligo-1,6-glucosidase [EC:3.2.1.10]
- HK; hexokinase [EC:2.7.1.1]
- GYS; glycogen synthase [EC:2.4.1.11]
- GYG1, GYG2; glycogenin [EC:2.4.1.186]
- GPI, pgi; glucose-6-phosphate isomerase [EC:5.3.1.9]
- GN5_6; glucan endo-1,3-beta-glucosidase 5/6 [EC:3.2.1.39]
- GN1_2_3; glucan endo-1,3-beta-glucosidase 1/2/3 [EC:3.2.1.39]
- gVA; maltose-6'-phosphate glucosidase [EC:3.2.1.122]
- gk; glucokinase [EC:2.7.1.2]
- glgX; glycogen debranching enzyme [EC:3.2.1.196]
- glgM; alpha-maltose-1-phosphate synthase [EC:2.4.1.342]
- glgE; starch synthase (maltosyl-transferring) [EC:2.4.1.99]
- glgC; glucose-1-phosphate adenylyltransferase [EC:2.4.1.21]
- glgA; starch synthase [EC:2.4.1.21]
- GCK; glucokinase [EC:2.7.1.2]
- GBE1, glgB; 1,4-alpha-glucan branching enzyme [EC:2.4.1.18]
- GANC; neutral alpha-glucosidase C [EC:3.2.1.20]
- GAA; lysosomal alpha-glucosidase [EC:3.2.1.20]
- G6PC; glucose-6-phosphatase [EC:3.1.3.9]
- ENPP1_3, CD203; ectonucleotide pyrophosphatase/phosphodiesterase fami
- EGLC; glucan endo-1,3-beta-D-glucosidase [EC:3.2.1.39]
- E3.2.1.86B, bglA; 6-phospho-beta-glucosidase [EC:3.2.1.86]
- E3.2.1.86A, celF; 6-phospho-beta-glucosidase [EC:3.2.1.86]
- E3.2.1.58; glucan 1,3-beta-glucosidase [EC:3.2.1.58]
- E3.2.1.4; endoglucanase [EC:3.2.1.4]
- E3.2.1.21; beta-glucosidase [EC:3.2.1.21]
- E2.7.1.4, scrK; fructokinase [EC:2.7.1.4]
- E2.4.1.7; sucrose phosphorylase [EC:2.4.1.7]
- E2.4.1.64; alpha-alpha-trehalose phosphorylase [EC:2.4.1.64]
- E2.4.1.4; amylosucrase [EC:2.4.1.4]
- E2.4.1.34; 1,3-beta-glucan synthase [EC:2.4.1.34]
- E2.4.1.20; cellobiose phosphorylase [EC:2.4.1.20]
- E2.4.1.14; sucrose-phosphate synthase [EC:2.4.1.14]
- E2.4.1.13; sucrose synthase [EC:2.4.1.13]
- cd, ma, npIT; cyclomaltodextrinase / maltogenic alpha-amylase / neopul
- CBH2, cbhA; cellulose 1,4-beta-cellobiosidase [EC:3.2.1.91]
- CBH1; cellulose 1,4-beta-cellobiosidase [EC:3.2.1.91]
- bglX; beta-glucosidase [EC:3.2.1.21]
- bglB; beta-glucosidase [EC:3.2.1.21]
- bcsA; cellulose synthase (UDP-forming) [EC:2.4.1.12]
- AMY, amyA, malS; alpha-amylase [EC:3.2.1.1]
- AGL; glycogen debranching enzyme [EC:2.4.1.25]



count

Supplemental Figure III-24. Counts of starch and sucrose metabolism specific path descriptors for symbiont and host, and an overview of the pathway with annotated transcripts only present in the symbiont bin in green (-1); those only in the host bin in red (1), and those present in both in grey (0). Given that multiple genes can be mapped to it a node, shaded nodes thus imply that some genes attributing to that node are exclusive to either symbiont or host bin. Open boxes represent genes not annotated in either transcriptome.

7. Supplementary Material References

- Bolger, Anthony M., Marc Lohse, and Bjoern Usadel. 2014. "Trimmomatic: A Flexible Trimmer for Illumina Sequence Data." *Bioinformatics* 30 (15): 2114–20. <https://doi.org/10.1093/bioinformatics/btu170>.
- Bryant, Donald M., Kimberly Johnson, Tia DiTommaso, Timothy Tickle, Matthew Brian Couger, Duygu Payzin-Dogru, Tae J. Lee, et al. 2017. "A Tissue-Mapped Axolotl De Novo Transcriptome Enables Identification of Limb Regeneration Factors." *Cell Reports* 18 (3): 762–76. <https://doi.org/10.1016/j.celrep.2016.12.063>.
- Grabherr, Manfred G, Brian J Haas, Moran Yassour, Joshua Z Levin, Dawn A Thompson, Ido Amit, Xian Adiconis, et al. 2011. "Full-Length Transcriptome Assembly from RNA-Seq Data Without a Reference Genome." *Nature Biotechnology* 29 (7): 644–52. <https://doi.org/10.1038/nbt.1883>.
- Kanehisa, Minoru, Yoko Sato, and Kanae Morishima. 2016. "BlastKOALA and GhostKOALA: KEGG Tools for Functional Characterization of Genome and Metagenome Sequences." *Journal of Molecular Biology* 428 (4): 726–31. <https://doi.org/10.1016/j.jmb.2015.11.006>.
- Kopylova, Evguenia, Laurent Noé, and Hélène Touzet. 2012. "SortMeRNA: Fast and Accurate Filtering of Ribosomal RNAs in Metatranscriptomic Data." *Bioinformatics* 28 (24): 3211–17. <https://doi.org/10.1093/bioinformatics/bts611>.
- Liu, Zhenfeng, Lisa Y. Mesrop, Sarah K. Hu, and David A. Caron. 2019. "Transcriptome of *Thalassicolla Nucleata* Holobiont Reveals Details of a Radiolarian Symbiotic Relationship." *Frontiers in Marine Science* 6 (June). <https://doi.org/10.3389/fmars.2019.00284>.
- Shen, Wei, Shuai Le, Yan Li, and Fuquan Hu. 2016. "SeqKit: A Cross-Platform and Ultrafast Toolkit for FASTA/Q File Manipulation." Edited by Quan Zou. *PLOS ONE* 11 (10): e0163962. <https://doi.org/10.1371/journal.pone.0163962>.

Supplementary Material 2:

Methods and analyses for differential expression

An online version containing all scripts and code underlying the analyses, as well as interactive graphics, can be found online at <https://doi.org/10.5281/zenodo.5105584> (Online Supplementary Material 2.1 and 2.2).

1. Intro

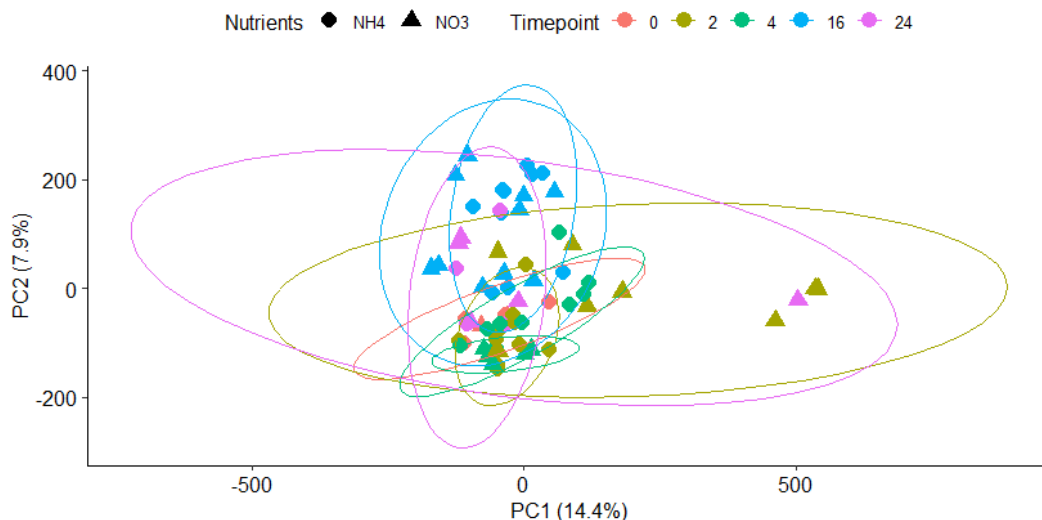
The split rnaSPAdes *de-novo* transcriptome was processed for differential transcript expression. Differential expression analyses were performed using EdgeR and limma packages. See session info for all specifics.

2. Differential expression testing

RSEM read count mappings are imported into the R environment, and prepared as a DGEList using EdgeR. Count data was transformed to counts per million (cpm). The counts per million data was filtered based on expression level, and normalised using TMM methods. Filtering was carried out to remove lowly (or non) expressed genes. Generally, only genes with at least 1 cpm in 4 (or smallest group size) or more samples are kept. This reduced the number of genes from 305580 to 40508 for the *Phaeocystis* bin and from 1803202 to 171106 for the non-*Phaeocystis* bin.

3. PCA analysis to assess similarity of samples

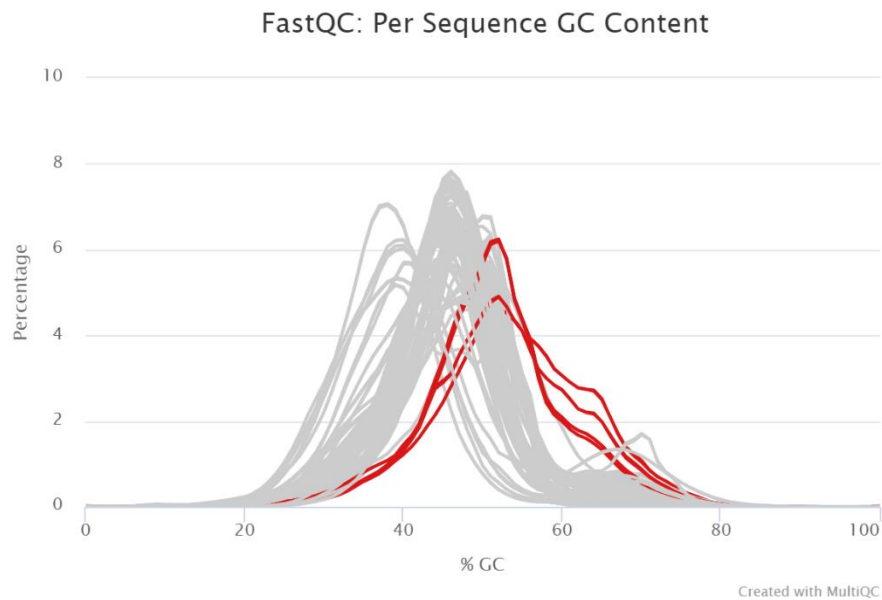
Sample relations are explored using principal component analyses, and can also be interactively explored using a Glimma non-metric multi-dimensional scaling plots in the online document.



Supplemental Figure III-25. Principal Component Analysis for the *Phaeocystis* transcriptome bin showing for the first 2 axes to identify sample relations of normalised and filtered log₂ cpm. Time point are indicated by colours and nutrient treatment by shape, for simplicity light or dark treatment is not shown. Even though no clear grouping by treatment condition can be observed, PC2 seems to be influenced by time. The samples D2NO₃_rep5, L24NO₃_rep1, L2NO₃_rep3, and L2NO₃_rep4 seem to be outliers. The PCA analysis for the non-*Phaeocystis* transcriptome bin can be found in Online Supplementary Material 2.2.

4. Outlier removal

Before differential expression analysis, the outliers identified in the PCA are now removed, as well as technical replicates. The outliers were identified as samples having aberrant GC profiles in the FASTQ analysis (**Supplemental Figure III-26**), as well as certain rRNA/cDNA quantity spikes as analysed by Bioanalyser (not shown). PCA showed technical replicates to be highly similar and warrants their removal. The total single-cell samples are now 54. The DGEList dataset was again normalised and filtered.

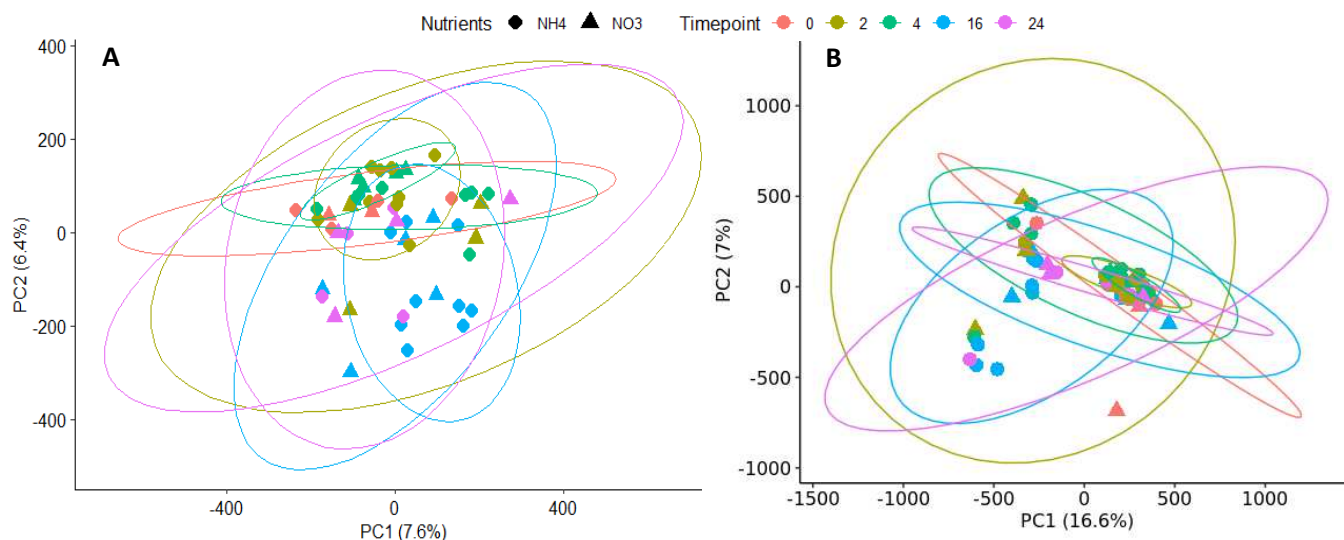


Supplemental Figure III-26. GC profiles of all samples, with outliers highlighted in red.

In this reduced sample set, of the total mapped transcripts in the *Phaeocystis* bin (305580), a total of 17560 transcripts had zero counts amongst all 54 samples. Removing the samples reduced the minimum number of samples per grouping and thus the filtering removed fewer transcripts. It reduced the number of transcripts from 305580 to 87365. For the Non-*Phaeocystis* bin a total of 108902 transcripts out of 1803202 had zero counts amongst all 54 samples. Filtering reduced the number of transcripts from 1803202 to 239420.

5. PCA analysis after sample removal

Sample relations are again explored using principal component analyses, and can also be interactively explored using a Glimma non-metric multi-dimensional scaling plot in the online document.



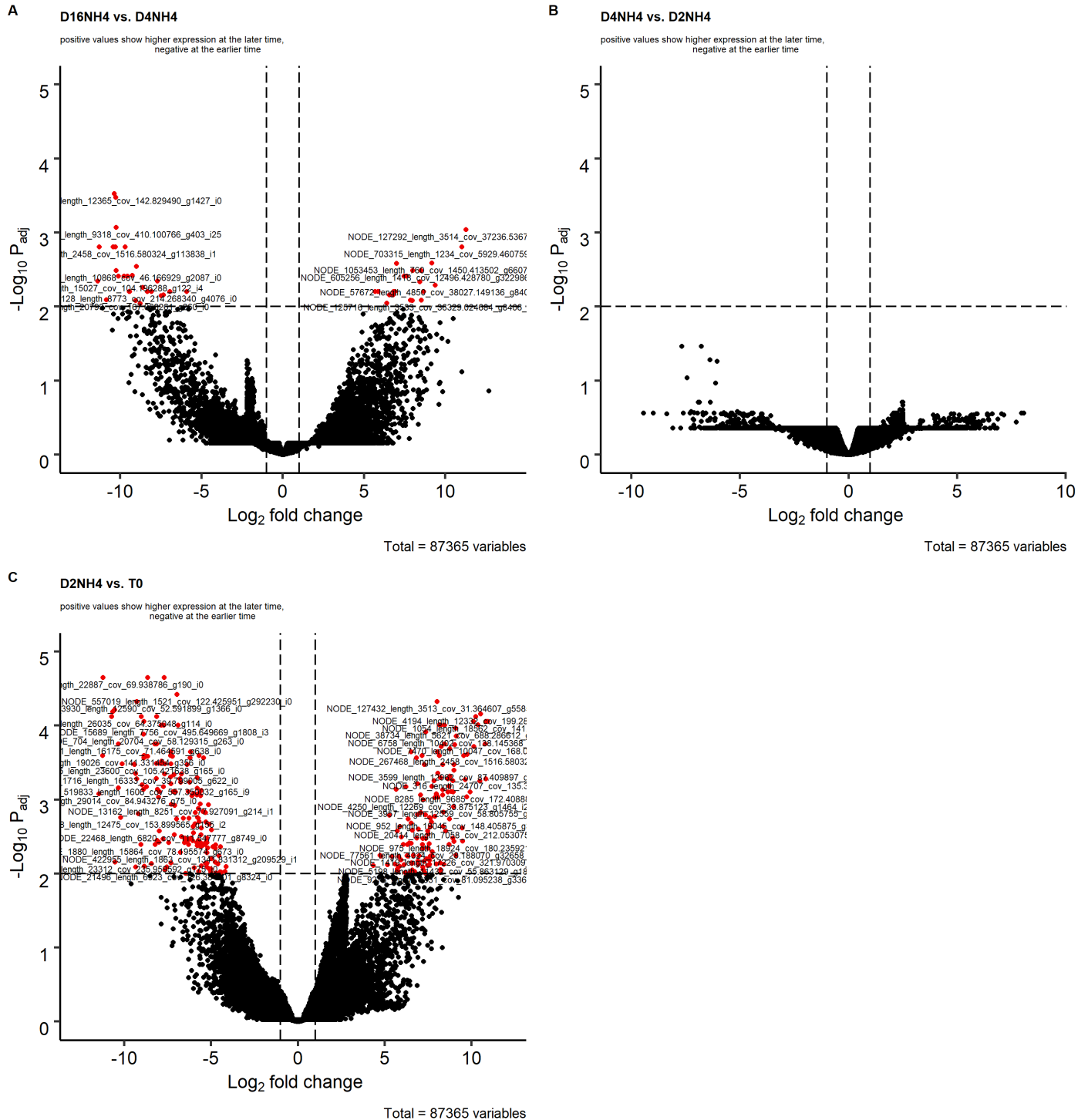
Supplemental Figure III-27. Principal Component Analysis for the *Phaeocystis* transcriptome bin (A) and non-*Phaeocystis* transcriptome bin (B) showing the first 2 axes to identify sample relations. With outliers and technical replicates removed, sample relations did not change. The timepoints are indicated by colours and nutrient treatment by shape, for simplicity light or dark treatment is not shown. Even though no clear grouping by treatment condition can be observed, PC2 of the *Phaeocystis* transcriptome bin seems to be influenced by time.

6. Differential Transcript Expression—Volcano plots

Data and pairwise comparisons are prepared for Differential Transcript Expression (DTE) analysis, the technical replicates and outliers are not included in this analysis. Pairwise comparisons are made for subsequent timepoints within each treatment group, as well as between treatments at the same timepoint. Volcano plots are plotted with significantly differentially expressed transcripts in red with cutoff at p-adjusted 0.01 and \log_2 fold change of $|1|$. Extra volcano plots can be found in the online supplemental material, and volcano plots can also be interactively explored with GO and KEGG annotations in separate online documents (<https://doi.org/10.5281/zenodo.5105584>).

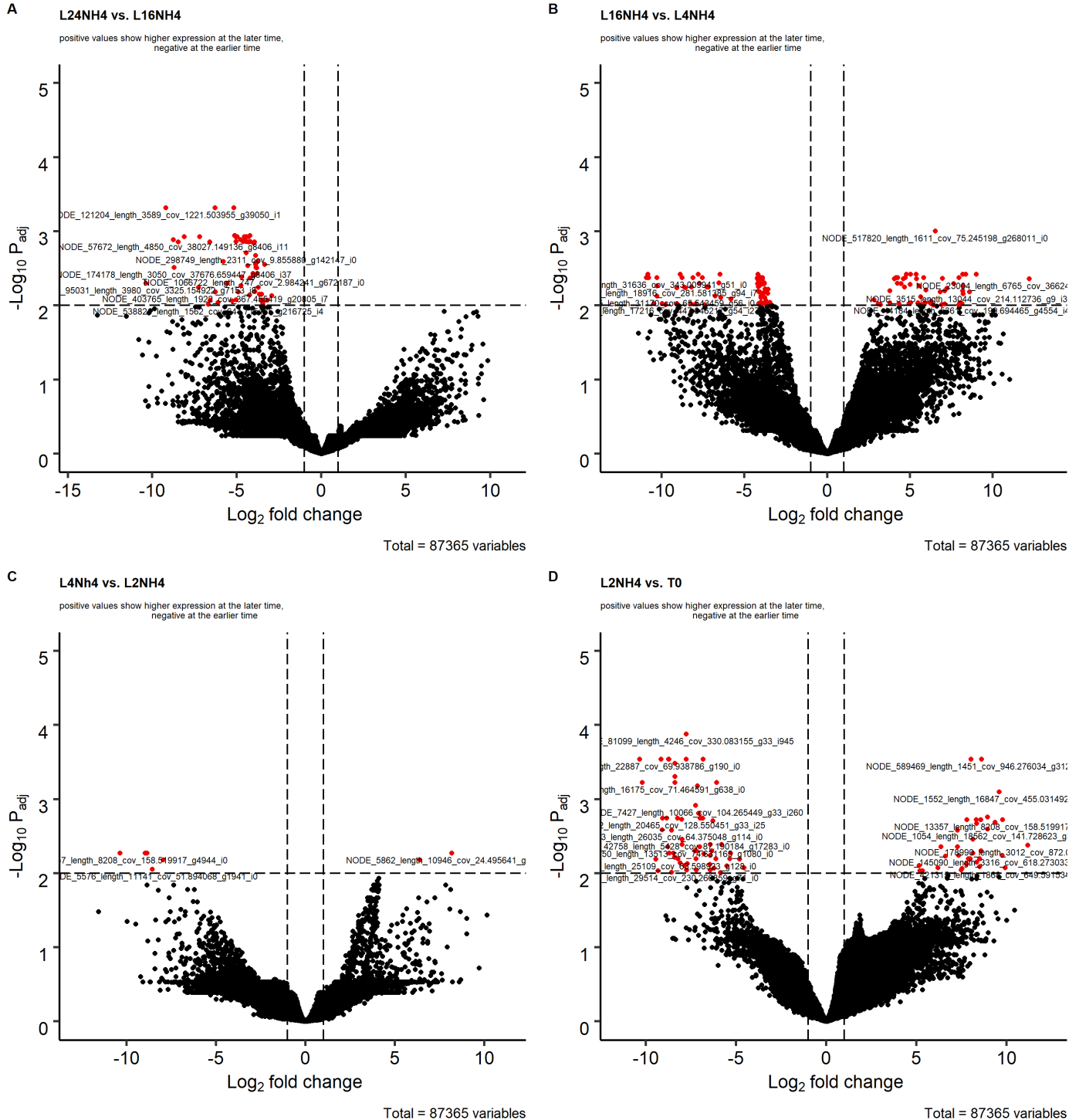
***Phaeocystis* transcriptome bin**

Time comparison, subsequent timepoint, NH4, dark



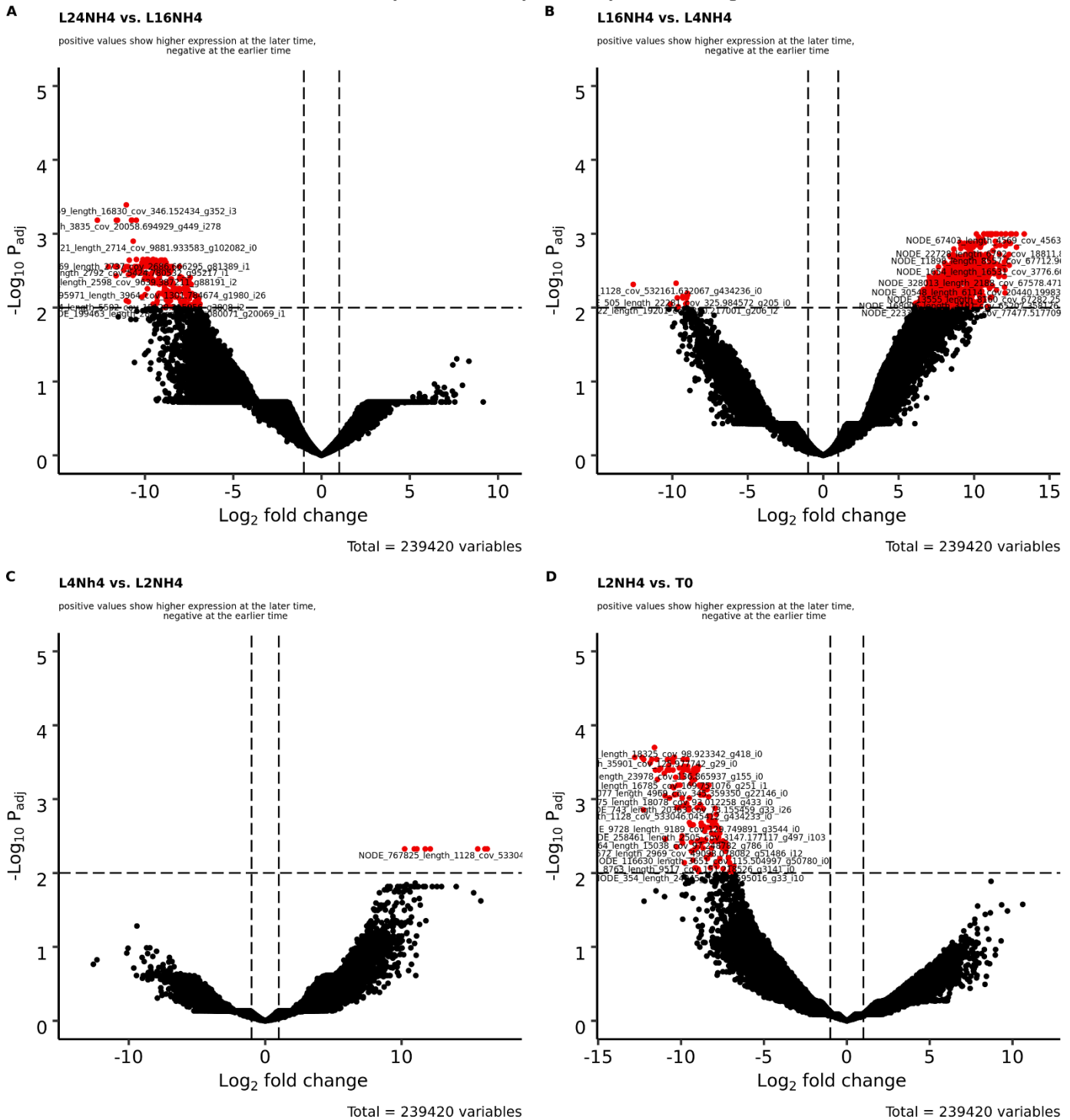
Supplemental Figure III-28. *Phaeocystis* assembly bin subsequent timepoint comparisons for samples incubated with ammonium in the dark. Timepoints are compared between 16 and 4 h (A), 4 and 2 h (B), and 2 and 0 h (C). The significance cut-offs for fold change and adjusted p-value are indicated with a dashed vertical and horizontal line respectively. The transcripts considered significantly differentially expressed are indicated in red, where a positive fold change indicates upregulation at the later timepoint and vice-versa.

***Phaeocystis* transcriptome bin**
Time comparison, subsequent timepoints, NH4, light



Supplemental Figure III-29. *Phaeocystis* assembly bin subsequent timepoint comparisons for samples incubated with ammonium under a normal light-dark cycle. Timepoints are compared between 24 and 16 h (A), 16 and 4 h (B), 4 and 2 h (C), and 2 and 0 h (D). The significance cut-offs for fold change and adjusted p-value are indicated with a dashed vertical and horizontal line respectively. The transcripts considered significantly differentially expressed are indicated in red, where a positive fold change indicates upregulation at the later timepoint and vice-versa.

Non-*Phaeocystis* transcriptome bin
Time comparison, subsequent timepoints, NH4, light



Supplemental Figure III-30. Non-*Phaeocystis* assembly bin subsequent timepoint comparisons for samples incubated with ammonium under a normal light-dark cycle. Timepoints are compared between 24 and 16 h (A), 16 and 4 h (B), 4 and 2 h (C), and 2 and 0 h (D). The significance cut-offs for fold change and adjusted p-value are indicated with a dashed vertical and horizontal line respectively. The transcripts considered significantly differentially expressed are indicated in red, where a positive fold change indicates upregulation at the later timepoint and vice-versa.

7. KEGG pathway set enrichment

KEGG pathway enrichment was explored for specific contrasts with the *kegga* function of the *limma* package. Considering that most differential expression is already observed at the 2 h time point, the contrast for L2NH₄, D2NH₄, and L16 NH₄ versus T0 (0 h control), were explored for enriched or depleted pathways. Additionally, tables with all significantly differentially expressed KEGG pathways for these comparisons, as well as KEGG pathway maps of pathways of interest with log₂ fold-change of significantly differentially expressed genes indicated, can be found in the online supplemental files (<https://doi.org/10.5281/zenodo.5105584>).

Supplemental Table III-7. *Phaeocystis* bin L16NH₄ versus T0 - Top enriched or depleted KEGG-terms.

Pathway	N	Up	Down	P.Up	P.Down	Name
ko00970	679	0	7	1	1.07 x10 ⁻⁴	Aminoacyl-tRNA biosynthesis
ko00260	482	0	6	1	1.22 x10 ⁻⁴	Glycine, serine and threonine metabolism
ko00020	514	1	6	0.75	1.73 x10 ⁻⁴	Citrate cycle (TCA cycle)
ko03018	535	2	6	0.42	2.14 x10 ⁻⁴	RNA degradation
ko00860	343	0	5	1	2.22 x10 ⁻⁴	Porphyrin and chlorophyll metabolism
ko00361	17	0	2	1	3.27 x10 ⁻⁴	Chlorocyclohexane and chlorobenzene degradation
ko00400	209	0	4	1	3.48 x10 ⁻⁴	Phenylalanine, tyrosine and tryptophan biosynthesis
ko03070	22	1	2	0.057	5.52 x10 ⁻⁴	Bacterial secretion system
ko00300	109	4	3	2.27 x10 ⁻⁴	7.01 x10 ⁻⁴	Lysine biosynthesis
ko00010	956	7	7	0.016	8.27 x10 ⁻⁴	Glycolysis / Gluconeogenesis

Supplemental Table III-8. Non-*Phaeocystis* bin L16NH₄ versus T0 - Top enriched or depleted KEGG-terms.

Pathway	N	Up	Down	P.Up	P.Down	Name
ko03018	583	3	3	0.87	2.74 x10 ⁻⁴	RNA degradation
ko00740	159	1	2	0.73	5.47 x10 ⁻⁴	Riboflavin metabolism
ko00730	172	3	2	0.18	6.39 x10 ⁻⁴	Thiamine metabolism
ko00900	196	1	2	0.81	8.28 x10 ⁻⁴	Terpenoid backbone biosynthesis
ko00071	276	1	2	0.90	0.002	Fatty acid degradation
ko00860	316	3	2	0.49	0.002	Porphyrin and chlorophyll metabolism
ko00250	344	1	2	0.94	0.003	Alanine, aspartate and glutamate metabolism
ko00230	1263	12	3	0.37	0.002	Purine metabolism
ko00520	381	8	2	0.016	0.003	Amino sugar and nucleotide sugar metabolism
ko03018	583	3	3	0.87	2.74 x10 ⁻⁴	RNA degradation

Chapter IV.3

Single-cell visualisation of carbon and nitrogen assimilation and translocation within endosymbiotic Acantharia

JS Mansour¹, C LeKieffre², J Decelle², B Gallet³, S Le Panse⁴ F Not¹

¹ CNRS and Sorbonne University, UMR7144, Adaptation and Diversity in Marine Environment (AD2M) Laboratory, Ecology of Marine Plankton Team, Station Biologique de Roscoff, Place Georges Teissier, Roscoff, France

² Univ. Grenoble Alpes, CNRS, CEA, INRAe, IRIG-LPCV, Grenoble, France.

³ Institut de Biologie Structurale (IBS), University Grenoble Alpes, CEA, CNRS, 38044 Grenoble, France

⁴ CNRS and Sorbonne University, Fr2424, Plateforme de imagerie Merimage, Station Biologique de Roscoff, Place Georges Teissier, Roscoff, France

Keywords: photosymbiosis, single-cell imaging, photosynthesis, oceanic plankton, NanoSIMS

In preparation

1. Methodology

1.1. Sample preparation for electron microscopy and chemical imaging

Sample preparations followed the methodology as described in Decelle et al., 2019, except that the samples in this study were chemically fixed prior to high-pressure freezing. Chemically fixed symbiotic Acantharia were individually picked and cryo-fixed in a batch of ~10 cells using high-pressure freezing (HPM100, Leica) in which cells were subjected to a pressure of 210 MPa at -196 °C, followed by freeze-substitution (EM ASF2, Leica). Freeze substitution and resin embedding of the Acantharia proceeded as in Decelle et al., 2019. That is, for the freeze substitution (FS), a mixture of dried acetone and 1% osmium tetroxide was used. The FS machine was programmed as follows: 72 h at -90 °C, heating rate of 2 °C h⁻¹ to -60 °C (15 h), 10 h at -60 °C, heating rate of 2 °C h⁻¹ to -30 °C (15 h), and 10 h at -30 °C. The cells were then washed four times in anhydrous acetone for 15 min at -30 °C. Subsequently, the cells were gradually embedded in anhydrous araldite, a resin that contains negligible levels of the elements and had been previously used in different analytical imaging studies. A graded resin/acetone (v/v) series was used (30, 50 and 70% resin) with each step lasting 2 h at increasing temperatures: 30% resin/acetone bath from -

30 °C to -10 °C; 50% resin/acetone bath from -10 °C to 10 °C; 70% resin/acetone bath from 10 °C to 20 °C. Samples were then placed in 100% resin for 8-10 h, and in 100% resin with accelerator (BDMA) for 8 h at room temperature. Resin polymerization finally occurred at 65 °C for 48 hours. The resin blocks and sections were stored in dry conditions before imaging (**Supplemental Figure III-32**).

1.2. Electron Microscopy

After trimming of the resin block, ultrathin sections of 60 nm thickness were cut for Transmission Electron Microscopy (TEM) using a diamond knife on a Leica ultracut UCT ultramicrotome and mounted onto copper grids. Sections were then stained in 1% uranyl acetate (10 min) and lead citrate (5 min). Micrographs were obtained using a JEOL JEM-1400 transmission electron microscope (JEOL, Tokyo, Japan), operating at 80 kV with a Gatan ultrascan camera. From the TEM images, the sectioning depth of interest was determined as sections showing at least three symbionts.

Thick sections (200 nm) were cut for Scanning Electron Microscopy (SEM), as well as NanoSIMS, and placed on 10 mm silicon wafers. SEM imaging was also used to locate the cells on the sections, verify the quality of structural preservation, and identify the relevant regions of interest for subsequent chemical imaging with NanoSIMS. The SEM micrographs were acquired at an electron energy of 5 kV using the secondary electron detector of the Zeiss Merlin VP Compact SEM at CEA, Grenoble.

1.3. NanoSIMS analyses

Prior to NanoSIMS analysis, SEM wafers were mounted on 10-mm aluminium plots with double-stick Cu-tape and coated with a ca. 10-nm thick gold layer. NanoSIMS analyses were done with a Cameca NanoSIMS L50 ion microprobe (Centre for Advanced Surface Analysis, EPFL – UNIL) based on SEM images to select the areas of interest to be imaged for their ^{13}C and ^{15}N distributions. The samples were processed as described in Lekieffre et al. 2020. Briefly, Acantharian cells were imaged with a 16 keV primary ion beam of Cs^+ focused to a beam spot of ca. 100–150 nm. The secondary molecular ions $^{12}\text{C}_2^-$, $^{13}\text{C}^{12}\text{C}^-$, $^{12}\text{C}^{14}\text{N}^-$ and $^{12}\text{C}^{15}\text{N}^-$ were collected simultaneously in electron multiplier detectors at a mass resolution of ca. 8000, enough to resolve potential interferences in the mass spectrum. Isotopic image dimensions ranged from $15 \times 15 \mu\text{m}$ to $50 \times 50 \mu\text{m}$ with 256×256 pixel resolution. For each image, at least 6 layers were acquired, drift corrected and superimposed using the software L'IMAGE (developed by Dr. Larry Nittler, Carnegie Institution of Washington DC, USA). Quantified $^{13}\text{C}/^{12}\text{C}$ and $^{15}\text{N}/^{14}\text{N}$ ratios were obtained as follows:

$$\delta^{13}\text{C} = \left(\left(\frac{{}^{13/12}\text{C}_{meas}}{{}^{13/12}\text{C}_{control}} \right) - 1 \right) \times 10^3$$

$$\delta^{15}\text{N} = \left(\left(\frac{{}^{15/14}\text{N}_{meas}}{{}^{15/14}\text{N}_{control}} \right) - 1 \right) \times 10^3$$

Where C_{meas} is the measured $^{12}\text{C}^{13}\text{C}^-/^{12}\text{C}_2^-$ ratio of the sample and $\text{C}_{control}$ is the average $^{12}\text{C}^{13}\text{C}^-/^{12}\text{C}_2^-$ ratio measured in unlabelled samples (control and 0 h incubations). Similarly, N_{meas} is the measured $^{12}\text{C}^{15}\text{N}^-/^{12}\text{C}^{14}\text{N}^-$ ratio of the sample and $\text{N}_{control}$ is the average $^{12}\text{C}^{15}\text{N}^-/^{12}\text{C}^{14}\text{N}^-$ ratio measured in unlabelled samples. The software L'IMAGE was used to determine the isotopic enrichments of the *in hospite*

Phaeocystis cells by drawing regions of interest on accumulated $^{12}\text{C}^{14}\text{N}$ images. A minimum of two symbionts were analysed from a minimum of two Acantharia cells (**Table III-7**).

Table III-7. Total cells analysed from NanoSIMS images per treatment and timepoint. The analysed number of host Acantharia is indicated, and the number of symbionts analysed for each Acantharia is separated by a semicolon.

Treatment	Number of Acantharia	Number of symbionts
^{13}C —4 h	2	2; 3
^{13}C —16 h	2	2; 5
$^{13}\text{C} + ^{15}\text{NH}_4^+$ —16 h	3	4; 3; 3



Figure III-9. Timeline for the light incubations and times at which samples were taken, indicated by an arrow. The pulse of nutrients (1 mM $\text{NaH}^{13}\text{CO}_3$; 1 mM $\text{NaH}^{13}\text{CO}_3 + 1 \mu\text{M Na}^{15}\text{NO}_3$ or 1 mM $\text{NaH}^{13}\text{CO}_3 + 0.4 \mu\text{M } ^{15}\text{NH}_4\text{Cl}$) is given at T0, samples were subsequently cleaned of enriched medium at T4 for the chase phase. Dark incubations were identical, but the light (day) period was kept in complete darkness.

2. Results

2.1. Electron microscopy observations

Electron microscopy photographs are presented in **Figure III-10**. The observed cellular features of the Acantharia in this study are congruent with those described for other Acantharia taxa (Decelle et al., 2019; Uwizeye et al., 2021). Notably are the many plastids of the *Phaeocystis* symbiont, whereas free-living *Phaeocystis* consistently have a maximum of 2 plastids (Decelle et al., 2019). Multiple nuclei are observed per Acantharia, with nucleoli at the periphery of the nucleus similar to in Collodaria (Anderson, 1976b). We also note large vacuoles in the symbionts, as well as vacuoles throughout the host cytoplasm

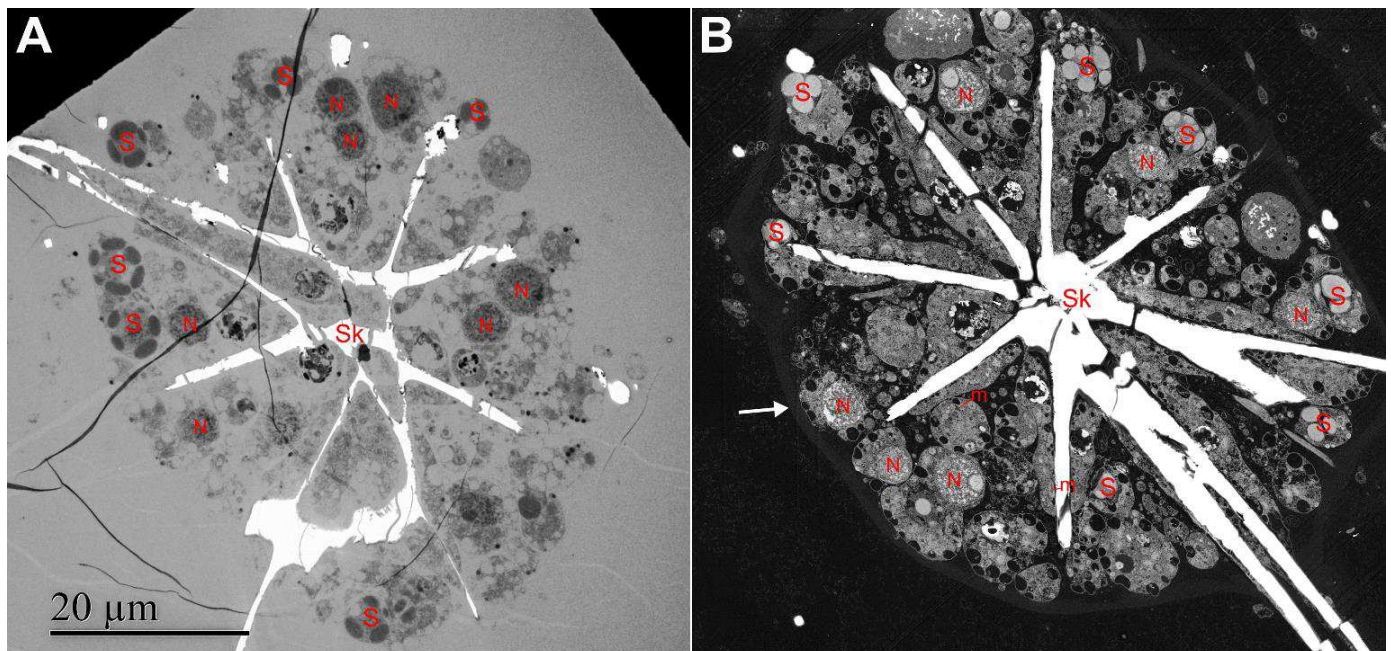


Figure III-10. Micrographs of the Acantharian central capsule by transmission electron microscopy (A) and a subsequent section by scanning electron microscopy (B). The spicules of the acantharian skeleton (Sk) are observed in white. The delineation of the endoplasm is indicated with a white arrow; symbionts are indicated with an “S”, host nuclei with “N”, and some mitochondria in the host with “m”. More detailed views are presented in **Supplemental Figure III-33** and **Supplemental Figure III-34**.

(**Supplemental Figure III-33**). These enlarged vacuoles might be artefacts attributed to the prolonged chemical fixation and low osmolarity of the PBS-based fixation solution. However, since large vacuoles have also been observed for samples processed with cryo-fixation, the vacuoles might be an inherent attribute, e.g., for metal reserves (Decelle et al., 2019, and pers. comm.).

2.2. Chemical imaging

NanoSIMS provided images of $^{15}\text{N}/^{14}\text{N}$ and $^{13}\text{C}/^{12}\text{C}$ ratios that could be correlated with SEM images of the corresponding cell structures, allowing the identification of the specific cellular structures where ^{15}N and ^{13}C are assimilated. Control samples (0 h) are used as reference values for isotopic enrichment calculations. Note that NanoSIMS analysis only allows the visualisation of assimilated compounds, soluble compounds such as those present in vacuoles are lost during sample preparation (Nomaki et al. 2018).

2.2.1 Assimilation of carbon within acantharian cells

Assimilation of ^{13}C after 4 h was only detected in the symbiont cell ($\delta^{13}\text{C} = 368.3 \pm 91 \text{ ‰}$, mean \pm SD, $n = 5$). However, there is one putative vesicle of ^{13}C assimilation observed in the host Acantharia at 4 h. Enrichment of ^{13}C was concentrated in symbiont plastids, though the symbiont nucleus was also ^{13}C -enriched (**Figure III-11**). After 4 h the supply of labelled material in the medium is removed, and incubation continued in the dark for another 12 hours, at 16 h the enrichment in the ^{13}C -enrichment in the *Phaeocystis* cells is significantly lower: $\delta^{13}\text{C} = 168 \pm 37 \text{ ‰}$, $n = 7$) (**Figure III-11**).

Under the addition of ammonium, the fixed carbon at 16 h is not significantly greater ($\delta^{13}\text{C} = 217.3 \pm 52 \text{ ‰}$, $n = 10$, **Figure III-12**), indicating similar assimilation, and translocation rates and possibly metabolic rates as without ammonium addition.

2.2.2 Assimilation of nitrogen within acantharian cells

Like ^{13}C , ^{15}N -enrichment by ammonium is strongest in the symbionts cell compartments. After 16 h of incubation, ^{15}N -enrichment by ammonium can be observed throughout the symbiont cell ($\delta^{15}\text{N} = 572 \pm 150 \text{ ‰}$, $n = 10$, **Figure III-12**). The ^{15}N -enrichment is predominantly found in the plastids, with also particular strong labelling in the nucleoli. Unidentified $\pm 1.1 \text{ }\mu\text{m}$ vesicles are ^{15}N -enriched in the host cell after these 16 h of incubation.

In addition to samples of earlier ammonium incubation timepoints, samples to investigate the capability of the holobiont to utilise nitrate need to still be analysed.

2.2.3 Uptake in the dark

Dark incubated samples that are aimed to investigate photosynthesis independent nitrogen uptake (nitrate and ammonium) need to still be analysed.

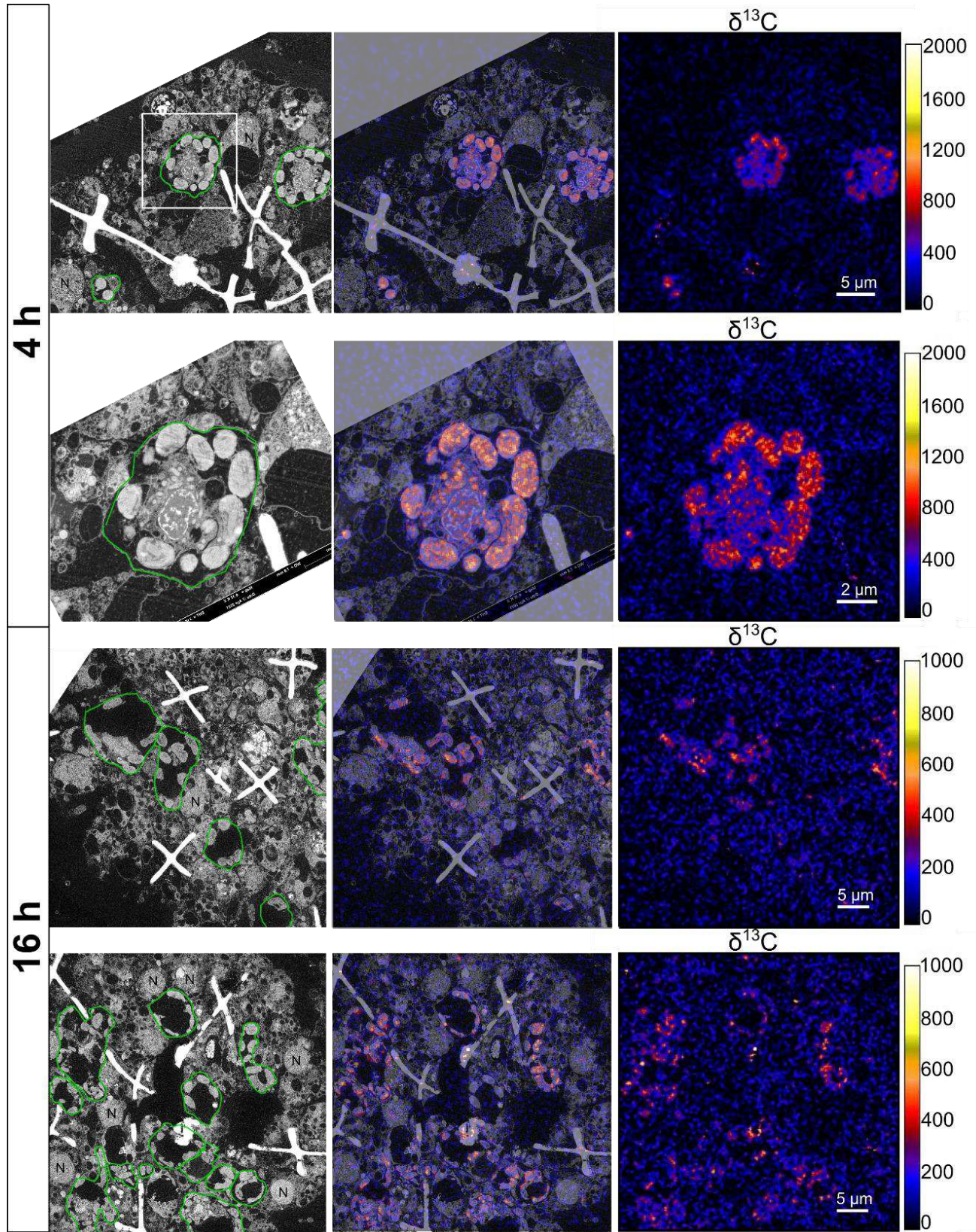


Figure III-11. Correlated Scanning Electron Microscopy and NanoSIMS images for carbon assimilation and remobilisation in the Acantharia holobiont. Each row contains a panel representing a SEM image of an Acantharia cell section (left); the corresponding $\delta^{13}\text{C}$ NanoSIMS image expressed in ‰ (right), and an overlay of SEM and NanoSIMS images (middle), obtained at 4 h of incubation (top 2 rows) in 1 mM $\text{NaH}^{13}\text{CO}_3$ (pulse phase) and after 12 h of subsequent incubation in unlabelled seawater (16 h, chase phase). Images at 4 h show a portion of an Acantharia cell and a focus on a symbiont. Images of 16 h show a different Acantharia on each row. The symbiont cell is roughly outlined in green on the SEM images. Colour scale indicates values in δ -notation, where black signifies no enrichment and white signifies highest enrichment (in ‰), note the differing scales between 4 h and 16 h.

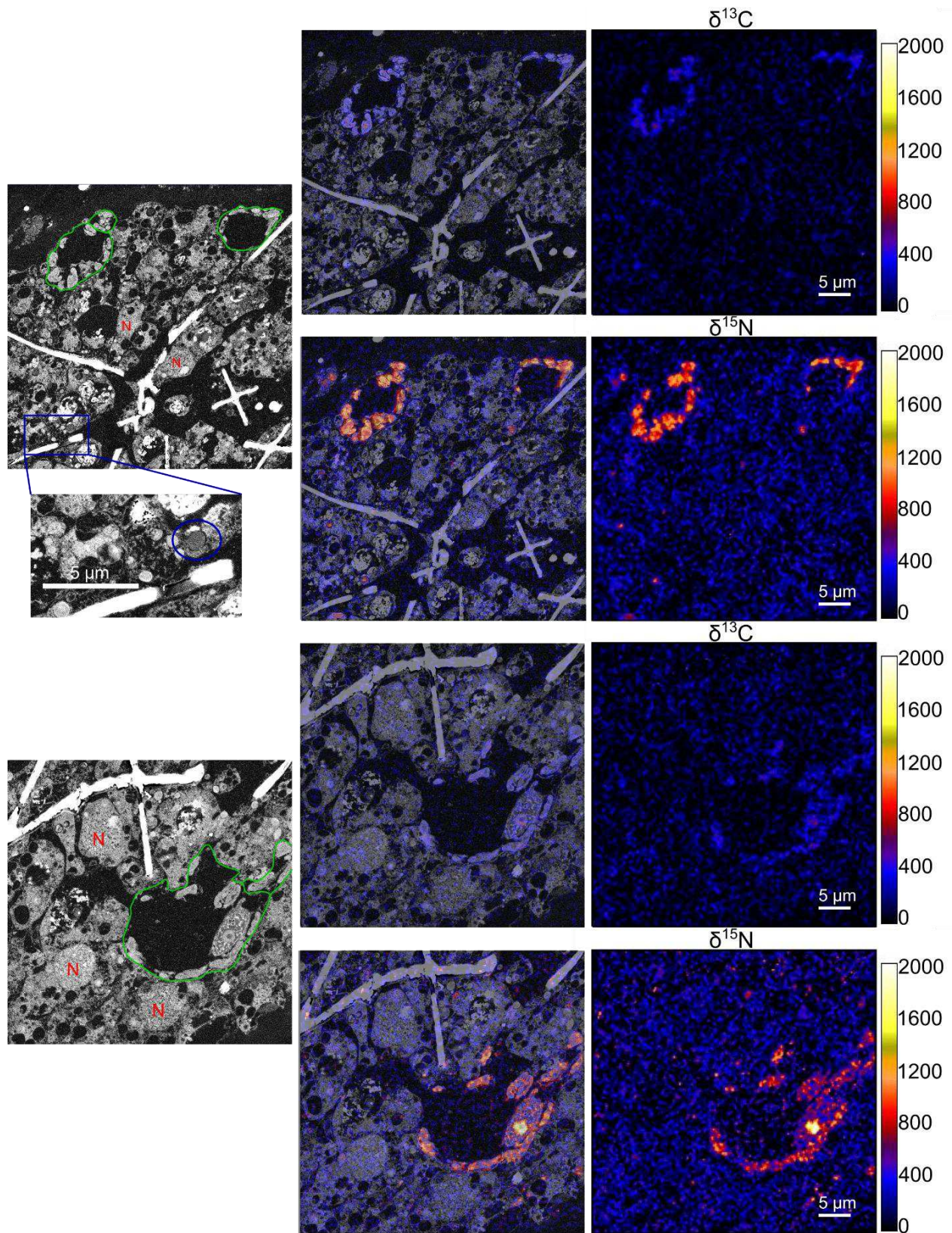


Figure III-12. Correlated Scanning Electron Microscopy and NanoSIMS images for enrichment of ^{13}C and ^{15}N in the Acantharia holobiont, showing the relative nitrogen and carbon assimilation following 16 h incubation with 1 mM $\text{NaH}^{13}\text{CO}_3$ and $0.4 \mu\text{M } ^{15}\text{NH}_4\text{Cl}$ during the chase phase (**Figure III-9**). Two parts of the same cell are shown, left column contains a panel representing a SEM image of an Acantharia cell section; the corresponding $\delta^{13}\text{C}$ or $\delta^{15}\text{N}$ NanoSIMS image expressed in ‰ (right), and an overlay of SEM and NanoSIMS images (middle), Colour scale indicates values in δ -notation, where black signifies no enrichment and white signifies enrichment higher than 2000‰. The symbiotic cell is roughly outlined in green on the SEM images. Nitrogen (ammonium) enrichment is most clearly observed in the symbiotic microalgae, more particularly in the nucleolus (yellow white hotspot, bottom row). Localised nitrogen enrichment is seen in several unidentified vesicles of the host cell, see zoom in panel outlined in cyan (top row). Carbon enrichment is relatively low, but seems apparent around the symbiont co-localised with nitrogen.

3. Discussion

3.1. Methodological considerations

The final isotope concentrations used are an approximate 20 times addition to the natural concentrations of nitrate and ammonium respectively (NO_3^{3-} : 0.5 μM , and NH_4^+ : 0.02 μM , in 2019 in the bay of Villefranche-sur-Mer, <https://www.somlit.fr/visualisation-des-donnees>), and could thereby represent elevated environmental levels of ammonium caused by nutrients enrichments in coastal water. However, the concentrations chosen here are in fact considerably lower than what is often used in similar studies exploring carbon or nitrogen assimilation (Pernice et al., 2012; LeKieffre et al., 2020; Lyndby et al., 2020). Though we here show that it is possible to analyse strongly enriched regions using lower nutrient concentrations that are closer to natural conditions, there is a lot of background noise. Hence, experiments using higher concentrations of isotopic enrichment might be more beneficial for the signal-to-noise ratio.

Our methodology used chemical fixation to cross-link and fix most proteins and amino acids, and was followed by high-pressure freezing, however, this still does not allow accurate tracking of low-molecular-weight compounds that are soluble and poor in amino groups (e.g. sugars). Such compounds are not successfully immobilized during the fixation protocol used in this study and are most likely extracted during the steps of sample preparation for microscopy (Nomaki et al. 2018). Only assimilated and fixed incorporation can thus be visualised. Therefore, uptake here represents incorporation into macromolecules - *i.e.* proteins, fatty acids, RNA, DNA, etc. representing the products of anabolic metabolism - and is an underestimation of the total uptake of the tracer. This additionally means that loss of labelling during the chase period of the experiment (16 h) cannot be fully elucidated. Lost carbon labelling could have, for example, been transferred into soluble compounds or used during respiration. Future studies intending to track metabolic activities should thus ideally proceed immediately from high-pressure freezing to cryo-NanoSIMS in order to immobilise all cell material. However, this is a highly specialised procedure with additional limitations for correlative microscopy (Decelle et al., 2020).

3.2. Carbon assimilation and transfer in the Acantharia holobiont

Carbon products derived from photosynthetically fixed carbon (photosynthates) exist among others in the forms of soluble compounds such as glycerol, glucose, amino acids (Whitehead and Douglas, 2003; Yellowlees et al., 2008; Davy et al., 2012). As previously indicated, such soluble compounds cannot be studied using this methodology. Other non-soluble carbon storage molecules are in the form of lipids, or starch grains (Ohlrogge and Browse, 1995; Jia et al., 2015; Kopp et al., 2015a; LeKieffre et al., 2018). For example, the transfer of photosynthates to and in the coral cell likely proceeds through lipid droplets (Kopp et al., 2015b).

We show that the symbionts are the primary location for carbon assimilation, and after a pulse of 4 h no ^{13}C labelling in the host can yet be observed. Other photosymbioses similarly show carbon uptake firstly in the photosymbiont cell. Already after 45 min, an increase in ^{13}C -labelling can be seen in the dinoflagellate symbionts of the foraminifera *Orbulina universa*, with the strongest enrichment in starch granules. At the same time, lipid droplets in the host cell are also already lightly enriched in ^{13}C , indicating the transfer of photosynthates (LeKieffre et al., 2018). In both the dinoflagellate symbionts of corals and

Collodaria (Radiolaria) newly assimilated carbon is also most evident in starch grains or lipid droplets of the symbionts (Kopp et al., 2015a; Decelle et al., 2021). Lipid droplets, mainly triacylglycerols, are a common storage molecule for haptophytes and dinoflagellates (Becker et al., 2018). Dinoflagellates, in contrast to plants, are known to synthesise starch in their cytosol, and not in their plastids (Michel et al., 2010). In the Acantharia holobiont we here do not observe assimilation in starch granules nor lipid droplets but rather at the site of the symbionts plastids. It might be that the synthesis of carbon storage molecules in *Phaeocystis*, the acantharian symbiont, proceeds in a manner more similar to plants—in their plastids, and could indicate that photosynthates are in fact primarily used for cell growth or repair (with minimal intermediate storage). This could be corroborated by the fact that we do not observe clear ^{13}C -enrichment in host cell compartments, whereas in other photosymbioses translocation, e.g. in lipid droplets, has been shown to happen already within the hour (Kopp et al., 2015a; LeKieffre et al., 2018). Additionally, Uwizeye et al. (2021) showed that in comparison to free-living *Phaeocystis* the symbiotic form downregulates genes related to (carbon) energy storage, such as triacylglycerol and starch biosynthesis, as was also seen for Collodaria (Liu et al., 2019). Though, low enrichment in Acantharia host cell compartments has previously been seen after 5 h (Uwizeye et al., 2021). It is possible that with our low level of ^{13}C enrichment and relatively high noise, less strongly enriched cellular compartments are not observed. Conversely, photosynthates might be translocated to the host in the form of soluble molecules, or used primarily for catabolic processes such as respiration, and thereby not observed in our study. However, we do note that there appears to be a carbon enriched vesicle in the host after 4 hours (**Figure III-11** second row), though this is only one instance and as such we cannot yet be certain of its validity without having analysed additional samples.

After 16 h incubation, during the chase phase, we observe a loss of ^{13}C labelling. This loss of ^{13}C -labelling in the algal symbionts during the chase (dark) period was already observed in other photosymbiotic associations, such as in dinoflagellates and coral or planktonic foraminifera symbioses (Kopp et al., 2015a; LeKieffre et al., 2018). The loss of ^{13}C -labelling in the algal symbionts during the chase (dark) period could indicate a transfer of ^{13}C -photosynthates within the holobiont or loss due to respiration. The exact nature of the translocation of ^{13}C during the chase phase cannot be determined, as no specific hotspots of fixed ^{13}C can be observed in the host cell. However, the clear disappearance of labelling in the algal symbionts indicates that previously fixed carbon is either used or transferred, either by the algal cells that initially fixed it or, if translocated, by the host, for example for respiration. Since no ^{13}C labelling is observed in the host, hypothetically transferred photosynthates are likely not fixed. As noted above, the soluble compounds are lost during sample preparation, thus we can only hypothesise that ^{13}C -photosynthates are transferred to the Acantharia host cell, but could not be visualised.

Currently, we do not observe a difference of carbon assimilation between treatments with and without ammonium, as is in agreement with previous bulk measurements (Chapter III). Though symbionts do use exogenous ammonium, as seen by the assimilation of labelled ammonium (also nitrate, see Chapter III), they would however have had access to host recycled nitrogen, reducing possible effects of extra exogenous ammonium. Even though an increase in photosynthesis might be expected with additional nitrogen sources, because N metabolism would profit from photosynthetically acquired energy, oppositely carbon assimilation has also been seen to be suppressed, and instead fixed reserves are utilised (e.g. starch) (Huppe and Turpin, 1994). Though here no effect of additional ammonium supply on carbon

fixation could be observed. Possibly, at the 16 h timepoint the signal might be too diluted to accurately make this comparison due to near-complete usage and translocation of enriched carbon over the 12 h night period. Ideally, the effect of nitrogen source on carbon assimilation would need to be compared at an earlier timepoint, during the pulse, with the currently available data this is however not yet possible. To further analyse this effect in photosymbiotic Acantharia we will analyse incubations with ammonium at earlier timepoints. In addition, the effect of nitrate on carbon uptake will be assessed by analysis of the respective samples.

3.3. Nitrogen assimilation and transfer in the Acantharia holobiont

Nitrogen assimilation from ammonium sources after 16 h (during the chase phase) is apparent in both symbiont and host. In the Acantharia holobiont, much like in Collodaria (Decelle et al., 2021), enriched nitrogen is observed throughout the entire symbiont cell and a particular high amount in the nucleoli. High N content is expected in the chloroplasts' light-harvesting proteins, pigments, and carbon fixation enzymes (e.g. Rubisco), as well as in the nucleus' DNA, RNA and ribosomes. The observed enriched in these cellular compartments indicates high activity and turnover in these compartments. The cell thus invests in both the resource acquisition machinery of the chloroplast and in growth machinery located in the nucleus.

The assimilation of ammonium in host vesicles cannot yet be attributed to either translocation or direct assimilation. Though in photosymbiotic corals or sponges host labelling due to enrichment is only seen in the chase phase and thus indicated indirect uptake and translocation from the symbionts (Pernice et al., 2012; Achlatis et al., 2018). Likewise, Collodaria NanoSIMS data suggested that nitrogen from ammonium was transferred from the symbiont into the Golgi (Decelle et al., 2021). Here we do not observe any enrichment in host Golgi, but in micrometre-sized unidentified vesicles. Such transfer might be in the form of amino acids as a transcriptome for Collodaria might suggest (Liu et al., 2019). To further verify the primary assimilation location and transfer of nitrogen obtained from ammonium, earlier timepoints (during the pulse phase) still need to be analysed.

Nitrate usage in photosymbiotic associations can be variable. For example, it is not observed in photosymbiotic *Cassiopea*, or in low amounts (Lyndby et al., 2020). This might have been attributed to the availability of other N sources (such as ammonium), and to recycling and preferential usage of host waste products. In other instances, nitrate is clearly assimilated, though in lower amounts and rates than ammonium (Grover et al., 2003; Tanaka et al., 2006; LeKieffre et al., 2020). In corals, the majority of nitrogen from nitrate was transferred to the host (Tanaka et al., 2006). We have previously verified nitrate uptake in Acantharia (Chapter III), but to ascertain its assimilation location and translocation, as well as synergy with carbon assimilation, further samples for NanoSIMS will be analysed.

4. Summary/conclusions

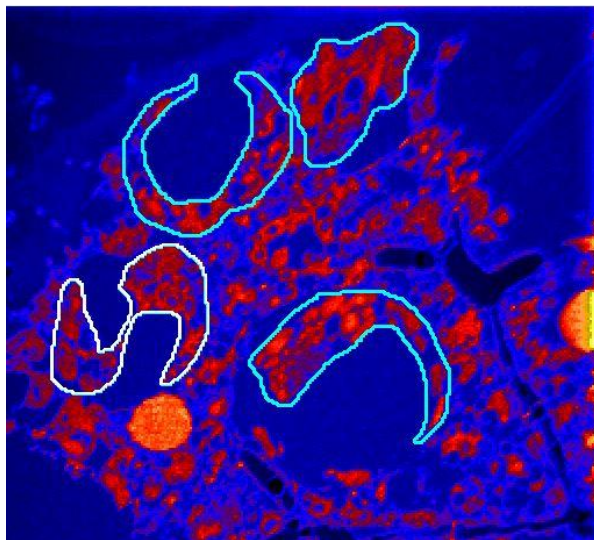
Increased levels of ^{13}C were observed within 4 hours in the symbiont cell, predominantly located in the symbiont's plastids and nucleus, indicating that the primary source of newly fixed carbon is in the symbiont cell. No clear transfer of ^{13}C -labelling is observed during the chase (dark) period. Carbon translocation might still occur in the form of undetected low molecular weight molecules or directly used for respiration and energy. The symbionts show strong ^{15}N -ammonium labelling still during the chase

period, showing that the symbionts at least fix external ammonium and not only utilise host waste product. Nitrogen from ammonium is also assimilated in the host, though it is still unclear if this has been transferred or directly assimilated. We hypothesise photosynthetic carbon uptake might be used for the maintenance of the symbionts (e.g. the plastids). Further investigation of nutrient transfer might be inferred by analysing samples as earlier timepoints for comparisons. Additionally, investigation of inorganic nutrient uptake in the dark could show the influence of photosynthesis-independent processes.

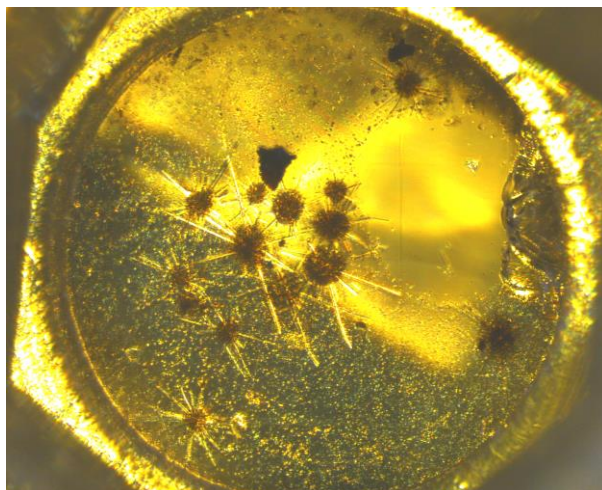
Supplementary Material to Chapter IV.3

Single-cell visualisation of carbon and nitrogen assimilation and translocation within endosymbiotic Acantharia

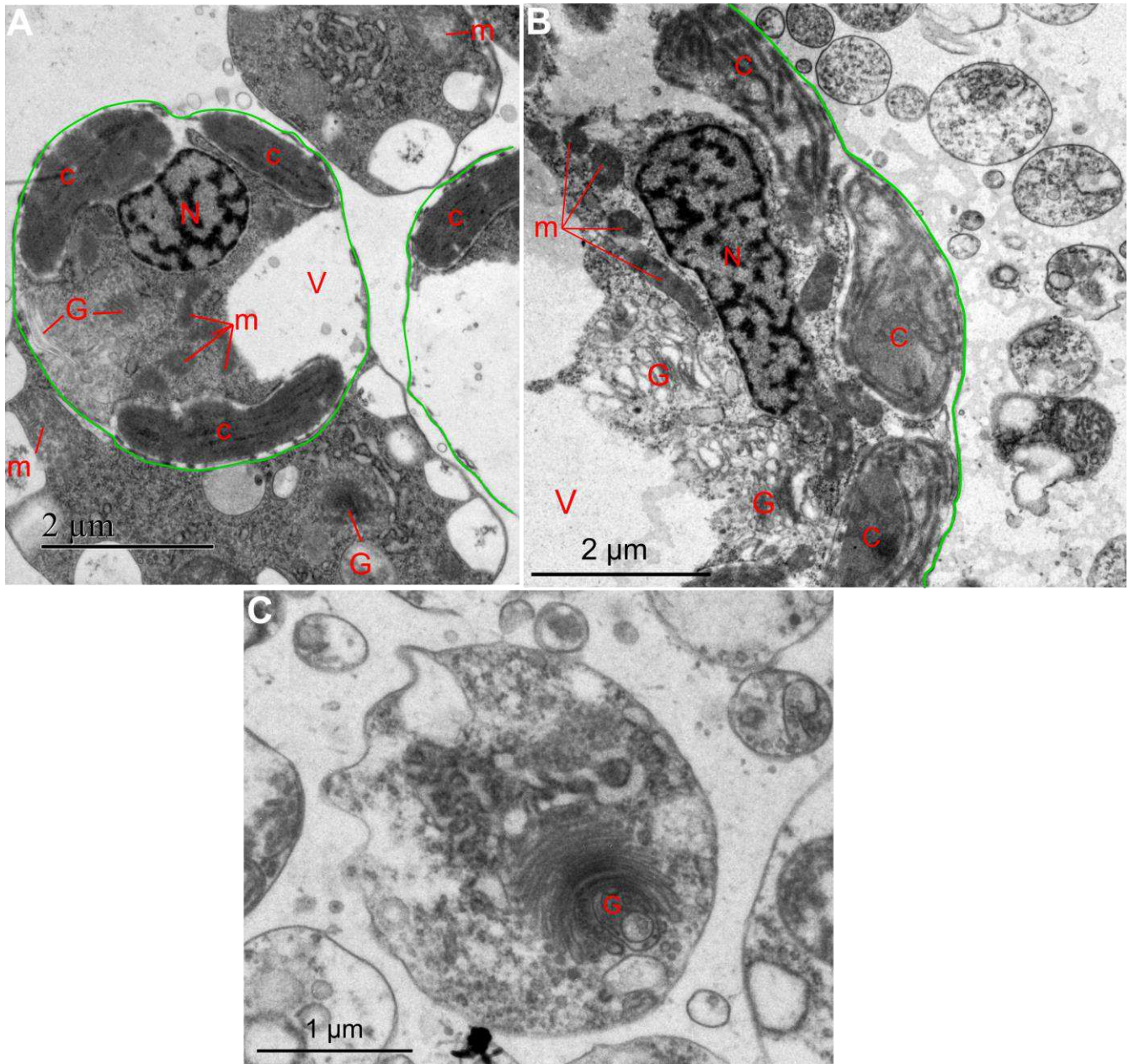
Supplementary Figures



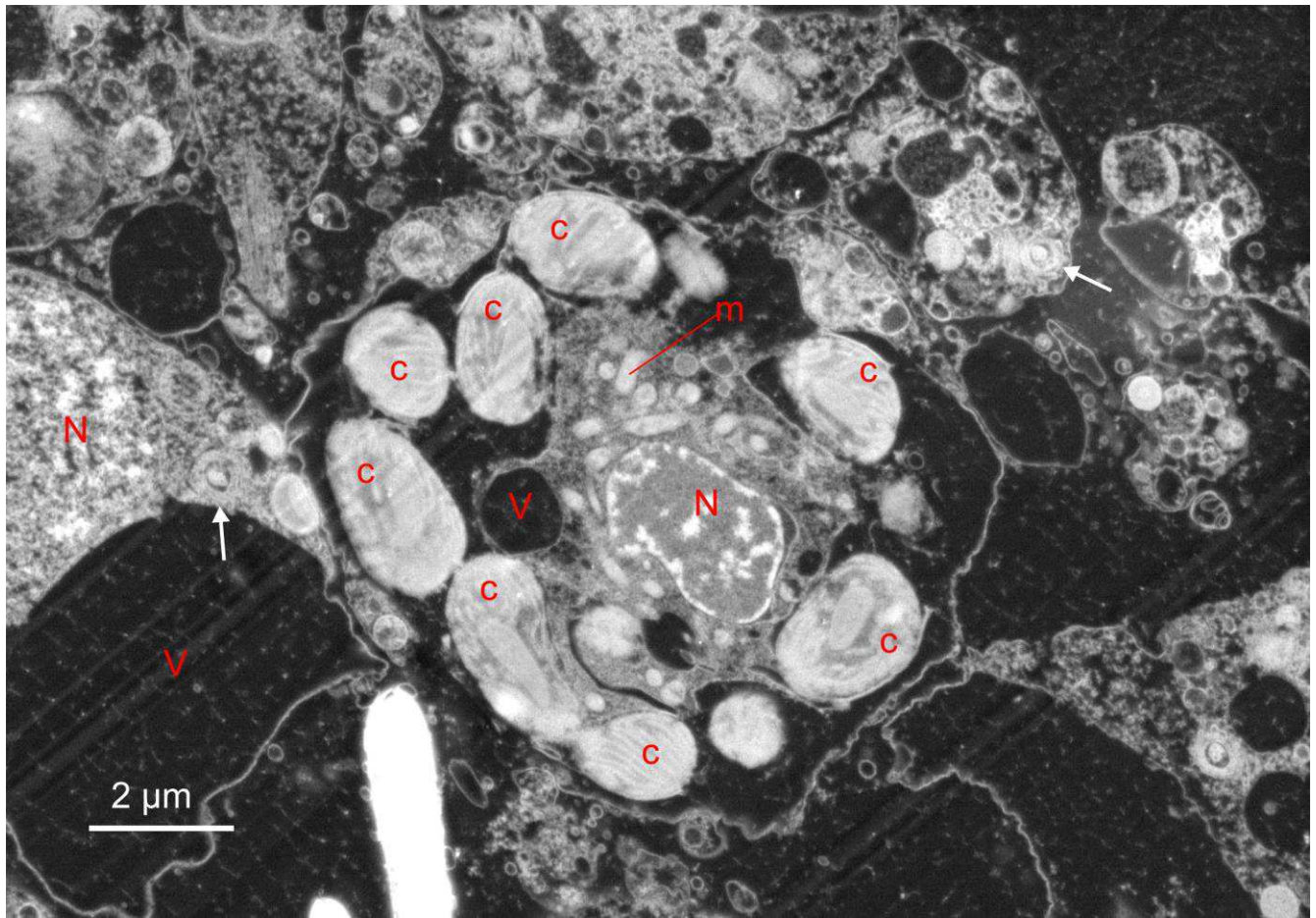
Supplemental Figure III-31. Example of region of interest (ROI) for analysis of the NanoSIMS images. Here the ROIs are the symbiont cells, excluding its large vacuole devoid of signal. Shown is a $^{14}\text{N}/^{12}\text{C}$ elemental image, thereby indicating structures rich in nitrogen as more red/yellow.



Supplemental Figure III-32. Acantharia embedded in resin prepared for electron microscopy. Block diameter is approximately 1 mm.



Supplemental Figure III-33. Transmission electron microscopy micrographs detailing the cellular structure of *Acantharia* and *Phaeocystis* symbionts. The symbiont is delineated with a green line (**A & B**). Host structures are or observed surrounding the symbiont in a drop-like shape. **C**) Details of such a structure. Symbiont chloroplasts: C; mitochondria: m; nucleus: N; Golgi: G; vacuole: V.



Supplemental Figure III-34. Scanning electron microscopy micrographs detailing the cellular structure of Acantharia and *Phaeocystis* symbionts. Symbiont chloroplasts are observed at the periphery of the symbiont cell with host structures surrounding the symbiont. Symbiont chloroplasts: C; mitochondria: m; nucleus: N; vacuole: V; Golgi in the host: white arrow.

Chapter IV.4

Chemical imaging and transcriptomics—Conclusions

The transfer of nutrients between host and symbionts is a central aspect for photosymbioses—assumed to be largely based on a trophic relationship. Photosymbionts are expected to benefit from a nitrogen-rich environment in the host, the host in turn would benefit from a supplemental energy source and inorganic carbon acquisition. A principal aim in the study of such photosymbioses is thus to understand if, how, and which compounds are translocated within the holobiont. Deducting such information from gene expression data only might not be possible, as it does not directly correlate to protein translation, due to processes such as post-transcriptional regulation.

Our combined experimental setup for single-cell transcriptomics and chemical imaging aimed to corroborate the capabilities in C and N assimilation of *Acantharia* from both a molecular and physiological angle. The chemical imaging approach was used to follow nutrient transport and localization over time using stable isotopes and NanoSIMS. Thereby we aimed to visualize and quantify carbon uptake, incorporation, and photosynthate translocation between symbionts and host over time, and the effect of nitrogen (nitrate or ammonium) thereon. The transcriptomics approach was utilised to assess gene expression differences under the same treatments and time series. Thereby investigating transcriptional difference, adaptability/plasticity of nutrient uptake when increased nutrients are present (eutrophication). As well as, N Metabolism adjustment and capabilities of symbiont and/or hosts). Separation of the holobiont transcriptome allows us additionally to disentangle specific processes, such as those involved in carbon and nitrogen metabolism, that are due to host or symbiont transcriptional activity.

The currently analysed samples show no measurable carbon transfer from symbiont to host, but do imply the usage of recently assimilated photosynthates. The specifics of photosynthate usages cannot yet be ascertained and might thus be used either directly at the symbiont or in the host cell. It would currently suggest that if the *Acantharia* obtains photosynthetically acquired carbon by translocation it is not assimilated in the host cell, but might still be used for catabolic processes to obtain energy. Additional samples of earlier time points would need to be analysed for their isotopic signature to ascertain this. Differential gene expression between symbiotic *Phaeocystis* and free-living *Phaeocystis* suggested that symbiotic *Phaeocystis* generally downregulates carbon storage pathways (Mars Brisbin 2020). We also

noted a decrease in expression in the TCA cycle of the *Phaeocystis* transcriptome bin after 16 h with ammonium under a normal light cycle. Likewise, fatty acid biosynthesis is downregulated at 2 h in the dark and light, as well as after 16 h with a normal light cycle. This would corroborate the observed absence of specific storage vesicles in the symbiont, and the lack of evidence for such carbon assimilation in the host further implies such photosynthates might be used for directly for respiration or energy. However, for samples 2 h in darkness, key genes in the TCA cycle show a log fold increase, and thus potential carbon storage might occur when photosynthesis is not possible (online supplementary material 2.1).

A photosynthesis-independent manner for carbon fixation might be possible through the identified urea pathway of the host. Carbonic anhydrase seems to be predominantly present in the host transcriptome. This enzyme catalyses a reaction resulting in bicarbonate that can, in turn, be used for photosynthesis, or in the ammonium pathway in conjunction with ammonia—allowing for inorganic carbon fixation in a photosynthesis-independent way. Such processes might account for the increased carbon fixation in the presence of ammonium that is seen in photosymbiotic corals in the dark (Cook et al., 1992; Ezzat et al., 2015), or a salamander-alga photosymbiosis (Burns et al., 2020). However, we here did not observe different inorganic carbon assimilation with or without ammonium. To further verify this and ascertain if any carbon fixation might be attributed to (heterotrophic) host processes we might further visualise carbon fixation of NanoSIMS samples, and analyse the expression of involved genes, in dark treatment samples.

Transcriptomic pathway analyses suggest that both symbiont and host could directly use nitrate, as well as ammonium. However, samples with nitrate treatment will need to be analysed to visualise and ascertain localised nitrate assimilation and translocation. Nonetheless, the symbiont would be able to benefit from host excreted ammonium, as well as urea. Ammonium assimilation that we observed in the host could have either been directly assimilated by the host or transferred from the symbiont. This might be compatible with previous suggestions that for both Acantharia and Collodaria holobionts the algal symbiont might transfer small nitrogen compounds rather than carbohydrates (Mars Brisbin 2020; Liu et al., 2019).

Acknowledgments

This work benefited from access to the Observatoire Océanologique de Villefranche sur Mer, an EMBRC-FR and EMBRC-ERIC Site, as well as the ABiMS bioinformatics platform of the Station Biologique de Roscoff. Stéphane Escrig and Anders Meibom are thanked for access and expertise with NanoSIMS imaging. Many thanks go to Konstantinos Anestis for both help in the lab and many discussions on transcriptomic data analyses. This work was supported by the European Union's Horizon 2020 research and innovation programme under grant agreement No. 766327 (project MixITiN). This project received funding from the ATIP-Avenir program, a Défi X-Life grant from CNRS, the LabEx GRAL (ANR-10-LABX-49-01), financed within the University Grenoble Alpes graduate school (Ecoles Universitaires de Recherche) CBH-EUR-GS (ANR-17-EURE-0003). We thank Guy Schoehn and Christine Moriscot, and the electron microscope facility, which is supported by the Rhône-Alpes Region, the Fondation Recherche Medicale (FRM), the fonds FEDER, the Centre National de la Recherche Scientifique (CNRS), the CEA, the University of Grenoble, EMBL, and the GIS-Infrastructures en Biologie Sante et Agronomie (IBISA).

Chapter V

Conclusions and Perspectives



“What is important is to spread confusion, not eliminate it.”

— Salvador Dalí

Conclusions and Perspectives

Mixoplanktic photosymbioses are ubiquitous in the global ocean and can be especially important to primary production in low nutrient ecosystems. Abundant in oligotrophic surface waters, the Acantharia-*Phaeocystis* (haptophyte algae) photosymbiosis is both an ecologically relevant system and additionally of interest from an evolutionary perspective. Their ubiquity and physiology make them great contributors to biogeochemical cycles, including strontium, and the vertical export of organic matter known as the biological carbon pump process. Furthermore, the Acantharia-*Phaeocystis* symbiosis is of evolutionary interest because symbionts are hosted in the central capsule (in lieu of the extracapsulum, as is the case in other Radiolaria) and the symbionts undergo extensive modification. Even though photosymbioses might generally be considered mutualistic, there has been an increasing amount of research questioning this fact, and symbionts may in fact not benefit in some cases (or vice-versa) (Kamel, Bishoy, 2016; Keeling and McCutcheon, 2017; Decelle et al., 2019; Uwizeye et al., 2021). In Acantharia, the symbiotic algae are no longer viable *ex hospite*, and are transformed for increased emphasis on photosynthetic resource acquisition and may be transitioning toward full integration as organelles.

1. Methodological and cell culturing challenges

Non-constitutive mixoplankton studies are generally not available from culture collections and this lack of cultures severely limits the possibilities to study them, as biomass and replications are needed. Study with organisms relatively fresh from nature is thus preferred and a necessity. Hence, specimens need to be always handpicked for experimentation; this makes experiments with high replication logistically extremely challenging where specimen quantity is limited. Additionally, this limits options for preliminary tests. Because of the uncultured nature of many mixotrophic lineages, among which are Acantharia, quantitative methods for assessing trophic and metabolic activities need both bulk, and by necessity, single-cell techniques. Single-cell techniques, like NanoSIMS or transcriptomics become increasingly interesting to integrate into future experiments. However, these single-cell methodologies cannot substitute bulk analysis for measurements of physiological rates, but complement by providing qualitative data and information for corroboration and forming of further hypotheses.

Photosynthetic contribution to the carbon budget of photosymbiotic association is generally difficult to estimate, because of carbon fluxes that occur between host and symbiont. The produced photosynthates might be employed in the maintenance of the originating structure (plastid/endosymbiont) and not contribute to the host's metabolism. Indeed, the allocation of assimilated carbon and nitrogen that we observed using NanoSIMS (Chapter III.2.2) might agree with such behaviour. Likewise, photosynthates may be preferentially used for respiration (Putt, 1990), thus lost as CO₂ rather than incorporated into host biomass. Respired photosynthates still contribute to the host metabolism but are not measurable using isotopic measurements that can only measure assimilated molecules. Indeed, respiration rates in some Radiolaria can be close to or higher than photosynthesis rates (Swanberg et al., 1986; Villar et al., 2018). Additionally, carbon derived from respiration might be recycled into the cell, and used in photosynthesis, diluting the used isotope pool relative to the pool present in the medium, ultimately causing underestimation of the photosynthetic rate due to the internal carbon recycling.

Despite that, the isotopic methods still provide a reliable measurement of net photosynthesis. However, it makes it difficult to quantify the overall gain that the organisms receive from the acquired phototrophy. In other organisms, this might have been assessed by comparison of the growth efficiency of the photosymbiotic species and purely heterotrophic ones. Since Radiolaria do not grow or proliferate under laboratory conditions, their longevity (and health by e.g., proxies of water column position, axopodial abundance, symbiont presence, or spicule degradation) might be assessed instead, similar to how Swanberg et al., (1985), and Anderson et al. (1989) looked at the survivability of Spumellaria in the lab. However, interspecific effects need to be taken into account since the same Acantharia species cannot be kept both symbiotic and non-symbiotic.

Efforts in cultivation (or improved maintenance) of Radiolaria will benefit the study of radiolarian physiology that are now severely hampered by specimen quantity and longevity of the specimens. It is clear that Acantharia would require both prey and light for survival. We have tested inorganic and organic (prey) nutrient uptake rates separately, though both might need to be combined to evaluate the effect of prey presence on photosynthesis. Photosynthetic rates have been shown to be tightly coupled to prey uptake, and prey concentration has been shown to be able to affect photosynthetic rates in other mixoplankton (Skovgaard et al., 2000; Hansen, 2011; Nielsen et al., 2012; Maselli et al., 2020). Here we did not evaluate survivability in absence of prey, but observations have indicated healthy acantharian specimens can be kept in a Petri dish with filtered seawater for at least a week. Maximal photochemical quantum yield remained unchanged for at least 5 days in the lab (data not shown). To assess possible improvements in acantharian survival, survivability could be tested with a minimal supply of prey. Additionally, the culture vessel might be rotated (e.g. as on a plankton wheel) to prevent the Acantharia from sticking to vessel, as well as better facilitate prey encounters. Alternatively, microfluidics approaches (Shapiro et al., 2016; Girault et al., 2019) could potentially sustain a single-cell with a constant flow of fresh medium, much like a mini chemostat. A cell trapped in a microfluidics set-up could then be monitored by automatic photography for its survival, and tested with different flow-through media to ascertain the best medium conditions. The flow-through medium could also contain prey items, which would thus allow predation and grazing rate assessments on a single cell, and thereby greatly improving the experimental throughput. Nevertheless, since the specifics of acantharian reproduction and the fate of its swimmers remains elusive, real cultures—in the sense of going through successive full life cycles—would persist to be far off.

2. Radiolarian cellular stoichiometry: carbon and nitrogen to volume ratios

The analyses of carbon and nitrogen content of several Rhizaria taxa presented in Chapter II are pivotal information for studies of ocean ecology and carbon or nitrogen-based models that require baseline carbon or nitrogen content of the organisms. Accordingly, knowledge and quantification of cellular C and N content of these abundant organisms is paramount in characterising oceanic ecosystems and C and N fluxes. We established biovolume to mass equations that can give more accurate predictions than mean C or N density or previously available central capsule normalised values. Overall, the measured carbon content of photosymbiotic, and thus mixotrophic, Radiolaria would have been heavily underestimated using generalised estimations/equations for protists. For example, using non-specific volume to carbon ratios for Acantharia would underestimate Acantharia carbon content by a factor of 35

(Chapter II). Importantly, the here established Radiolaria specific carbon and nitrogen content to volume estimation will provide a first step towards better incorporation of these mixotrophic organisms in, e.g., organismal or biochemical models.

3. Phototrophy and phagotrophy of Acantharia

Subsequent research focused on the Acantharia. In particular, we aimed to establish phototrophic and phagotrophic rates for Acantharia and elucidate the metabolic connectivity between host and symbiont. Photosynthetic rates by Acantharia have only been established once, with a very high standard deviation (816.7 ± 875 pg C Acantharia⁻¹h⁻¹, Michaels, 1991). Here, we established a more precise estimate for the total inorganic carbon uptake rate of Acantharia as 1112.7 ± 82.1 pg C h⁻¹ Acantharia⁻¹. Considering that such carbon uptake rates would only account for little more than a tenth of the acantharian cell mass, we suspect photosynthetic carbon uptake would not allow growth and might mainly be used for energy or survival (Chapter III). Conversely, a Spumellaria was shown to require food uptake and light for prolonged survival (Swanberg and Anderson, 1985). Photosynthesis might thus mainly be used for energy, and preferentially usage of photosynthates for respiration has been previously suggested for mixotrophic ciliates (Putt, 1990). Localisation of assimilated inorganic nutrients further showed that both carbon and nitrogen are predominantly assimilated at the symbiont's plastids, and nitrogen assimilation is especially prominent in the nucleolus of the symbiont. Inorganic carbon translocation over time from symbiont to host could not be seen, which could further suggest that photosynthates are used mainly for respiration or transferred in low molecular weight compounds that could indeed be an energy source. Whereas nitrogen assimilation in the symbionts plastid and nucleolus would also suggest allocation of nutrients to photosynthesis machinery maintenance (Chapter IV), congruent with evidence of prolonged symbiont maintenance (Mars Brisbin et al., 2018; Uwizeye et al., 2021).

Current data suggests that photosynthesis in Acantharia mainly constitutes an energy source and would need to be supplemented with organic nutrients from predation for growth, as was similarly suggested for Collodaria (Swanberg, 1983). Predation rates for Acantharia could not be accurately established, though the inorganic carbon uptake rates suggest a major role for organic nutrition for the Acantharia. The lack of predation results could have a plethora of reasons, among which could be a methodological limitation (Chapter III) or organism inherent. For example, prey preference might be more specific than imagined, and the right prey might not have been tested. Many protists show specific prey preference (Hansen et al., 2013; Maselli et al., 2020). Indeed as stated in Flynn et al., (2019): "Simply catching these organisms in the act of eating is a problem. It may only need to eat one prey a day to acquire its P or Fe quota. Did we observe that event in our incubation? Do we know whether the time of day is important for the event? Is the prey presented for possible consumption in the experiment an appropriate species, and in the correct nutritional state?" Alternatively, we suggest that, if indeed, photosynthesis is used mainly for energy, and predation for growth, then predation might not be of importance in mature live stages where growth might not be of primary concern.

The algal symbiont in Acantharia is heavily modified to favour photosynthetic resource acquisition, however, the increase in inorganic carbon uptake seems mainly linked to an increase in symbiont size (Chapter III). Thus photosynthetic carbon uptake is predominantly increased by a multiplication of the

photosynthetic machinery. The Acantharia could further benefit from the increased size of the symbiont as a sink for sulphur, iron, and cobalt (Decelle et al., 2019). The sulphur compounds in the symbiont could be associated with antioxidant compounds that would alleviate the stress associated with reactive oxygen species due to photosynthetic activity (Deschaseaux et al., 2014; Gardner et al., 2016; Royer et al., 2021). Increased accumulation of (trace) metals in the symbionts is also associated with photosynthesis and antioxidant protection and might be common in photosymbioses (Ferrier-Pagès et al., 2018; Reich et al., 2020).

Taken together, the currently presented results could designate predation - organic nutrition - as a major part of the acantharian metabolism. Since photosynthetically acquired carbon might not suffice for growth. In which case the metabolic role of the symbiont would mostly be to fulfil energetic needs; as means for nitrogen recycling, or as a sink for metals (Decelle et al., 2019). Furthermore, chemical imaging did not indicate assimilation of photosynthates, and would suggest that these are mainly used for respiration. The assessment of predation rates for Acantharia was however indeterminate and would require further testing. Using lower prey culture density and a higher Acantharia to prey ratio might improve such experiments. Alternative experiments using stable isotopically labelled prey could produce clearer results, though these experiments suffer from increased specimen needs and thereby do not easily allow multiple prey species testing.

The natural isotopic ratio of these mixotrophic Radiolaria were observed to vary seasonally, *i.e.*, a lower $\delta^{13}\text{C}$ ratio around spring and higher around autumn. Based on these natural isotopic ratios I hypothesised these Radiolaria rely more on heterotrophy and external food sources around spring (concurrent with algal spring blooms), whereas summer and autumn would be a period where phototrophy is exploited. Further investigation on the natural isotopic ratios of these Radiolaria in comparison to other organisms in the local food web might help identify their reliance on either phototrophy or phagotrophy.

4. Inorganic nitrogen uptake by Acantharia

Acantharia are shown to utilise extraneous ammonium and nitrate (Chapter III). Nitrogen is assimilated from ammonium in both the host Acantharia cell and symbiont (Chapter IV). It remains yet unclear if the host can directly assimilate ammonium. Though, pathways for ammonium assimilation have been found in the Acantharia host transcriptome, and taken together with NanoSIMS chemical images give an indication of ammonium metabolism by the host. Carbon and nitrogen metabolism are intrinsically linked since both share a carbon source and energy. Additionally, extraneous inorganic carbon might be used in the urea cycle for the uptake of ammonium (also independent from photosynthesis). Our currently analysed samples are only for ammonium assimilation after 16 h, this was at the end of the night. To have a clearer idea of ammonium uptake and assimilation, earlier timepoints or complete darkness treatments need to be analysed. If localisation of ammonium assimilation during complete darkness shows assimilation in the host it would give a clear indication on photosynthesis independent assimilation. Data from earlier time points during a normal light cycle, combined with the identified pathways in the holobiont transcriptome, will help deduce the translocation of nitrogen compounds in the holobiont.

As for ammonium, pathways for nitrate assimilation appear present in both symbiont and host, though samples for NanoSIMS analyses will have to verify the fate of nitrate in the holobiont. The specifics of nitrate metabolism in the *Acantharia-Phaeocytis* holobiont thus remains a question open for research.

5. Endosymbiotic Acantharia in mixoplankton models

The fact that a majority of plankton can combine phototrophy and phagotrophy trophic modes is no longer perceived as an oddity, but is starting to be accepted as the ‘new normal’, resulting in increased study in mixotrophy. Yet, detailed knowledge on mixotrophic nutrient acquisition in plankton are still lacking. Among, and within, mixoplankton groups physiological traits are highly diverse, posing difficulties for modelling (Flynn and Mitra, 2009). Even though, efforts have been made to incorporate mixoplankton in models (Flynn and Mitra, 2009; Andersen et al., 2015; Ward and Follows, 2016; Berge et al., 2017; Ghyoot et al., 2017a; Anschütz and Flynn, 2020), mixotrophy is still not included in most biogeochemical models or models describing plankton nutrient dynamics, neglecting among others the carbon fixed by non-constitutive mixoplankton through photosynthesis. Effectively skewing climatic models predictions, and thereby our ability to understand and prevent future effects of global change. Increased knowledge of mixoplankton physiology is thus paramount to improve eco-physiological and biogeochemical models. The fundamental data acquired in this thesis might be used as a baseline in models to open new perspectives and hypotheses of acantharian (or radiolarian) ecology, and for further aimed experimentation.

Bibliography

- Abelmann, A., and Nimmergut, A. (2005). Radiolarians in the Sea of Okhotsk and their ecological implication for paleoenvironmental reconstructions. *Deep. Res. Part II Top. Stud. Oceanogr.* 52, 2302–2331. doi:10.1016/j.dsr2.2005.07.009.
- Abràmoff, M. D., Magalhães, P. J., and Ram, S. J. (2004). Image processing with imageJ. *Biophotonics Int.* 11, 36–41. doi:10.1201/9781420005615.ax4.
- Achlatis, M., Pernice, M., Green, K., Guagliardo, P., Kilburn, M. R., Hoegh-Guldberg, O., et al. (2018). Single-cell measurement of ammonium and bicarbonate uptake within a photosymbiotic bioeroding sponge. *ISME J.* 12, 1308–1318. doi:10.1038/s41396-017-0044-2.
- Allen, A. E., Dupont, C. L., Oborník, M., Horák, A., Nunes-Nesi, A., McCrow, J. P., et al. (2011). Evolution and metabolic significance of the urea cycle in photosynthetic diatoms. *Nature* 473, 203–207. doi:10.1038/nature10074.
- Amacher, J., Neuer, S., Anderson, I., and Massana, R. (2009). Molecular approach to determine contributions of the protist community to particle flux. *Deep. Res. Part I Oceanogr. Res. Pap.* 56, 2206–2215. doi:10.1016/j.dsr.2009.08.007.
- Andersen, K. H., Aksnes, D. L., Berge, T., Fiksen, Ø., and Visser, A. (2015). Modelling emergent trophic strategies in plankton. *J. Plankton Res.* 37, 862–868. doi:10.1093/plankt/fbv054.
- Anderson, O., and Gupta, S. (1998). Evidence of binary division in mature central capsules of a Collosphaerid colonial radiolarians: implications for shell ontogenetic patterns in modern and fossil species. *Palaeontol. Electron.*, 1–13. doi:10.26879/98002.
- Anderson, O. R. (1976a). Fine structure of a collodarian radiolarian (*Sphaerozoum punctatum* Müller 1858) and cytoplasmic changes during reproduction. *Mar. Micropaleontol.* 1, 287–297. doi:10.1016/0377-8398(76)90012-8.
- Anderson, O. R. (1976b). Ultrastructure of a colonial radiolarian *Collozoum inerme* and a cytochemical determination of the role of its zooxanthellae. *Tissue Cell* 8, 195–208. doi:10.1016/0040-8166(76)90046-X.
- Anderson, O. R. (1978). Light and electron microscopic observations of feeding behaviour, nutrition, and reproduction in laboratory cultures of *Thalassicolla nucleata*. *Tissue Cell* 10, 401–412. doi:10.1016/S0040-8166(16)30336-6.
- Anderson, O. R. (1983). *Radiolaria*. Springer New York Available at: <https://books.google.fr/books?id=kSnUBwAAQBAJ> [Accessed April 4, 2018].
- Anderson, O. R., Bennett, P., and Bryan, M. (1989). Experimental and observational studies of radiolarian physiological ecology: 3. Effects of temperature, salinity and light intensity on the growth and survival of *Spongaster tetras tetras* maintained in laboratory culture. *Mar. Micropaleontol.* 14, 275–282. doi:10.1016/0377-8398(89)90014-5.
- Anderson, O. R., Swanberg, N. R., and Bennett, P. (1983). Assimilation of symbiont-derived photosynthates in some solitary and colonial radiolaria. *Mar. Biol.* 77, 265–269. doi:10.1007/BF00395815.
- Anderson, O. R., Swanberg, N. R., and Bennett, P. (1984). An estimate of predation rate and relative preference for algal versus crustacean prey by a spongiöse skeletal radiolarian. *Mar. Biol.* 78, 205–207. doi:10.1007/BF00394702.
- Andrews, S. (2010). FastQC A Quality Control tool for High Throughput Sequence Data. *Babraham Bioinforma.* Available at: <http://www.bioinformatics.babraham.ac.uk/projects/fastqc/>.

- Anschütz, A. A., and Flynn, K. J. (2020). Niche separation between different functional types of mixoplankton: results from NPZ-style N-based model simulations. *Mar. Biol.* 167, 1–21. doi:10.1007/s00227-019-3612-3.
- Arenovski, A. L., Lim, L., Caron, D. A., Lim, E. L., and Caron, D. A. (1995). Mixotrophic nanoplankton in oligotrophic surface waters of the Sargasso Sea may employ phagotrophy to obtain major nutrients. *J. Plankton Res.* 17, 801–820. doi:10.1093/plankt/17.4.801.
- Ayala, D. J., Munk, P., Lundgreen, R. B. C., Traving, S. J., Jaspers, C., Jørgensen, T. S., et al. (2018). Gelatinous plankton is important in the diet of European eel (*Anguilla anguilla*) larvae in the Sargasso Sea. *Sci. Rep.* 8, 1–10. doi:10.1038/s41598-018-24388-x.
- Badger, M. R., Andrews, T. J., Whitney, S. M., Ludwig, M., Yellowlees, D. C., Leggat, W., et al. (1998). The diversity and coevolution of Rubisco, plastids, pyrenoids, and chloroplast-based CO₂-concentrating mechanisms in algae. *Can. J. Bot.* 76, 1052–1071. doi:10.1139/b98-074.
- Baker, D. M., Freeman, C. J., Wong, J. C. Y., Fogel, M. L., and Knowlton, N. (2018). Climate change promotes parasitism in a coral symbiosis. *ISME J.* 12, 921–930. doi:10.1038/s41396-018-0046-8.
- Balzano, S., Corre, E., Decelle, J., Sierra, R., Wincker, P., Da Silva, C. D., et al. (2015). Transcriptome analyses to investigate symbiotic relationships between marine protists. *Front. Microbiol.* 6, 98. doi:10.3389/fmicb.2015.00098.
- Bănanu, D., Carlotti, F., Barani, A., Grégori, G., Neffati, N., and Harmelin-Vivien, M. (2014). Seasonal variation of stable isotope ratios of size-fractionated zooplankton in the Bay of Marseille (NW Mediterranean Sea). *J. Plankton Res.* 36, 145–156. doi:10.1093/plankt/fbt083.
- Beardall, J. (1989). Photosynthesis and photorespiration in marine phytoplankton. *Aquat. Bot.* 34, 105–130. doi:10.1016/0304-3770(89)90052-1.
- Becker, K. W., Collins, J. R., Durham, B. P., Groussman, R. D., White, A. E., Fredricks, H. F., et al. (2018). Daily changes in phytoplankton lipidomes reveal mechanisms of energy storage in the open ocean. *Nat. Commun.* 9, 1–9. doi:10.1038/s41467-018-07346-z.
- Berge, T., Chakraborty, S., Hansen, P. J., and Andersen, K. H. (2017). Modeling succession of key resource-harvesting traits of mixotrophic plankton. *ISME J.* 11, 212–223. doi:10.1038/ismej.2016.92.
- Bernstein, R. E., Betzer, P. R., Feely, R. A., Byrne, R. H., Lamb, M. F., and Michaels, A. F. (1987). Acantharian fluxes and strontium to chlorinity ratios in the North Pacific Ocean. *Science* 237, 1490–1494. doi:10.1126/science.237.4821.1490.
- Biard, T., Krause, J. W., Stukel, M. R., and Ohman, M. D. (2018). The significance of giant phaeodarians (Rhizaria) to biogenic silica export in the California Current Ecosystem. *Global Biogeochem. Cycles* 32, 987–1004. doi:10.1029/2018GB005877.
- Biard, T. M. (2015). Diversité, biogéographie et écologie des Collodaires (Radiolaires) dans l’océan mondial. doi:tel-01298213.
- Biard, T., and Ohman, M. D. (2020). Vertical niche definition of test-bearing protists (Rhizaria) into the twilight zone revealed by in situ imaging. *Limnol. Oceanogr.*, 1–42. doi:10.1002/lno.11472.
- Biard, T., Pillet, L., Decelle, J., Poirier, C., Suzuki, N., and Not, F. (2015). Towards an Integrative Morpho-molecular Classification of the Collodaria (Polycystinea, Radiolaria). *Protist* 166, 374–388. doi:10.1016/j.protis.2015.05.002.
- Biard, T., Stemmann, L., Picheral, M., Mayot, N., Vandromme, P., Hauss, H., et al. (2016). In situ imaging reveals the biomass of giant protists in the global ocean. *Nature* 532, 504–507. doi:10.1038/nature17652.
- Bolger, A. M., Lohse, M., and Usadel, B. (2014). Trimmomatic: A flexible trimmer for Illumina sequence data. *Bioinformatics* 30, 2114–2120. doi:10.1093/bioinformatics/btu170.

- Boltovskoy, D., Anderson, O. R., and Correa, N. M. (2016). "Radiolaria and Phaeodaria," in *Handbook of the Protists*, eds. J. Archibald, A. Simpson, and C. Slamovits (Springer, Cham). doi:10.1007/978-3-319-32669-6.
- Bottazzi, E. M. (1978). Systematic-ecological aspects of radiolaria with special reference to acantharia. *Bolletino di Zool.* 45, 133–144. doi:10.1080/11250007809440123.
- Bryant, D. M., Johnson, K., DiTommaso, T., Tickle, T., Couger, M. B., Payzin-Dogru, D., et al. (2017). A tissue-mapped axolotl de novo transcriptome enables identification of limb regeneration factors. *Cell Rep.* 18, 762–776. doi:10.1016/j.celrep.2016.12.063.
- Burki, F., and Keeling, P. J. (2014). Rhizaria. *Curr. Biol.* 24, R103–R107. doi:10.1016/j.cub.2013.12.025.
- Burns, J. A., Kerney, R., and Duhamel, S. (2020). Heterotrophic carbon fixation in a salamander-alga symbiosis. *Front. Microbiol.* 11, 1815. doi:10.3389/fmicb.2020.01815.
- Capella-Gutiérrez, S., Silla-Martínez, J. M., and Gabaldón, T. (2009). trimAl: A tool for automated alignment trimming in large-scale phylogenetic analyses. *Bioinformatics* 25, 1972–1973. doi:10.1093/bioinformatics/btp348.
- Caron, D. A. (2016). Mixotrophy stirs up our understanding of marine food webs. *Proc. Natl. Acad. Sci.* 113, 2806–2808. doi:10.1073/pnas.1600718113.
- Caron, D. A., Michaels, A. F., Swanberg, N. R., and Howse, F. A. (1995). Primary productivity by symbiont-bearing planktonic sarcodines (Acantharia, Radiolaria, Foraminifera) in surface waters near Bermuda. *J. Plankton Res.* 17, 103–129. doi:10.1093/plankt/17.1.103.
- Chan, Y. F., Chiang, K. P., Ku, Y., and Gong, G. C. (2019). Abiotic and Biotic Factors Affecting the Ingestion Rates of Mixotrophic Nanoflagellates (Haptophyta). *Microb. Ecol.* 77, 607–615. doi:10.1007/s00248-018-1249-2.
- Colin, S., Coelho, L. P., Sunagawa, S., Bowler, C., Karsenti, E., Bork, P., et al. (2017). Quantitative 3D-imaging for cell biology and ecology of environmental microbial eukaryotes. *Elife* 6. doi:10.7554/eLife.26066.
- Cook, C. B., Muller-Parker, G., and D'Elia, C. F. (1992). Ammonium enhancement of dark carbon fixation and nitrogen limitation in symbiotic zooxanthellae: Effects of feeding and starvation of the sea anemone *Aiptasia pallida*. *Limnol. Oceanogr.* 37, 131–139. doi:10.4319/lo.1992.37.1.0131.
- Cooney, E. C., Okamoto, N., Cho, A., Hehenberger, E., Richards, T. A., Santoro, A. E., et al. (2020). Single cell transcriptomics of *Abedinium* reveals a new early-branching dinoflagellate lineage. *Genome Biol. Evol.* doi:10.1093/gbe/evaa196.
- Coplen, T. B., Brand, W. A., Gehre, M., Gröning, M., Meijer, H. A. J., Toman, B., et al. (2006). New guidelines for $\delta^{13}\text{C}$ measurements. *Anal. Chem.* 78, 2439–2441. doi:10.1021/ac052027c.
- Dagenais-Bellefeuille, S., and Morse, D. (2013). Putting the N in dinoflagellates. *Front. Microbiol.* 4, 369. doi:10.3389/fmicb.2013.00369.
- Davy, S. K., Allemand, D., and Weis, V. M. (2012). Cell Biology of Cnidarian-Dinoflagellate Symbiosis. *Microbiol. Mol. Biol. Rev.* 76, 229–261. doi:10.1128/mmbr.05014-11.
- De Vargas, C., Audic, S., Henry, N., Decelle, J., Mahé, F., Logares, R., et al. (2015). Eukaryotic plankton diversity in the sunlit ocean. *Science* 348, 1261605. doi:10.1126/science.1261605.
- Decelle, J. (2013). New perspectives on the functioning and evolution of photosymbiosis in plankton. *Commun. Integr. Biol.* 6, e24560. doi:10.4161/cib.2456.
- Decelle, J., Colin, S., and Foster, R. A. (2015). "Photosymbiosis in marine planktonic protists," in *Marine Protists: Diversity and Dynamics* (Tokyo: Springer Japan), 465–500. doi:10.1007/978-4-431-55130-0_19.

- Decelle, J., Martin, P., Paborstava, K., Pond, D. W., Tarling, G., Mahé, F., et al. (2013). Diversity, Ecology and Biogeochemistry of Cyst-Forming Acantharia (Radiolaria) in the Oceans. *PLoS One* 8, e53598. doi:10.1371/journal.pone.0053598.
- Decelle, J., Probert, I., Bittner, L., Desdevises, Y., Colin, S., de Vargas, C., et al. (2012a). An original mode of symbiosis in open ocean plankton. *Proc. Natl. Acad. Sci.* 109, 18000–18005. doi:10.1073/pnas.1212303109.
- Decelle, J., Siano, R., Probert, I., Poirier, C., and Not, F. (2012b). Multiple microalgal partners in symbiosis with the acantharian *Acanthochiasma* sp. (Radiolaria). *Springer Sci.* 58, 233–244. doi:10.1007/s13199-012-0195-x.
- Decelle, J., Stryhanyuk, H., Gallet, B., Veronesi, G., Schmidt, M., Balzano, S., et al. (2019). Algal remodeling in a ubiquitous planktonic photosymbiosis. *Curr. Biol.* 29, 968–978. doi:10.1016/J.CUB.2019.01.073.
- Decelle, J., Suzuki, N., Mahé, F., de Vargas, C., and Not, F. (2012c). Molecular Phylogeny and Morphological Evolution of the Acantharia (Radiolaria). *Protist* 163, 435–450. doi:10.1016/j.protis.2011.10.002.
- Decelle, J., Veronesi, G., Gallet, B., Stryhanyuk, H., Benettoni, P., Schmidt, M., et al. (2020). Subcellular Chemical Imaging: New Avenues in Cell Biology. *Trends Cell Biol.* 30, 173–188. doi:10.1016/j.tcb.2019.12.007.
- Decelle, J., Veronesi, G., LeKieffre, C., Gallet, B., Chevalier, F., Stryhanyuk, H., et al. (2021). Subcellular architecture and metabolic connection in the planktonic photosymbiosis between Collodaria (radiolarians) and their microalgae. *Environ. Microbiol.*, 1462–2920. doi:10.1111/1462-2920.15766.
- Dennett, M. R., Caron, D. A., Michaels, A. F., Gallagher, S. M., and Davis, C. S. (2002). Video plankton recorder reveals high abundances of colonial Radiolaria in surface waters of the central North Pacific. *J. Plankton Res.* 24, 797–805. doi:10.1093/plankt/24.8.797.
- Deschaseaux, E. S. M., Jones, G. B., Deseo, M. A., Shepherd, K. M., Kiene, R. P., Swan, H. B., et al. (2014). Effects of environmental factors on dimethylated sulfur compounds and their potential role in the antioxidant system of the coral holobiont. *Limnol. Oceanogr.* 59, 758–768. doi:10.4319/lo.2014.59.3.0758.
- Dittami, S., Arboleda, E., Auguet, J.-C., Bigalke, A., Briand, E., Cardenas, P., et al. (2020). A community perspective on the concept of marine holobionts: current status, challenges, and future directions. *PeerJ Prepr.* 27519, ver. 4 peer reviewed and recommended by PCI Ecolog. doi:10.5281/zenodo.3696771.
- Djehri, N., Stibor, H., Lebeau, O., and Pondaven, P. (2020). $\delta^{13}\text{C}$, $\delta^{15}\text{N}$, and C:N ratios as nutrition indicators of zooxanthellate jellyfishes: insights from an experimental approach. *J. Exp. Mar. Bio. Ecol.* 522. doi:10.1016/j.jembe.2019.151257.
- Dobberfuhl, D. R., and Elser, J. J. (2000). Elemental stoichiometry of lower food web components in arctic and temperate lakes. *J. Plankton Res.* 22, 1341–1354. doi:10.1093/PLANKT/22.7.1341.
- Douglas, A. E. (1998). Host benefit and the evolution of specialization in symbiosis. *Heredity (Edinb).* 81, 599–603. doi:10.1038/sj.hdy.6884550.
- Elrifi, I. R., and Turpin, D. H. (1986). Nitrate and ammonium induced photosynthetic suppression in N-Limited *Selenastrum minutum*. *Plant Physiol.* 81, 273–279. doi:10.1104/pp.81.1.273.
- Erez, J. (2003). The source of ions for biomineralization in foraminifera and their implications for paleoceanographic proxies. *Rev. Mineral. Geochemistry* 54, 115–149. doi:10.2113/0540115.
- Ewels, P., Magnusson, M., Lundin, S., and Källér, M. (2016). MultiQC: Summarize analysis results for multiple tools and samples in a single report. *Bioinformatics* 32, 3047–3048. doi:10.1093/bioinformatics/btw354.
- Ezzat, L., Maguer, J.-F., Grover, R., and Ferrier-Pagès, C. (2015). New insights into carbon acquisition and exchanges within the coral–dinoflagellate symbiosis under NH_4^+ and NO_3^- supply. *Proc. R. Soc. B Biol. Sci.* 282, 20150610. doi:10.1098/rspb.2015.0610.

- Falkowski, P. G., Barber, R. T., and Smetacek, V. (1998). Biogeochemical controls and feedbacks on ocean primary production. *Science* 281, 200–206. doi:10.1126/science.281.5374.200.
- Falkowski, P. G., Dubinsky, Z., Muscatine, L., and Porter, J. W. (1984). Light and the Bioenergetics of a Symbiotic Coral. Available at: <https://academic.oup.com/bioscience/article/34/11/705/249447> [Accessed January 29, 2021].
- Fasham, M. J. R., Ducklow, H. W., and McKelvie, S. M. (1990). A nitrogen-based model of plankton dynamics in the oceanic mixed layer. *J. Mar. Res.* 48, 591–639. doi:10.1357/002224090784984678.
- Faure, E., Not, F., Benoiston, A.-S., Labadie, K., Bittner, L., and Ayata, S.-D. (2019). Mixotrophic protists display contrasted biogeographies in the global ocean. *ISME J.* 13, 1072–1083. doi:10.1038/s41396-018-0340-5.
- Febvre-Chevalier, C., and Febvre, J. (1986). Motility mechanisms in the actinopods (Protozoa): A review with particular attention to axopodial contraction/extension, and movement of nonactin filament systems. *Cell Motil. Cytoskeleton* 6, 198–208. doi:10.1002/cm.970060219.
- Febvre, J. (1981). The myoneme of the Acantharia (Protozoa): A new model of cellular motility. *BioSystems* 14, 327–336. doi:10.1016/0303-2647(81)90039-3.
- Ferreira, G., Calbet, A., Not, F., Mansour, J., Hansen, P., Medić, N., et al. (2021). “Development and validation of new methods for measuring predation rates in mixoplanktonic protists,” in *Novel Approaches For Investigating Marine Planktonic Mixotrophy*, eds. K. Anestis, J. S. Mansour, G. D. Ferreira, C. Albert, A. Mitra, and K. J. Flynn (Zenodo). doi:10.5281/zenodo.5148500.
- Ferrier-Pagès, C., Peirano, A., Abbate, M., Cocito, S., Negri, A., Rottier, C., et al. (2011). Summer autotrophy and winter heterotrophy in the temperate symbiotic coral *Cladocora caespitosa*. *Limnol. Oceanogr.* 56, 1429–1438. doi:10.4319/lo.2011.56.4.1429.
- Ferrier-Pagès, C., Sauzéat, L., and Balter, V. (2018). Coral bleaching is linked to the capacity of the animal host to supply essential metals to the symbionts. *Glob. Chang. Biol.* 24, 3145–3157. doi:10.1111/gcb.14141.
- Ferrier-Pagès, C., and Leal, M. C. locatie (2018). Stable isotopes as tracers of trophic interactions in marine mutualistic symbioses. *Ecol. Evol.*, 1–18. doi:10.1002/ece3.4712.
- Field, C. B., Behrenfeld, M. J., Randerson, J. T., and Falkowski, P. (1998). Primary production of the biosphere: Integrating terrestrial and oceanic components. *Science* 281, 237–240. doi:10.1126/science.281.5374.237.
- Flöder, S., Hansen, T., and Ptacnik, R. (2006). Energy-Dependent Bacterivory in *Ochromonas minima* - A Strategy Promoting the Use of Substitutable Resources and Survival at Insufficient Light Supply. *Protist* 157, 291–302. doi:10.1016/j.protis.2006.05.002.
- Flynn, K. J., and Mitra, A. (2009). Building the “perfect beast”: Modelling mixotrophic plankton. *J. Plankton Res.* 31, 965–992. doi:10.1093/plankt/fbp044.
- Flynn, K. J., Mitra, A., Anestis, K., Anschütz, A. A., Calbet, A., Ferreira, G. D., et al. (2019). Mixotrophic protists and a new paradigm for marine ecology: where does plankton research go now? *J. Plankton Res.* 41, 375–391. doi:10.1093/plankt/fbz026.
- Flynn, K. J., Stoecker, D. K., Mitra, A., Raven, J. A., Glibert, P. M., Hansen, P. J., et al. (2013). Misuse of the phytoplankton-zooplankton dichotomy: The need to assign organisms as mixotrophs within plankton functional types. *J. Plankton Res.* 35, 3–11. doi:10.1093/plankt/fbs062.
- Franks, P. J. S. (2002). NPZ models of plankton dynamics: Their construction, coupling to physics, and application. *J. Oceanogr.* 58, 379–387. doi:10.1023/A:1015874028196.
- Freeman, C. J., Stoner, E. W., Easson, C. G., Matterson, K. O., and Baker, D. M. (2016). Symbiont carbon and nitrogen assimilation in the *Cassiopea*-Symbiodinium mutualism. *Mar. Ecol. Prog. Ser.* 544, 281–286. doi:10.3354/meps11605.

- Frost, B. W. (1972). Effects of size and concentration of food particles on the feeding behavior of the marine planktonic copepod *Calanus pacificus*. *Limnol. Oceanogr.* 17, 805–815. doi:10.4319/lo.1972.17.6.0805.
- Fry, B. (2006). *Stable Isotope Ecology*. New York: Springer New York Available at: <https://link.springer.com/content/pdf/10.1007/0-387-33745-8.pdf> [Accessed February 12, 2019].
- Fry, B., and Sherr, E. B. (1989). “ $\delta^{13}\text{C}$ measurements as indicators of carbon flow in marine and freshwater ecosystems,” in (Springer, New York, NY), 196–229. doi:10.1007/978-1-4612-3498-2_12.
- Fulton, J. F. (1921). Concerning the vitality of *Actinia bermudensis*: A study in symbiosis. *J. Exp. Zool.* 33, 352–364. doi:10.1002/jez.1400330203.
- Furla, P., Richier, S., and Allemand, D. (2011). “Physiological adaptation to symbiosis in cnidarians,” in *Coral Reefs: An Ecosystem in Transition* (Springer, Dordrecht), 187–195. doi:10.1007/978-94-007-0114-4_12.
- García-Portela, Reguera, Gago, Gac, and Rodríguez (2020). Uptake of Inorganic and Organic Nitrogen Sources by *Dinophysis acuminata* and *D. acuta*. *Microorganisms* 8, 187. doi:10.3390/microorganisms8020187.
- Gardner, S. G., Nielsen, D. A., Laczka, O., Shimmon, R., Beltran, V. H., Ralph, P. J., et al. (2016). Dimethylsulfoniopropionate, superoxide dismutase and glutathione as stress response indicators in three corals under short-term hyposalinity stress. *Proc. R. Soc. B Biol. Sci.* 283. doi:10.1098/rspb.2015.2418.
- Gast, R. J., and Caron, D. A. (2001). Photosymbiotic associations in planktonic foraminifera and radiolaria. in *Hydrobiologia*, 1–7. doi:10.1023/A:1012710909023.
- Ghyoot, C., Flynn, K. J., Mitra, A., Lancelot, C., and Gypens, N. (2017a). Modeling Plankton Mixotrophy: A Mechanistic Model Consistent with the Shuter-Type Biochemical Approach. *Front. Ecol. Evol.* 5. doi:10.3389/fevo.2017.00078.
- Ghyoot, C., Lancelot, C., Flynn, K. J., Mitra, A., and Gypens, N. (2017b). Introducing mixotrophy into a biogeochemical model describing an eutrophied coastal ecosystem: The Southern North Sea. *Prog. Oceanogr.* 157, 1–11. doi:10.1016/j.pocean.2017.08.002.
- Girault, M., Beneyton, T., del Amo, Y., and Baret, J. C. (2019). Microfluidic technology for plankton research. *Curr. Opin. Biotechnol.* 55, 134–150. doi:10.1016/j.copbio.2018.09.010.
- Gonçalves Leles, S., Bruggeman, J., Polimene, L., Blackford, J., Flynn, K. J., and Mitra, A. (2021). Differences in physiology explain succession of mixoplankton functional types and affect carbon fluxes in temperate seas. *Prog. Oceanogr.* 190, 102481. doi:10.1016/j.pocean.2020.102481.
- González-Olalla, J. M., Medina-Sánchez, J. M., and Carrillo, P. (2019). Mixotrophic trade-off under warming and UVR in a marine and a freshwater alga. *J. Phycol.* 55, 1028–1040. doi:10.1111/jpy.12865.
- Gowing, M. M. (1989). Abundance and feeding ecology of Antarctic phaeodarian radiolarians. *Mar. Biol.* 103, 107–118. doi:10.1007/BF00391069.
- Grabherr, M. G., Haas, B. J., Yassour, M., Levin, J. Z., Thompson, D. A., Amit, I., et al. (2011). Full-length transcriptome assembly from RNA-Seq data without a reference genome. *Nat. Biotechnol.* 29, 644–652. doi:10.1038/nbt.1883.
- Grover, R., Maguer, J. F., Allemand, D., and Ferrier-Pagès, C. (2003). Nitrate uptake in the scleractinian coral *Stylophora pistillata*. *Limnol. Oceanogr.* 48, 2266–2274. doi:10.4319/lo.2003.48.6.2266.
- Grover, R., Maguer, J. F., Reynaud-Vaganay, S., and Ferrier-Pagès, C. (2002). Uptake of ammonium by the scleractinian coral *Stylophora pistillata*: Effect of feeding, light, and ammonium concentrations. *Limnol. Oceanogr.* 47, 782–790. doi:10.4319/lo.2002.47.3.0782.
- Guidi, L., Chaffron, S., Bittner, L., Eveillard, D., Larhlimi, A., Roux, S., et al. (2016). Plankton networks driving carbon export in the oligotrophic ocean. *Nature* 532, 465–470. doi:10.1038/nature16942.

- Gutierrez-Rodriguez, A., Pillet, L., Biard, T., Said-Ahmad, W., Amrani, A., Simó, R., et al. (2017). Dimethylated sulfur compounds in symbiotic protists: A potentially significant source for marine DMS(P). *Limnol. Oceanogr.* 62, 1139–1154. doi:10.1002/lno.10491.
- Gutierrez-Rodriguez, A., Stukel, M. R., Lopes dos Santos, A., Biard, T., Scharek, R., Vaultot, D., et al. (2019). High contribution of Rhizaria (Radiolaria) to vertical export in the California Current Ecosystem revealed by DNA metabarcoding. *ISME J.* 13, 964–976. doi:10.1038/s41396-018-0322-7.
- Haeckel, E. (1887). Report on radiolaria collected by H. M. S. Challenger during the years 1873–1876. *Rep. Sci. Results Voyag. H.M.S. Chall. years 1873-1876 Zoology XV*, 1–1803. Available at: <http://ci.nii.ac.jp/naid/10003918762/en/> [Accessed May 19, 2020].
- Haeckel, E. H. (1862). *Die Radiolarien. (Rhizopoda Radiaria.)*.
- Hansen, P. J. (2011). The role of photosynthesis and food uptake for the growth of marine mixotrophic dinoflagellates. *J. Eukaryot. Microbiol.* 58, 203–214. doi:10.1111/j.1550-7408.2011.00537.x.
- Hansen, P. J., Anderson, R., Stoecker, D. K., Decelle, J., Altenburger, A., Blossom, H. E., et al. (2019). *Mixotrophy among freshwater and marine protists*. 4th ed. , ed. Thomas M. Schmidt Elsevier Inc. doi:10.1016/B978-0-12-809633-8.20685-7.
- Hansen, P. J., Miranda, L., and Azanza, R. (2004). Green *Noctiluca scintillans*: A dinoflagellate with its own greenhouse. *Mar. Ecol. Prog. Ser.* 275, 79–87. doi:10.3354/meps275079.
- Hansen, P. J., Nielsen, L. T., Johnson, M., Berge, T., and Flynn, K. J. (2013). Acquired phototrophy in *Mesodinium* and *Dinophysis* - A review of cellular organization, prey selectivity, nutrient uptake and bioenergetics. *Harmful Algae* 28, 126–139. doi:10.1016/j.hal.2013.06.004.
- Hansen, P. J., Ojamäe, K., Berge, T., Trampe, E. C. L., Nielsen, L. T., Lips, I., et al. (2016). Photoregulation in a kleptochloroplastidic dinoflagellate, *Dinophysis acuta*. *Front. Microbiol.* 7, 785. doi:10.3389/fmicb.2016.00785.
- Heinbokel, J. F. (1978). Studies on the functional role of tintinnids in the Southern California Bight. I. Grazing and growth rates in laboratory cultures. *Mar. Biol.* 47, 177–189. doi:10.1007/BF00395638.
- Hillebrand, H., Dürselen, C. D., Kirschtel, D., Pollinger, U., and Zohary, T. (1999). Biovolume calculation for pelagic and benthic microalgae. *J. Phycol.* 35, 403–424. doi:10.1046/j.1529-8817.1999.3520403.x.
- Hood, R. R., Laws, E. A., Armstrong, R. A., Bates, N. R., Brown, C. W., Carlson, C. A., et al. (2006). Pelagic functional group modeling: Progress, challenges and prospects. *Deep Sea Res. Part II Top. Stud. Oceanogr.* 53, 459–512. doi:10.1016/j.dsr2.2006.01.025.
- Hughes, E. A., Maselli, M., Sørensen, H., and Hansen, P. J. (2021). Metabolic reliance on photosynthesis depends on both irradiance and prey availability in the mixotrophic ciliate, *Strombidium cf. basimorphum*. *Front. Microbiol.* 12, 1577. doi:10.3389/fmicb.2021.642600.
- Hughes, T. P., Baird, A. H., Bellwood, D. R., Card, M., Connolly, S. R., Folke, C., et al. (2003). Climate Change, Human Impacts, and the Resilience of Coral Reefs. *Science* 301, 929–933. Available at: <http://science.sciencemag.org/> [Accessed September 10, 2019].
- Huppe, H. C., and Turpin, D. H. (1994). Integration of carbon and nitrogen metabolism in plant and algal cells. *Annu. PHYSIOL.PLANT MOL.BIOL.* 45, 577–607. doi:10.1146/annurev.pp.45.060194.003045.
- Huxley, T. (1851). Zoological notes and observations made on board H.M.S Rattlesnake. III. Upon Thalassicolla, a new zoophyte. *Ann. Mag. Nat. Hist.* 8, 433–442.
- Ikenoue, T., Kimoto, K., Okazaki, Y., Sato, M., Honda, M. C., Takahashi, K., et al. (2019). Phaeodaria: An Important Carrier of Particulate Organic Carbon in the Mesopelagic Twilight Zone of the North Pacific Ocean. *Global Biogeochem. Cycles* 33, 1146–1160. doi:10.1029/2019GB006258.

- Izumo, A., Fujiwara, S., Oyama, Y., Satoh, A., Fujita, N., Nakamura, Y., et al. (2007). Physicochemical properties of starch in *Chlorella* change depending on the CO₂ concentration during growth: Comparison of structure and properties of pyrenoid and stroma starch. *Plant Sci.* 172, 1138–1147. doi:10.1016/j.plantsci.2007.03.001.
- Jeong, H. J., du Yoo, Y., Kim, J. S., Seong, K. A., Kang, N. S., and Kim, T. H. (2010). Growth, feeding and ecological roles of the mixotrophic and heterotrophic dinoflagellates in marine planktonic food webs. *Ocean Sci. J.* 45, 65–91. doi:10.1007/s12601-010-0007-2.
- Jia, J., Han, D., Gerken, H. G., Li, Y., Sommerfeld, M., Hu, Q., et al. (2015). Molecular mechanisms for photosynthetic carbon partitioning into storage neutral lipids in *Nannochloropsis oceanica* under nitrogen-depletion conditions. *Algal Res.* 7, 66–77. doi:10.1016/j.algal.2014.11.005.
- Johnson, M. D. (2015). Inducible mixotrophy in the dinoflagellate *Prorocentrum minimum*. *J. Eukaryot. Microbiol.* 62, 431–443. doi:10.1111/jeu.12198.
- Kamel, Bishoy, S. (2016). Homology, Homoplasmy and The Holobiont: A Comparative Genomics Approach. doi:10.5822/978-1-59726-228-6_3_WATER.
- Kanehisa, M., Sato, Y., and Morishima, K. (2016). BlastKOALA and GhostKOALA: KEGG Tools for Functional Characterization of Genome and Metagenome Sequences. *J. Mol. Biol.* 428, 726–731. doi:10.1016/j.jmb.2015.11.006.
- Kaplan, A., and Reinhold, L. (1999). CO₂ concentrating mechanisms in photosynthetic microorganisms. *Annu. Rev. Plant Physiol. Plant Mol. Biol.* 50, 539–570. doi:10.1146/annurev.arplant.50.1.539.
- Katoh, K., Kuma, K. I., Toh, H., and Miyata, T. (2005). MAFFT version 5: Improvement in accuracy of multiple sequence alignment. *Nucleic Acids Res.* 33, 511–518. doi:10.1093/nar/gki198.
- Keeling, P. J., and McCutcheon, J. P. (2017). Endosymbiosis: The feeling is not mutual. *J. Theor. Biol.* 434, 75–79. doi:10.1016/j.jtbi.2017.06.008.
- Keller, M. D., Shapiro, L. P., Haugen, E. M., Cucci, T. L., Sherr, E. B., and Sherr, B. F. (1994). Phagotrophy of fluorescently labeled bacteria by an oceanic phytoplankter. *Microb. Ecol.* 28, 39–52. doi:10.1007/BF00170246.
- Kimoto, K., Yuasa, T., and Takahashi, O. (2011). Molecular identification of reproductive cells released from *Cypris irregularis* Nigrini (Radiolaria). *Environ. Microbiol. Rep.* 3, 86–90. doi:10.1111/j.1758-2229.2010.00191.x.
- Kopp, C., Domart-Coulon, I., Escrig, S., Humbel, B. M., Hignette, M., and Meibom, A. (2015a). Subcellular investigation of photosynthesis-driven carbon assimilation in the symbiotic reef coral *Pocillopora damicornis*. *MBio* 6. doi:10.1128/mBio.02299-14.
- Kopp, C., Pernice, M., Domart-Coulon, I., Djediat, C., Spangenberg, J. E., Alexander, D. T. L., et al. (2013). Highly dynamic cellular-level response of symbiotic coral to a sudden increase in environmental nitrogen. *MBio* 4. doi:10.1128/mBio.00052-13.
- Kopp, C., Wisztorski, M., Revel, J., Mehiri, M., Dani, V., Capron, L., et al. (2015b). MALDI-MS and NanoSIMS imaging techniques to study cnidarian-dinoflagellate symbioses. *Zoology* 118, 125–131. doi:10.1016/j.zool.2014.06.006.
- Kopylova, E., Noé, L., and Touzet, H. (2012). SortMeRNA: Fast and accurate filtering of ribosomal RNAs in metatranscriptomic data. *Bioinformatics* 28, 3211–3217. doi:10.1093/bioinformatics/bts611.
- Labarre, A., Obiol, A., Wilken, S., Forn, I., and Massana, R. (2020). Expression of genes involved in phagocytosis in uncultured heterotrophic flagellates. *Limnol. Oceanogr.* 65, S149–S160. doi:10.1002/lno.11379.

Bibliography

- LaJeunesse, T. C., Parkinson, J. E., Gabrielson, P. W., Jeong, H. J., Reimer, J. D., Voolstra, C. R., et al. (2018). Systematic revision of Symbiodiniaceae highlights the antiquity and diversity of coral endosymbionts. *Curr. Biol.* 28, 2570-2580.e6. doi:10.1016/j.cub.2018.07.008.
- Lampitt, R. S., Salter, I., and Johns, D. (2009). Radiolaria: Major exporters of organic carbon to the deep ocean. *Global Biogeochem. Cycles* 23, GB1010. doi:10.1029/2008GB003221.
- Langmead, B., and Salzberg, S. L. (2012). Fast gapped-read alignment with Bowtie 2. *Nat. Methods* 9, 357–359. doi:10.1038/nmeth.1923.
- Larsson, A. (2014). AliView: A fast and lightweight alignment viewer and editor for large datasets. *Bioinformatics* 30, 3276–3278. doi:10.1093/bioinformatics/btu531.
- Law, C. W., Chen, Y., Shi, W., and Smyth, G. K. (2014). Voom: Precision weights unlock linear model analysis tools for RNA-seq read counts. *Genome Biol.* 15, 1–17. doi:10.1186/gb-2014-15-2-r29.
- Lekieffre, C., Jauffrais, T., Geslin, E., Jesus, B., Bernhard, J. M., Giovani, M. E., et al. (2018). Inorganic carbon and nitrogen assimilation in cellular compartments of a benthic kleptoplastic foraminifer. *Sci. Rep.* 8. doi:10.1038/s41598-018-28455-1.
- LeKieffre, C., Spero, H. J., Fehrenbacher, J. S., Russell, A. D., Ren, H., Geslin, E., et al. (2020). Ammonium is the preferred source of nitrogen for planktonic foraminifer and their dinoflagellate symbionts. *Proc. R. Soc. B Biol. Sci.* 287, 20200620. doi:10.1098/rspb.2020.0620.
- LeKieffre, C., Spero, H. J., Russell, A. D., Fehrenbacher, J. S., Geslin, E., and Meibom, A. (2018). Assimilation, translocation, and utilization of carbon between photosynthetic symbiotic dinoflagellates and their planktic foraminifera host. *Mar. Biol.* 165, 104. doi:10.1007/s00227-018-3362-7.
- Leles, S. G., Mitra, A., Flynn, K. J., Stoecker, D. K., Hansen, P. J., Calbet, A., et al. (2017). Oceanic protists with different forms of acquired phototrophy display contrasting biogeographies and abundance. *Proc. R. Soc. B Biol. Sci.* 284, 20170664. doi:10.1098/rspb.2017.0664.
- Lesser, M. P., Stat, M., and Gates, R. D. (2013). The endosymbiotic dinoflagellates (*Symbiodinium sp.*) of corals are parasites and mutualists. *Coral Reefs* 32, 603–611. doi:10.1007/s00338-013-1051-z.
- Li, B., and Dewey, C. N. (2011). RSEM: Accurate transcript quantification from RNA-Seq data with or without a reference genome. *BMC Bioinformatics* 12, 1–16. doi:10.1186/1471-2105-12-323.
- Liu, Z., Mesrop, L. Y., Hu, S. K., and Caron, D. A. (2019). Transcriptome of *Thalassicolla nucleata* holobiont reveals details of a radiolarian symbiotic relationship. *Front. Mar. Sci.* 6, 284. doi:10.3389/fmars.2019.00284.
- Llopis Monferrer, N., Boltovskoy, D., Tréguer, P., Sandin, M. M., Not, F., and Leynaert, A. (2020). Estimating Biogenic Silica Production of Rhizaria in the Global Ocean. *Global Biogeochem. Cycles* 34, e2019GB006286. doi:10.1029/2019GB006286.
- López-García, P., Eme, L., and Moreira, D. (2017). Symbiosis in eukaryotic evolution. *J. Theor. Biol.* 434, 20–33. doi:10.1016/j.jtbi.2017.02.031.
- López-Sandoval, D. C., Delgado-Huertas, A., and Agustí, S. (2018). The ¹³C method as a robust alternative to ¹⁴C-based measurements of primary productivity in the Mediterranean Sea. *J. Plankton Res.* 40, 544–554. doi:10.1093/plankt/fby031.
- Lowe, C. D., Minter, E. J., Cameron, D. D., and Brockhurst, M. A. (2016). Shining a Light on Exploitative Host Control in a Photosynthetic Endosymbiosis. *Curr. Biol.* 26, 207–211. doi:10.1016/j.cub.2015.11.052.
- Lyndby, N. H., Rådecker, N., Bessette, S., Helene, L., Jensen, S., Escrig, S., et al. (2020). Amoebocytes facilitate efficient carbon and nitrogen assimilation in the *Cassiopea*-Symbiodiniaceae symbiosis. *Proc. R. Soc. B Biol. Sci.* 287, 20202393. doi:10.1098/rspb.2020.2393.

- Manni, M., Berkeley, M. R., Seppey, M., Simão, F. A., and Zdobnov[†], E. M. (2021). BUSCO update: novel and streamlined workflows along with broader and deeper phylogenetic coverage for scoring of eukaryotic, prokaryotic, and viral genomes. Available at: <https://arxiv.org/abs/2106.11799v1> [Accessed July 14, 2021].
- Mansour, J., Anestis, K., Not, F., and John, U. (2021a). cDNA library preparation from total RNA extracts of Single-cell marine protists (e.g. Acantharia, *Strombidium basimorphum*, and *Prymnesium parvum*) for transcriptome sequencing V.2. *protocols.io*. doi:10.17504/protocols.io.brw3m7gn.
- Mansour, J., Anestis, K., Not, F., and John, U. (2021b). Single-cell total RNA extraction from marine protists (e.g. Acantharia, *Strombidium cf basimorphum*, and *Prymnesium parvum*) V.2. *protocols.io*. doi:10.17504/protocols.io.bp6xmrfn.
- Mansour, J., and Not, F. (2021). Isolation of clean single-cell samples for physiological or molecular experiments (Radiolaria, Acantharia) V.2. *protocols.io*. doi:10.17504/protocols.io.bqvrnw56.
- Mansour, J. S., and Anestis, K. (2021). Eco-Evolutionary Perspectives on Mixoplankton. *Front. Mar. Sci.* 8, 666160. doi:10.3389/fmars.2021.666160.
- Mansour, J. S., Norlin, A., Llopis Monferrer, N., L'Helguen, S., and Not, F. (2021c). Carbon and nitrogen content to biovolume relationships for marine protist of the Rhizaria lineage (Radiolaria and Phaeodaria). *Limnol. Oceanogr.* 66, 1703–1717. doi:10.1002/lno.11714.
- Mars Brisbin, M. (2020). Characterization of Acantharea-Phaeocystis photosymbioses: distribution, abundance, specificity, maintenance and host-control.
- Mars Brisbin, M., Brunner, O. D., Grossmann, M. M., and Mitarai, S. (2020). Paired high-throughput, in situ imaging and high-throughput sequencing illuminate acantharian abundance and vertical distribution. *Limnol. Oceanogr.*, lno.11567. doi:10.1002/lno.11567.
- Mars Brisbin, M., Mesrop, L. Y., Grossmann, M. M., and Mitarai, S. (2018). Intra-host symbiont diversity and extended symbiont maintenance in photosymbiotic Acantharea (clade F). *Front. Microbiol.* 9, 1998. doi:10.3389/fmicb.2018.01998.
- Martínez, R. A., Isari, S., and Calbet, A. (2014). Use of live, fluorescently-labeled algae for measuring microzooplankton grazing in natural communities. *J. Exp. Mar. Bio. Ecol.* 457, 59–70. doi:10.1016/j.jembe.2014.03.007.
- Maselli, M., Altenburger, A., Stoecker, D. K., and Hansen, P. J. (2020). Ecophysiological traits of mixotrophic *Strombidium* spp. *J. Plankton Res.* 42, 485–496. doi:10.1093/plankt/fbaa041.
- Matsuoka, A. (1992). Skeletal growth of a spongioid radiolarian *Dictyocoryne truncatum* in laboratory culture. *Mar. Micropaleontol.* 19, 287–297. doi:10.1016/0377-8398(92)90034-H.
- Matsuoka, A. (2007). Living radiolarian feeding mechanisms: New light on past marine ecosystems. *Swiss J. Geosci.* 100, 273–279. doi:10.1007/s00015-007-1228-y.
- Mayzaud, P., and Razouls, S. (1992). Degradation of gut pigment during feeding by a subantarctic copepod : importance of feeding history and digestive acclimation. *Limnol. Oceanogr.* 37, 393–404. doi:10.2307/2838015.
- McAuley, P. (1994). Interactions between hosts and symbionts in algal invertebrate intracellular symbioses. *Bot. J. Scotl.* 47, 97–112. doi:10.1080/03746609408684820.
- Menden-Deuer, S., and Lessard, E. J. (2000). Carbon to volume relationships for dinoflagellates, diatoms, and other protist plankton. *Limnol. Oceanogr.* 45, 569–579. doi:10.4319/lo.2000.45.3.0569.
- Meng, A., Marchet, C., Corre, E., Peterlongo, P., Alberti, A., Da Silva, C., et al. (2018). A de novo approach to disentangle partner identity and function in holobiont systems. *Microbiome* 6, 105. doi:10.1186/s40168-018-0481-9.

Bibliography

- Michaels, A. F. (1988). Vertical distribution and abundance of Acantharia and their symbionts. *Mar. Biol.* 97, 559–569. doi:10.1007/BF00391052.
- Michaels, A. F. (1991). Acantharian abundance and symbiont productivity at the VERTEX seasonal station. *J. Plankton Res.* 13, 399–418. doi:10.1093/plankt/13.2.399.
- Michaels, A. F., Caron, D. A., Swanberg, N. R., Howse, F. A., and Michaels, C. M. (1995). Planktonic sarcodines (Acantharia, Radiolaria, Foraminifera) in surface waters near Bermuda: abundance, biomass and vertical flux. *J. Plankton Res.* 17, 131–163. doi:10.1093/plankt/17.1.131.
- Michel, G., Tonon, T., Scornet, D., Cock, J. M., and Kloareg, B. (2010). Central and storage carbon metabolism of the brown alga *Ectocarpus siliculosus*: Insights into the origin and evolution of storage carbohydrates in Eukaryotes. *New Phytol.* 188, 67–81. doi:10.1111/j.1469-8137.2010.03345.x.
- Mies, M. (2019). Evolution, diversity, distribution and the endangered future of the giant clam–Symbiodiniaceae association. *Coral Reefs* 38, 1067–1084. doi:10.1007/s00338-019-01857-x.
- Mitra, A., Flynn, K. J., Burkholder, J. M., Berge, T., Calbet, A., Raven, J. A., et al. (2014). The role of mixotrophic protists in the biological carbon pump. *Biogeosciences* 11, 995–1005. doi:10.5194/bg-11-995-2014.
- Mitra, A., Flynn, K. J., Tillmann, U., Raven, J. A., Caron, D., Stoecker, D. K., et al. (2016). Defining planktonic protist functional groups on mechanisms for energy and nutrient acquisition: Incorporation of diverse mixotrophic strategies. *Protist* 167, 106–120. doi:10.1016/j.protis.2016.01.003.
- Moodley, L., Middelburg, J. J., Soetaert, K., Boschker, H. T. S., Herman, P. M. J., and Heip, C. H. R. (2005). Similar rapid response to phytodetritus deposition in shallow and deep-sea sediments. *J. Mar. Res.* 63, 457–469. doi:10.1357/0022240053693662.
- Moore, C. A., and Gelder, S. R. (1983). The role of the “blunt” granules in hemocytes of *Mercenaria mercenaria* following phagocytosis. *J. Invertebr. Pathol.* 41, 369–377. doi:10.1016/0022-2011(83)90254-9.
- Müller, J. P. (1858). Über die Thalassicollen, Polycystinen und Acanthometren des Mittelmeeres. *K. Preuss. Akad. der Wissenschaften zu Berlin, Abhandlungen, Jahre 1858*, 1–62.
- Muscatine, L., Falkowski, P. G., Dubinsky, Z., Cook, P. A., and McCloskey, L. R. (1989). The effect of external nutrient resources on the population dynamics of zooxanthellae in a reef coral. *Proc. - R. Soc. London, B* 236, 311–324. doi:10.1098/rspb.1989.0025.
- Nakamura, Y., Somiya, R., Suzuki, N., Hidaka-Umetsu, M., Yamaguchi, A., and Lindsay, D. J. (2017). Optics-based surveys of large unicellular zooplankton: A case study on radiolarians and phaeodarians. *Plankt. Benthos Res.* 12, 95–103. doi:10.3800/pbr.12.95.
- Nakamura, Y., Tuji, A., Kimoto, K., Yamaguchi, A., Hori, R. S., and Suzuki, N. (2021). Ecology, Morphology, Phylogeny and Taxonomic Revision of Giant Radiolarians, *Orodaria* ord. nov. (Radiolaria; Rhizaria; SAR). *Protist* 172, 125808. doi:10.1016/j.protis.2021.125808.
- Nielsen, L. T., Krock, B., and Hansen, P. J. (2012). Effects of light and food availability on toxin production, growth and photosynthesis in *Dinophysis acuminata*. *Mar. Ecol. Prog. Ser.* 471, 37–50. doi:10.3354/meps10027.
- Not, F., Gausling, R., Azam, F., Heidelberg, J. F., and Worden, A. Z. (2007). Vertical distribution of picoeukaryotic diversity in the Sargasso Sea. *Environ. Microbiol.* 9, 1233–1252. doi:10.1111/j.1462-2920.2007.01247.x.
- Not, F., Probert, I., Ribeiro, C. G., Crenn, K., Guillou, L., Jeanthon, C., et al. (2016). “Photosymbiosis in marine pelagic environments,” in *The Marine Microbiome: An Untapped Source of Biodiversity and Biotechnological Potential*, eds. L. Stal and M. S. Cretoiu (Cham: Springer International Publishing), 305–332. doi:10.1007/978-3-319-33000-6_11.

- Ohdera, A. H., Abrams, M. J., Ames, C. L., Baker, D. M., Suescún-Bolívar, L. P., Collins, A. G., et al. (2018). Upside-down but headed in the right direction: Review of the highly versatile *Cassiopea xamachana* system. *Front. Ecol. Evol.* 6, 35. doi:10.3389/fevo.2018.00035.
- Ohlrogge, J., and Browse, J. (1995). Lipid biosynthesis. *Plant Cell* 7, 957–970. doi:10.1105/tpc.7.7.957.
- Ok, J. H., Jeong, H. J., Lim, A. S., You, J. H., Kang, H. C., Kim, S. J., et al. (2019). Effects of light and temperature on the growth of *Takayama helix* (Dinophyceae): mixotrophy as a survival strategy against photoinhibition. *J. Phycol.* 55, 1181–1195. doi:10.1111/jpy.12907.
- Olson, R. J., Zettler, E. R., Chisholm, S. W., and Dusenberry, J. A. (1991). “Advances in Oceanography through Flow Cytometry,” in *Particle Analysis in Oceanography*, ed. S. Demers (Berlin: Springer-Verlag), 351–399. doi:10.1007/978-3-642-75121-9_15.
- Oulhen, N., Schulz, B. J., and Carrier, T. J. (2016). English translation of Heinrich Anton de Bary’s 1878 speech, ‘Die Erscheinung der Symbiose’ (‘De la symbiose’). *Symbiosis* 69, 131–139. doi:10.1007/s13199-016-0409-8.
- Paul, D., Skrzypek, G., and Fórizs, I. (2007). Normalization of measured stable isotopic compositions to isotope reference scales - A review. *Rapid Commun. Mass Spectrom.* 21, 3006–3014. doi:10.1002/rcm.3185.
- Pernice, M., Meibom, A., Van Den Heuvel, A., Kopp, C., Domart-Coulon, I., Hoegh-Guldberg, O., et al. (2012). A single-cell view of ammonium assimilation in coral-dinoflagellate symbiosis. *ISME J.* 6, 1314–1324. doi:10.1038/ismej.2011.196.
- Polet, S., Berney, C., Fahrni, J., and Pawlowski, J. (2004). Small-subunit ribosomal RNA gene sequences of *Phaeodarea* challenge the monophyly of Haeckel’s Radiolaria. *Protist* 155, 53–63. doi:10.1078/1434461000164.
- Post, D. M. (2002). Using stable isotopes to estimate trophic position: models, methods, and assumptions. *Ecology* 83, 703–718. doi:10.2307/3071875.
- Probert, I., Siano, R., Poirier, C., Decelle, J., Biard, T., Tuji, A., et al. (2014). *Brandtodinium* gen. nov. and *B.nutricula* comb. Nov. (Dinophyceae), a dinoflagellate commonly found in symbiosis with polycystine radiolarians. *J. Phycol.* 50, 388–399. doi:10.1111/jpy.12174.
- Putt, M. (1990). Metabolism of photosynthate in the chloroplast-retaining ciliate *Laboea strobila*. *Mar. Ecol. Prog. Ser.* 60, 271–282. doi:10.3354/meps060271.
- Raven, J. A. (1997). Inorganic carbon acquisition by marine autotrophs. *Adv. Bot. Res.* 27, 85–209. doi:10.1016/S0065-2296(08)60281-5.
- Reich, H. G., Rodriguez, I. B., LaJeunesse, T. C., and Ho, T. Y. (2020). Endosymbiotic dinoflagellates pump iron: differences in iron and other trace metal needs among the Symbiodiniaceae. *Coral Reefs* 39, 915–927. doi:10.1007/s00338-020-01911-z.
- Riemann, L., Alfredsson, H., Hansen, M. M., Als, T. D., Nielsen, T. G., Munk, P., et al. (2010). Qualitative assessment of the diet of European eel larvae in the Sargasso Sea resolved by DNA barcoding. *Biol. Lett.* 6, 819–822. doi:10.1098/rsbl.2010.0411.
- Rivkin, R. B., and Seliger, H. H. (1981). Liquid scintillation counting for ¹⁴C uptake of single algal cells isolated from natural samples. *Limnol. Oceanogr.* 26, 780–785. doi:10.4319/lo.1981.26.4.0780.
- Robinson, M. D., McCarthy, D. J., and Smyth, G. K. (2009). edgeR: A Bioconductor package for differential expression analysis of digital gene expression data. *Bioinformatics* 26, 139–140. doi:10.1093/bioinformatics/btp616.
- Rost, B., Richter, K. U., Riebesell, U., and Hansen, P. J. (2006). Inorganic carbon acquisition in red tide dinoflagellates. *Plant, Cell Environ.* 29, 810–822. doi:10.1111/j.1365-3040.2005.01450.x.

- Roth, M. S. (2014). The engine of the reef: Photobiology of the coral-algal symbiosis. *Front. Microbiol.* 5. doi:10.3389/fmicb.2014.00422.
- Röthig, T., Puntin, G., Wong, J. C. Y., Burian, A., McLeod, W., and Baker, D. M. (2021). Holobiont nitrogen control and its potential for eutrophication resistance in an obligate photosymbiotic jellyfish. *Microbiome* 9, 1–16. doi:10.1186/s40168-021-01075-0.
- Royer, C., Gypens, N., Cardol, P., Borges, A. V., and Roberty, S. (2021). Response of dimethylsulfoniopropionate (DMSP) and dimethylsulfoxide (DMSO) cell quotas to oxidative stress in three phytoplankton species. *J. Plankton Res.* 00, 2021. doi:10.1093/plankt/fbab052.
- Sachs, J. L., and Wilcox, T. P. (2006). A shift to parasitism in the jellyfish symbiont *Symbiodinium microadriaticum*. *Proc. R. Soc. B Biol. Sci.* 273, 425–429. doi:10.1098/rspb.2005.3346.
- Saffo, M. (1992). Coming to terms with a field: words and concepts in symbiosis. *Symbiosis* 14, 17–31. Available at: <https://www.researchgate.net/publication/281240992> [Accessed September 9, 2019].
- Sandin, M. M. (2019). Diversité et évolution des Nassellaires et Spumellaires (Radiolaires).
- Sandin, M. M., Pillet, L., Biard, T., Poirier, C., Bigeard, E., Romac, S., et al. (2019). Time Calibrated Morpho-molecular Classification of Nassellaria (Radiolaria). *Protist* 170, 187–208. doi:10.1016/j.protis.2019.02.002.
- Schewiakoff, W. (1926). *Fauna e Flora del Golfo di Napoli, Die Acantharia.*, eds. D. . Bardi and R. Friedlander Stazione Zoologica di Napoli.
- Schmied, C., and Jambor, H. K. (2020). Effective image visualization for publications – a workflow using open access tools and concepts. *F1000Research* 9, 1373. doi:10.12688/f1000research.27140.1.
- Schneider, L., Anestis, K., Mansour, J., Anschütz, A., Gypens, N., Hansen, P., et al. (2020a). A dataset on trophic modes of aquatic protists. *Biodivers. Data J.* 8, e56648. doi:10.3897/bdj.8.e56648.
- Schneider, L. K., Flynn, K. J., Herman, P. M. J., Troost, T. A., and Stolte, W. (2020b). Exploring the trophic spectrum: Placing mixoplankton into marine protist communities of the Southern North Sea. *Front. Mar. Sci.* 7, 586915. doi:10.3389/fmars.2020.586915.
- Schoener, D. M., and McManus, G. B. (2017). Growth, grazing, and inorganic C and N uptake in a mixotrophic and a heterotrophic ciliate. *J. Plankton Res.* 39, 379–391. doi:10.1093/plankt/fbx014.
- Selosse, M. A., Charpin, M., and Not, F. (2017). Mixotrophy everywhere on land and in water: the grand écart hypothesis. *Ecol. Lett.* 20, 246–263. doi:10.1111/ele.12714.
- Shapiro, O. H., Kramarsky-Winter, E., Gavish, A. R., Stocker, R., and Vardi, A. (2016). A coral-on-a-chip microfluidic platform enabling live-imaging microscopy of reef-building corals. *Nat. Commun.* 7. doi:10.1038/ncomms10860.
- Sibbald, S. J., and Archibald, J. M. (2020). Genomic insights into plastid evolution. *Genome Biol. Evol.* 20, 978–990. doi:10.1093/gbe/evaa096.
- Skovgaard, A., Hansen, P. J., and Stoecker, D. K. (2000). Physiology of the mixotrophic dinoflagellate *Fragilidium subglobosum*. I. Effects of phagotrophy and irradiance on photosynthesis and carbon content. *Mar. Ecol. Prog. Ser.* 201, 129–136. doi:10.3354/meps201129.
- Smalley, G. W., Coats, D. W., and Stoecker, D. K. (2003). Feeding in the mixotrophic dinoflagellate *Ceratium furca* is influenced by intracellular nutrient concentrations. *Mar. Ecol. Prog. Ser.* 262, 137–151. doi:10.3354/meps262137.
- Smith, M., and Hansen, P. J. (2007). Interaction between *Mesodinium rubrum* and its prey: Importance of prey concentration, irradiance and pH. *Mar. Ecol. Prog. Ser.* 338, 61–70. doi:10.3354/meps338061.

- Stamatakis, A. (2014). RAxML version 8: a tool for phylogenetic analysis and post-analysis of large phylogenies. *Bioinformatics* 30, 1312–1313. Available at: <https://academic.oup.com/bioinformatics/article/30/9/1312/238053> [Accessed July 4, 2020].
- Stemmann, L., Youngbluth, M., Robert, K., Hosia, A., Picheral, M., Paterson, H., et al. (2008). Global zoogeography of fragile macrozooplankton in the upper 100–1000 m inferred from the underwater video profiler. *ICES J. Mar. Sci.* 65, 433–442. doi:10.1093/icesjms/fsn010.
- Sterner, R. ., and Elser, J. . (2002). *Ecological Stoichiometry: The Biology of Elements from Molecules to the Biosphere*. Princeton University Press. Available at: <https://www.amazon.com/Ecological-Stoichiometry-Elements-Molecules-Biosphere/dp/0691074917> [Accessed July 5, 2020].
- Stoecker, D. K., Hansen, P. J., Caron, D. A., and Mitra, A. (2017). Mixotrophy in the marine plankton. *Ann. Rev. Mar. Sci.* 9, 311–335. doi:10.1146/annurev-marine-010816-060617.
- Stoecker, D. K., Johnson, M. D., De Vargas, C., and Not, F. (2009). Acquired phototrophy in aquatic protists. *Aquat. Microb. Ecol.* 57, 279–310. doi:10.3354/ame01340.
- Stukel, M. R., Biard, T., Krause, J., and Ohman, M. D. (2018). Large Phaeodaria in the twilight zone: Their role in the carbon cycle. *Limnol. Oceanogr.* 63, 2579–2594. doi:10.1002/lno.10961.
- Sugiyama, K., Hori, R. S., Kusunoki, Y., and Matsuoka, A. (2008). Pseudopodial features and feeding behavior of living nassellarians *Eucyrtidium hexagonatum* Haeckel, *Pterocorys zancleus* (Müller) and *Dictyocodon prometheus* Haeckel. *Paleontol. Res.* 12, 209–222. doi:10.2517/1342-8144-12.3.209.
- Suzuki, N., and Not, F. (2015). “Biology and ecology of Radiolaria,” in *Marine Protists: Diversity and Dynamics*, eds. S. Ohtsuka, T. Suzuki, T. Horiguchi, N. Suzuki, and F. Not (Tokyo: Springer), 179–222. doi:10.1007/978-4-431-55130-0.
- Swanberg, N. R. (1979). The ecology of colonial radiolarians : their colony morphology, trophic interactions and associations, behavior, distribution, and the photosynthesis of their symbionts. *Ph.D. thesis*. doi:10.1575/1912/2214.
- Swanberg, N. R. (1983). The trophic role of colonial Radiolaria in oligotrophic oceanic environments. *Limnol. Oceanogr.* 28, 655–666. doi:10.4319/lo.1983.28.4.0655.
- Swanberg, N. R., and Anderson, O. R. (1985). The nutrition of radiolarians: Trophic activity of some solitary Spumellaria. *Limnol. Oceanogr.* 30, 646–652. doi:10.4319/lo.1985.30.3.0646.
- Swanberg, N. R., Anderson, O. R., Lindsey, J. L., and Bennett, P. (1986). The biology of *Physematium muelleri*: trophic activity. *Deep Sea Res. Part A, Oceanogr. Res. Pap.* 33, 913–922. doi:10.1016/0198-0149(86)90006-3.
- Swanberg, N. R., and Caron, D. A. (1991). Patterns of sarcodine feeding in epipelagic oceanic plankton. *J. Plankton Res.* 13, 287–312. doi:10.1093/plankt/13.2.287.
- Tada, K., Pithakpol, S., Yano, R., and Montani, S. (2000). Carbon and nitrogen content of *Noctiluca scintillans* in the Seto Inland Sea, Japan. *J. Plankton Res.* 22, 1203–1211. doi:10.1093/plankt/22.6.1203.
- Takahashi, O., Mayama, S., and Matsuoka, A. (2003). Host-symbiont associations of polycystine Radiolaria: epifluorescence microscopic observation of living Radiolaria. *Mar. Micropaleontol.* 49, 187–194. doi:10.1016/S0377-8398(03)00035-5.
- Tanaka, Y., Miyajima, T., Koike, I., Hayashibara, T., and Ogawa, H. (2006). Translocation and conservation of organic nitrogen within the coral-zooxanthella symbiotic system of *Acropora pulchra*, as demonstrated by dual isotope-labeling techniques. *J. Exp. Mar. Bio. Ecol.* 336, 110–119. doi:10.1016/j.jembe.2006.04.011.

- Taylor, D. L. (1978). Nutrition of algal-invertebrate symbiosis. II. Effects of exogenous nitrogen sources on growth, photosynthesis and the rate of excretion by algal symbionts in vivo and in vitro. *Proc. R. Soc. London - Biol. Sci.* 201, 401–412. doi:10.1098/rspb.1978.0052.
- Terrado, R., Pasulka, A. L., Lie, A. A.-Y., Orphan, V. J., Heidelberg, K. B., and Caron, D. A. (2017). Autotrophic and heterotrophic acquisition of carbon and nitrogen by a mixotrophic chrysophyte established through stable isotope analysis. *ISME J.* 11, 2022–2034. doi:10.1038/ismej.2017.68.
- Tittel, J., Bissinger, V., Zippel, B., Gaedke, U., Bell, E., Lorke, A., et al. (2003). Mixotrophs combine resource use to outcompete specialists: Implications for aquatic food webs. *Proc. Natl. Acad. Sci. U. S. A.* 100, 12776–12781. doi:10.1073/pnas.2130696100.
- Trench, R. K. (1979). The cell biology of plant-animal symbiosis. *Ann. Rev. Plant Physiol.* 30, 485–531. Available at: www.annualreviews.org [Accessed August 11, 2021].
- Turpin, D. H. (1991). Effects of Inorganic N availability on algal photosynthesis and carbon metabolism. *J. Phycol.* 27, 14–20. doi:10.1111/j.0022-3646.1991.00014.x.
- Uthicke, S., and Altenrath, C. (2010). Water column nutrients control growth and C:N ratios of symbiont-bearing benthic foraminifera on the Great Barrier Reef, Australia. *Limnol. Oceanogr.* 55, 1681–1696. doi:10.4319/lo.2010.55.4.1681.
- Uwizeye, C., Brisbin, M. M., Gallet, B., Chevalier, F., LeKieffre, C., Schieber, N. L., et al. (2021). Cytoklepty in the plankton: A host strategy to optimize the bioenergetic machinery of endosymbiotic algae. *Proc. Natl. Acad. Sci.* 118, e2025252118. doi:<https://doi.org/10.1101/2020.12.08.416644>.
- Vernette, C., Henry, N., Lecubin, J., de Vargas, C., Hingamp, P., and Lescot, M. (2021). The Ocean Barcode Atlas: a web service to explore the biodiversity and biogeography of marine organisms. *Mol. Ecol. Resour.*, 1–12. doi:10.1111/1755-0998.13322.
- Villar, E., Dani, V., Bigeard, E., Linhart, T., Mendez-Sandin, M., Bachy, C., et al. (2018). Symbiont chloroplasts remain active during bleaching-like response induced by thermal stress in *Collozoum pelagicum* (Collodaria, Retaria). *Front. Mar. Sci.* 5, 387. doi:10.3389/fmars.2018.00387.
- Vitousek, P. M., and Howarth, R. W. (1991). Nitrogen limitation on land and in the sea: How can it occur? *Biogeochem.* 1991 132 13, 87–115. doi:10.1007/BF00002772.
- Vizzini, S., and Mazzola, A. (2006). Sources and transfer of organic matter in food webs of a Mediterranean coastal environment: Evidence for spatial variability. *Estuar. Coast. Shelf Sci.* 66, 459–467. doi:10.1016/j.ecss.2005.10.004.
- von Wirén, N., Gazzarrini, S., Gojon, A., and Frommer, W. B. (2000). The molecular physiology of ammonium uptake and retrieval. *Curr. Opin. Plant Biol.* 3, 254–261. doi:10.1016/S1369-5266(00)80074-6.
- Ward, B. A., and Follows, M. J. (2016). Marine mixotrophy increases trophic transfer efficiency, mean organism size, and vertical carbon flux. *Proc. Natl. Acad. Sci.* 113, 2958–2963. doi:10.1073/pnas.1517118113.
- Watanabe, T., Nagai, S., Kawakami, Y., Asakura, T., Kikuchi, J., Inaba, N., et al. (2021). 18S rRNA gene sequences of leptocephalus gut contents, particulate organic matter, and biological oceanographic conditions in the western North Pacific. *Sci. Rep.* 11, 5488. doi:10.1038/s41598-021-84532-y.
- Wever, P. De, Dumitrica, P., Caulet, J., Nigrini, C., and Caridroit, M. (2002). *Radiolarians in the Sedimentary Record*. Gordon & Breach Science Publishers doi:10.1201/9781482283181.
- Whitehead, L. F., and Douglas, A. E. (2003). Metabolite comparisons and the identity of nutrients translocated from symbiotic algae to an animal host. *J. Exp. Biol.* 206, 3149–3157. doi:10.1242/jeb.00539.
- Wilken, S., Choi, C. J., and Worden, A. Z. (2020). Contrasting mixotrophic lifestyles reveal different ecological niches in two closely related marine protists. *J. Phycol.* 56, 52–67. doi:10.1111/jpy.12920.

- Wilken, S., Huisman, J., Naus-Wiezer, S., and Van Donk, E. (2013). Mixotrophic organisms become more heterotrophic with rising temperature. *Ecol. Lett.* 16, 225–233. doi:10.1111/ele.12033.
- Wilken, S., Schuurmans, J. M., and Matthijs, H. C. P. (2014). Do mixotrophs grow as photoheterotrophs? Photophysiological acclimation of the chrysophyte *Ochromonas danica* after feeding. *New Phytol.* 204, 882–889. doi:10.1111/NPH.12975.
- Xu, Z., Wang, M., Wu, W., Li, Y., Liu, Q., Han, Y., et al. (2018). Vertical Distribution of Microbial Eukaryotes From Surface to the Hadal Zone of the Mariana Trench. *Front. Microbiol.* 9, 2023. doi:10.3389/fmicb.2018.02023.
- Yamada, N., Bolton, J. J., Trobajo, R., Mann, D. G., Dąbek, P., Witkowski, A., et al. (2019). Discovery of a kleptoplastic ‘dinotom’ dinoflagellate and the unique nuclear dynamics of converting kleptoplastids to permanent plastids. *Sci. Rep.* 9. doi:10.1038/s41598-019-46852-y.
- Yellowlees, D., Rees, T. A. V., and Leggat, W. (2008). Metabolic interactions between algal symbionts and invertebrate hosts. *Plant, Cell Environ.* 31, 679–694. doi:10.1111/j.1365-3040.2008.01802.x.
- Yuasa, T., Kawachi, M., Horiguchi, T., and Takahashi, O. (2019). *Chrysochromulina andersonii* sp. nov. (Prymnesiophyceae), a new flagellate haptophyte symbiotic with radiolarians. doi:10.1080/00318884.2018.1541271.
- Yuasa, T., and Takahashi, O. (2014). Ultrastructural morphology of the reproductive swarms of *Sphaerozoum punctatum* (Huxley) from the East China Sea. *Eur. J. Protistol.* 50, 194–204. doi:10.1016/j.ejop.2013.12.001.
- Yuasa, T., and Takahashi, O. (2016). Light and electron microscopic observations of the reproductive swarmer cells of nassellarian and spumellarian polycystines (Radiolaria). *Eur. J. Protistol.* 54, 19–32. doi:10.1016/j.ejop.2016.02.007.

ANNEX I

Public presentations

- 36th annual International Society of Chemical Ecology meeting– September 2021 – Online conference, South Africa:
Presentation: Carbon and nitrogen uptake and translocation between the single cell marine protist Acantharia and their symbionts
<https://isce2021.carlamani.com/abstracts/Chemical%20Ecology%20of%20Marine%20Holobionts%20combined%20abstracts.pdf>
- Young Researchers Day ([JJC](#)) – February 2021 – Roscoff, France:
Flash-Talk: Radiolaria back to the future
- International Conference on Mixoplankton – January 2021 – Online:
Presentation: Oceanic Greenhouses, the endosymbiotic nonconstitutive mixoplanktonic Radiolaria
<https://www.mixotroph.org/wp-content/uploads/2020/12/20201217-Conference-Timetable-D12.pdf>
- Young Researchers Day ([JJC](#)) – January 2020 – Roscoff, France:
Flash-Talk: Study on endosymbiotic Radiolaria
- MixITiN Symposium – October 2019 – Heraklion, (Crete) Greece:
Presentation: Physiological and genetic interactions between symbionts and eSNCM hosts— Radiolaria
- 7th European Phycological Congress – August 2019 – Zagreb, Croatia:
Presentation: Photosynthetic C & N uptake of symbiotic Radiolaria assessed by stable isotope analysis. Keynote and Oral Papers, European Journal of Phycology, 54:sup1, 31-117, DOI: <https://doi.org/10.1080/09670262.2019.1626627>
- [MOOSE-GE Seminar](#) – June 2019 – shipboard in the Mediterranean Sea:
Seminar: Mixoplankton

Oceanographic Expedition

- MOOSE-GE 2019: Thalassa research vessel
Mediterranean Ocean Observing System for the Environment

Awards/grants

- Assemble Plus, 5th call 2019, project: Radiolaria Metabolic Budget—RAMB

MixITiN Project Deliverables

- Publication of e-newsletters, public and (social)media engagement interactions – www.mixotroph.org
- Mid-term results: New tools and protocols for genomic sampling of mixotrophic protists – *Confidential (19 p)*
- Mid-term results: new approaches to estimate predation rates in mixotrophic protists – *Confidential (18 p)*
- Preliminary report on field and experimental data – *Confidential (54 p)*
- Reporting new tools and protocols for genomic sampling of mixotrophic protists – *Confidential (39 p)*
- Report of the role of NCM ecophysiology affecting trophic dynamic studies – *Confidential (76 p)*
- Reporting interpretative toolkit to enable the use of genomic data aligned with physiological status for representative mixotrophs – *Public Document, DOI: to be disclosed*
- Guide for field studies and environmental monitoring of mixotrophic populations – *Public Document, DOI: <http://doi.org/10.5281/zenodo.5054916>*
- Manual Reporting Novel Approaches For Investigating Marine Planktonic Mixotrophy. Aditee Mitra, Kevin J Flynn, Konstantinos Anestis, Joost S Mansour, Guilherme D Ferreira, Albert Calbet (Editors), 2021. Published by Zenodo, <http://doi.org/10.5281/Zenodo.5148500>
 - Section 2: Mansour J, Anestis K, Maselli M, Hansen PJH, Not F, John U (2021) Genomic sampling protocols for application to mixoplankton.
 - Section 3: Ferreira GD, Calbet A, Not F, Mansour JS, Hansen PJ, Medić N, Pitta P, Romano F, Flynn KJ, Mitra A (2021) Development And Validation Of New Methods For Measuring Predation Rates In Mixoplanktonic Protists.
 - Section 4: Anestis K, Mansour JS, Maselli M, Hansen PJ, Not F, John U (2021) Reporting interpretative toolkit to enable the use of genomic data aligned with physiological status for representative mixoplankton.

ANNEX II
Other Publications and Collaborations



Data Paper

A dataset on trophic modes of aquatic protists

Lisa K. Schneider^{‡,§}, Konstantinos Anestis[‡], **Joost Mansour[¶]**, Anna A. Anschütz^{#,§}, Nathalie Gypens[§], Per J Hansen[¶], Uwe John^{‡,¶}, Kerstin Klemm[‡], Jon Lapeya Martin[§], Nikola Medic[¶], Fabrice Not[¶], Willem Stolte[‡]

‡ Deltares, Delft, Netherlands

§ Université Libre de Bruxelles, Bruxelles, Belgium

‡ Alfred-Wegener-Institute Helmholtz Center for Polar and Marine Research, Bremerhaven, Germany

¶ Sorbonne University, CNRS, Roscoff, France

School of Earth and Ocean Sciences, Cardiff University, Cardiff, United Kingdom

¶ Marine Biological Laboratory, University of Copenhagen, Copenhagen, Denmark

¶ Helmholtz Institute for Functional Marine Biodiversity, Oldenburg, Germany

¶ CNRS, Roscoff, France

Corresponding author: Lisa K. Schneider (lisa.schneider@deltares.nl)

Academic editor: Anne Thessen

Received: 17 Jul 2020 | Accepted: 08 Sep 2020 | Published: 23 Oct 2020

Citation: Schneider LK, Anestis K, Mansour JS, Anschütz AA, Gypens N, Hansen PJ, John U, Klemm K, Martin JL, Medic N, Not F, Stolte W (2020) A dataset on trophic modes of aquatic protists. Biodiversity Data Journal 8: e56648. <https://doi.org/10.3897/BDJ.8.e56648>

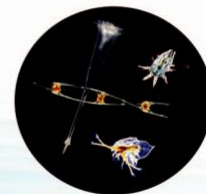
Abstract

Background

An important functional trait of organisms is their trophic mode. It determines their position within food webs, as well as their function within an ecosystem. For the better part of the 20th century, aquatic protist communities were thought to consist mainly of producers (phytoplankton) and consumers (protozooplankton). Phytoplankton cover their energy requirements through photosynthesis (phototrophy), while protozooplankton graze on prey and organic particles (phagotrophy). However, over the past decades, it was shown that another trophic group (mixoplankton) comprise a notable part of aquatic protist communities. Mixoplankton employ a third trophic mode by combining phototrophy and phagotrophy (mixotrophy). Due to the historical dichotomy, it is not straightforward to gain adequate and correct information on the trophic mode of aquatic protists. Long hours of literature research or expert knowledge are needed to correctly assign trophic modes. Additionally, aquatic protists also have a long history of undergoing taxonomic changes which make it difficult to compare past and present literature. While WoRMS, the World Register of Marine Species, keeps track of the taxonomic changes and assigns each species a unique AphiaID that can be linked to its various historic and present taxonomic hierarchy, there is currently no machine-readable database to query aquatic protists for their trophic modes.

New information

This paper describes a dataset that was submitted to WoRMS and links aquatic protist taxa, with a focus on marine taxa, to their AphiaID and their trophic mode. The bulk of the data used for this dataset stems from (routine) monitoring stations in the North Sea and the Baltic Sea. The data were augmented and checked against state-of-the-art knowledge on mixoplankton taxa by consulting literature and experts. Thus, this dataset provides a first attempt to make the trophic mode of aquatic protists easily accessible in both a human- and machine-readable format.



J. Plankton Res. (2019) 41(4): 375–391. First published online July 15, 2019 doi:10.1093/plankt/fbz026

HORIZONS

Mixotrophic protists and a new paradigm for marine ecology: where does plankton research go now?

Kevin J Flynn^{1*}, Aditee Mitra¹, Konstantinos Anestis², Anna A Anschutz¹, Albert Calbet³, Guilherme D Ferreira³, Nathalie Gypens⁴, Per J Hansen⁵, Uwe John^{2,6}, Jon Lapeyra Martin⁴, **Joost S Mansour**⁷, Maira Maselli⁵, Nikola Medić⁵, Andreas Norlin¹, Fabrice Not⁷, Paraskevi Pitta⁸, Filomena Romano⁸, Enric Saiz³, Lisa Schneider⁹, Willem Stolte⁹, Claudia Traboni³

¹ Biosciences, Swansea University, Swansea SA2 8PP, UK, ² Alfred-Wegener-Institute Helmholtz Centre for Polar and Marine Research, Am Handelshafen 12, 27570 Bremerhaven, Germany, ³ Institut de Ciències del Mar (ICM, CSIC). Passeig Marítim de la Barceloneta 37-49, 08003, Barcelona, Spain, ⁴ Université Libre de Bruxelles, Écologie des Systèmes Aquatiques, CP-221, Boulevard du Triomphe, 1050 Brussels, Belgium, ⁵ Marine Biological Section, University of Copenhagen, DK-3000, Helsingør, Denmark, ⁶ Helmholtz Institute for Functional Marine Biodiversity (HIFMB), Ammaländer Heerstr. 231, 23129 Oldenburg, Germany, ⁷ Sorbonne University, CNRS, UMR7144, Adaptation and Diversity in Marine Environment (AD2M) Laboratory, Ecology of marine plankton team, Station Biologique de Roscoff, Place Georges Teissier, 29680, Roscoff, France, ⁸ Institute of Oceanography, Hellenic Centre for Marine Research, PO Box 2214, 71003 Heraklion, Greece, ⁹ Deltares, Boussinesqweg 1, 2629 HV Delft, The Netherlands

*corresponding author: k.j.flynn@swansea.ac.uk

Received March 22, 2019; editorial decision May 24, 2019; accepted May 24, 2019; Corresponding editor: John Dolan

Many protist plankton are mixotrophs, combining phototrophy and phagotrophy. Their role in freshwater and marine ecology has emerged as a major developing feature of plankton research over recent decades. To better aid discussions, we suggest these organisms are termed “mixoplankton”, as “planktonic protist organisms that express, or have potential to express, phototrophy and phagotrophy”. The term “phytoplankton” then describes phototrophic organisms incapable of phagotrophy. “Protozooplankton” describes phagotrophic protists that do not engage in acquired phototrophy. The complexity of the changes to the conceptual base of the plankton trophic web caused by inclusion of mixoplanktonic activities are such that we suggest that the restructured description is termed the “mixoplankton paradigm”. Implications and opportunities for revision of survey and fieldwork, of laboratory experiments and of simulation modelling are considered. The main challenges are not only with taxonomic and functional identifications, and with measuring rates of potentially competing processes within single cells, but with decades of inertia built around the traditional paradigm that assumes a separation of trophic processes between different organisms. In keeping with the synergistic nature of cooperative photo- and phagotrophy in mixoplankton, a comprehensive multidisciplinary approach will be required to tackle the task ahead.

Kevin J Flynn, Aditee Mitra, Konstantinos Anestis, Anna A Anschutz, Albert Calbet, Guilherme Duarte Ferreira, Nathalie Gypens, Per J Hansen, Uwe John, Jon Lapeyra Martin, **Joost S Mansour**, Maira Maselli, Nikola Medić, Andreas Norlin, Fabrice Not, Paraskevi Pitta, Filomena Romano, Enric Saiz, Lisa K Schneider, Willem Stolte, Claudia Traboni, Mixotrophic protists and a new paradigm for marine ecology: where does plankton research go now?, *Journal of Plankton Research*, , fbz026, <https://doi.org/10.1093/plankt/fbz026>

Eco-Evolutionary Perspectives on Mixoplankton

Frontiers in Marine Science, Global Change and the Future Ocean.
ICYMARE - Early Career Researchers in Marine Science

Joost Samir Mansour¹

Konstantinos Anestis^{2,3}

¹CNRS and Sorbonne University, UMR7144 Adaptation and Diversity in Marine Environment (AD2M) Laboratory, Ecology of Marine Plankton Team, Station Biologique de Roscoff, Roscoff, France, ²Department of Ecological Chemistry, Alfred-Wegener-Institute Helmholtz Centre for Polar and Marine Research, Bremerhaven, Germany, ³Faculty of Biology/Chemistry, University of Bremen, Bremen, Germany

Keywords: Evolution, mixotrophy, endosymbiosis, plankton, kleptoplasty, plastids

Citation: Mansour, J. S., and Anestis, K. (2021). Eco-Evolutionary Perspectives on Mixoplankton. *Front. Mar. Sci.* 8, 666160. doi:10.3389/fmars.2021.666160.

Continues on next page



Eco-Evolutionary Perspectives on Mixoplankton

Joost Samir Mansour^{1†} and Konstantinos Anestis^{2,3*†}

¹CNRS and Sorbonne University, UMR7144 Adaptation and Diversity in Marine Environment (AD2M) Laboratory, Ecology of Marine Plankton Team, Station Biologique de Roscoff, Roscoff, France, ²Department of Ecological Chemistry, Alfred-Wegener-Institute Helmholtz Centre for Polar and Marine Research, Bremerhaven, Germany, ³Faculty of Biology/Chemistry, University of Bremen, Bremen, Germany

OPEN ACCESS

Edited by:

Viola Liebich,
Bremen Society for Natural Sciences,
Germany

Reviewed by:

Elisabeth Hehenberger,
GEOMAR Helmholtz Center for
Ocean Research Kiel, Germany
Patricia M. Glibert,
University of Maryland Center for
Environmental Science (UMCES),
United States

*Correspondence:

Konstantinos Anestis
kanestis@awi.de

[†]These authors have contributed
equally to this work

*ORCID:

Joost Samir Mansour
orcid.org/0000-0002-9505-1673
Konstantinos Anestis
orcid.org/0000-0002-8208-6789

Specialty section:

This article was submitted to
Marine Biology,
a section of the journal
Frontiers in Marine Science

Received: 09 February 2021

Accepted: 29 April 2021

Published: 26 May 2021

Citation:

Mansour JS and Anestis K (2021)
Eco-Evolutionary Perspectives
on Mixoplankton.
Front. Mar. Sci. 8:666160.
doi: 10.3389/fmars.2021.666160

Mixotrophy, i.e., the capability of both phototrophy and phagotrophy within a single organism, is a prominent trophic mode in aquatic ecosystems. Mixotrophic strategies can be highly advantageous when feeding or photosynthesis alone does not sustain metabolic needs. In the current review, we discuss the functional types of mixotrophic marine protists (herein mixoplankton) within the context of evolution. Permanent plastids have been established in large due to gene transfer from prey and/or endosymbionts to the host cell. In some kleptoplastidic mixoplankton, prior gene transfers and active transcription of plastid related genes in the host can help maintain and extend retention of the current kleptoplast. In addition to kleptoplasts, the prey nucleus is also sometimes retained and actively transcribed to help maintain and even replicate the kleptoplasts. Endosymbiotic relations vary considerably in the extent to which hosts affect symbionts. For example, some endosymbionts are heavily modified to increase photosynthetic efficiency, or are controlled in their cell division. It can be proposed that many kleptoplasts and endosymbionts are in fact *en route* to becoming permanent plastids. Conditions such as increased temperature and limiting nutrients seem to favor phagotrophy in mixoplankton. However, responses of mixoplankton to changing environmental conditions like light irradiance, temperature, nutrient, and prey availability are variable and species-specific. Studying mixotrophs with temporary plastids could elucidate past and future evolutionary mechanisms and dynamics of processes such as phagotrophy and the establishment of (secondary) permanent plastids.

Keywords: evolution, mixotrophy, endosymbiosis, plankton, kleptoplasty, plastids

INTRODUCTION TO MIXOTROPHY

All living organisms need resources (micronutrients and macronutrients) in order to sustain their structure, basic cellular functions, and their overall existence. Various strategies (e.g., phototrophy, phagotrophy, chemotrophy, or osmotrophy) have evolved in order to acquire these important resources. The two most well-known strategies for nutrient acquisition distinguish organisms into two functional categories, those that make use of light to fix carbon (phototrophs/primary producers) and those that feed on others (heterotrophs/consumers). However, there is a third category to consider – mixotrophs. As indicated by the name, mixotrophy refers to a mixed trophic mode, thereby combining both phototrophic and heterotrophic modes of nutrition in order to fulfill cellular nutrient requirements.

We focus here on marine mixotrophic protists, but mixotrophy is an important trait for organisms both on land, and in water (Selosse et al., 2017). A well-known land example being the carnivorous plants that feed on insects. In aquatic ecosystems, mixotrophy is much more prevalent and widespread than initially thought. It can be found in a plethora of different organisms, from unicellular eukaryotes to multicellular metazoa such as jellyfishes or sea slugs that use endosymbionts or acquired plastids for photosynthesis (Cruz et al., 2013; Selosse et al., 2017). Plankton research has traditionally been based on the division of plankton between photosynthetic phytoplankton and heterotrophic zooplankton. The increasing focus on mixotrophy has changed the perception of plankton dynamics and interactions within plankton communities (Flynn et al., 2013). As more examples of mixotrophic marine organisms became known, it was realized that mixotrophy is not a rare occurrence in aquatic ecosystems, but fairly common (Mitra et al., 2014; Caron, 2017).

Mixoplankton

In the last decades, mixotrophic protists were referred to using definitions combining the two contradicting terms of phytoplankton and phagotrophy. The term mixotroph was used for photosynthetic organisms that take up dissolved organic carbon by osmotrophy, as well as for those using phagotrophy (Burkholder et al., 2008; Sforza et al., 2012). An emerging need to formally define mixotrophic protists (Flynn et al., 2013) with regards to their nutritional mode led to the first efforts to categorize mixotrophs in groups with distinct features. In an attempt to group protists based on their nutritional mode and function, Mitra et al. (2016) proposed a comprehensive terminology. Following the definitions of functional groups for mixotrophic protists, Flynn et al. (2019) suggested the use of the term *mixoplankton* – “*planktonic protists that express, or have potential to express, phototrophy and phagotrophy*” – as is the nomenclature we herein follow.

The functional classification of mixoplankton is based on how the cell incorporates photosynthesis. Mixotrophic protists (i.e., mixoplankton), as defined by Mitra et al. (2016) and Flynn et al. (2019), are functionally distinguished between *constitutive mixoplankton (CM)* and *non-constitutive mixoplankton (NCM)*. A CM has an inherent capability for both phototrophy and phagotrophy. *Constitutive mixoplankton* are found in most eukaryotic microalgal lineages (e.g., green algae, euglenophytes, cryptophytes, chrysophytes, haptophytes, and dinoflagellates; **Figure 1**). *Non-constitutive mixoplankton*, which are defined by the need to acquire their photosynthetic ability through external means, are found mostly among ciliates, dinoflagellates, Foraminifera, and Radiolaria (**Figure 1**). Phototrophic activity in NCM can broadly be achieved in three ways which further divide NCM into sub-groups: (1) stealing chloroplasts of (any) prey (*generalist non-constitutive mixoplankton, GNCM*); (2) stealing chloroplasts from specific prey (*plastidic specialist non-constitutive mixoplankton pSNCM*); and (3) harboring photosynthetically active endosymbionts (*endosymbiotic specialist non-constitutive mixoplankton, eSNCM*; acquired phototrophy

reviewed in Stoecker et al., 2009). Even though, we currently make a functional separation between GNCM and pSNCM, it is possible that some pSNCM lean more toward GNCM. Often very few data are available to support the GNCM assumption, making GNCM appear as pSNCM. The main differences between GNCM and pSNCM definitions rest simply on the rate of success in utilizing plastids from prey, and on the observed specificity of the prey from which plastids can be acquired.

Similar to the distinction of GNCM and pSNCM, the classification of mixoplankton into functional types is greatly influenced by current knowledge or lack thereof. Often the metabolic contribution of predation vs. photosynthesis is poorly understood (Anschütz and Flynn, 2020). By default, an organism would be either phototroph or heterotroph, while to identify a mixotroph both phagotrophic and phototrophic capabilities need to have been identified (Beisner et al., 2019; Hansen et al., 2019; Ferreira and Calbet, 2020). Considering the relative ease to identify a photosynthetic organism (by fluorescence signal of plastid pigments, and/or optical and electron microscopy to characterize the cell) it is tempting to immediately classify it as a (pure) phototroph (Anderson et al., 2017; Beisner et al., 2019). In contrast, phagotrophy rarely has clear external identifiers, instead it requires meticulous experimentation to identify phagotrophic potential in an organism (Anderson et al., 2017; Beisner et al., 2019). Even then, the absence of observed phagotrophy might just imply that not all conditions were met—time, type or state of prey, or state of the potential predator. Transcriptomics and genomics-based approaches and subsequent gene-based predictive models can help indicate mixotrophic potential (Burns et al., 2018). Identification of genetic potential for both phototrophy and phagotrophy does not forego the need for physiological experimentation and knowledge of photosynthetic and feeding rates. When the potential for a nutritional mode is observed, one could expect this potential to be used or otherwise lost over evolutionary time. Though, a nutritional mode might only be used under certain conditions. An organism could rely on (yet unobserved) instances of e.g., phagotrophy in space or time, which can be exceedingly difficult confirm.

The different functional groups of mixoplankton possess traits, such as phagotrophy and acquired photosynthesis that play a major part in evolutionary processes. Studying mixotrophy in its different forms offers an opportunity to gain a better understanding of major ecological and evolutionary processes that have been crucial in the creation of life as we know it today. Mixotrophy has not only been pivotal in the past with visible effects still identifiable today (such as the establishment of permanent organelles through endosymbiosis), but also it is still a prevalent biological phenomenon with a considerable fraction of marine plankton identified as mixoplankton (Flynn et al., 2019; Schneider et al., 2020; **Figure 1**). In mixotrophic organisms, we may have a glimpse of how life used to look in the past, and how things could change in the future. In the following sections, we address evolutionary theories and their relation to different functional types of mixoplankton, to gain a general overview of the possible role of mixotrophy as a transient

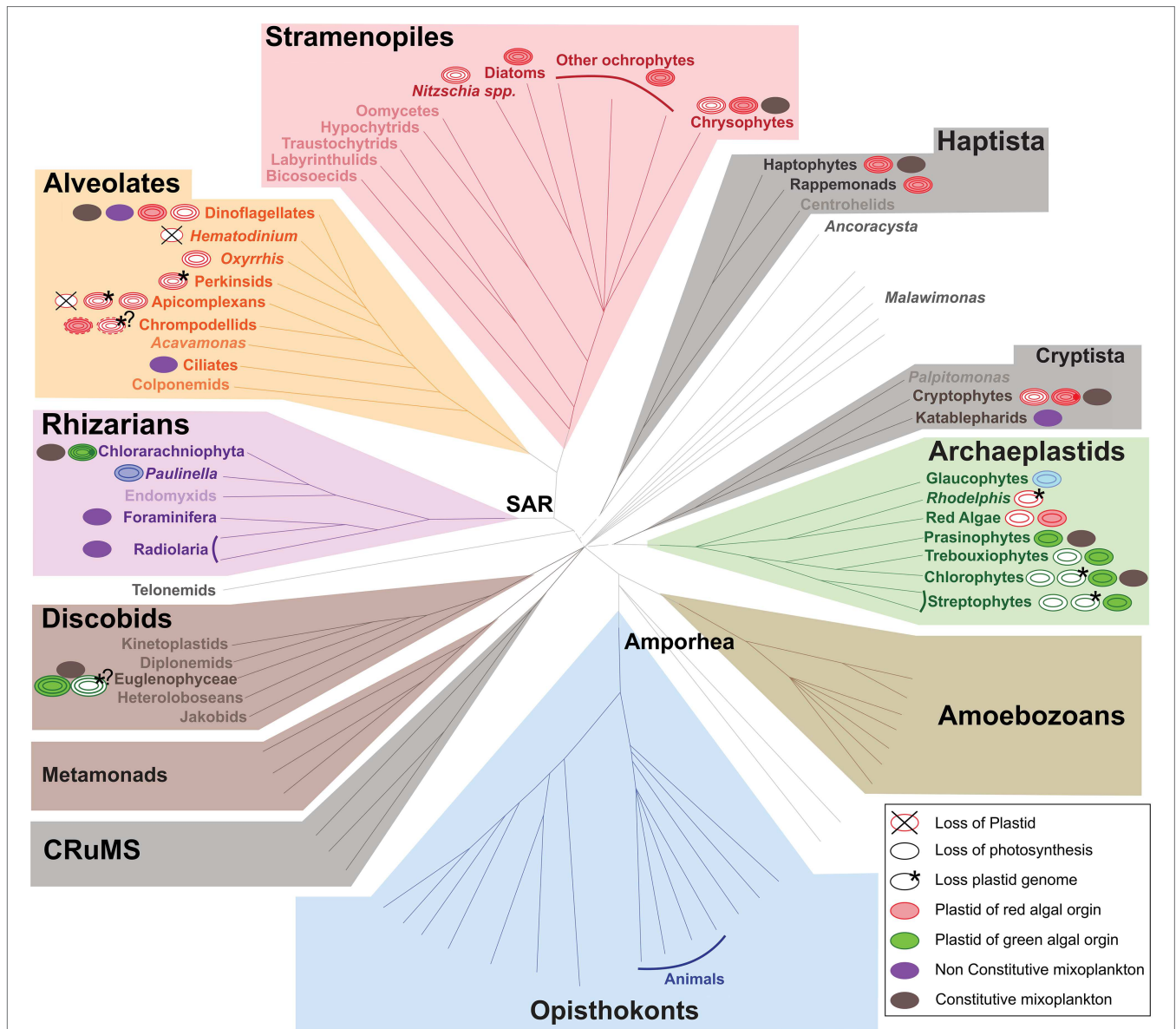


FIGURE 1 | Distribution of (non-)photosynthetic plastids and mixoplankton among eukaryotes. The schematic representation of the eukaryotic tree of life shows the distribution of plastids and protist mixoplankton among major taxonomic lineages. The tree topology is based on (Keeling and Burki, 2019). Dashed gray lines of certain deep branches indicate yet unclear relationships. Mixoplankton indicated with a purple non-constitutive mixoplankton (NCM) or dark gray constitutive mixoplankton (CM) circle is attributed if at least one member of the lineage can be indicated as such, this does not exclude that other taxa in the lineage use trophic modes such as purely heterotrophic (phagotrophic) or phototrophic. The focus here is on mixoplankton, hence kleptoplasty and photosymbiosis in animals is not indicated. Plastids and their origins are indicated by a circle, primary plastids are bounded by two membranes, while secondary, tertiary, or alternatively quaternary plastids (complex plastids) are bounded either by three or four membranes as schematically shown by the number and color of circular lines. The primary plastids, arising from a single primary endosymbiosis, of Archaeplastida including glaucophytes (bright blue), red algae (red), green algae, and land plants (green) are bounded by two membranes (two circular lines). The plastid of *Paulinella chromatophora* (Rhizaria) represents an example of another independent primary endosymbiosis, and is also depicted bound by two membranes (dark blue). Complex plastids of red algal origin can be found in Stramenopiles (plastids bounded by four membranes), Alveolata (plastids bounded by three or four membranes), haptophytes and cryptophytes (both containing plastids bounded by four membranes). Both photosynthetic and non-photosynthetic plastids can be found among Stramenopiles, dinoflagellates, chrompodellids, and cryptophytes. Plastids present in Apicomplexa and perkinsid taxa, as well as *Oxhhmis* are all non-photosynthetic (uncertain number of membranes). Chlorarachniophyta (Rhizaria; plastids bounded by four membranes) and Euglenophyceae (Discobids, Excavata; plastids bounded by three membranes) arose via two independent secondary endosymbioses of green algae. Evidence for the loss of photosynthesis and retention of non-photosynthetic plastids exists among Euglenophyceae (white circle, three green circular lines). Nucleomorphs, leftover nuclei of endosymbionts, are present between the second and the third plastid membranes of Chlorarachniophyta (dark green dot) and cryptophytes (dark red dot). Complete plastid loss (crossed circles) is found in some Apicomplexa and dinoflagellates, while genome-less non-photosynthetic plastids occur among perkinsids, and *Rhodelphis* (asterisk) and likely also among chrompodellids and Euglenophyceae (asterisks with question marks). The outermost fourth membrane of chrompodellids is indicated by a dashed circular line, because it is yet uncertain if colpodellids have three or four membranes. Figure modified from Keeling and Burki (2019) with permission from Elsevier. Plastid details are mainly derived from Hadariová et al. (2018) and Sibbald and Archibald (2020), see also **Supplementary Table 1**.

state between stable evolutionary states. Given the driving force of a changing environment in protist evolution, we further discuss environmental factors that have an impact on mixoplankton and could explain their current prevalence and success.

EVOLUTION OF PLASTIDS IN RELATION TO MIXOTROPHY

Eukaryotic life as we know it today is very likely only possible due to phagocytosis (Yutin et al., 2009). Many eukaryotic cells still possess the mechanisms for phagocytosis, that is, the engulfment and internalization of particles with a diameter bigger than 0.4 μm (Haas, 2007). Phagocytosis facilitated the evolution of permanent plastids. However, how and when phagocytosis first evolved remains a major question in evolutionary biology (as discussed in Mills, 2020) and many theories have been proposed about explaining its connection to eukaryogenesis and organellogenesis (Sagan, 1967; Martin and Müller, 1998; Cavalier-Smith, 2002; Lane, 2005; Koonin, 2010; Martijn and Ettena, 2013; Booth and Doolittle, 2015; Hampl et al., 2019). These theories are mainly orientated toward the evolution of mitochondria and will not be treated in further detail here. Phylogenetic analyses have shown the high diversity of the molecular systems involved in phagocytosis and indicate that from early phagocytosis-like engulfment modern-type phagocytosis has independently evolved within many lineages (Yutin et al., 2009). Regardless of how and when phagocytosis first appeared, it is a trait retained by a considerable portion of marine unicellular life and plays a crucial role in ecosystem dynamics (without it, there would be no microbial loop).

The primary source of photosynthesis in eukaryotes is generally agreed upon to be established by the uptake and permanent retention of a photosynthetic cyanobacterium by a eukaryote – “primary endosymbiosis” (Schimper, 1883; Mereschkowsky, 1905; Cavalier-Smith, 1987; Zimorski et al., 2014). In essence, this resulted in the first mixotroph, capable of ingestion and photosynthesis. This primary endosymbiosis gave rise to Archaeplastida, and subsequent evolution of the plastids found in both plants and algae (with exception of the recent primary plastid acquisition of *Paulinella*, **Box 1**; **Figure 1**; Rodríguez-Ezpeleta et al., 2005; Adl et al., 2012; Jackson and Reyes-Prieto, 2014). For discussions on the monophyly, or polyphyly of Archaeplastida, see e.g., Larkum et al., 2007; Howe et al., 2008; Kim and Maruyama, 2014. Subsequent events of secondary and tertiary symbioses (uptake of eukaryotic alga with a primary plastid and secondary plastid, respectively) in eukaryotic algae have spread chloroplasts throughout the (eukaryotic) tree of life (see also Keeling, 2013 and references therein). To this day, it remains unresolved how many independent secondary and tertiary endosymbiotic events have occurred (Sibbald and Archibald, 2020).

Endosymbiont Gene Transfer for the Establishment of Permanent Plastids

Endosymbiosis has indisputably played a critical role in the evolution of eukaryotes and cellular plastids (reviewed in

Keeling, 2013). However, the distinction between endosymbionts and permanent plastids or organelles has become constantly more blurred (Theissen and Martin, 2006; Keeling et al., 2015). In the current review, endosymbionts are considered “organisms non-permanently and autonomously living within their host – they keep their organellar integrity and are spatially separated from the host.” The symbiosis can be beneficial for both host and symbiont, and the endosymbionts are often still viable outside of their host. To be able to discuss endosymbionts in the context of mixoplankton classifications and ecology this definition of an endosymbiont should be considered. The reader, though, needs to be aware that the difference between an endosymbiont and a permanent organelle is all but clear-cut – with various examples discovered that bridge somewhere between the two concepts.

In the evolutionary context, a permanent plastid is the result of endosymbiosis and is stably maintained in the host organism over long periods of evolutionary time. A permanent plastid is not established simply through the engulfment of another alga. For the establishment of permanent plastids (organellogenesis), it is considered a prerequisite that genes for plastid functioning are transferred (from the endosymbiont) and integrated into the host nucleus, conjointly with a reduction of the endosymbiont plastid genome, and the establishment of a protein-targeting system to move nuclear-encoded proteins into the plastid (Larkum et al., 2007; Zimorski et al., 2014; Archibald, 2015). The transfer of genes from the endosymbiont to the host nucleus is known as EGT (Timmis et al., 2004). EGT allows the establishment of a genetic connection between the functions of host and symbiont. Before plastid retention, maintenance, and continuity are achieved EGT or gene loss can total up to 90% of the endosymbiont genome (Archibald, 2015; Qiu et al., 2017). In effect, most of the transferred genes are not involved in processes associated with photosynthesis or plastid maintenance, but in other essential biosynthetic pathways. Loss of such genes creates increased metabolic integration in the host.

BOX 1 | *Paulinella*.

The case of the photosynthetic euglyphid testate amoeba *Paulinella chromatophora* (Cercozoa, Rhizaria) is an interesting one. First discovered in 1894 by Robert Lauterborn, *P. chromatophora* was found to have one or two kidney-shaped intracellular symbionts per cell, and unlike its sister species does not seem to feed on cyanobacteria but relies solely on photosynthesis (Nowack et al., 2008). The symbionts, now called chromatophores or cyanelles, were found to be related to *Synechococcus/Prochlorococcus* and function as “normal” plastids (Kies and Kremer, 1979; Marin et al., 2005; Yoon et al., 2006). Furthermore, the cyanelles have a significantly reduced genome, though less than canonical plastids, and also divide synchronously with the host (Kies and Kremer, 1979; Marin et al., 2005; Yoon et al., 2006). Besides the phylogenetic origin, the different origin of cyanelles is further supported by the distinct protein targeting mechanisms used by cyanelles and plastids of Archaeplastida (Marin et al., 2005; Nowack and Grossman, 2012; Nowack, 2014). With evidence of endosymbiont gene transfer (EGT) and protein trafficking, the cyanelle can be considered an organelle, though at a more recent evolutionary stage than canonical plastids, due to its relatively large genome and the thick wall still surrounding it (Nakayama and Ishida, 2009; Nowack, 2014). *Paulinella chromatophora* is now considered the most recent and only known case of independent primary plastid acquisition, other than the Archaeplastida plastids, making it a model organism for understanding the evolution of primary endosymbiotic events.

Why EGT to the Hosts' Nuclear Genome?

Incorporation of genes into the nuclear genome could impart the selective advantage of decreased mutation by moving the genetic material away from the reactive oxygen species producing plastids (Allen and Raven, 1996). For organellar genes, which are present in relatively small copy numbers, detrimental mutations would spread quickly. Nuclear genes have the advantage of sexual recombination, which could aid in the repair of mutations (whereas there are no repair mechanisms in organelles) and improve fitness in ever-changing environments. The advantage of less genetic material at the plastid site is proposed to further enhance the plastids metabolic efficiency by limiting the volume occupied by DNA and ribosomes (Cavalier-Smith, 1987; Timmis et al., 2004).

Why Keep Genes in the Plastid?

A hypothesis proposed by Allen (1993), known as the co-location (of gene and gene product) for redox reaction (CoRR) hypothesis, attempts to explain why any genes are left in the plastids at all. The underlying concept behind this hypothesis is that core regulatory plastid genes have an advantage by remaining in the plastid genome. In prokaryotes, which are the origin of plastids, the redox state can regulate gene expression. The close spatial contact of genes and their product in the same intercellular compartment permits immediate feedback and regulation after a change in redox state in the light reaction centers of chloroplasts, or the mitochondrial oxidative phosphorylation system (Allen, 2017). Indeed, genes found in the organelles are essential for the proper functioning of the electron transport chain of the photosynthetic reaction centers of chloroplasts or the oxidative phosphorylation pathway in mitochondria (Pfannschmidt et al., 1999; Allen and Martin, 2016; Allen, 2017). For example, as shown in extracted chloroplasts, *in vitro*, there is direct and rapid redox control of chloroplast transcription at the plastoquinone site, more rapid than possible by comparable nuclear genes (Pfannschmidt et al., 1999). Björkholm et al. (2015) further proposed that selective pressure on highly hydrophobic membrane proteins caused these genes to remain in plastid genomes.

How Are Imported Gene Products Targeted to Their Destination?

Crucial for the establishment of permanent plastids is the targeting of nuclear-encoded genes toward the plastid. von Heijne (1986) hypothesized that the hydrophobicity of nuclear precursor products would pose issues in endo-cellular protein transfer among cellular components. Due to hydrophobicity, protein targeting to the plastid could be misdirected toward the wrong cellular compartment (i.e., the endoplasmic reticulum; Björkholm et al., 2015). As a result, transport of proteins would be the main obstacle for effective EGT. Yet, many examples exist of nuclear-encoded hydrophobic proteins directed to the plastids. Proteins of the light-harvesting chlorophyll *b* or fucoxanthin chlorophyll *a/c* are all hydrophobic and need to move across several membranes before reaching

the thylakoids (Allen and Raven, 1996). In effect, it is not only that genes need to be transferred to the host nucleus, but also maybe more importantly, transporter and protein-targeting systems need to be established. Arguably, this is the most complex and critical step toward the establishment of permanent plastids (Cavalier-Smith, 1999; Bodył et al., 2009).

Briefly, in early evolution, protein targeting could have been achieved by early forms of the complex TIC and TOC plastid translocons of the inner and outer chloroplast membranes, respectively (Bodył et al., 2009). The subunits of TIC-TOC translocons suggest a diverse origin, with genes involved from both prokaryotic (mainly cyanobacterial) and eukaryotic origin (reviewed in Reumann et al., 2005). Further targeting mechanisms involve the transit peptides on most nucleus-encoded proteins, which serve as a signal for import to a specific cellular component. Proteins can be targeted to, and recognized by, the plastid before being post-translationally imported through the TIC-TOC translocons. Additionally, this allows import through an endomembrane system involving the endoplasmic reticulum and Golgi system, further facilitating flexibility to target multiple cellular locations (Bodył et al., 2009). Whether the initial system and driver of plastid evolution revolved around a TIC-TOC-like system or an endomembrane system is not generally agreed upon (Cavalier-Smith, 2006; Bhattacharya et al., 2007; Bodył et al., 2009).

What Are the Actual Origins of Imported Nuclear Genes?

Recently, the interestingly coined “shopping bag model” hypothesized that nuclear genes for plastid proteins encompass varying phylogenetic origins, and builds on the fact that protists readily take up cytosolic DNA into their nucleus (Larkum et al., 2007; Howe et al., 2008). This DNA can remain for significant periods of time. DNA from lysed plastids will thus not unlikely result in integrations of plastid DNA into the nuclear genome. Before the final establishment of a permanent plastid, there could thus have been genetic contributions of many different origins over time. Transient relations like kleptoplasty, where a plastid is only temporarily retained (more in section “Temporary plastids: On their way to becoming permanent?”), could result in DNA entering the host nucleus. The kleptoplastic dinoflagellate *Dinophysis*, or likewise the Ross Sea dinoflagellate, which itself does not harbor a permanent plastid, does harbor genes of diverse phylogenetic origin encoding for plastid-related proteins (Hehenberger et al., 2019; Hongo et al., 2019).

If a stable plastid were to be established, the genetics underlying the plastid machinery would finally be a mixture of the current stably established plastid and from previously acquired DNA. Cases of such chimeric genomes can be found in a great diversity of taxa (Dorrell et al., 2017). Certain dinoflagellates, for example, express isoforms for plastid-targeted proteins from several different phylogenetic origins, proteins such as cysteine synthase and psbU (*Karlodinium*, Patron et al., 2006), or isoprenoid and heem biosynthesis (*Dinophysis*, Hongo et al., 2019). Likewise, for the diatom genome, Morozov and Galachyants (2019), and earlier cases discussed in Dagan and Martin (2009)

and Deschamps and Moreira (2012), illustrated supposed ancient gene transfers from green algae, in addition to genetic information from the current red algal plastid.

Eukaryotic cells readily take up DNA into the nucleus. Obviously, though, not all foreign DNA is integrated, nor do all endosymbionts become permanent plastids. The conversion of an endosymbiont to permanent organelle is a long evolutionary process that requires specific and complex protein transport mechanisms. The simple transfer of genes is not enough. The apparent complexity of the needed protein transport mechanisms makes it that plastids are less likely to become permanent and be sustained, than is endosymbiosis or temporal plastid retention in the host.

Secondary Loss of Trophic Functions Photosynthesis

The acquisition of photosynthetic ability is considered to be well established in (plankton) evolution, yet, it is by no means always permanent (Cavalier-Smith, 1987). Secondary reduction of photosynthetic plastids has been recorded many times. When heterotrophy is retained, phototrophy may not be essential to a cell's survival anymore. Consequently, the loss of a plastid can occur when the ecological situation changes and the functions of the plastid are no longer entirely needed, or even potentially detrimental (Williams and Keeling, 2003; Burki, 2016). Transcriptomic surveys of heterotrophic and mixotrophic chrysophytes have revealed genetic adaptations to a gradual loss of chloroplasts (Beisser et al., 2017; Graupner et al., 2018). The gene expression in these cases tends to be downregulated for photosynthesis-related processes. The gradual reduction of plastids, both in genome and size, leads to the formation of non-photosynthetic structures that could be described as "cryptic" plastids (reviewed in Hadariová et al., 2018).

Non-photosynthetic plastids are not uncommon and have been recorded across the eukaryotic tree, from Alveolata and Stramenophiles to cryptophytes, Euglenophyceae, red and green algae, as well as (parasitic) land plants (Hadariová et al., 2018; **Figure 1**). For example, several diatoms, mostly of the genus *Nitzschia*, are apochlorotic, that is with non-photosynthetic plastids (Li and Volcani, 1987). Though the plastids are genomically reduced and no longer photosynthetically active, transcriptomics show that the plastids still play an indispensable role in among others glycolysis and gluconeogenesis (Kamikawa et al., 2017). The reduced chloroplasts—the apicoplasts—of plasmodium parasites no longer function for photosynthesis but carry out other biosynthetic processes for which the cell is dependent on the plastids (McFadden and Yeh, 2017; Janouskovec et al., 2019). Likewise, the recently described phagotrophic genus *Rhodolphis* was found to still host cryptic plastids involved in heem synthesis (Gawryluk et al., 2019). Here, the involvement in the heem synthesis pathway is likely the reason the plastids have not been entirely lost.

Even though reduction of plastids has been reported in many taxa, the complete loss of a plastid seems more difficult

due to the importance of the plastid in many biochemical/metabolic pathways (Barbrook et al., 2006). Though it is rare, cases of complete plastid loss have been suggested for taxa belonging to oomycetes, ciliates, and dinoflagellates (Saldarriaga et al., 2001; Archibald, 2008; Reyes-Prieto et al., 2008). In the case of ciliates, the presence of proteins of plastid-origin suggests gene transfer from either algal prey or a putative photosynthetic history; however, in most cases evidence of a plastid harboring ancestor is not clear (Reyes-Prieto et al., 2008). Complete plastid loss is only unambiguously defined for several apicomplexan group parasites, e.g., *Cryptosporidium* and *Hematodinium* (Abrahamsen et al., 2004; **Figure 1**). While apicomplexans are evolutionarily descended from a mixotroph through the primary endosymbiotic event, the current parasitic live style could have been a major cause for the loss of dependency on the photosynthetic functions of the plastid (Archibald, 2015). *Hematodinium*, and also Amoebozoa, independently retain limited functions from their ancestral plastidic pathways, but as they live and fulfill their metabolic needs from their hosts the plastid would be redundant and is lost entirely (Gornik et al., 2015; John et al., 2019). Interestingly, free-living organisms tend to retain their plastid, possibly indicating that replacing lost metabolic pathways is more challenging (Janouskovec et al., 2017). Some cases are also known for dinoflagellates where, over evolutionary time, plastid loss is followed by the replacement with another (Keeling, 2013). This shows the relevant adaptability and evolutionary transitions between nutritional modes as a response to changing environmental factors.

Phagocytosis

In essence, all eukaryotic microalgal lineages (e.g., cryptophytes, haptophytes, Euglenophyceae, Stramenophiles, or dinoflagellates) have the capacity of predation, though it may have been lost in species of each lineage. Phagocytosis was lost on multiple occasions, proposed as owing to the lack of need for this mode of nutritional uptake, i.e., when photosynthetic plastids were acquired. Indeed, extant red algae or glaucophytes harboring primary plastids, as well as diatoms, have lost their phagotrophic ability (Raven et al., 2009). Phagocytosis is most often kept in those taxa harboring secondary or tertiary plastids – many of which are mixoplankton. The fact that it is specifically those species with secondary and tertiary plastid that retain phagotrophy has been hypothesized to be an artifact of time (Kim and Maruyama, 2014). That is to say, these secondary plastids species are younger and current selective pressures keep these species mixotrophic, whereas this might not have been the case after the establishment of primary plastids.

Temporary Plastids: On Their Way to Becoming Permanent?

"The mitochondria and plastids we see today may, accordingly, have only been the luckiest of a longstanding series of doomed endosymbionts who were saved by transfer of genes to the nucleus." – Keeling et al. (2015)

GNCM and pSNCM: Stolen Plastids

Unlike a permanent plastid, a stolen plastid or kleptoplast is transient. Kleptoplasty refers to the acquisition of solely the plastid from a plastid-containing prey. Kleptoplasty is a relatively common phenomenon that has been observed in various protists taxa including dinoflagellates, ciliates, and Foraminifera (Stoecker et al., 2009; Pillet and Pawlowski, 2013; Park et al., 2014). An exceptional case of animal kleptoplasty is of sacoglossan sea slugs (Pierce et al., 2003) and some flatworms (Van Steenkiste et al., 2019). The critical aspect of the kleptoplasty definition is that plastids remain only transiently functional within the kleptoplastic host. Depending on the taxa, the stolen plastids exhibit a wide range of origins and varying retention times. Retention time can be from days to months, after which the photosynthetic activity is lost and/or the plastid digested. Both the ability of the host to control the upkeep of the plastid, and the inherent stability of the original plastid can affect the retention time (Green et al., 2005). Even though kleptoplasts can have a positive impact on the energy budget of the host, there are also “side effects” due to the functioning of kleptoplasts. The host has to deal with the stress invoked due to the generation of reactive oxygen species as well as maintain the plastid with the perspective of assuring its functionality (Uzuka et al., 2019).

Studies of the *Dinophysis*-*Mesodinium*-Cryptophyta complex have contributed substantially to our understanding of the dynamics of kleptoplasty and the route toward a potential tertiary plastid establishment. Kleptoplastidic *Mesodinium* sp. (ciliate) does not only steal the plastid (kleptoplasts) from its cryptophyte prey but also the nucleus (kleptokaryon; Hansen et al., 2013, 2016). The kleptoplastids significantly contribute to the energetic budget of the cell with a large proportion of the total carbon needs (Hansen et al., 2013). The ability to retain fully functional plastids for a long period of time is in large part due to the additional retention of the prey nucleus (Johnson et al., 2007; Kim et al., 2017). The kleptokaryon becomes enlarged, and recent advances in transcriptomic and genomic data from both the ciliate and cryptophyte suggest that the sequestered nucleus is transcriptionally active and could account for approximately half of the total transcriptome of the ciliate (Altenburger et al., 2020). The kleptokaryon expresses genes responsible for both the maintenance of chloroplasts and the biosynthesis of metabolites for which *Mesodinium* lacks the genetic toolkit (Lasek-Nesselquist et al., 2015; Kim et al., 2016). This allows *Mesodinium* to replicate and exploit the plastids for a few months before being degraded (Smith and Hansen, 2007; Hansen et al., 2013). Interestingly, no photosynthesis-related genes were found to be transcribed by the genome of the ciliate (Altenburger et al., 2020). Instead, differential gene expression analysis indicates *Mesodinium* alters the gene expression of the kleptokaryon compared to when the nucleus is in its original host (Lasek-Nesselquist et al., 2015; Kim et al., 2016).

Kleptoplasts and kleptokaryon usage have also been observed in the (freshwater) dinoflagellate *Nusuttodinium aeruginosum* (Onuma and Horiguchi, 2015). The nucleus of cryptomonad origin undergoes extensive remodeling, accompanied by the

enlargement of the kleptoplast (Onuma et al., 2020). The remodeling includes polyploidization, upregulated gene expression of pathways that involve among others, metabolism, gene translation, and DNA replication, as well as downregulation of certain genes like those involved in motility. In both *Mesodinium rubrum* and *Nusuttodinium aeruginosum* the transcriptional regulation of the kleptokaryon is no longer affected by light-regime. These transcriptional changes, and especially polyploidization, are common ground among kleptoplastic organisms and are also seen in permanently established plastids (Bendich, 1987). This suggests that polyploidization and transcriptional regulation could be a prerequisite in plastid evolution and prospective organelles. These modifications are also observed in the permanent diatom endosymbiont of *Durinskia baltica* – made possible by its polyploidy – the diatom nucleus can undergo karyostenosis during cell division (Tippit and Pickett Heaps, 1976; Yamada et al., 2019).

Dinophysis (Dinoflagellata) are known to sequester plastids of cryptophyte origin, but not the nucleus (Park et al., 2014). The difference to other kleptoplastidic organisms is that in this case the acquisition is indirect and solely after the consumption of *Mesodinium* sp. (note that *Mesodinium* sp. itself has a kleptoplast; Park et al., 2014; Hansen et al., 2016). Several *Dinophysis* nuclear transcripts are involved in photosynthesis-related processes including plastid maintenance or pigment biosynthesis (Hongo et al., 2019). Even though the acquired plastids originate from a cryptophyte, genes involved in their maintenance originate from: haptophytes, dinoflagellates, chlorarachniophytes, cyanobacteria, and cryptophytes (Hongo et al., 2019). This indicates the complexity of gene transfer to the nuclear genome of the host and gives an idea about their evolutionary past, and previous interactions, and also advocates for the “shopping bag” hypothesis (see section “Endosymbiont gene transfer for the establishment of permanent plastids”). The aforementioned NCM highlight different methods for the control of acquired plastids. The first one involves the acquisition of the prey nucleus, which is actively expressed and allows extended use and even replication of the kleptoplasts, without EGT of plastid related genes (the case of *Mesodinium*). The second strategy does involve EGT. Host-encoded genes facilitate extended use of the plastid, and possible plastid division, instead of a kleptokaryon (the case of *Dinophysis*; Rusterholz et al., 2017). The incapability to enslave the nucleus of the prey could have resulted in stronger selective forces for EGT. Yet, both strategies ultimately yield an increased survival in absence of food (Hansen et al., 2013), and could potentially evolve host-governed organelles.

A recent study by Hehenberger et al. (2019) has provided substantial insights into the fine lines between temporary and permanent plastids. The kleptoplastic Antarctic Ross Sea dinoflagellate belongs to the Kareniaceae lineage, but unlike its sister taxa, it does not have permanent plastids (Gast et al., 2007). The unusual long retention (up to 22 months) of the kleptoplast in the host suggests the presence of genes to stabilize the plastid (Sellers et al., 2014). Transcriptomic analysis of the Ross Sea dinoflagellate revealed host-encoded genes for

kleptoplast-targeted proteins (Hehenberger et al., 2019). This includes photosynthesis related genes that are also found in permanent plastids harboring relatives of the Ross Sea dinoflagellate. Interestingly, such plastid-targeted genes appear to come from various phylogenetic sources, the majority of which do not share origin with the kleptoplast, indicating ancestral establishment of plastid-targeting mechanisms. The early establishment of such mechanisms would facilitate the further usage and possible integration of subsequent plastids (of different origin), such as the haptophyte kleptoplast of the Ross Sea dinoflagellate. A critical factor for the permanent integration of the kleptoplast, as indicated in Hehenberger et al. (2019), is the level of transcriptional regulation of the host on plastid-targeted nuclear genes. The Ross Sea dinoflagellate only has transcriptional regulation for a subset of plastid-related genes, as depicted by the response (or lack thereof) to different light and temperature conditions. Indications of the establishment of transcriptional regulation mechanisms, which are important for the control of modern-day plastids, would suggest progress toward permanent plastid integration.

eSNCM: Plastids Through Photosymbiosis

The internalization of a phototroph by a heterotrophic organism characterizes one of the first steps toward a permanent plastid (section “Endosymbiont gene transfer for the establishment of permanent plastids”). Many extant examples exist of such endosymbioses, without *per se* being permanent plastids (reviewed in Stoecker et al., 2009). Upon entering a host cell an endosymbiont is encapsulated in a vacuole-like unit called a symbiosome. Endosymbionts can (most of the time) divide within the host, foregoing the need for continuous replenishment of photosymbionts. Well-known endosymbioses are cnidarians, like corals, with dinoflagellate endosymbionts. Other (photo)endosymbioses include among others: marine Rhizaria, bivalves, and gastropods with dinoflagellate symbionts; Acantharia with haptophytes and a dinoflagellate (*Noctiluca scintillans*) with green prasinophyte algal symbionts (*Pedimonas noctilucae*; Anderson, 2012; Decelle et al., 2015; Clavijo et al., 2018).

In a photosymbiosis (or other endosymbiosis), where the symbiont provides energy or photosynthates, a prerequisite for a stable relation is that the interaction is beneficial to the host. The host must be dependent on the symbiont, otherwise, the symbiont would be expendable and the relation forfeited. The relation would thus naturally be driven toward exploitation of the symbiont by the host (Keeling and McCutcheon, 2017). For the symbiosis to be evolutionarily viable to the endosymbiont it needs to be able to reproduce itself. Indeed, many photosymbionts have been extracted and cultured from their host systems, illustrating that they are capable of independent existence and reproduction (Trench and Thinh, 1995; Probert et al., 2014). However, this is not always the case, thus creating an evolutionary dead-end for the symbiont.

In the Acantharia-*Phaeocystis* symbiosis, the Acantharia host cell recruits environmental *Phaeocystis* as endosymbionts. The acquisition of symbionts is suspected to be purely horizontal, and symbionts need to be reacquired for each individual.

The symbionts *in hospite* are modified in several physiological aspects, among which are an increased number and volume of plastids, and more dense thylakoids, thereby increasing the photosynthetic efficiency (Decelle et al., 2019). The symbiosome of mature symbionts intrudes into the symbiont cell, further indicating a permanent change of the endosymbiont (Uwizeye et al., 2020). These modifications are thought to be a major reason as to why the symbionts are not viable after extraction from the host. The modifications made to the symbiont in this symbiosis show several similarities to the plastid acquisition of *Paulinella*, possibly representing steps toward more complete plastid integration. Genomic or transcriptomic studies of this symbiosis are still lacking; hence it remains unknown if there have been EGT events. Evidence of EGT could show further integration and hijacking of the functions of the symbiont besides the already observed modifications.

In endosymbiotic dinotoms – dinoflagellates in symbiosis with diatoms – like other endosymbioses, the symbiotic diatom is surrounded by a membrane, a symbiosome that separates it spatially from the cytosol of the host (Tomas et al., 1973; Jeffrey and Vesik, 1976). It should be noted that in this endosymbiosis, the diatom is not fully intact as it loses its silica frustule during uptake, and unlike a permanent plastid, genome reduction and EGT are lacking, and major cellular components of the diatom remain (Hehenberger et al., 2016; Yamada et al., 2019). The symbionts of endosymbiotic dinotoms, e.g., *Durinskia kwazulunatalensis*, *D. baltica*, and *Glenodinium foliaceum*, are structurally and transcriptionally autonomous from the host dinoflagellate and can replicate independently, yet DNA replication of the diatom endosymbiont seems to coincide closely with the cell division of the host (Figueroa et al., 2009; Yamada et al., 2019). This allows permanent retention of the diatom symbiont and vertical symbiont transfer. In contrast, in the kleptoplastidic dinotom *Durinskia capensis*, an internalized diatom gradually loses most of its organelles leaving only the plastids until those are also degraded (Yamada et al., 2019). The diatoms cannot be permanently retained as no nucleus control mechanisms are developed in the host, thus converting them into temporary kleptoplasts that will need to be reobtained in subsequent generations. The synchronized karyokinesis of host and endosymbiont, as in *D. baltica* or *D. kwazulunatalensis*, seems critical for the development of a more stable relationship between host and endosymbiont.

NCM as a Transition to Permanent Plastids

Bodył (2018) hypothesized that red algal derived secondary plastids, like those of dinoflagellates, evolved not necessarily by phagocytotic uptake, but *via* kleptoplastidy. In fact, it can be proposed that many of the previously explored kleptoplastidic and endosymbiotic relations are in effect new plastids *en route* to becoming permanent plastids, a “work in progress” situation. The establishment of permanent plastids is preceded by genomic reduction, and increased control of the host on its symbiont to the point that the symbiont is no longer able to reproduce *in hospite* nor *ex hospite* once released from the host. Progressively there would be increased genetic integration (EGT) of

photosynthetic genes from the transient symbiont/kleptoplast associations (see targeting-ratchet model in Keeling, 2013). *Dinophysis* and *Mesodinium* both use a kleptoplast obtained from the same source, though EGT has yet only occurred in *Dinophysis*. Apart from EGT, the Ross Sea dinoflagellate exemplifies the importance of establishing transcriptional regulation mechanisms for transferred genes. The acantharian symbiont *Phaeocystis* has already been suggested to possibly be a form of kleptoplasty instead of symbiosis, due to the restrictions in proliferation and modifications on the symbiont (Decelle et al., 2012, 2019). Similar modifications are observed for the kleptoplast of *Nusuttodinium*. Dinotoms have varying levels of endosymbiont integration and karyokinesis in concert with their own (Yamada et al., 2019). Considering the insights into gene transfer, metabolic connectivity and protein-targeting between plastid/endosymbiont and host, we could hypothesize that kleptoplastic or endosymbiotic mixotrophs are an evolutionary intermediate toward a permanent plastid (Figure 2; Keeling, 2013; Keeling and McCutcheon, 2017; Hehenberger et al., 2019). However, this is not to say that all these systems are heading in the same direction, but could offer a chance to compare potential stages of evolving systems.

Alternatively, temporary plastids could be an advantageous adaptation as opposed to permanent organelles. Unlike genetic adaptation, and thus the establishment of permanent plastids, temporary plastids could allow for more plasticity within an environmental range. This could be thought of in light of Acantharia that acquire and maintain locally adapt *Phaeocystis* symbionts as directed by the environment (Decelle et al., 2012; Mars Brisbin et al., 2018). Corals can also shuffle their symbiont populations when stress events mandate it (Lewis and Coffroth, 2004; LaJeunesse et al., 2009, 2010). This allows the host to better adapt to changing environments by shuffling and swapping symbionts. Additionally, acquired plastids possibly impose less energy investment and could be converted into host biomass, whereas this is not possible for permanent plastids (Flynn and Hansen, 2013).

WHY, WHEN, AND HOW TO MIXOTROPH

Protists are often limited in their growth capabilities, pure phototrophs by nutrients or light, and pure phagotrophs by prey availability. This holds particularly true in oligotrophic

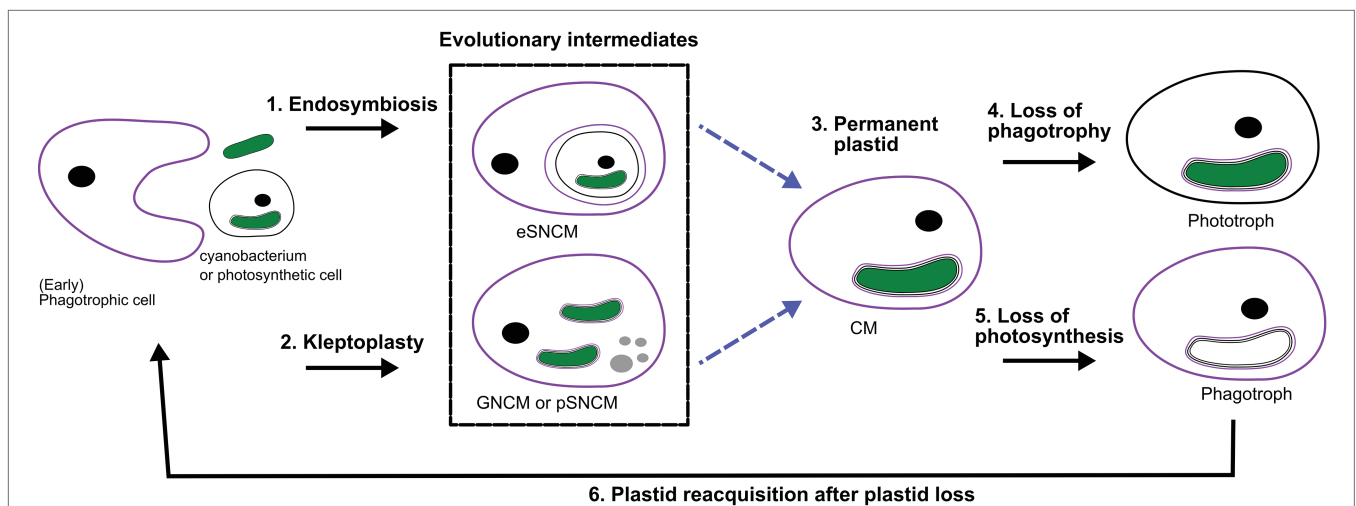


FIGURE 2 | Perspective of protist plastid evolution and the role of mixotrophy. Conceptual illustration of plastid evolution depicting non-constitutive mixoplankton as hypothetical intermediate stages to permanent plastids. The cell nucleus is shown as a black circle, kleptokaryons as gray circles, and photosynthetic plastids in green. For the initial primary plastid acquisition, the plastid came from a cyanobacterium (green oval; see also “Box 1 *Paulinella*” for a possible exception), the acquired primary plastid would be bound by only two membranes as depicted in the photosynthetic cell on the left. While complex permanent plastids gained by secondary or tertiary endosymbiosis are bound by three or four membranes, respectively as illustrated by the number of lines around the plastid. In secondary and higher plastid acquisition, the photosynthetic cell can be either a CM or phototroph with primary, secondary or higher-order plastid. Illustrated here is secondary plastid acquisition with the host membrane in purple. Blue dashed lines are the hypothetical route toward permanent plastid retention. (1) Uptake of a photosynthetic alga and internalization of the entire organism as a symbiont (in a symbiosome) e.g., *Radiolaria*, *Noctiluca*. (2) Kleptoplasty shows the phagotrophic uptake of photosynthetic algae (prey), keeping the chloroplasts temporarily functional. The photosynthetic prey can be with primary, secondary (or higher) plastids. For example, the kleptoplastic ciliates like *Strombidium* sp. In some cases, the prey nucleus (gray circles) is also retained e.g., *Mesodinium rubrum* (which feeds on secondary plastid holding cryptophytes), and *Nusuttodinium aeruginosum*. (3) The establishment of permanent plastids. Primary plastids by uptake of a cyanobacterium, with the plastid bound by only two membranes, e.g., as retained in most Archaeplastida including glaucophytes, red and green algae, as well as land plants and the more recent primary plastid of *Paulinella chromatophora*. Secondary plastids bound by three or more membranes are found in Euglenophyceae, haptophytes, cryptophytes, and SAR organisms. Tertiary plastid acquisitions have only been clearly documented in Dinoflagellates. (4) Indicated here is the secondary loss of phagotrophy, we assume all pure phototrophs lost phagotrophy somewhere along their phylogeny e.g., diatoms. (5) Loss of photosynthesis, though only in rare cases is the plastid completely lost, the non-photosynthetic plastid is depicted lacking green color. Evidence for such primary plastid loss is found in e.g., *Rhodolphis* sp., *Helicosporidium* sp. Loss of photosynthesis after secondary (or higher) permanent plastid acquisition can be found, for example, in some Euglenophyceae, Stramenopiles like apochlorotic diatoms, dinoflagellates, cryptophytes, perkinsids, and Apicomplexa like *Cryptosporidium*. Complete plastid loss can, for example, be seen in *Polytoma* sp., *Cryptosporidium*, and *Hematodinium* (see also Figure 1). (6) Plastid reacquisition after loss of phototrophy is only known in dinoflagellates.

ecosystems, where mixotrophy proved to be more beneficial (Stoecker et al., 2017). In such nutrient poor environments, mixotrophy can thus be especially widespread. Since mixoplankton can meet their metabolic demands through a mixture of photosynthesis and prey ingestion, they can supplement one nutrient source with another.

Trade-Offs

Even though mixotrophy offers flexibility in nutrient and energy acquisition, mixoplankton are not prevailing everywhere. Therefore, certain trade-offs (benefits and costs) to mixed nutrition seem apparent (Raven, 1997). Both phototrophy and phagotrophy involve mechanisms and structures that incur costs. In the case of a phototroph, this is primarily the maintenance of the photosynthetic machinery. For phagotrophs, it includes costs related to all the required mechanisms for the internalization of food particles and/or production of secondary metabolites, like toxins that mediate prey capture. Investments into the photosynthetic (or phagotrophic) machinery involve nutrient costs, estimated as up to 50% (or 10%) of the cell's nutrient currency (e.g., carbon, nitrogen, and phosphorus; Raven, 1984, 1997). Resources used to maintain chloroplasts could have otherwise been used for other processes, like growth or reproduction. This is likewise the case for traits associated with, for example, phagotrophy, dissolved nutrient uptake, prey detection, capture or defense (Andersen et al., 2015). This inevitably has an impact on the growth rate, as "costs" are to be paid in order to make use of each of these processes. Costs that are also incurred by the fundamentals such as DNA, RNA, and ribosome maintenance and multiplication (Flynn and Mitra, 2009; Stoecker et al., 2009; Ward et al., 2011).

Besides the basic trade-offs in cell maintenance, more plastid-specific trade-offs have also been researched. Giovanardi et al. (2017) showed more tightly compressed thylakoids in plastids of mixotrophic *Neochloris oleoabundans* than in autotrophically grown samples, thereby the compressed thylakoids would lose on fluidity. It has been hypothesized that more appressed thylakoids would preserve or delay the degradation of the photosystems (Giovanardi et al., 2017). However, in turn, decreased fluidity could impair plasticity for stressors such as temperature change (Mansour et al., 2018).

Along with phototrophy come high-affinity nutrient transporters for the import of dissolved nutrients into the cell. An increase in nutrient uptake sites for dissolved nutrients, facilitates higher affinity and an increase in nutrient uptake. Simultaneously, these sites could also be costly due to being potential entry points for viruses (Menge and Weitz, 2009). From that perspective, a lower affinity to dissolved nutrients could mitigate viral entry. For mixotrophs, the loss of these sites and the involved costs would be minimized when nutrient uptake can be achieved and supplemented through phagotrophy. Predation, in turn, requires encounters with other cells, which could also incur indirect costs due to increased encounters with potential predators (Broglio et al., 2001; Kiørboe, 2011). Phagotrophy would further exclude a rigid cell wall and thereby limit protection, as in diatoms with rigid cell walls but having lost phagotrophic capability.

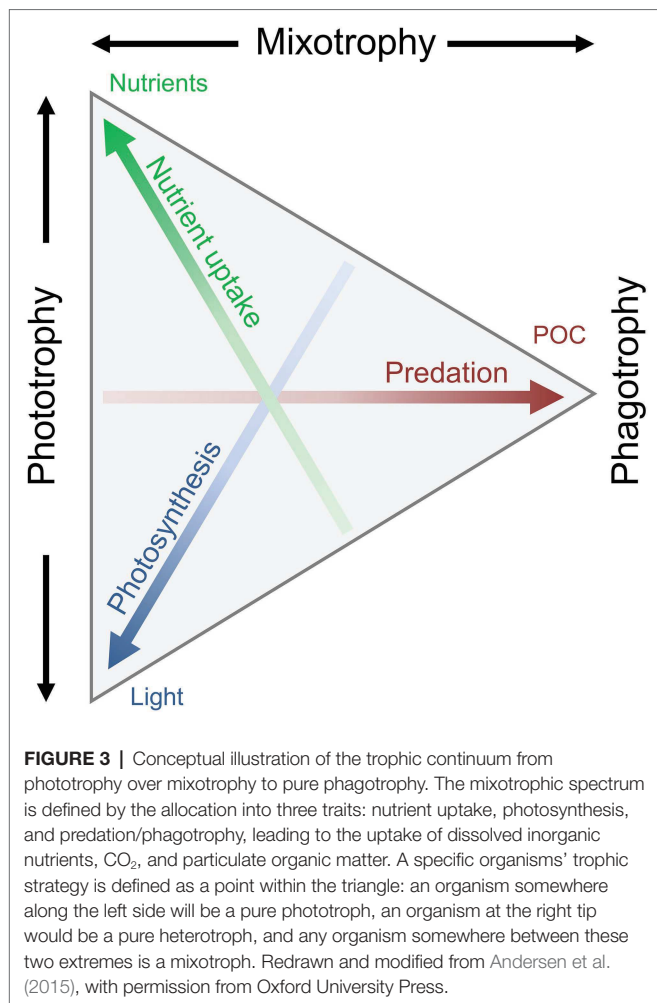
Mixotrophic Gradient Under Changing Biotic and Abiotic Factors

An increasing number of both field and laboratory studies have contributed to our understanding of the dynamics and different aspects of mixotrophy. A mixotrophic lifestyle is often flexible. The biological investment in phagotrophy or phototrophy can vary depending on the prevailing biotic and abiotic environmental conditions. The reliance on either photosynthesis or prey consumption can be partial or complete. We thus refer to a gradient of mixotrophy, toward either more phototrophy or phagotrophy, considering their relative contribution to an organism's metabolic needs (Figure 3). This mixotrophic spectrum is further affected by the degree of investment into nutrient uptake (Andersen et al., 2015), to which previously discussed potential trade-offs apply. How mixotrophy and mixotrophic communities change in response to environmental changes is a current scientific challenge (González-Olalla et al., 2019). Environmental conditions discussed here include light irradiance, temperature, and nutrients in the perspective of feeding and growth.

Light

The ability to photosynthesize prerequisites the availability of light in order to grow. Irradiance generally increases growth up to a point of saturation, though often the highest growth rates are achieved if prey is available (Li et al., 1999). There are, however, exceptions of mixoplankton that rely mainly on either photosynthesis (e.g., *Gymnodinium splendens*; Skovgaard, 2000) or phagotrophic feeding (e.g., *Fragilidium* sp. or *Ochromonas*; Skovgaard, 1996; Flöder et al., 2006). In these cases, mixotrophy seems to be a survival strategy for when a single trophic mode does not suffice (Keller et al., 1994; Flöder et al., 2006; Anderson et al., 2018), for example, during long polar winters (Stoecker and Lavrentyev, 2018).

Under low light conditions, two different isolates of *Ochromonas* showed contrasting physiological responses. Whereas one isolate moved toward an increased focus on photosynthesis by compensating the lower light intensity with more cellular chlorophyll *a*, the other isolate substituted the focus on photosynthesis with an increased rate of bacterivory (Wilken et al., 2020), as is similarly seen for *Heterocapsa rotundata* (Millette et al., 2017). Increased irradiance has been shown to cause a positive feedback chain for *Karlodinium veneficum*, where higher light increased photosynthesis as well as feeding rate; the increased phagotrophy in turn increased photosynthetic capacity (Li et al., 1999). In contrast, the feeding rate of *M. rubrum* is not affected by irradiance (Smith and Hansen, 2007). *Karlodinium veneficum*, and some other dinoflagellates, cannot grow (or are only sustained) in the dark even when prey is available, that is to say, it is an obligate phototroph. Other dinoflagellate species, or chrysophytes such as *Ochromonas* sp., can grow in constant darkness if supplied with food (Caron et al., 1993; Ok et al., 2019). Thus, predation can, but does not always, compensate for the inability to use chloroplasts in the dark. Fischer et al. (2017) investigated the effect of light on the success of mixotrophic flagellates, and showed



that mixotrophic bacterivorous flagellates prevail in high light and low nutrients conditions. Oppositely, pure heterotrophs and pure autotrophs prevail in low-light and nutrient-rich ecosystems.

Nutrients

Research has mostly focused on the availability of non-carbon elements such as nitrogen and phosphorus. When one or both of these nutrients are inadequate mixotrophy can be vital, as prey ingestion is the only alternative to obtain missing nutrients. Many examples are recorded of species feeding on either bacteria or eukaryotic prey under short- or long-term starvations of nitrogen and phosphorus. *Nephroselmis pyriformis*, for example, can achieve normal growth even when nutrient-limited by compensation *via* bacterivory (Anderson et al., 2018). Other seemingly non-phagotrophic species can be induced to perform phagotrophy by nutrient-limited treatments, e.g., in dinoflagellates (Smalley et al., 2003; Johnson, 2015), haptophytes (Chan et al., 2019), and cryptophytes (González-Olalla et al., 2019). The use of diluted media to provoke starvation indicates the complexity in understanding in detail the principal factors that could induce phagotrophy and identify mixotrophy.

Nutrients that are usually found in low concentrations, such as iron, micronutrients, and vitamins are mostly understudied (Anderson et al., 2018), but can have major effects on growth rates (Reich et al., 2020). It is believed that (N)CM obtain micro-nutrients mainly through the ingestion of prey (Hansen et al., 2019). However, there remains a lot to learn about nutrient acquisition dynamics in NCM, and the role of endosymbionts in acquiring dissolved nutrients.

Temperature

The general theory of metabolism in ecology suggests a shift to heterotrophy when temperature increases (Allen et al., 2005; Rose and Caron, 2007; Franzè and Lavrentyev, 2014). As in many biological systems, the relation of phagotrophy and temperature is Gaussian, and delimited by an organism's temperature tolerance. Higher temperature implies higher metabolic rates and concomitantly an increased need for energy, and possible stress incurrence. Studies have indeed shown higher ingestion rates in response to temperature increase in many species (Princiotta et al., 2016; Cabrerizo et al., 2019; Ok et al., 2019). This validates the applicability of the general theory of metabolism in marine protists. A combined increase of phagotrophy and a decrease in photosynthetic capacity with higher temperatures strongly decreased the relative contribution of phototrophy in mixotrophic *Ochromonas* sp., allowing growth rates to keep increasing under temperatures where photosynthetic growth rate already declined (Wilken et al., 2013). This effect of temperature on the autotrophic, mixotrophic, and heterotrophic growth of *Ochromonas* sp. has highlighted the trade-offs in its trophic strategy and temperature tolerance. The increased temperature can be considered as a stressor that needs to be alleviated by reduced photosynthetic activity, and/or compensated for with nutrients from phagotrophy (Cabrerizo et al., 2019). This might be achieved by using nutrients from phagotrophy to repair or maintain photosystems.

Role of Mixotrophy in a Future Scenario

We found the physiological research on mixoplankton is generally biased toward CM. Yet, within this group there is already a large taxonomic and physiological diversity resulting in ambiguous responses to environmental factors. Especially among dinoflagellates – which can be CM, NCM, pure phagotrophs, or pure phototrophs – there is a wide spectrum of responses to food availability and abiotic conditions (Hansen, 2011). Efforts to understand the effects of varying conditions, such as nutrients, light irradiance, temperature, and prey availability have given diverse results, thus making it difficult to highlight general patterns.

Changing environmental conditions can shift mixoplankton toward a higher prevalence of either phototrophy or phagotrophy (Figure 4). Such shifts have apparent effects on the plankton community composition and the energy transfer between trophic levels (Rose and Caron, 2007; O'Connor et al., 2009). Though not unambiguous, the general trends seem to show mostly a phagotrophic increase with increased temperature. Decreased nutrients can induce or promote phagotrophy, oppositely,

phototrophy seems preferred when sufficient nutrients are available. Whereas light is directly fueling phototrophy, it can promote both phototrophy and phagotrophy. In some cases, limiting inorganic nutrients is a critical factor for expressing mixotrophy, while in other cases mixotrophy is a de-facto state independent of nutrient regime (Johnson, 2015). The combination of low nutrients and high light is suggested to favor mixotrophy, as it is suboptimal for either pure phagotrophy or phototrophy (Mitra et al., 2014; Hansen et al., 2019). Seasonally such conditions can already show increased mixoplankton abundance, e.g., in summer (mature ecosystem states; Hansen et al., 2019). It has also been proposed that polar regions, characterized by extremes in solar

irradiance and nutrient-limitation, select for mixotrophy (Stoecker and Lavrentyev, 2018). The *grand écart* hypothesis proposed by Selsosse et al. (2017) further attempts to explain the ubiquity of mixotrophy. The open ocean ecosystem is usually limited in non-carbon elements, and summer stratification limits the recycling of sinking particles or nutrients back into the water column and upper layers. The biological carbon pump further exports carbon and other nutrients from the upper photic layers. This results in light being available in the upper layers, while other essential nutrients are separated toward deeper layers. This imbalance in resources (light and nutrients) favors and selects for mixotrophs that can supplement the lack of resources by feeding.

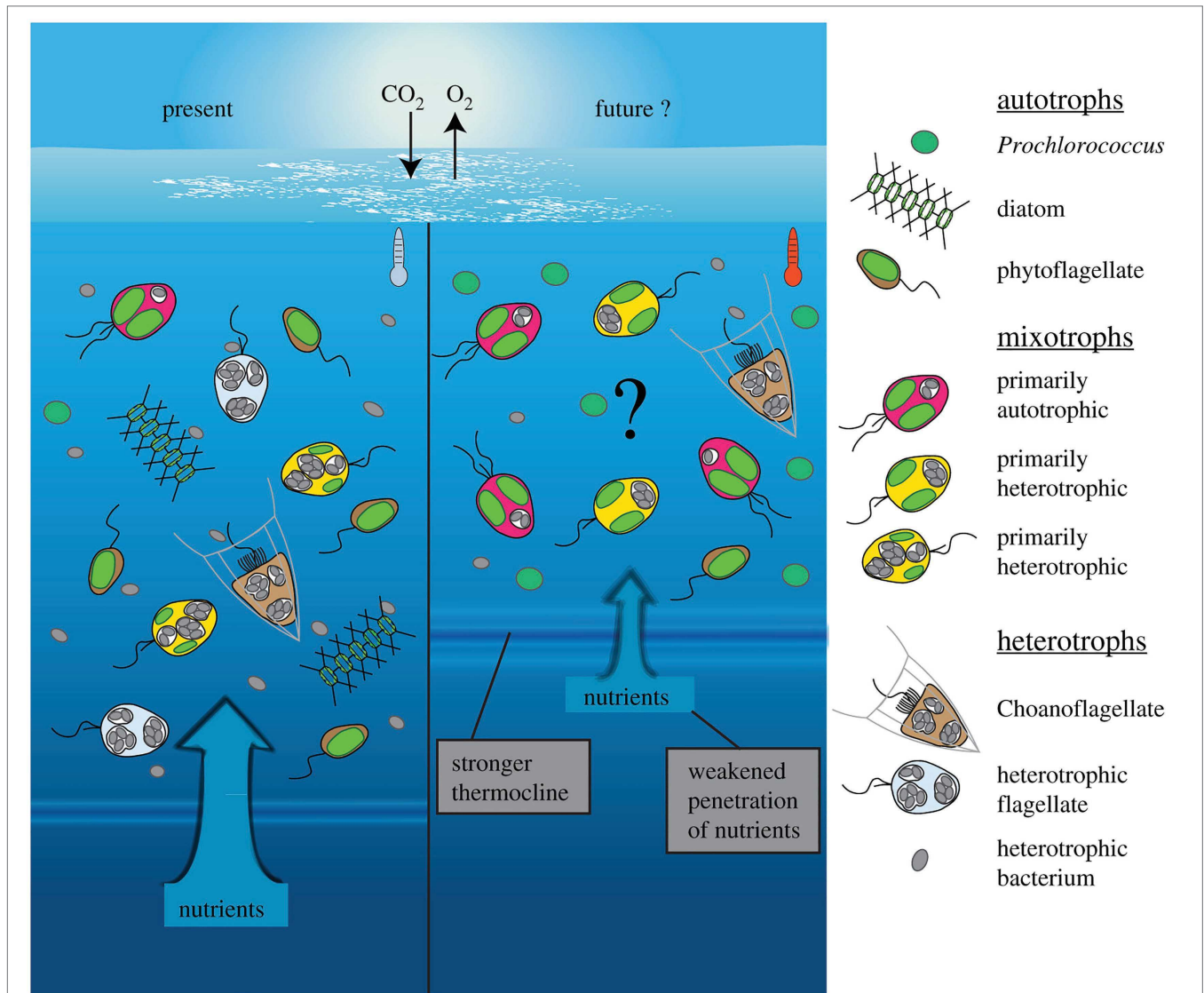


FIGURE 4 | Conceptual depiction of plankton community shift under a climate change scenario in the open ocean. Future changes involve warmer, more oligotrophic water and higher light irradiance, due to stronger water stratification and a shallower mixed layer depth (right). Protists with photosynthetic ability contain plastids (green), while phagotrophic ability is indicated by food vacuoles containing bacterial prey (gray). The limiting nutrients in this future scenario are expected to favor more nutrient competitive species like *Prochlorococcus* (cyanobacteria), while no generalized effects can yet be accurately predicted for mixoplankton. Generally, the flexibility in nutritional modes by mixoplankton renders them more competitive than pure photototrophs or heterotrophs, thus a general increase in relative mixoplankton abundance could be expected. Species-specific responses could shift over the mixotrophic continuum either toward more heterotrophy (in red) or more photosynthesis (in yellow). Reprinted from Wilken et al. (2019), with permission from Royal Society.

CONCLUSION

Phagotrophy rests at the origin of the different functional types of mixoplankton. The complete digestion of prey, the retention of prey organelles, or whole cells as endosymbionts indicates the diversity of responses after phagocytosis of “external” material. Constitutive mixoplankton benefits from having alternative ways of nutrient acquisition that each can be exploited under certain conditions. In non-constitutive mixoplankton, undigested organelles can either be perceived as the inability of the host to degrade (or digest) the organelles (incidental retention), or as the active retention of them for further use (deliberate retention). The longevity of an organelle within the host as well as the level of usage, integration, and connectivity is species-specific and variable (Gast et al., 2007; Stoecker et al., 2009; Yamada et al., 2019). The broad diversity in exploitation and handling of acquired organelles, as well as the acquisition and/or loss of phagocytosis or photosynthesis, is indicative of the adaptation of organisms to environmental conditions over their evolutionary history.

Mixotrophs with temporary plastids could depict evolutionary intermediates of permanent plastids (Figure 2). In species with temporary plastids, evolutionary force could still drive toward fixing phototrophic potential. That is, of course, given that the trade-offs for having potential for both photosynthesis and phagotrophy do not pose too strong a counterforce. With ever-changing environmental conditions, even seasonally, temporary plastids can give more flexibility by allowing a change to better-adapted plastids and are thereby more beneficial. Conversely, when either organic matter or light is constantly available, maintaining phagotrophy as well as photosynthesis can be costly. When the costs for maintaining multiple structures do not offset the benefits, evolution might be driven toward permanent plastids in lieu of temporary plastids, or toward pure heterotrophy. It is thus interesting to note that mixoplankton have been associated with oligotrophic environments (Mitra et al., 2014; Hansen et al., 2019), as the imbalance in resource availability “forces” more efficient use and alternative means of resource acquisition.

So far, eco-physiological studies to understand the role of environmental conditions in the prevalence of mixotrophy are mostly done on cultures. Many taxa thus remain understudied due to difficulties in culturing them. This is especially true for fragile protists and grazers (often NCM), where the successful isolation of both the predator and the prey is required. Field experiments are thus especially useful as the effects of parameters such as light, temperature, prey, and nutrients availability can

be tested on understudied uncultured taxa. New technologies including single-cell genomics (Labarre et al., 2020), transcriptomics (Cooney et al., 2020), and chemical imaging (Decelle et al., 2020) allow us to study the biological role of individual cells. The potential of such techniques could reinforce the study of rare and unculturable NCM taxa. Comparative genomics has already helped to better understand how temporary plastids become permanent (Sibbald and Archibald, 2020). Combined knowledge from comparative genomics and new eco-physiological studies on mixotrophs could give further insights in the evolutionary fate of extant temporary plastids and NCM, as well as resolve evolutionary histories and their early intermediates. Jointly, knowledge of the evolutionary fate of such trophic dynamics shaping traits will assist in predictions of oceanic ecosystems.

AUTHOR CONTRIBUTIONS

All authors listed have made a substantial, direct and intellectual contribution to the work, and approved it for publication.

FUNDING

This work was supported by European Union’s Horizon 2020 research and innovation programme under grant agreement No. 766327.

ACKNOWLEDGMENTS

We thank the MixITiN consortium (www.mixotroph.org) for helpful comments and criticism on early versions of the manuscript, in particular Fabrice Not, Uwe John, Maira Maselli, Lisa Schneider, Claudia Traboni, Kevin Flynn, and Aditee Mitra. We also want to thank the editor and the reviewers of the manuscript for their constructive comments.

SUPPLEMENTARY MATERIAL

The Supplementary Material for this article can be found online at: <https://www.frontiersin.org/articles/10.3389/fmars.2021.666160/full#supplementary-material>

REFERENCES

- Abrahamsen, M. S., Templeton, T. J., Enomoto, S., Abrahante, J. E., Zhu, G., Lancto, C. A., et al. (2004). Complete genome sequence of the apicomplexan, *Cryptosporidium parvum*. *Science* 304, 441–445. doi: 10.1126/science.1094786
- Adl, S. M., Simpson, A. G. B., Lane, C. E., Lukeš, J., Bass, D., Bowser, S. S., et al. (2012). The revised classification of eukaryotes. *J. Eukaryot. Microbiol.* 59, 429–493. doi: 10.1111/j.1550-7408.2012.00644.x
- Allen, J. F. (1993). Control of gene expression by redox potential and the requirement for chloroplast and mitochondrial genomes. *J. Theor. Biol.* 165, 609–631. doi: 10.1006/jtbi.1993.1210
- Allen, J. F. (2017). The CoRR hypothesis for genes in organelles. *J. Theor. Biol.* 434, 50–57. doi: 10.1016/j.jtbi.2017.04.008
- Allen, A. P., Gillooly, J. F., and Brown, J. H. (2005). Linking the global carbon cycle to individual metabolism. *Funct. Ecol.* 19, 202–213. doi: 10.1111/j.1365-2435.2005.00952.x
- Allen, J. F., and Martin, W. F. (2016). Why have organelles retained genomes? *Cell Syst.* 2, 70–72. doi: 10.1016/j.cels.2016.02.007
- Allen, J. F., and Raven, J. A. (1996). Free-radical-induced mutation vs redox regulation: costs and benefits of genes in organelles. *J. Mol. Evol.* 42, 482–492. doi: 10.1007/BF02352278
- Altenburger, A., Cai, H., Li, Q., Drumm, K., Kim, M., Zhu, Y., et al. (2020). Limits to the cellular control of sequestered cryptophyte prey in the marine

- ciliate *Mesodinium rubrum*. *ISME J.* 15, 1056–1072. doi: 10.1038/s41396-020-00830-9
- Andersen, K. H., Aksnes, D. L., Berge, T., Fiksen, Ø., and Visser, A. (2015). Modelling emergent trophic strategies in plankton. *J. Plankton Res.* 37, 862–868. doi: 10.1093/plankt/fbv054
- Anderson, O. R. (2012). Living together in the plankton: a survey of marine protist symbioses. *Acta Protozool.* 52, 1–10. doi: 10.4467/16890027AP13.006.1085
- Anderson, R., Charvet, S., and Hansen, P. (2018). Mixotrophy in chlorophytes and haptophytes—effect of irradiance, macronutrient, micronutrient and vitamin limitation. *Front. Microbiol.* 9:1704. doi: 10.3389/FMICB.2018.01704
- Anderson, R., Jürgens, K., and Hansen, P. J. (2017). Mixotrophic phytoflagellate bacterivory field measurements strongly biased by standard approaches: a case study. *Front. Microbiol.* 8:1398. doi: 10.3389/fmicb.2017.01398
- Anschütz, A. A., and Flynn, K. J. (2020). Niche separation between different functional types of mixoplankton: results from NPZ-style N-based model simulations. *Mar. Biol.* 167, 1–21. doi: 10.1007/s00227-019-3612-3
- Archibald, J. M. (2008). Plastid evolution: remnant algal genes in ciliates. *Curr. Biol.* 18, R663–R665. doi: 10.1016/j.cub.2008.06.031
- Archibald, J. M. (2015). Endosymbiosis and eukaryotic cell evolution. *Curr. Biol.* 25, R911–R921. doi: 10.1016/j.cub.2015.07.055
- Barbrook, A. C., Howe, C. J., and Purton, S. (2006). Why are plastid genomes retained in non-photosynthetic organisms? *Trends Plant Sci.* 11, 101–108. doi: 10.1016/j.tplants.2005.12.004
- Beisner, B. E., Grossart, H. P., and Gasol, J. M. (2019). A guide to methods for estimating phago-mixotrophy in nanophytoplankton. *J. Plankton Res.* 41, 77–89. doi: 10.1093/plankt/fbz008
- Beisser, D., Graupner, N., Bock, C., Wodniok, S., Grossmann, L., Vos, M., et al. (2017). Comprehensive transcriptome analysis provides new insights into nutritional strategies and phylogenetic relationships of chrysophytes. *PeerJ* 5:e2832. doi: 10.7717/peerj.2832
- Bendich, A. J. (1987). Why do chloroplasts and mitochondria contain so many copies of their genome? *Bioessays* 6, 279–282. doi: 10.1002/bies.950060608
- Bhattacharya, D., Archibald, J. M., Weber, A. P. M., and Reyes-Prieto, A. (2007). How do endosymbionts become organelles? Understanding early events in plastid evolution. *Bioessays* 29, 1239–1246. doi: 10.1002/bies.20671
- Björkholm, P., Harish, A., Hagström, E., Ernst, A. M., and Andersson, S. G. E. (2015). Mitochondrial genomes are retained by selective constraints on protein targeting. *Proc. Natl. Acad. Sci. U. S. A.* 112, 10154–10161. doi: 10.1073/pnas.1421372112
- Bodyl, A. (2018). Did some red alga-derived plastids evolve via kleptoplastidy? A hypothesis. *Biol. Rev. Camb. Philos. Soc.* 93, 201–222. doi: 10.1111/brv.12340
- Bodyl, A., Mackiewicz, P., and Stiller, J. W. (2009). Early steps in plastid evolution: current ideas and controversies. *Bioessays* 31, 1219–1232. doi: 10.1002/bies.200900073
- Booth, A., and Doolittle, W. F. (2015). Eukaryogenesis, how special really? *Proc. Natl. Acad. Sci. U. S. A.* 112, 10278–10285. doi: 10.1073/pnas.1421376112
- Brisbin, M. M., Mesrop, L. Y., Grossmann, M. M., and Mitarai, S. (2018). Intra-host symbiont diversity and extended symbiont maintenance in photosymbiotic Acantharea (clade F). *Front. Microbiol.* 9:1998. doi: 10.3389/fmicb.2018.01998
- Broglio, E., Johansson, M., and Jonsson, P. R. (2001). Trophic interaction between copepods and ciliates: effects of prey swimming behavior on predation risk. *Mar. Ecol. Prog. Ser.* 220, 179–186. doi: 10.3354/meps220179
- Burkholder, J. A. M., Glibert, P. M., and Skelton, H. M. (2008). Mixotrophy, a major mode of nutrition for harmful algal species in eutrophic waters. *Harmful Algae* 8, 77–93. doi: 10.1016/j.hal.2008.08.010
- Burki, F. (2016). Mitochondrial evolution: going, going, gone. *Curr. Biol.* 26, R410–R412. doi: 10.1016/j.cub.2016.04.032
- Burns, J. A., Pittis, A. A., and Kim, E. (2018). Gene-based predictive models of trophic modes suggest asgard archaea are not phagocytotic. *Nat. Ecol. Evol.* 2, 697–704. doi: 10.1038/s41559-018-0477-7
- Cabrero, M. J., González-Olalla, J. M., Hinojosa-López, V. J., Peralta-Cornejó, F. J., and Carrillo, P. (2019). A shifting balance: responses of mixotrophic marine algae to cooling and warming under UVR. *New Phytol.* 221, 1317–1327. doi: 10.1111/nph.15470
- Caron, D. A. (2017). Acknowledging and incorporating mixed nutrition into aquatic protistan ecology, finally. *Environ. Microbiol. Rep.* 9, 41–43. doi: 10.1111/1758-2229.12514
- Caron, D. A., Sanders, R. W., Lim, E. L., Marrasé, C., Amaral, L. A., Whitney, S., et al. (1993). Light-dependent phagotrophy in the freshwater mixotrophic chrysophyte *Dinobryon cylindricum*. *Microb. Ecol.* 25, 93–111. doi: 10.1007/BF00182132
- Cavalier-Smith, T. (1987). The simultaneous symbiotic origin of mitochondria, chloroplasts, and microbodies. *Ann. N. Y. Acad. Sci.* 503, 55–71. doi: 10.1111/j.1749-6632.1987.tb40597.x
- Cavalier-Smith, T. (1999). Principles of protein and lipid targeting in secondary symbiogenesis: euglenoid, dinoflagellate, and sporozoan plastid origins and the eukaryote family tree. *J. Eukaryot. Microbiol.* 46, 347–366. doi: 10.1111/j.1550-7408.1999.tb04614.x
- Cavalier-Smith, T. (2002). The phagotrophic origin of eukaryotes and phylogenetic classification on protozoa. *Int. J. Syst. Evol. Microbiol.* 52, 297–354. doi: 10.1099/00207713-52-2-297
- Cavalier-Smith, T. (2006). Origin of mitochondria by intracellular enslavement of a photosynthetic purple bacterium. *Proc. Biol. Sci.* 273, 1943–1952. doi: 10.1098/rspb.2006.3531
- Chan, Y. F., Chiang, K. P., Ku, Y., and Gong, G. C. (2019). Abiotic and biotic factors affecting the ingestion rates of mixotrophic nanoflagellates (Haptophyta). *Microb. Ecol.* 77, 607–615. doi: 10.1007/s00248-018-1249-2
- Clavijo, J. M., Donath, A., Seródio, J., and Christa, G. (2018). Polymorphic adaptations in metazoans to establish and maintain photosymbioses. *Biol. Rev. Camb. Philos. Soc.* 93, 2006–2020. doi: 10.1111/brv.12430
- Cooney, E. C., Okamoto, N., Cho, A., Hehenberger, E., Richards, T. A., Santoro, A. E., et al. (2020). Single cell transcriptomics of *Abedinium* reveals a new early-branching dinoflagellate lineage. *Genome Biol. Evol.* 12, 2417–2428. doi: 10.1093/gbe/evaa196
- Cruz, S., Calado, R., Seródio, J., and Cartaxana, P. (2013). Crawling leaves: photosynthesis in sacoglossan sea slugs. *J. Exp. Bot.* 64, 3999–4009. doi: 10.1093/jxb/ert197
- Dagan, T., and Martin, W. (2009). Seeing green and red in diatom genomes. *Science* 324, 1651–1652. doi: 10.1126/science.1175765
- Decelle, J., Colin, S., and Foster, R. A. (2015). “Photosymbiosis in marine planktonic protists” in *Marine Protists*. eds. S. Ohtsuka, T. Suzuki, T. Horiguchi, N. Suzuki and F. Not (Tokyo, Japan: Springer), 465–500.
- Decelle, J., Probert, I., Bittner, L., Desdevises, Y., Colin, S., de Vargas, C., et al. (2012). An original mode of symbiosis in open ocean plankton. *Proc. Natl. Acad. Sci. U. S. A.* 109, 18000–18005. doi: 10.1073/pnas.1212303109
- Decelle, J., Stryhanyuk, H., Gallet, B., Veronesi, G., Schmidt, M., Balzano, S., et al. (2019). Algal remodeling in a ubiquitous planktonic photosymbiosis. *Curr. Biol.* 29, 968–978. doi: 10.1016/j.cub.2019.01.073
- Decelle, J., Veronesi, G., Gallet, B., Stryhanyuk, H., Benettoni, P., Schmidt, M., et al. (2020). Subcellular chemical imaging: new avenues in cell biology. *Trends Cell Biol.* 30, 173–188. doi: 10.1016/j.tcb.2019.12.007
- Deschamps, P., and Moreira, D. (2012). Reevaluating the green contribution to diatom genomes. *Genome Biol. Evol.* 4, 683–688. doi: 10.1093/gbe/evs053
- Dorrell, R. G., Gile, G., McCallum, G., Méheust, R., Baptiste, E. P., Klinger, C. M., et al. (2017). Chimeric origins of ochrophytes and haptophytes revealed through an ancient plastid proteome. *elife* 6:e23717. doi: 10.7554/eLife.23717
- Ferreira, G. D., and Calbet, A. (2020). Caveats on the use of rotenone to estimate mixotrophic grazing in the oceans. *Sci. Rep.* 10:3899. doi: 10.1038/s41598-020-60764-2
- Figueroa, R. I., Bravo, I., Fraga, S., Garcés, E., and Llaveria, G. (2009). The life history and cell cycle of *Kryptoperidinium foliaceum*, a dinoflagellate with two eukaryotic nuclei. *Protist* 160, 285–300. doi: 10.1016/j.protis.2008.12.003
- Fischer, R., Giebel, H.-A., Hillebrand, H., and Ptacnik, R. (2017). Importance of mixotrophic bacterivory can be predicted by light and loss rates. *Oikos* 126, 713–722. doi: 10.1111/oik.03539
- Flöder, S., Hansen, T., and Ptacnik, R. (2006). Energy-dependent bacterivory in *Ochromonas minima*—a strategy promoting the use of substitutable resources and survival at insufficient light supply. *Protist* 157, 291–302. doi: 10.1016/j.protis.2006.05.002
- Flynn, K. J., and Hansen, P. J. (2013). Cutting the canopy to defeat the “selfish gene”: conflicting selection pressures for the integration of phototrophy in mixotrophic protists. *Protist* 164, 811–823. doi: 10.1016/j.protis.2013.09.002
- Flynn, K. J., and Mitra, A. (2009). Building the “perfect beast”: modelling mixotrophic plankton. *J. Plankton Res.* 31, 965–992. doi: 10.1093/plankt/fbp044

- Flynn, K. J., Mitra, A., Anestis, K., Anschütz, A. A., Calbet, A., Ferreira, G. D., et al. (2019). Mixotrophic protists and a new paradigm for marine ecology: where does plankton research go now? *J. Plankton Res.* 41, 375–391. doi: 10.1093/plankt/fbz026
- Flynn, K. J., Stoecker, D. K., Mitra, A., Raven, J. A., Glibert, P. M., Hansen, P. J., et al. (2013). Misuse of the phytoplankton-zooplankton dichotomy: the need to assign organisms as mixotrophs within plankton functional types. *J. Plankton Res.* 35, 3–11. doi: 10.1093/plankt/fbs062
- Franzè, G., and Lavrentyev, P. J. (2014). Microzooplankton growth rates examined across a temperature gradient in the Barents Sea. *PLoS One* 9:e86429. doi: 10.1371/journal.pone.0086429
- Gast, R. J., Moran, D. M., Dennett, M. R., and Caron, D. A. (2007). Kleptoplasty in an antarctic dinoflagellate: caught in evolutionary transition? *Environ. Microbiol.* 9, 39–45. doi: 10.1111/j.1462-2920.2006.01109.x
- Gawryluk, R. M. R., Tikhonenkov, D. V., Hehenberger, E., Husnik, F., Mylnikov, A. P., and Keeling, P. J. (2019). Non-photosynthetic predators are sister to red algae. *Nature* 572, 240–243. doi: 10.1038/s41586-019-1398-6
- Giovanardi, M., Poggioli, M., Ferroni, L., Lespinasse, M., Baldisserotto, C., Aro, E. M., et al. (2017). Higher packing of thylakoid complexes ensures a preserved photosystem II activity in mixotrophic *Neochloris oleoabundans*. *Algal Res.* 25, 322–332. doi: 10.1016/j.algal.2017.05.020
- González-Olalla, J. M., Medina-Sánchez, J. M., and Carrillo, P. (2019). Mixotrophic trade-off under warming and UVB in a marine and a freshwater alga. *J. Phycol.* 55, 1028–1040. doi: 10.1111/jpy.12865
- Gornik, S. G., Cassin, A. M., MacRae, J. I., Ramaprasad, A., Rchiad, Z., McConville, M. J., et al. (2015). Endosymbiosis undone by stepwise elimination of the plastid in a parasitic dinoflagellate. *Proc. Natl. Acad. Sci. U. S. A.* 112, 5767–5772. doi: 10.1073/pnas.1423400112
- Graupner, N., Jensen, M., Bock, C., Marks, S., Rahmann, S., Beisser, D., et al. (2018). Evolution of heterotrophy in chrysophytes as reflected by comparative transcriptomics. *FEMS Microbiol. Ecol.* 94, 1–11. doi: 10.1093/femsec/fiy039
- Green, B. J., Fox, T. C., and Rumpho, M. E. (2005). Stability of isolated algal chloroplasts that participate in a unique mollusc/kleptoplast association. *Symbiosis* 40, 31–40.
- Haas, A. (2007). The phagosome: compartment with a license to kill. *Traffic* 8, 311–330. doi: 10.1111/j.1600-0854.2006.00531.x
- Hadariová, L., Vesteg, M., Hampl, V., and Krajčovič, J. (2018). Reductive evolution of chloroplasts in non-photosynthetic plants, algae and protists. *Curr. Genet.* 64, 365–387. doi: 10.1007/s00294-017-0761-0
- Hampl, V., Čepička, I., and Eliáš, M. (2019). Was the mitochondrion necessary to start eukaryogenesis? *Trends Microbiol.* 27, 96–104. doi: 10.1016/j.tim.2018.10.005
- Hansen, P. J. (2011). The role of photosynthesis and food uptake for the growth of marine mixotrophic dinoflagellates. *J. Eukaryot. Microbiol.* 58, 203–214. doi: 10.1111/j.1550-7408.2011.00537.x
- Hansen, P. J., Anderson, R., Stoecker, D. K., Decelle, J., Altenburger, A., Blossom, H. E., et al. (2019). “Mixotrophy among freshwater and marine protists” in *Encyclopedia of Microbiology*. ed. T. M. Schmidt (Amsterdam, Netherlands: Elsevier Ltd.), 199–210.
- Hansen, P. J., Nielsen, L. T., Johnson, M., Berge, T., and Flynn, K. J. (2013). Acquired phototrophy in *Mesodinium* and *Dinophysis*—a review of cellular organization, prey selectivity, nutrient uptake and bioenergetics. *Harmful Algae* 28, 126–139. doi: 10.1016/j.hal.2013.06.004
- Hansen, P. J., Ojamäe, K., Berge, T., Trampe, E. C. L., Nielsen, L. T., Lips, I., et al. (2016). Photoregulation in a kleptochloroplastidic dinoflagellate, *Dinophysis acuta*. *Front. Microbiol.* 7:785. doi: 10.3389/fmicb.2016.00785
- Hehenberger, E., Burki, F., Kolisko, M., and Keeling, P. J. (2016). Functional relationship between a dinoflagellate host and its diatom endosymbiont. *Mol. Biol. Evol.* 33, 2376–2390. doi: 10.1093/molbev/msw109
- Hehenberger, E., Gast, R. J., and Keeling, P. J. (2019). A kleptoplastidic dinoflagellate and the tipping point between transient and fully integrated plastid endosymbiosis. *Proc. Natl. Acad. Sci. U. S. A.* 116, 17934–17942. doi: 10.1073/pnas.1910121116
- Hongo, Y., Yabuki, A., Fujikura, K., and Nagai, S. (2019). Genes functioned in kleptoplastids of *Dinophysis* are derived from haptophytes rather than from cryptophytes. *Sci. Rep.* 9, 1–11. doi: 10.1038/s41598-019-45326-5
- Howe, C. J., Barbrook, A. C., Nisbet, R. E. R., Lockhart, P. J., and Larkum, A. W. D. (2008). The origin of plastids. *Philos. Trans. R. Soc. B Biol. Sci.* 363, 2675–2685. doi: 10.1098/rstb.2008.0050
- Jackson, C. J., and Reyes-Prieto, A. (2014). The mitochondrial genomes of the glaucophytes *gloeochaete wittrockiana* and cyanopytyche *gloeocystis*: multilocus phylogenetics suggests amonophyletic archaeplastida. *Genome Biol. Evol.* 6, 2774–2785. doi: 10.1093/gbe/evu218
- Janouskovec, J., Gavelis, G. S., Burki, F., Dinh, D., Bachvaroff, T. R., Gornik, S. G., et al. (2017). Major transitions in dinoflagellate evolution unveiled by phylotranscriptomics. *Proc. Natl. Acad. Sci. U. S. A.* 114, E171–E180. doi: 10.1073/pnas.1614842114
- Janouskovec, J., Paskerova, G. G., Miroliubova, T. S., Mikhaiiov, K. V., Birley, T., Aieoshin, V. V., et al. (2019). Apicomplexan-like parasites are polyphyletic and widely but selectively dependent on cryptic plastid organelles. *elife* 8:e49662. doi: 10.7554/eLife.49662
- Jeffrey, S. W., and Vesik, M. (1976). Further evidence for a membrane-bound endosymbiont within the dinoflagellate *Peridinium foliaceum*. *J. Phycol.* 12, 450–455. doi: 10.1111/j.1529-8817.1976.tb02872.x
- John, U., Lu, Y., Wohlrab, S., Groth, M., Janouškovec, J., Kohli, G. S., et al. (2019). An aerobic eukaryotic parasite with functional mitochondria that likely lacks a mitochondrial genome. *Sci. Adv.* 5, 1–12. doi: 10.1126/sciadv.aav1110
- Johnson, M. D. (2015). Inducible mixotrophy in the dinoflagellate *Prorocentrum minimum*. *J. Eukaryot. Microbiol.* 62, 431–443. doi: 10.1111/jeu.12198
- Johnson, M. D., Oldach, D., Delwiche, C. F., and Stoecker, D. K. (2007). Retention of transcriptionally active cryptophyte nuclei by the ciliate *Myrionecta rubra*. *Nature* 445, 426–428. doi: 10.1038/nature05496
- Kamikawa, R., Moog, D., Zauner, S., Tanifuji, G., Ishida, K. I., Miyashita, H., et al. (2017). A non-photosynthetic diatom reveals early steps of reductive evolution in plastids. *Mol. Biol. Evol.* 34, 2355–2366. doi: 10.1093/molbev/msx172
- Keeling, P. J. (2013). The number, speed, and impact of plastid endosymbioses in eukaryotic evolution. *Annu. Rev. Plant Biol.* 64, 583–607. doi: 10.1146/annurev-arplant-050312-120144
- Keeling, P. J., and Burki, F. (2019). Progress towards the tree of eukaryotes. *Curr. Biol.* 29, R808–R817. doi: 10.1016/j.cub.2019.07.031
- Keeling, P. J., and McCutcheon, J. P. (2017). Endosymbiosis: the feeling is not mutual. *J. Theor. Biol.* 434, 75–79. doi: 10.1016/j.jtbi.2017.06.008
- Keeling, P. J., McCutcheon, J. P., and Doolittle, W. F. (2015). Symbiosis becoming permanent: survival of the luckiest. *Proc. Natl. Acad. Sci. U. S. A.* 112, 10101–10103. doi: 10.1073/pnas.1513346112
- Keller, M. D., Shapiro, L. P., Haugen, E. M., Cucci, T. L., Sherr, E. B., and Sherr, B. F. (1994). Phagotrophy of fluorescently labeled bacteria by an oceanic phytoplankter. *Microb. Ecol.* 28, 39–52. doi: 10.1007/BF00170246
- Kies, L., and Kremer, B. P. (1979). Function of cyanelles in the thecamoeba *Paulinella chromatophora*. *Naturwissenschaften* 66, 578–579. doi: 10.1007/BF00368819
- Kim, M., Drumm, K., Daughjerg, N., and Hansen, P. J. (2017). Dynamics of sequestered cryptophyte nuclei in *Mesodinium rubrum* during starvation and refeeding. *Front. Microbiol.* 8:423. doi: 10.3389/fmicb.2017.00423
- Kim, G. H., Han, J. H., Kim, B., Han, J. W., Nam, S. W., Shin, W., et al. (2016). Cryptophyte gene regulation in the kleptoplastidic, karyokleptic ciliate *Mesodinium rubrum*. *Harmful Algae* 52, 23–33. doi: 10.1016/j.hal.2015.12.004
- Kim, E., and Maruyama, S. (2014). A contemplation on the secondary origin of green algal and plant plastids. *Acta Soc. Bot. Pol.* 83, 331–336. doi: 10.5586/asbp.2014.040
- Kjørboe, T. (2011). How zooplankton feed: mechanisms, traits and trade-offs. *Biol. Rev.* 86, 311–339. doi: 10.1111/j.1469-185X.2010.00148.x
- Koonin, E. V. (2010). The origin and early evolution of eukaryotes in the light of phylogenomics. *Genome Biol.* 11:209. doi: 10.1186/gb-2010-11-5-209
- Labarre, A., Obiol, A., Wilken, S., Forn, I., and Massana, R. (2020). Expression of genes involved in phagocytosis in uncultured heterotrophic flagellates. *Limnol. Oceanogr.* 65, S149–S160. doi: 10.1002/lno.11379
- LaJeunesse, T. C., Smith, R. T., Finney, J., and Oxenford, H. (2009). Outbreak and persistence of opportunistic symbiotic dinoflagellates during the 2005 Caribbean mass coral “bleaching” event. *Proc. R. Soc. B Biol. Sci.* 276, 4139–4148. doi: 10.1098/rspb.2009.1405
- LaJeunesse, T. C., Smith, R., Walther, M., Pinzón, J., Pettay, D. T., McGinley, M., et al. (2010). Host-symbiont recombination versus natural selection in the response of coral-dinoflagellate symbioses to environmental disturbance. *Proc. Biol. Sci.* 277, 2925–2934. doi: 10.1098/rspb.2010.0385
- Lane, N. (2005). *Power, Sex, Suicide: Mitochondria and the Meaning of Life*. Oxford, United Kingdom: Oxfords University Press.

- Larkum, A. W. D., Lockhart, P. J., and Howe, C. J. (2007). Shopping for plastids. *Trends Plant Sci.* 12, 189–195. doi: 10.1016/j.tplants.2007.03.011
- Lasek-Nesselquist, E., Wisecaver, J. H., Hackett, J. D., and Johnson, M. D. (2015). Insights into transcriptional changes that accompany organelle sequestration from the stolen nucleus of *Mesodinium rubrum*. *BMC Genomics* 16:805. doi: 10.1186/s12864-015-2052-9
- Lewis, C. L., and Coffroth, M. A. (2004). The acquisition of exogenous, algal symbionts by an octocoral after bleaching. *Science* 304, 1490–1492. doi: 10.1126/science.1097323
- Li, A., Stoeker, D. K., and Adolf, J. E. (1999). Feeding, pigmentation, photosynthesis and growth of the mixotrophic dinoflagellate *Gyrodinium galatheanum*. *Aquat. Microb. Ecol.* 19, 163–176. doi: 10.3354/ame019163
- Li, C. W., and Volcani, B. E. (1987). Four new apochlorotic diatoms. *Br. Phycol. J.* 22, 375–382. doi: 10.1080/00071618700650441
- Mansour, J. S., Pollock, F. J., Díaz-Almeyda, E., Iglesias-Prieto, R., and Medina, M. (2018). Intra- and interspecific variation and phenotypic plasticity in thylakoid membrane properties across two *Symbiodinium* clades. *Coral Reefs* 37, 841–850. doi: 10.1007/s00338-018-1710-1
- Marin, B., Nowack, E. C. M., and Melkonian, M. (2005). A plastid in the making: evidence for a second primary endosymbiosis. *Protist* 156, 425–432. doi: 10.1016/j.protis.2005.09.001
- Martijn, J., and Ettena, T. J. G. (2013). From archaeon to eukaryote: the evolutionary dark ages of the eukaryotic cell. *Biochem. Soc. Trans.* 41, 451–457. doi: 10.1042/BST20120292
- Martin, W., and Müller, M. (1998). The hydrogen hypothesis for the first eukaryote. *Nature* 392, 37–41. doi: 10.1038/32096
- McFadden, G. I., and Yeh, E. (2017). The apicoplast: now you see it, now you don't. *Int. J. Parasitol.* 47, 137–144. doi: 10.1016/j.ijpara.2016.08.005
- Menge, D. N. L., and Weitz, J. S. (2009). Dangerous nutrients: evolution of phytoplankton resource uptake subject to virus attack. *J. Theor. Biol.* 257, 104–115. doi: 10.1016/j.jtbi.2008.10.032
- Mereschkowsky, C. (1905). Über natur und ursprung der chromatophoren im pflanzenreiche. *Biol. Cent.* 25, 593–604. (English translation in Martin, W., Kowallik, K. V. (1999). Annotated English translation of Mereschkowsky's 1905 paper 'Über Natur und Ursprung der Chromatophoren im Pflanzenreiche'. *Eur. J. Phycol.* 34, 287–295).
- Millette, N. C., Pierson, J. J., Aceves, A., and Stoeker, D. K. (2017). Mixotrophy in *Heterocapsa rotundata*: a mechanism for dominating the winter phytoplankton. *Limnol. Oceanogr.* 62, 836–845. doi: 10.1002/lno.10470
- Mills, D. B. (2020). The origin of phagocytosis in earth history. *Interface Focus* 10:20200019. doi: 10.1098/rsfs.2020.0019
- Mitra, A., Flynn, K. J., Burkholder, J. M., Berge, T., Calbet, A., Raven, J. A., et al. (2014). The role of mixotrophic protists in the biological carbon pump. *Biogeosciences* 11, 995–1005. doi: 10.5194/bg-11-995-2014
- Mitra, A., Flynn, K. J., Tillmann, U., Raven, J. A., Caron, D., Stoeker, D. K., et al. (2016). Defining planktonic protist functional groups on mechanisms for energy and nutrient acquisition: incorporation of diverse mixotrophic strategies. *Protist* 167, 106–120. doi: 10.1016/j.protis.2016.01.003
- Morozov, A. A., and Galachyants, Y. P. (2019). Diatom genes originating from red and green algae: implications for the secondary endosymbiosis models. *Mar. Genomics* 45, 72–78. doi: 10.1016/j.margen.2019.02.003
- Nakayama, T., and Ishida, K. I. (2009). Another acquisition of a primary photosynthetic organelle is underway in *Paulinella chromatophora*. *Curr. Biol.* 19, R284–R285. doi: 10.1016/j.cub.2009.02.043
- Nowack, E. C. M. (2014). *Paulinella chromatophora*—rethinking the transition from endosymbiont to organelle. *Acta Soc. Bot. Pol.* 83, 387–397. doi: 10.5586/asbp.2014.049
- Nowack, E. C. M., and Grossman, A. R. (2012). Trafficking of protein into the recently established photosynthetic organelles of *Paulinella chromatophora*. *Proc. Natl. Acad. Sci. U. S. A.* 109, 5340–5345. doi: 10.1073/pnas.1118800109
- Nowack, E. C. M., Melkonian, M., and Glöckner, G. (2008). Chromatophore genome sequence of *Paulinella* sheds light on acquisition of photosynthesis by eukaryotes. *Curr. Biol.* 18, 410–418. doi: 10.1016/j.cub.2008.02.051
- O'Connor, M. I., Piehler, M. F., Leech, D. M., Anton, A., and Bruno, J. F. (2009). Warming and resource availability shift food web structure and metabolism. *PLoS Biol.* 7:e1000178. doi: 10.1371/journal.pbio.1000178
- Ok, J. H., Jeong, H. J., Lim, A. S., You, J. H., Kang, H. C., Kim, S. J., et al. (2019). Effects of light and temperature on the growth of *Takayama helix* (Dinophyceae): mixotrophy as a survival strategy against photoinhibition. *J. Phycol.* 55, 1181–1195. doi: 10.1111/jpy.12907
- Onuma, R., Hirooka, S., Kanesaki, Y., Fujiwara, T., Yoshikawa, H., and Miyagishima, S. (2020). Changes in the transcriptome, ploidy, and optimal light intensity of a cryptomonad upon integration into a kleptoplast dinoflagellate. *ISME J.* 14, 2407–2423. doi: 10.1038/s41396-020-0693-4
- Onuma, R., and Horiguchi, T. (2015). Kleptochloroplast enlargement, karyoklepty and the distribution of the cryptomonad nucleus in *Nusuttodinium* (= *Gymnodinium*) *aeruginosum* (Dinophyceae). *Protist* 166, 177–195. doi: 10.1016/j.protis.2015.01.004
- Park, M. G., Kim, M., and Kim, S. (2014). The acquisition of plastids/phototrophy in heterotrophic dinoflagellates. *Acta Protozool.* 53, 39–50. doi: 10.4467/16890027AP.14.005.1442
- Patron, N. J., Waller, R. F., and Keeling, P. J. (2006). A tertiary plastid uses genes from two endosymbionts. *J. Mol. Biol.* 357, 1373–1382. doi: 10.1016/j.jmb.2006.01.084
- Pfannschmidt, T., Nilsson, A., and Allen, J. F. (1999). Photosynthetic control of chloroplast gene expression. *Nature* 397, 625–628. doi: 10.1038/17624
- Pierce, S. K., Massey, S. E., Hanten, J. J., and Curtis, N. E. (2003). Horizontal transfer of functional nuclear genes between multicellular organisms. *Biol. Bull.* 204, 237–240. doi: 10.2307/1543594
- Pillet, L., and Pawlowski, J. (2013). Transcriptome analysis of foraminiferan *Elphidium margaritaceum* questions the role of gene transfer in kleptoplastidy. *Mol. Biol. Evol.* 30, 66–69. doi: 10.1093/molbev/mss226
- Princiotta, S. D. V., Smith, B. T., and Sanders, R. W. (2016). Temperature-dependent phagotrophy and phototrophy in a mixotrophic chrysophyte. *J. Phycol.* 52, 432–440. doi: 10.1111/jpy.12405
- Probert, I., Siano, R., Poirier, C., Decelle, J., Biard, T., Tuji, A., et al. (2014). *Brandtodinium* gen. nov. and *B. nutricula* comb. Nov. (Dinophyceae), a dinoflagellate commonly found in symbiosis with polycystine radiolarians. *J. Phycol.* 50, 388–399. doi: 10.1111/jpy.12174
- Qiu, H., Lee, J. M., Yoon, H. S., and Bhattacharya, D. (2017). Hypothesis: gene-rich plastid genomes in red algae may be an outcome of nuclear genome reduction. *J. Phycol.* 53, 715–719. doi: 10.1111/jpy.12514
- Raven, J. A. (1984). A cost-benefit analysis of photon absorption by photosynthetic unicells. *New Phytol.* 98, 593–625. doi: 10.1111/j.1469-8137.1984.tb04152.x
- Raven, J. A. (1997). Phagotrophy in phototrophs. *Limnol. Oceanogr.* 42, 198–205. doi: 10.4319/lo.1997.42.1.0198
- Raven, J. A., Beardall, J., Flynn, K. J., and Maberly, S. C. (2009). Phagotrophy in the origins of photosynthesis in eukaryotes and as a complementary mode of nutrition in phototrophs: relation to darwin's insectivorous plants. *J. Exp. Bot.* 60, 3975–3987. doi: 10.1093/jxb/erp282
- Reich, H. G., Rodriguez, I. B., Lajeunesse, T. C., and Ho, T. Y. (2020). Endosymbiotic dinoflagellates pump iron: differences in iron and other trace metal needs among the Symbiodiniaceae. *Coral Reefs* 39, 915–927. doi: 10.1007/s00338-020-01911-z
- Reumann, S., Inoue, K., and Keegstra, K. (2005). Evolution of the general protein import pathway of plastids (review). *Mol. Membr. Biol.* 22, 73–86. doi: 10.1080/09687860500041916
- Reyes-Prieto, A., Moustafa, A., and Bhattacharya, D. (2008). Multiple genes of apparent algal origin suggest ciliates may once have been photosynthetic. *Curr. Biol.* 18, 956–962. doi: 10.1016/j.cub.2008.05.042
- Rodriguez-Ezpeleta, N., Brinkmann, H., Burey, S. C., Roure, B., Burger, G., Löffelhardt, W., et al. (2005). Monophyly of primary photosynthetic eukaryotes: green plants, red algae, and glaucophytes. *Curr. Biol.* 15, 1325–1330. doi: 10.1016/j.cub.2005.06.040
- Rose, J. M., and Caron, D. A. (2007). Does low temperature constrain the growth rates of heterotrophic protists? Evidence and implications for algal blooms in cold waters. *Limnol. Oceanogr.* 52, 886–895. doi: 10.4319/lo.2007.52.2.0886
- Rusterholz, P. M., Hansen, P. J., and Daugbjerg, N. (2017). Evolutionary transition towards permanent chloroplasts?—division of kleptochloroplasts in starved cells of two species of *Dinophysis* (Dinophyceae). *PLoS One* 12:e0177512. doi: 10.1371/journal.pone.0177512
- Sagan, L. (1967). On the origin of mitosing cells. *J. Theor. Biol.* 14, 225–IN6. doi: 10.1016/0022-5193(67)90079-3
- Saldarriaga, J. F., Taylor, F. J. R., Keeling, P. J., and Cavalier-Smith, T. (2001). Dinoflagellate nuclear SSU rRNA phylogeny suggests multiple plastid losses and replacements. *J. Mol. Evol.* 53, 204–213. doi: 10.1007/s002390010210

- Schimper, A. F. W. (1883). Über die entwicklung der chlorophyllkörner und farbkörper. *Bot. Zeit.* 41, 105–114.
- Schneider, L., Anestis, K., Mansour, J., Anschutz, A., Gypens, N., Hansen, P., et al. (2020). A dataset on trophic modes of aquatic protists. *Biodivers. Data J.* 8:e56648. doi: 10.3897/bdj.8.e56648
- Sellers, C. G., Gast, R. J., and Sanders, R. W. (2014). Selective feeding and foreign plastid retention in an Antarctic dinoflagellate. *J. Phycol.* 50, 1081–1088. doi: 10.1111/jpy.12240
- Selosse, M. A., Charpin, M., and Not, F. (2017). Mixotrophy everywhere on land and in water: the grand écart hypothesis. *Ecol. Lett.* 20, 246–263. doi: 10.1111/ele.12714
- Sforza, E., Cipriani, R., Morosinotto, T., Bertuccio, A., and Giacometti, G. M. (2012). Excess CO₂ supply inhibits mixotrophic growth of *Chlorella protothecoides* and *Nannochloropsis salina*. *Bioresour. Technol.* 104, 523–529. doi: 10.1016/j.biortech.2011.10.025
- Sibbald, S. J., and Archibald, J. M. (2020). Genomic insights into plastid evolution. *Genome Biol. Evol.* 12, 978–990. doi: 10.1093/gbe/evaa096
- Skovgaard, A. (1996). Mixotrophy in *Fragilidium subglobosum* (Dinophyceae): growth and grazing responses as functions of light intensity. *Mar. Ecol. Prog. Ser.* 143, 247–253. doi: 10.3354/meps143247
- Skovgaard, A. (2000). A phagotrophically derivable growth factor in the plastidic dinoflagellate *Gyrodinium resplendens* (Dinophyceae). *J. Phycol.* 36, 1069–1078. doi: 10.1046/j.1529-8817.2000.00009.x
- Smalley, G. W., Coats, D. W., and Stoecker, D. K. (2003). Feeding in the mixotrophic dinoflagellate *Ceratium furca* is influenced by intracellular nutrient concentrations. *Mar. Ecol. Prog. Ser.* 262, 137–151. doi: 10.3354/meps262137
- Smith, M., and Hansen, P. J. (2007). Interaction between *Mesodinium rubrum* and its prey: importance of prey concentration, irradiance and pH. *Mar. Ecol. Prog. Ser.* 338, 61–70. doi: 10.3354/meps338061
- Stoecker, D. K., Hansen, P. J., Caron, D. A., and Mitra, A. (2017). Mixotrophy in the marine plankton. *Annu. Rev. Mar. Sci.* 9, 311–335. doi: 10.1146/annurev-marine-010816-060617
- Stoecker, D. K., Johnson, M. D., De Vargas, C., and Not, F. (2009). Acquired phototrophy in aquatic protists. *Aquat. Microb. Ecol.* 57, 279–310. doi: 10.3354/ame01340
- Stoecker, D. K., and Lavrentyev, P. J. (2018). Mixotrophic plankton in the polar seas: a pan-Arctic review. *Front. Mar. Sci.* 5:292. doi: 10.3389/fmars.2018.00292
- Theissen, U., and Martin, W. (2006). The difference between organelles and endosymbionts. *Curr. Biol.* 16, R1016–R1017. doi: 10.1016/j.cub.2006.11.020
- Timmis, J. N., Ayliff, M. A., Huang, C. Y., and Martin, W. (2004). Endosymbiotic gene transfer: organelle genomes forge eukaryotic chromosomes. *Nat. Rev. Genet.* 5, 123–135. doi: 10.1038/nrg1271
- Tippit, D. H., and Heaps, J. D. P. (1976). Apparent amitosis in the binucleate dinoflagellate *Peridinium balticum*. *J. Cell Sci.* 21, 273–289. doi: 10.1242/jcs.21.2.273
- Tomas, R. N., Cox, E. R., and Steidinger, K. A. (1973). *Peridinium balticum* (Levander) Lemmermann, and unusual dinoflagellate with a mesocaryotic and an eucaryotic nucleus. *J. Phycol.* 9, 91–98. doi: 10.1111/j.0022-3646.1973.00091.x
- Trench, R. K., and Thinh, L. V. (1995). *Gymnodinium linucheae* sp. Nov.: the dinoflagellate symbiont of the jellyfish *Linuche unguiculata*. *Eur. J. Phycol.* 30, 149–154. doi: 10.1080/09670269500650911
- Uwizeye, C., Brisbin, M. M., Gallet, B., Chevalier, F., Lekieffre, C., Schieber, N., et al. (2020). Cytokleptin in the plankton: a host strategy to optimize the bioenergetic machinery of endosymbiotic algae. *bioRxiv*. [Preprint]. doi: 10.1101/2020.12.08.416644
- Uzuka, A., Kobayashi, Y., Onuma, R., Hirooka, S., Kanesaki, Y., Yoshikawa, H., et al. (2019). Responses of unicellular predators to cope with the phototoxicity of photosynthetic prey. *Nat. Commun.* 10:5606. doi: 10.1038/s41467-019-13568-6
- Van Steenkiste, N. W. L., Stephenson, I., Herranz, M., Husnik, F., Keeling, P. J., and Leander, B. S. (2019). A new case of kleptoplasty in animals: marine flatworms steal functional plastids from diatoms. *Sci. Adv.* 5:eaaw4337. doi: 10.1126/sciadv.aaw4337
- von Heijne, G. (1986). Why mitochondria need a genome. *FEBS Lett.* 198, 1–4. doi: 10.1016/0014-5793(86)81172-3
- Ward, B. A., Dutkiewicz, S., Barton, A. D., and Follows, M. J. (2011). Biophysical aspects of resource acquisition and competition in algal mixotrophs. *Am. Nat.* 178, 98–112. doi: 10.1086/660284
- Wilken, S., Choi, C. J., and Worden, A. Z. (2020). Contrasting mixotrophic lifestyles reveal different ecological niches in two closely related marine protists. *J. Phycol.* 56, 52–67. doi: 10.1111/jpy.12920
- Wilken, S., Huisman, J., Naus-Wiezer, S., and Van Donk, E. (2013). Mixotrophic organisms become more heterotrophic with rising temperature. *Ecol. Lett.* 16, 225–233. doi: 10.1111/ele.12033
- Wilken, S., Yung, C. C. M., Hamilton, M., Hoadley, K., Nzongo, J., Eckmann, C., et al. (2019). The need to account for cell biology in characterizing predatory mixotrophs in aquatic environments. *Philos. Trans. R. Soc. Lond. Ser. B Biol. Sci.* 374:20190090. doi: 10.1098/rstb.2019.0090
- Williams, B. A. P., and Keeling, P. J. (2003). Cryptic organelles in parasitic protists and fungi. *Adv. Parasitol.* 54, 9–68. doi: 10.1016/S0065-308X(03)54001-5
- Yamada, N., Bolton, J. J., Trobajo, R., Mann, D. G., Dąbek, P., Witkowski, A., et al. (2019). Discovery of a kleptoplastic ‘dinotom’ dinoflagellate and the unique nuclear dynamics of converting kleptoplastids to permanent plastids. *Sci. Rep.* 9:10474. doi: 10.1038/s41598-019-46852-y
- Yoon, H. S., Reyes-Prieto, A., Melkonian, M., and Bhattacharya, D. (2006). Minimal plastid genome evolution in the *Paulinella* endosymbiont. *Curr. Biol.* 16, 670–672. doi: 10.1016/j.cub.2006.08.018
- Yutin, N., Wolf, M. Y., Wolf, Y. I., and Koonin, E. V. (2009). The origins of phagocytosis and eukaryogenesis. *Biol. Direct* 4, 1–26. doi: 10.1186/1745-6150-4-9
- Zimorski, V., Ku, C., Martin, W. F., and Gould, S. B. (2014). Endosymbiotic theory for organelle origins. *Curr. Opin. Microbiol.* 22, 38–48. doi: 10.1016/j.mib.2014.09.008

Conflict of Interest: The authors declare that the research was conducted in the absence of any commercial or financial relationships that could be construed as a potential conflict of interest.

Copyright © 2021 Mansour and Anestis. This is an open-access article distributed under the terms of the Creative Commons Attribution License (CC BY). The use, distribution or reproduction in other forums is permitted, provided the original author(s) and the copyright owner(s) are credited and that the original publication in this journal is cited, in accordance with accepted academic practice. No use, distribution or reproduction is permitted which does not comply with these terms.

Mixotrophy of photosymbiotic Radiolaria

Summary

Mixoplanktic photosymbioses are ubiquitous trophic relationships among marine plankton in the global ocean and can be important to ecosystems functioning, in particular in low nutrient settings. Radiolaria (Rhizaria) are abundant and ubiquitous single-celled eukaryotes (i.e. protists), many of which harbour photosynthetic endosymbionts. The abundance and mixotrophic physiology of photosymbiotic Radiolaria makes them both significant producers and consumers in oceanic food webs, as well as great contributors to biogeochemical cycles, including silicon, strontium, and the vertical export of organic matter. Because photosymbiotic Radiolaria cannot currently be cultured, physiological information for these organisms is limited and depends on cultivation-independent approaches. Research on Radiolaria will be important to understand photosymbiotic processes in planktic protists. Additionally, understanding their nutrient uptake capabilities will help to predict plankton dynamics by providing data for (e.g. system dynamics or global ocean) model input. In this thesis my primary objective aimed at elucidating the mixotrophic physiology of photosymbiotic Radiolaria.

Analyses of carbon and nitrogen content of specific planktic organisms are pivotal information for studies of ocean ecology and in particular for carbon or nitrogen-based models. In Chapter 2, we established biovolume to mass equations for several Rhizaria taxa, giving more accurate predictions than mean or central capsule normalised C and N density values previously available. Overall, we demonstrate that the carbon content of photosymbiotic Radiolaria has been underestimated several fold by using generalised estimations for protists. The Radiolaria-specific carbon content to volume estimations provides a first step to better incorporate these mixotrophic organisms into predictive models.

Subsequent chapters focus on the photosymbiotic association between Acantharia (Radiolaria) and *Phaeocystis* (haptophyte algae). In particular, we aimed to establish phototrophic and phagotrophic rates for Acantharia using bulk stable isotope analyses. As well as elucidate the metabolic connectivity between host and symbiont using single-cell NanoSIMS and transcriptomic methods. We established the estimate for total inorganic carbon uptake rate of Acantharia as $1112.7 \pm 82.1 \text{ pg C h}^{-1} \text{ Acantharia}^{-1}$. Despite that the grazing rates of Acantharia remained unclear, based on our experiments and considering that the observed photosynthetic carbon uptake rates would only account for 14.5% of the acantharian carbon content, we suggest photosynthetic carbon uptake might thus mainly be used for energy. Therefore, photosynthates could be preferentially used for respiration. Transcriptomic analyses show an overall rapid gene expressional response to nutrient changes within the first few hours for genes from the photosymbionts. Concurrently, localisation of assimilated inorganic nutrients showed that both carbon and nitrogen are predominantly assimilated at the symbiont's plastids, and nitrogen assimilation is most prominent in the symbiont's nucleolus. Carbon translocation from symbionts to host could not be seen in our experiments and further suggest that photosynthates are used mainly for respiration or, transferred in low molecular weight compounds. Nitrogen assimilation in the symbiont's plastids and nucleolus suggest allocation of nutrients to photosynthesis machinery maintenance. Gene expression data further shows pathways present in nitrate metabolism in both host and symbiont, and certain photosynthesis-related genes might be present in the Acantharia host, further indicating the intertwined nature of the Acantharia and symbiont.

Taken together, we propose Acantharia can use both nitrate and ammonium as inorganic nitrogen sources and use photosynthesis mainly as an energy source, and we suggest that carbon acquired by predation would be preferentially allocated (and is needed for) to growth.

Keywords: Physiology; Acantharia; Radiolaria; Photosymbiosis; Transcriptomics; Isotopes; Nutrients; Mixotrophy